Mitochondrial respiration is essential for early B cell development and the humoral immune response

Mitochondriale Zellatmung ist essenziell für die frühe B Zell Entwicklung und die humorale Immunantwort

Der Naturwissenschaftlichen Fakultät

der Friedrich-Alexander-Universität Erlangen-Nürnberg

zur

Erlangung des Doktorgrades Dr. rer. nat.

vorgelegt von

Sophia Johanna Urbanczyk

aus Nürnberg

Als Dissertation genehmigt von der Naturwissenschaftlichen Fakultät

der Friedrich-Alexander-Universität Erlangen-Nürnberg

Tag der mündlichen Prüfung: 06.05.2022

Gutachter: Prof. Dr. Lars Nitschke

Prof. Dr. rer. nat. Dr. habil. med. Dirk Mielenz

"*I cannot consider the organism without its environment … from a formal point of view the two may be regarded as equivalent phases between which dynamic contact is maintained by the membranes that separate and link them "*

(Peter Mitchell)

"Jedermanns Schüler
Und mein eigener Meister…
Es lebe das Leben
Auf immer und ewig
In Liebe ergeben."

(Robert Gwisdek alias Käptn Peng)

Table of contents

1. Summary

The prevention and treatment of cancer and autoimmune diseases but also the development and improvement of vaccines require a deep understanding of the underlying molecular immunological processes. The past few years have shown that metabolism plays a crucial and decisive role for several immune cell types. Within the B cell lineage, the pro B to pre B cell transition is accompanied by a metabolic downregulation and a switch towards oxidative metabolism. Conversely, activated B cells upregulate oxidative and glycolytic metabolism, while anergy is induced via metabolic suppression. Yet, a detailed analysis of mitochondrial metabolism at central and peripheral B cell differentiation stages are missing. Therefore, in this thesis I tested the hypothesis that mitochondrial respiration is essential for early B cell development and peripheral activation, and that consequently mitochondrial function is ensured and selected for at certain checkpoints. The establishment of a mouse line that expresses a dominant-negative mutant of the mitochondrial helicase Twinkle (DNT) in conjunction with IRES-GFP specifically in B cells using the Cre-loxP system, resulted in decreased mitochondrial (mt) DNA abundance in B cells. Since essential respiratory chain subunits are encoded in mtDNA, these cells consequently have impaired mitochondrial respiration. This enabled the analysis of mitochondrial respiration specifically in early B cell development and during B cell activation by using mb1Cre and CD23Cre mice, respectively. Expression of DNT in B cell progenitors via mb1Cre revealed an essential requirement of mtDNA replication and mitochondrial respiration at the pro to pre B cell transition, as these mice exhibited a developmental block at the pre B cell stage. Furthermore, transitional B cells with higher mtDNA content are selected into the pool of marginal zone B cells. This is in accordance with other results obtained in this thesis that showed the highest mtDNA content in marginal zone B cells and plasma cells, especially in the bone marrow. In accordance, the generation of plasma cells and basal as well as induced humoral immune responses to T cell-dependent and -independent antigens are highly dependent on functional mtDNA replication and mitochondrial respiration in B cells, as shown by the analysis of DNTxCD23Cre mice. The decreased oxidative phosphorylation in lipopolysaccharide activated B cells led to an aberrant flux of the TCA cycle and to decreased abundance of saturated phosphatidic acid. Consequently, mTORC1 activity and BLIMP1 expression were reduced, whereas pAMPK, HIF1α, and glycolysis were increased.

In summary, mitochondrial respiration in B cells is essential for early B cell development in the bone marrow at the pro to pre B cell transition. Furthermore, marginal zone B cells and BM plasma cells have the highest mtDNA content in the B cell lineage. Lastly, replication of mtDNA, which provides essential subunits of the respiratory chain, in mature B cells is crucial for B cell activation, subsequent plasma cell differentiation, and consequently the humoral immune response.

2. Zusammenfassung

Sowohl die Vorbeugung und Behandlung von Krebs und Autoimmunerkrankungen als auch die Entwicklung und Verbesserung von Impfstoffen setzen ein tiefgreifendes Verständnis von zugrunde liegenden molekularen, immunologischen Prozessen voraus. Studien aus jüngerer Vergangenheit konnten zeigen, dass der Stoffwechsel eine essenzielle und entscheidende Rolle in diversen Immunzelltypen spielt. Innerhalb der B Zell Linie wird der Stoffwechsel während der pro zu prä B Zell Transition runter reguliert und wechselt zu überwiegend oxidativen Stoffwechselwegen. Aktivierte B Zellen erhöhen sowohl oxidative als auch glykolytische Stoffwechselwege, wohingegen Anergie in B Zellen durch Suppression des Stoffwechsels erreicht wird. Jedoch fehlen bisher detaillierte Analysen der Rolle des mitochondrialen Stoffwechsels an zentralen und peripheren Kontrollpunkten während der B Zell Differenzierung. Daher teste ich in dieser Arbeit die Hypothese, dass die mitochondriale Zellatmung eine essenzielle Rolle während der frühen B Zell Entwicklung und während der peripheren Aktivierung spielt, und dass folglich B Zellen mit funktionellen Mitochondrien an bestimmten Kontrollpunkten selektiert werden. Die Cre-loxP vermittelte Generierung einer Mauslinie, die eine dominant-negative Mutante der mitochondrialen Helikase Twinkle (DNT), gekoppelt an IRES-GFP, spezifisch in B Zellen exprimiert, führt zu reduzierter mitochondrialer DNA in B Zellen. Da essenzielle Untereinheiten der Atmungskette im mitochondrialen Genom kodiert sind, ist die mitochondriale Zellatmung folglich gestört in diesen Zellen. Das ermöglicht die Untersuchung der mitochondrialen Zellatmung während der frühen B Zell Entwicklung durch Kreuzung mit mb1Cre Mäusen und während der B Zell Aktivierung durch Kreuzung mit CD23Cre Mäusen. Die mb1Cre vermittelte DNT Expression in pro B Zellen zeigte, dass mitochondriale Zellatmung eine essenzielle Rolle während der pro zu prä B Zell Transition spielt, da diese Mäuse in diesem Stadium einen Entwicklungsblock aufwiesen. Außerdem werden transitionale B Zellen mit funktioneller Replikation der mitochondrialen DNA in das Kompartment von Marginalzonen B Zellen selektiert. Damit übereinstimmend konnte in dieser Dissertation gezeigt werden, dass Marginalzonen B Zellen und Plasma Zellen den höchsten Gehalt an mitochondrialer DNA innerhalb der B Zell Linie aufweisen. Die Analyse von DNT x CD23Cre Mäusen zeigte, dass die Generierung von Plasma Zellen und humorale Immunantworten, sowohl basal als auch T Zell-abhängig oder -unabhängig induziert, stark von funktioneller Replikation der mitochondrialen DNA und mitochondrialer Zellatmung abhängig sind. Reduzierte oxidative Phosphorylierung in Lipopolysaccharid-aktivierten B Zellen führt zu aberrantem Fluss des Citratzyklus und verringerten Vorkommen an Phosphatidat. Folglich waren mTORC1 Aktivität und BLIMP1 Expression verringert, wohingegen pAMPK, HIF1α, und Glykolyse erhöht waren. Zusammenfassend konnte im Rahmen dieser Arbeit gezeigt werden, dass mitochondriale Zellatmung in B Zellen eine essenzielle Rolle während der frühen B Zell Entwicklung im Knochenmark spielt. Außerdem zeigen Marginalzonen B Zellen und Plasma

Zellen den höchsten Gehalt an mitochondrialer DNA innerhalb der B Zell Linie auf. Und schließlich ist die Replikation mitochondrialer DNA in reifen B Zellen essenziell für die B Zell Aktivierung und darauffolgende Plasma Zell Differenzierung, und somit folglich für die humorale Immunantwort.

3. Preface

Writing this sentence and thesis during a lockdown caused by a pandemic that has started 2 years ago and cost so far over 3 million lives, that is heavily affecting the global economy and social life and that will leave permanent scars on individual but also on collective level, makes it more than clear how important our understanding of the immune system is. The generation and improvement of vaccines that protect us collectively from otherwise harmful or even deadly pathogens, but also the prevention and treatment of cancer and autoimmune diseases that represent a further burden on individual well-being but also society as a whole, require a deep understanding of the underlying molecular, immunological processes.

4. Introduction

4.1 Mitochondria

Mitochondria are found in basically all eukaryotes as double membrane-bounded organelles and originate from a monophyletic endosymbiosis where an archaea acquired α-proteobacteria. This unique evolutionary event gave rise to complex life, precisely eukaryotes, indicating its importance. Due to its bacterial origin, mitochondria have their own genome and although the majority of genes were lost or transferred to the nucleus over time, they preserved a small part that ranges ~16.6 kb in mammalian species (Fig. 1) (Gray, 2012). It encodes 11 mRNAs that are translated to 13 proteins, which are all essential subunits of the mitochondrial respiratory chain (mtRC). It furthermore encodes 2 rRNAs and 22 tRNAs that are required for the translation within the mitochondrial matrix of mtDNA encoded genes (Gustafsson et al., 2016). The replication of mtDNA is executed by a specific set of nucleus-encoded proteins that differ from the replication machinery of nuclear DNA. The minimal replisome consists of the hexameric mtDNA helicase TWINKLE, the heterotrimeric mtDNA polymerase (POLG), and the tetrameric single-stranded DNA-binding protein (mtSSB). TWINKLE is homologous to the T7 phage gene 4 protein and it initiates unwinding of mtDNA in the 5' to 3' direction that is required for subsequent replication. It is the only replicative DNA helicase in mammalian mitochondria and loss of TWINKLE causes embryonic lethality at ~E8.5 (Milenkovic et al., 2013). Long stretches of single-stranded DNA formed at the replication fork are stabilized by tetramer-forming mtSSB, which also functions as a stimulator for TWINKLE and POLγ, the polymerase executing the replication of mtDNA (Gustafsson et al., 2016). Although the exact mechanisms of how mtDNA copy number is controlled are unknown, it has been shown that TWINKLE plays a crucial role in this context: Increased TWINKLE expression results in increased mtDNA copy number, whereas knockout of TWINKLE lead to a profound drop in mtDNA copy numbers (Gustafsson et al., 2016). The accumulation of mtDNA deletions in muscle and peripheral nerve cells is responsible for diseases, such as SANDO, which is a syndrome characterized by sensory ataxic neuropathy, dysarthria, and ophthalmoparesis (Angelini, 2014). In fact, a single mutation in the N-terminus of the TWINKLE gene that changes lysine to glutamate (K319E) results in a SANDO phenotype in humans, highlighting the importance of functional TWINKLE and mtDNA replication *in vivo*. (Hudson et al., 2005).

Mitochondria can be separated into six distinct compartments: The outer membrane, the inner membrane, the cristal membrane, the intracristal space, the intermembrane space, and the matrix (Rossignol et al., 2004). In textbooks mitochondria are typically termed the "powerhouse of the cell" because they provide the cell with most of the ATP that is needed for cellular function. Yet, over the past decades it became clear that mitochondria participate in numerous

ways beyond the production of ATP to cellular function, such as the induction of apoptosis, modulating Ca2+ signaling, and balancing the redox system (McCarron et al., 2013). The shape, number, and localization of mitochondria within the cell depends on the cell type an can even vary within individual cells, indicating different functions of individual mitochondria. (McCarron et al., 2013). Furthermore, mitochondria are transported through the cell in a kinesin- and dynein-dependent manner and they are able to initiate morphological remodelling by combining and separating mitochondria in processes termed fusion and fission, respectively. These dynamic processes, namely fusion and fission, are mediated by large guanosine triphosphatases (GTPases) in the dynamin family: mitochondrial fission is mediated by Drp1 whereas Mfn1, Mfn2, and Opa1 are required for mitochondrial fusion (Chang and Blackstone, 2007). Importantly, mitochondria are more fused when performing OxPhos, indicating that these processes influence mitochondrial function and vice versa. Additionally, mitochondrial fusion promotes the complementation between damaged mitochondria and is furthermore induced by for instance inhibition of protein synthesis or inhibition of mTOR (Youle and van der Bliek, 2012). Mitochondrial dynamics also play a crucial role during apoptotic cell death: high levels of stress preceding apoptosis result in excessive fission of mitochondria. In parallel, the pro-apoptotic Bcl-2 family member Bax is translocated from the cytosol into mitochondria and cytochrome c is being released (Youle and van der Bliek, 2012). While the role of mitochondria during apoptotic cell death is well known it is important to highlight mitochondria require a functional respiratory chain that for this purpose. There are several studies showing that cells devoid of mtDNA (ρ^0 cells) are protected against apoptosis: Human osteosarcoma cells lacking mtDNA (143B ρ^0 cells) are strongly protected from ER stress-induced apoptosis and mitochondria-initiated apoptosis (Kwong et al., 2007).

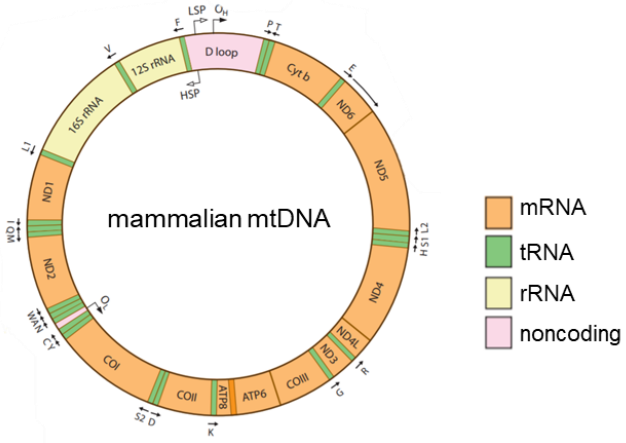

Figure 1 | Depiction of mammalian mitochondrial DNA

Mammalian mitochondrial DNA (mtDNA) is a double-stranded, circular molecule that encodes 13 mRNAs, which are all essential subunits of the oxidative phosphorylation machinery. In addition, 22 tRNAs and 2 rRNAs encoded that are needed for the translation of these mRNAs within the mitochondrial matrix are encoded.

Figure adapted and modified from Larsson et. al. (Larsson, 2010).

4.2 Metabolism

Metabolism portrays the entirety of life-sustaining chemical reactions that can be divided into anabolic and catabolic processes. While the former describes the synthesis of compounds, such as nucleic acids, proteins, carbohydrates, and lipids, the latter describes the break-down of compounds, such as glucose or amino acids. In general, it can be said that catabolic processes are energy releasing, while anabolic processes are energy consuming. These chemical reactions are organized into metabolic pathways, where compounds are transformed in a stepwise manner, each step being executed by a specific enzyme (Fig 2).

4.2.1 Glycolysis

Glycolysis describes the conversion of glucose that takes place within the cytoplasm in a sequence of 10 enzymatic reactions that ultimately result in the generation of two molecules of NADH, H_2O, pyruvate, and ATP each.

Glucose enters the cells via specific transporter proteins (GLUT1-GLUT14) and is then phosphorylated by ATP to form glucose-6-phosphate. The next step is the isomerization of glucose-6-phosphate to fructose-6-phosphate. Next, fructose-1,6-bisphosphate is generated at the expense of ATP. Fructose-1,6-bosphosphate is then cleaved into glyceraldehyde 3 -phosphate (GAP) and dihydroxyacetone phosphate (DHAP). After GAP is converted into 1,3-bisphosphoglycerate (1,3-BPG), phosphoglycerate kinase catalyses the transfer of the phosphoryl group to ADP, thereby generating ATP and 3-phosphoglycerate with the reduction of NAD+ to NADH. In the remaining steps, 3-phosphoglycerate is converted into pyruvate which produces a second molecule of ATP. Under aerobic conditions, the generated pyruvate is preferentially imported into mitochondria to fuel the TCA cycle and electron transport chain (ETC). However, even in the presence of oxygen, glycolysis may also be used for energy production under certain circumstances in a process termed aerobic glycolysis, or “Warburg effect” in the case of cancer cells, where pyruvate is converted to lactate which is then secreted by the cell (Berg et al., 2002c). While the production of ATP represents the catabolic aspect of glycolysis, this pathway also participates in anabolic processes by supplying metabolites that serve as precursors for instance in the pentose phosphate pathway (PPP) and synthesis of phospholipids (Fig 2).

The glycolytic enzymes are regulated by gene expression, allostery, protein-protein interactions, post-translational modifications, and localization (Locasale, 2018). Due to the saturation of glycolytic enzymes, high abundance of glucose does generally not increase the glycolysis rate. However, the activity of certain glycolytic master TFs, namely c-Myc and HIF1α, can increase the maximum reaction rate V^{max} by several fold for multiple glycolytic enzymes simultaneously (Locasale, 2018). In turn, the activity of these TFs is regulated by

signal transduction pathways that respond to extracellular signals and abundance of growth factors or nutrients.

The glycolysis pathway also plays an important role in B cells, as its upregulation upon BCR crosslinking supports cell growth and proliferation in a PI3K/Akt dependent manner (Caro-Maldonado et al., 2014; Doughty et al., 2006). Furthermore, in this context the glycolytic upregulation is dependent on c-Myc, but HIF1α-independent. Importantly, B cells rely on glycolytic flux for proliferation and antibody (Ab) production (Caro-Maldonado et al., 2014).

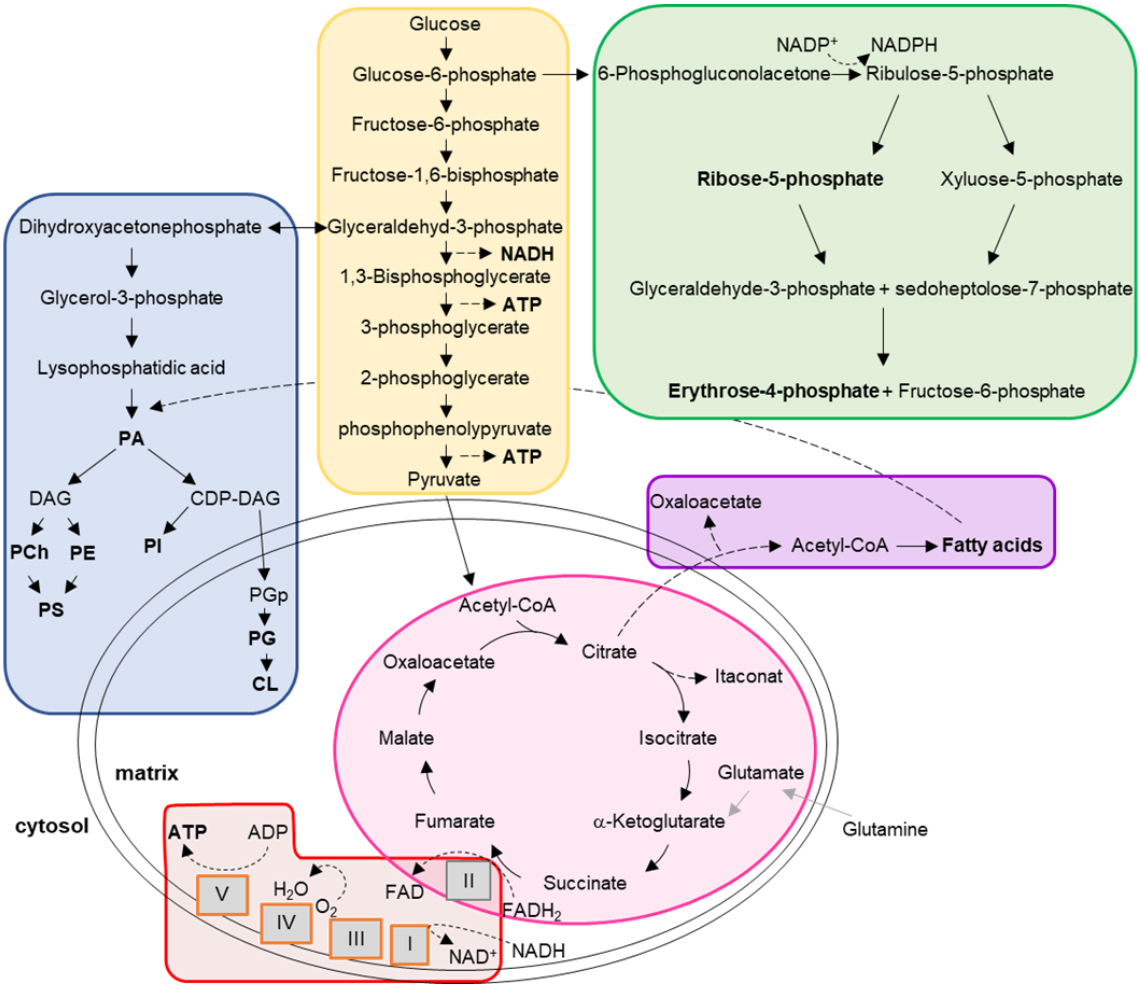

Figure 2 | Overview of metabolic pathways

Schematic depiction of glycolysis (yellow), pentose phosphate pathway (green), TCA cycle (pink), oxidative phosphorylation (red), fatty acid (purple) and phospholipid synthesis (blue). Roman letters indicate OxPhos complexes I-V (grey), and complexes outlined in orange contain essential mtDNA-encoded subunits. Metabolic products are highlighted in bold. Indicated double membrane represents mitochondria. PA, phosphatidic acid; CDP-DAG, cytidinediphosphate-diacylglycerol; DAG, diacylglycerol; PCh, phosphatidylcholine; PE, phosphatidylethanolamine; PI, phosphatidylinositol; PGp, phosphatidylglycerol phosphate; PS, phosphatidylserine; PG, phosphatidylglycerol; CL, cardiolipin.

4.2.2 Pentose phosphate pathway

The PPP is an important aspect of glucose metabolism and branches after the first step of glycolysis using the intermediate glucose 6-phosphate as substrate (Fig 2). Therefore, these two pathways are tightly linked and interdependent. In contrast to glycolysis or aerobic oxidation, this pathway does not provide ATP but instead supplies the cell with ribose 5-phosphate (R5P), erythrose 4-phosphate (E4P), and NADPH, which are vital substrates for survival and proliferation: While R5P is required for the synthesis of nucleic acids, E4P is the precursor for aromatic amino acids. NADHP, on the other hand, is the reducing power for the synthesis of fatty acids, nucleotides, and non-essential amino acids but also important for cellular antioxidant defences. In fact, the PPP is the largest contributor of cytosolic NADPH, which is required for the reduction of glutathione disulfide (GSSG) to the sulfhydryl form glutathione (GSH), thereby salvaging oxidative stress (Ge et al., 2020; Stincone et al., 2015; Xiao et al., 2018). The PPP is separated into the oxidative and non-oxidative branch, both of which take place in the cytosol. In the oxidative phase, glucose 6-phosphate is converted into ribulose 5-phosphate, which is subsequently converted into E4P and fructose 6-phosphate in the non-oxidative branch (Ge et al., 2020; Stincone et al., 2015).

The specific functions and requirements of the PPP at different B cells stages remains largely elusive. However, it was shown that PP2A activity, a serine/threonine-protein phosphatase that was identified as a tumor suppressor in multiple types of cancer, is required during B cell development in the bone marrow. It redirects glucose carbon utilization from glycolysis to the PPP to salvage oxidative stress and its deletion results in a developmental block at the pre-BCR stage (Xiao et al., 2018). One important consequence of PP2A deletion was a reduced NADPH/NADP ratio, which consequently decreased the GSH/GSGG ratio, indicating exhaustion of reductive reserves in these cells. Interestingly, inducible deletion of PP2A under cell culture conditions in established BCR-positive, mature B cells resulted in acute cell death, highlighting the importance of glucose diversion into the PPP also for survival of mature B cells (Xiao et al., 2018). Apparently, glucose diversion into the PPP also plays an important role during B cell activation: Activated B cells (αCD40/IL4, 24h) increase their glucose uptake and mainly divert it into the PPP to produce R5P that in this context is required for the synthesis of ribonucleotides (Waters et al., 2018).

4.2.3 Phospholipid synthesis

A further metabolic pathway that is linked to glycolysis as well as the TCA cycle is the synthesis of phospholipids (Fig 2). First, phosphatidic acid (diacylglycerol 3-phosphate, PA) needs to be generated, due to its functions as a precursor for the synthesis of phospholipids necessary for both, membranes and triacylglycerols for energy storage (Athenstaedt and Daum, 1999; Berg et al., 2002a). For this purpose, glycerol 3-phosphate is acetylated by the coenzyme acyl CoA to form lysophosphatidic acid that is further acetylated by acyl CoA to generate PA. And while glycerol 3-phosphate is primarily formed by the reduction of dihydroxyacetone phosphate (DHAP), which is a glycolytic intermediate, the required acyl CoA origins from succinate, which is a TCA cycle intermediate (Berg et al., 2002a; Gnoni et al., 2009). Therefore, glucose derived carbon in the form of pyruvate is imported into mitochondria and decarboxylated to form citrate, which can be exported via the malate-citrate shuttle system and used as substrate for ATP-citrate lyase (ACLY) that catalyses the formation of acetyl-CoA (Dufort et al., 2014). An alternative source for citrate is the glutamine-dependent reductive carboxylation pathway, which is preferentially used by cells with defective mitochondria or under hypoxia (Mullen et al., 2011). For this purpose, glutamine is imported into mitochondria and converted into glutamate which is subsequently converted into alpha-ketoglutarate (α-KG). The generated α-KG can either participate in the TCA cycle supporting OxPhos or route into the reductive carboxylation pathway (Yoo et al., 2020).

Importantly, PA plays an additional vital role as messenger that signals the presence of sufficient lipid precursors for membrane biosynthesis, cell growth, and proliferation via its ability to directly activate mTOR (Fang et al., 2001; Foster, 2013; Yoon et al., 2011a).

This glucose-dependent *de novo* lipid synthesis pathway plays an important role in the B cell lineage and is essential during plasma blast differentiation: Stimulation of B cells with LPS activates the PI3K/Akt pathway, which stimulates the activity of ACLY, resulting in increased levels of several phospholipids (PCh, PE, PI, PS, CL). Analysing incorporation of [^{14}C] glucose showed no detectable incorporation into lipids in unstimulated B cells, but increased incorporation upon LPS stimulation. This is also the case after α-BCR/CD40/IL4 stimulation, although the relative amounts into the individual lipids differ (Dufort et al., 2014). Inhibition of ACLY blocks glucose derived incorporation into lipids and results in decreased ER expansion, decreased expression of CD138 and BLIMP1, which both are surface markers for plasma blasts and plasma cells (PB/PCs), and decreased IgM secretion (Dufort et al., 2014).

4.2.4 TCA cycle and OxPhos

The tricarboxylic acid (TCA) cycle is a series of enzymatic reactions that take place inside mitochondria and is formed in a closed loop (Fig 2). It is the gateway to aerobic metabolism and the final common pathway for the oxidation of fuel molecules such as amino acids and fatty acids. The reactions in the TCA cycle are executed by eight enzymes, which completely oxidize acetyl-CoA into two molecules of CO_2 and H_2O each. The primary source of acetyl-CoA is glycolysis derived pyruvate, although it may also be obtained from fatty acid oxidation via β-oxidation. First, acetyl-CoA and oxaloacetate (OAA) are combined to generate citrate that becomes converted into isocitrate in a second step. Next, a-ketoglutarate (a-KG) is generated that subsequently forms succinyl-CoA. This step generates two molecules of CO_2 and NADH each. Succinyl-CoA is then enzymatically converted to succinate that becomes oxidized to fumarate which is accompanied by the reduction of FAD to $FADH_2$. Next, malate is produced by hydration of fumarate and is finally oxidized to oxaloacetate which is accompanied by the reduction of NAD to NADH (Berg et al., 2002b; Krebs, 1948).

The TCA cycle and oxidative phosphorylation (OxPhos) are tightly linked and interdependent (Fig 2): First, the NADH and FADH2 molecules produced in the TCA cycle act as reducing agents for the electron transport chain (ETC). Second, the succinate dehydrogenase (SDH) participates in both, the TCA cycle and as complex II in the ETC. The ETC consists of 4 complexes: 3 proton pumps (CI, CIII, and CIV) and complex II (CII), which is the physical link to the TCA cycle (Fig 3).

Complex I (CI) transfers a pair of electrons from NADH to coenzyme Q and subsequently to complex II and III while protons are transported from the matrix side to the cytosolic side of the inner membrane, thereby contributing to the generation of the proton motive force.

Complex II (CII), the only TCA cycle enzyme residing in the mitochondrial inner membrane (MIM), oxidizes FADH2 and reduces coenzyme Q without the transport of protons.

Complex III (CIII) mediates the electron transport from coenzyme Q to cytochrome c and

Complex IV (CIV) transfers electrons from cytochrome c to reduce the essential terminal electron acceptor O_2 to H_2O on the matrix side. Both, CIII and CIV, are transporting protons across the MIM (Berg et al., 2002c; Garrett, n.d.).

A proton motive force, Δp that is essential for OxPhos is generated by the ETC. It consists of an electrical gradient, Δψμ that is negative inside the matrix, and a pH gradient, ΔpH that is alkaline inside the matrix (Rottenberg, 1975).

OxPhos describes the synthesis of ATP that is coupled to the flow of electrons from NADH or $FADH_2$ to O_2 by a proton gradient across the mitochondrial inner membrane, which has been established by the ETC. The flow of protons back through the ATP synthase, complex V of the OxPhos system (CV), provides the force for the rotation of the enzyme complex resulting in the synthesis of ATP (Fig 3) (Berg et al., 2002c).

Whereas the metabolism of glucose to lactate generates 2 molecules of ATP per molecule of glucose, the complete oxidation of glucose in OxPhos generates 36 molecules of ATP (Vander Heiden et al., 2009). Therefore, oxidative metabolism is highly efficient, however it requires the presence of O_2. Furthermore, mitochondrial metabolism is a major source of reactive oxygen species (ROS): 1-2% of mitochondrial consumed O_2 is diverted into the formation of ROS, mainly at complex I and complex III of the ETC (Circu and Aw, 2010). ROS are highly reactive oxygen ions (superoxide $O_2^{\cdot-}$) or oxygen-containing radicals (hydroxyl, $OH^{\cdot-}$) formed by the reduction of O_2. Additional cellular compartments that contribute to ROS production are ER-bound enzymes, cytoplasmic enzyme systems and the surface of the plasma membrane. Besides being produced as a by-product of cellular respiration, endogenous ROS also arises from NADPH oxidases (NOX1-4) that play an important role in phagocytes such as neutrophiles and macrophages during the process of bacterial killing (Auten and Davis, 2009). The functions of ROS depend critically on its location and concentration: It is an important 2nd messenger that activates multiple signal transduction pathways, thereby facilitating the actions of growth factors, cytokines, and calcium signaling. However, at higher concentrations ROS can cause direct injury to lipids, proteins, and nucleic acids and is involved in multiple pathways of cell death (Auten and Davis, 2009).

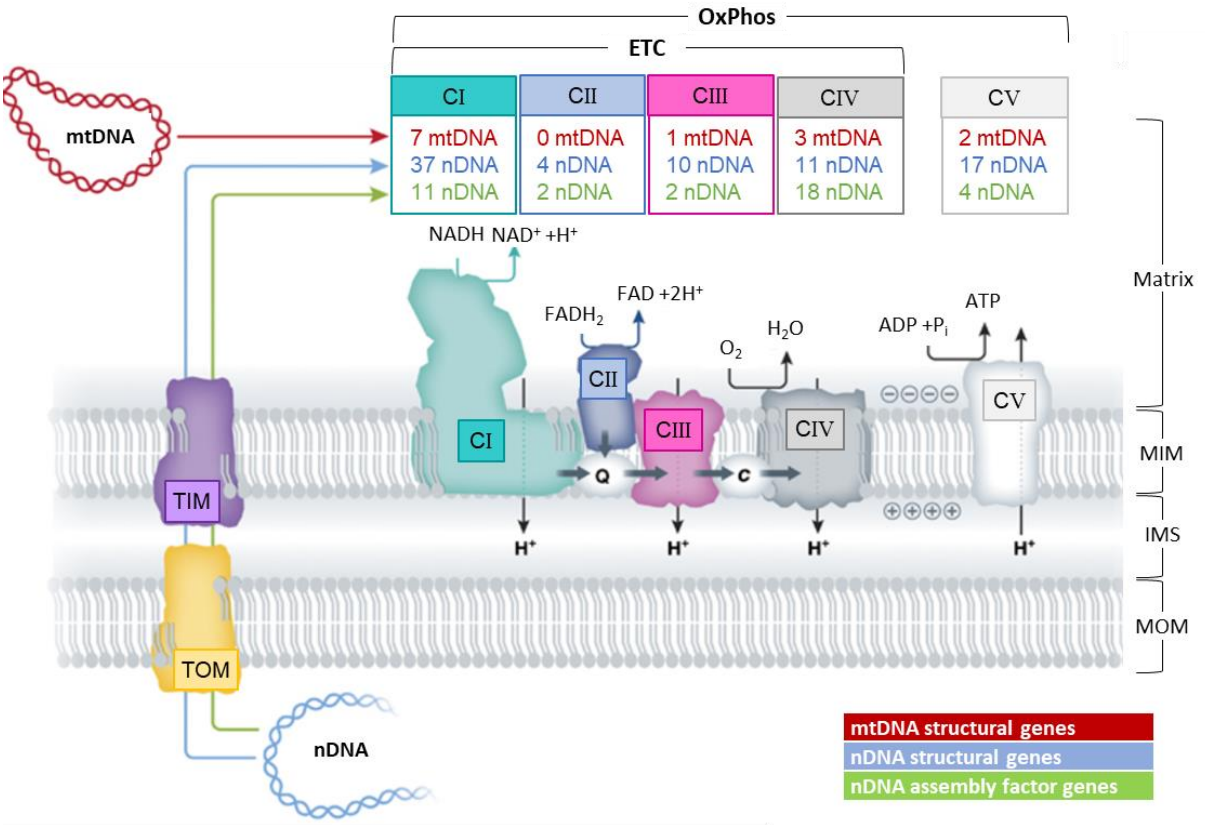

Figure 3 | Schematic depiction of Oxidative Phosphorylation

Genetic origin and assembly of the electron transport chain (ETC) and oxidative phosphorylation (OxPhos) system that consists of five multisubunit complexes (CI-CV) residing in the mitochondrial inner membrane (MIM). IMS, inner mitochondrial membrane; MOM, mitochondrial outer membrane; TIM, translocase of inner membrane; TOM, translocase of outer membrane; nDNA, nuclear DNA, mtDNA, mitochondrial DNA. *Adapted and modified from Koopman et al., 2013.*

In B cells OxPhos activity increases upon TLR4 or BCR stimulation (Caro-Maldonado et al., 2014). Apparently BLIMP1 expression is essential in this context as it mediates a stepwise upregulation of nucleus encoded OxPhos genes (Price et al., 2018). Moreover, this increased oxidative metabolism in PBs is required for Ab secretion as its inhibition results in decreased Ab titers (Price et al., 2018).

Gene Set Enrichment Analysis (GSEA) on RNA-seq datasets confirmed increased expression of TCA cycle and OxPhos genes also in anti-CD40/IL4 activated B cells (24h) compared to naïve B cells (Waters et al., 2018). Furthermore, they showed increased TCA metabolite levels in activated B cells indicating increased TCA flux. However, labelled glucose and pyruvate did not contribute carbon atoms for the formation of these intermediates. Therefore, activated B cells may utilize alternative nutrients to fuel the TCA cycle, such as lipids or glutamine.

4.2.5 Purinergic signaling

The form of extracellular signaling that is mediated by purine nucleotides and nucleosides, such as ATP and adenosine, is termed purinergic signaling. It comprises of 3 basic elements: (i) mechanisms that produce and release ATP into the pericellular space, (ii) the expression of purinergic receptors that recognize ATP and its metabolites and elicit intracellular signals that regulate cell function, and (iii) mechanisms that terminate the purinergic signaling cascade by breakdown of ATP, and cellular uptake or simple diffusion of extracellular ATP and its metabolites (Ledderose and Junger, 2020). The release of ATP is executed via vesicular exocytosis or ATP-permeable membrane channels, including connexin hemichannels, pannexin channels, calcium homeostasis modulator 1, maxi-anion channels, and volume-regulated anion channels. Under basal conditions cells release only a small portion of ATP, but the stimulation of cell surface receptors, such as TCR or chemokine receptors on T cells as well as anti-Ig or CpG stimulation of human B cells, results in a rapid burst of ATP release (Ledderose and Junger, 2020; Schena et al., 2013). The binding of ATP and its metabolites is mediated by purinergic receptors that are classified in two groups: P1 receptors that are selective for adenosine, and P2 receptors that are selective for ATP, ADP and UDP (Fig 4) (Burnstock et al., 2012). The P1 receptors comprises of four members, namely A_1, A_{2a}, A_{2b}, and A_3 that are all coupled to G-proteins and modulate adenylate cyclase activity in an either inhibitory (A_1, A_3) or stimulatory (A_{2a}, A_{2b}) manner, thereby resulting in cAMP changes. The probably most famous and appreciated adenosine-receptor antagonists is caffeine (Ribeiro and Sebastião, 2010). P2 receptors are divided into two families, namely P2X and P2Y, based on their molecular structure, transduction mechanism, and pharmacological properties. P2X receptors are ligand-gated ion channels, that, when activated by extracellular ATP, induce a flow of cations (Na^+, K^+, and Ca^{2+}) across the plasma membrane. There are seven subtypes recognized, termed $P2X_1$-$P2X_7$, that all mediate fast signaling, however differ their localization, function, and pharmacological properties. P2Y receptors represent a subclass of the super-family of G-coupled receptors, each containing seven transmembrane domains. The principal transduction pathway involves phospholipase C, which leads to the formation of inositol 1,4,5-triphosphate (InsP3), which regulates cell growth and DNA replication, and the mobilization of intracellular calcium. The conversion of ATP to adenosine is either achieved through spontaneous hydrolysis or through the activity of ectoenzymes, such as 5'-ectonucleotidases, ecto-ADPases, or ecto-ATPases (Burnstock et al., 2012). One of these enzymes, namely Ectonucleoside triphosphate diphosphohydrolase-1 (NTPDase1, CD39) is an ectonucleotidase that transforms ATP into ADP and AMP. Subsequently, ecto-5'- nucleotidase (5'-NT, CD73) hydrolyses AMP to adenosine (Fig 4) (Przybyła et al., 2018). The pericellular concentration of adenosine is maintained at constant levels and its availability as ligand for P1 receptors is determined by the rates of its synthesis and degradation.

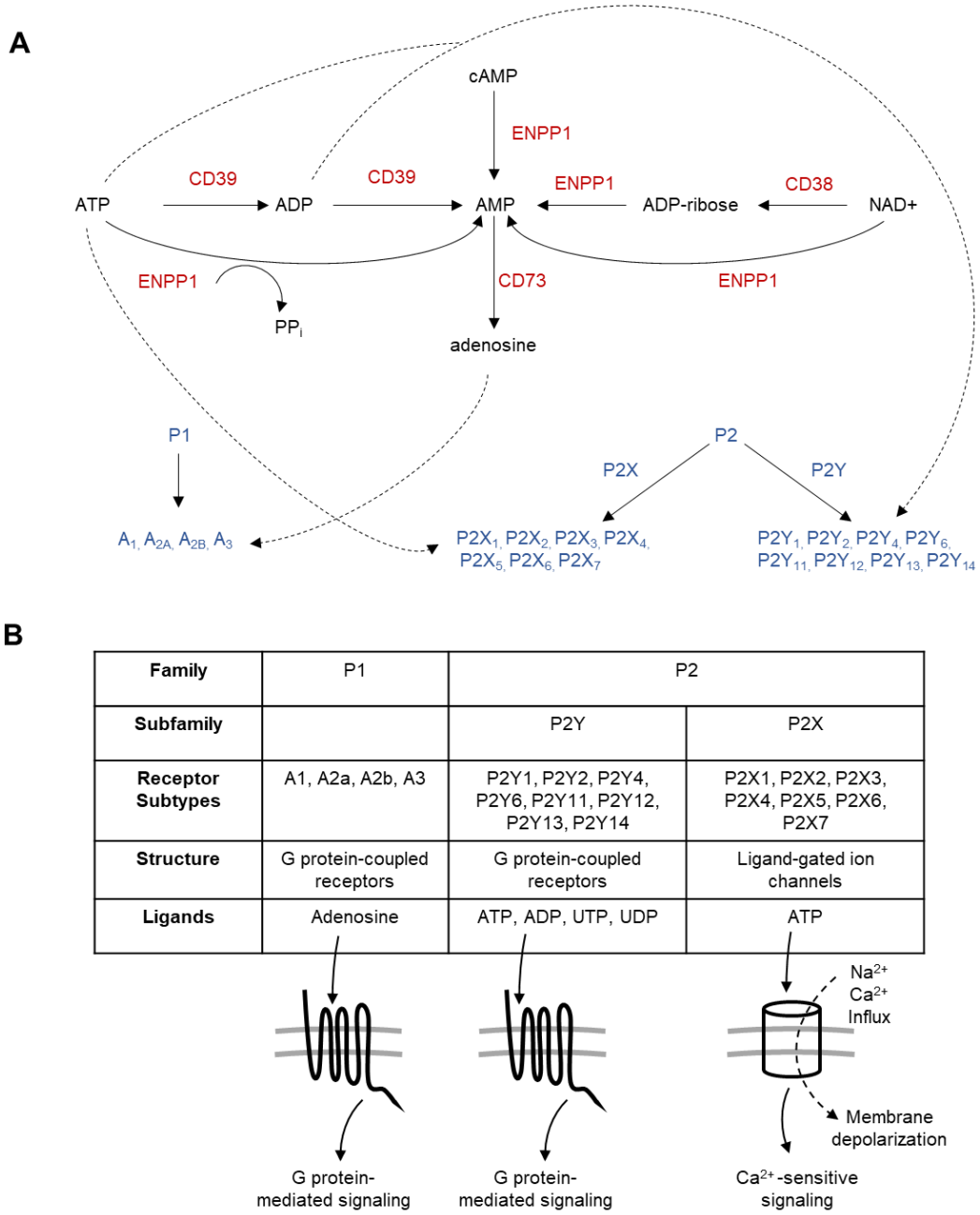

Figure 4 | Overview of purinergic receptors and their activity

A) Diagram of ATP metabolizing ectoenzyme function and purinergic receptors: Adenine nucleotides that are present in all cells (ATP > NAD > cAMP) are released in response to cell necrosis, apoptosis, or various factors that open membrane channels. This diagram shows some of the enzymes that participate in the extracellular conversion of ATP, NAD+, or cyclic AMP to adenosine. CD38, cyclic ADP-ribose hydrolase 1/NAD+ nucleosidase; CD39 (ENTPD1), ectonucleoside triphosphate diphosphohydrolase 1; ENPP1, ectonucleotide pyrophosphatase/phosphodiesterase; CD73 (NT5E), ecto-5-nucleotidase. Ectoenzymes are shown in red, and purinergic receptors are shown in blue. Adapted and modified from (Yu et al., 2018) **B) Overview of the purinergic receptor family:** classification, structure and singaling pathway: The family of purinergic repectors comprises major 2 groups: adenosine-activated P1 receptors and nucleotide-activated P2 receptors. The latter is further categorized in 2 subfamilies, namely P2X receptors and P2Y receptors, based on their pharmacological profile and molecular structure. P2X receptors (composing of 7 subtypes) are trimeric ATP-gated plasma membrane channels, whereas P2Y receptors are classic G protein-coupled receptors. P2Y receptors are further divided in 8 subtypes, based on their ligand selectivity.

4.2.6 Role of cellular metabolism in immune cell migration

The migration of immune cells is a fundamental process during homeostasis and infection. To achieve directed movement, cells organize and maintain spatial and functional asymmetry with a defined leading edge and trailing edge (uropod) that each contain specific cell parts: While the machinery for actin polymerization and gradient sensing are localized in the leading edge, the uropod contains certain adhesion molecules, the microtubule organization center (MTOC), and the majority of cellular organelles and cytoplasmic volume (Campello et al., 2006; del Pozo et al., 1998). The migratory capacity depends firstly on the combination of the expressed chemokine receptors and integrins, secondly on the ability to dynamically remodel the cytoskeleton and thirdly on sufficient metabolic support to meet bioenergetic demands (Guak and Krawczyk, 2020). While there are interesting reports on the function of mitochondria during cell migration in T cells and neutrophiles, insights on how mitochondria affect the migration B cell remain elusive. In neutrophiles from zebrafish the genetic inhibition of mtDNA replication by disruption of the mtDNA polymerase γ polg resulted in reduced velocity of neutrophil interstitial migration, thus indicating a direct link between mtDNA replication and migratory capacity (Zhou et al., 2018). Immune cells predominantly perform amoeboid movements with leading edge protrusions and contraction of the cell body (Friedl and Weigelin, 2008), which is an energy demanding process that requires most notably ATP for actin polymerisation, but also GTP for GTPases and microtubules. It appears that both glycolysis and OxPhos are important in this context: Although OxPhos is more efficient, glycolysis is also required for immune cell migration and in fact several glycolytic enzymes are associated with the cytoskeleton (Guak and Krawczyk, 2020). Interestingly, it has been shown in migrating T cells that mitochondria are transported to the uropod along microtubules in response to the chemokines C-X-C motif chemokine 12 (CXCL12) or C-C motif ligand 21 (CCL21), probably to ensure high ATP levels at this particular localization, where myosin II proteins are selectively localized (Campello et al., 2006). Furthermore, functional mitochondrial fission is required for their re-localization, and processes that shift the balance towards mitochondrial fusion interfere with the relocation of the mitochondria to the uropod which results in impaired polarization and migration (Campello et al., 2006). Intriguingly, there are also reports for T cells and neutrophiles showing that a small portion of mitochondria with higher membrane potential are located at the front of the migrating cell where they are required for continuous ATP production that is necessary for purinergic signaling via P2 receptors (Fig 5) (Bao et al., 2015; Ledderose et al., 2018). Moreover, continuously fuelling of purinergic signaling was an essential contribution to the migration of immune cells and was stimulated by the cytokine CXCL12: CXCL12 triggered mitochondrial ATP production and release and an accumulation of mitochondria with P2X4 receptors near the front of the cell. P2X4 receptors facilitate Ca2+

influx to maintain local mitochondrial ATP production at levels that are needed for migration, but also to promote cytoskeletal remodeling. This ensures a feed-forward signaling mechanism that promotes Ca2+ influx and sustains ATP synthesis at levels sufficient for pseudopod protrusion, polarization, and migration (Ledderose et al., 2018).

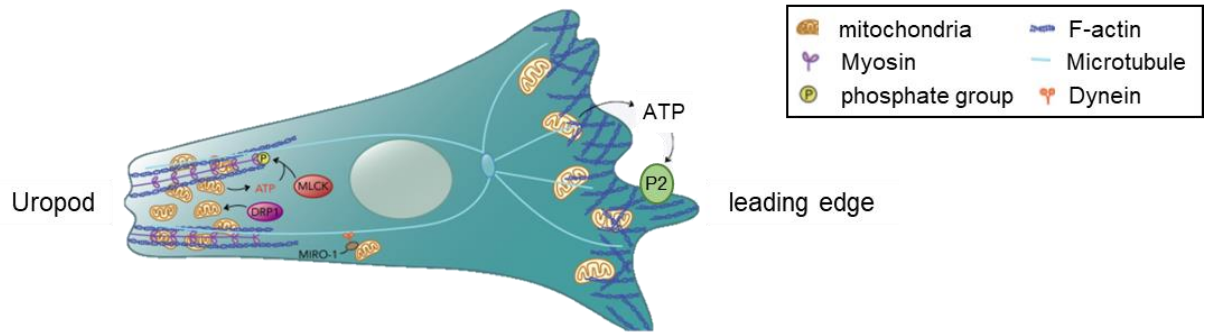

Figure 5 | Regulated redistribution of mitochondria in migrating immune cells
A small portion of mitochondria with relatively high membrane potential accumulate at the leading edge of migrating cells. ATP derived from these mitochondria is released and acts on purinergic P2 receptors, promoting the formation of actin protrusions. The majority of mitochondria with lower membrane potential are localized at the uropod in a DRP1-dependent manner. They facilitate contraction of the uropod by providing ATP for myosin light chain kinase (MLCK) phosphorylation. Adapted and modified from Guak and Krawczyk.

4.3 The immune system

The immune system is a network of cells and biological processes that protect the organism from diseases induced by pathogens such as viruses, bacteria, parasites, and fungi but also from cancer. These pathogens can infect humans for instance via direct contact, inhalation, or ingestion. Almost all living organisms, even bacteria, have an immune system, indicating its importance in life. Vertebrates have developed two subsystems, the innate immune system and the adaptive immune system, that also work tightly together (Fig 6). The innate immune system is evolutionary considerably older and consists of antimicrobial peptides, phagocytic cells, small molecules such as complement proteins, but also physical barriers, such as epithelial cell layers or secreted mucus layer in respiratory, gastrointestinal, and genitourinary tracts. The innate immune response represents the first line of defence and is partially constitutively active and partially inducible upon infection. The second line of defence is the adaptive immune system that is highly specialized, effective, and long-lasting. The adaptive immune system primarily consists of T lymphocytes and B lymphocytes that express a repertoire of millions diverse receptors, each specifically recognizing a different antigen and thereby providing protection against a vast variety of pathogens. This repertoire is generated by the rearrangement of gene segments in a process termed VDJ recombination. Both the

innate and the adaptive immune system include cell-mediated immune components and humoral immune components. In the case of the adaptive immune system the former is T cell mediated and the latter B cell mediated. Therefore, B cells represent a crucial part of the humoral immune response: First, by developing long-lived plasma cells that continuously secrete antibodies with high specificity and affinity, which circulate through the blood and bind foreign antigen. Secondly, B cells mediate immunological memory by developing into memory B cells (Bmem), that provide a faster and enhanced immune response upon repeated encounter with previously encountered pathogens. Yet, the aforementioned generation of this highly diverse repertoire comes at a high prize: all autoimmune diseases are immune responses from the adaptive immune system against self-antigens (Medzhitov and Janeway Jr, 2000). Receptors of the innate immune system are fully encoded in the germline and constantly under evolutionary pressure, ensuring that no autoreactive receptors are generated. Receptors of the adaptive immune system on the other hand are generated by gene rearrangement, that enables the generation of receptors recognizing host structures, such as dsDNA in the case of SLE. This implies that the ability to distinguish self from non-self is a further central function of the adaptive immune system (Chaplin, 2010). Therefore, the development and activation of T and B cells must be tightly controlled which is ensured by heavy and strict selection at defined checkpoints.

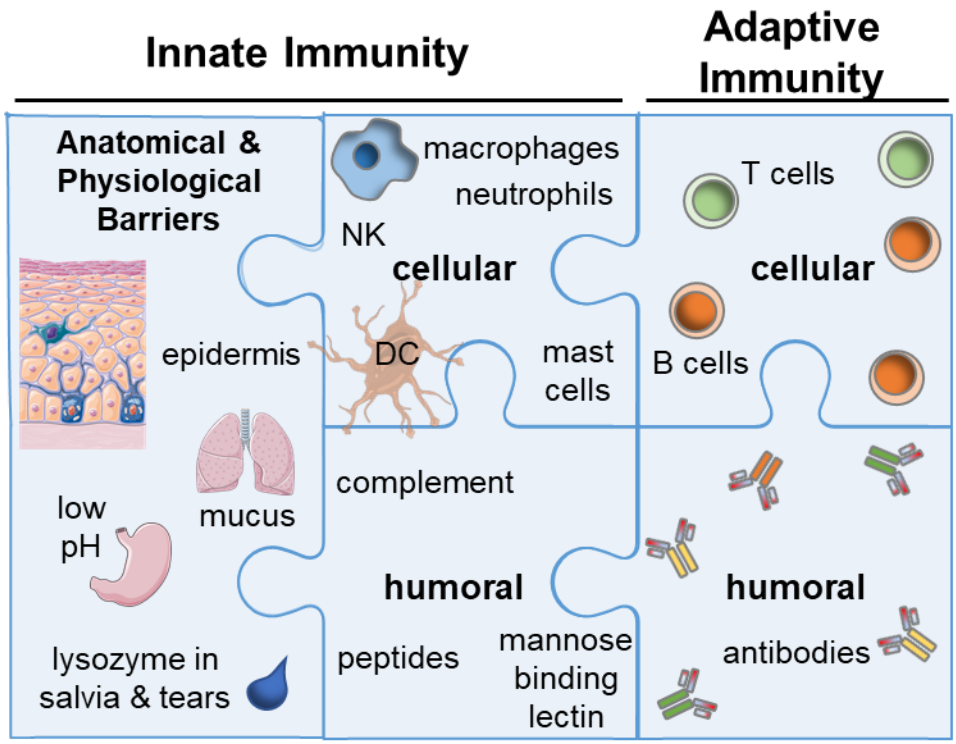

Figure 6 | Overview of the immune system
The immune system can be separated into the innate and adaptive immune system. Both comprise of cellular and humoral parts and the former also include anatomical and physiological barriers. B cells are an important part of the adaptive immune system, mainly by differentiating into longlived plasma cells that secrete high amounts of antibodies and memory B cells that provide an immunological memory.

4.3.1 B cell development and maturation

4.3.1.1 Early B cell development in the bone marrow

B cells develop in mammals in the bone marrow from pluripotent hematopoietic stem cells (pHSC) in a succession of defined stages: hematopoietic stem cells (HSC), common lymphoid progenitors (CLPs), B cell-biased lymphoid progenitors (BLPs), pre-pro B cells, pro B cells, and pre B cells (Fig 7A). The process is executed by the expression of defined sets of transcription factors in addition to external stimuli that steer the B cell development and migration through the respective niches (Fig 7B). The first step of B cell development is controlled by the TFs PU.1 and Ikaros (IKZF1), both of which are expressed in CLPs that can give rise to B, T, natural killer (NK), and dendritic cells (DCs). The subsequent commitment to the B cell lineage is mediated by the expression of the TFs E2A, EBF-1, and Pax5, and by expression of the proteins B220 and CD19 (Busslinger, 2004; Hagman and Lukin, 2006). Rag1/2 expression is induced in these generated pre-pro B cells leading to recombination of D_H/J_H segments in the µ heavy chain (µHC) locus and to recombination of $V_H/D_H/J_H$ segments

later in pro B cells (Sadofsky, 2001; Urbanczyk et al., 2018). The µHCs, even without the formation of a pre B cell receptor (pre-BCR), signal to close the second allele to avoid expression of two different µHCs by one B cell (Melchers, 2015). Successful rearrangements result in the expression of µHC that subsequently assembles with the surrogate light chain (SLC) and Igα and Igβ to form a pre-BCR in large pre B cells (Clark et al., 2014). Signaling via the pre-BCR in these pre B cells counteracts apoptosis by inducing 2-7 cell divisions, depending on the relative fitness of the pre-BCR, and furthermore it initiates the downregulation of SLC expression (Melchers, 2015). The formation of these pre-BCR+, large, cycling pre II B cells is accompanied by the downregulation of the proteins ckit and IL7Rα and upregulation of CD25. The downregulation of SLC expression leads to decreased proliferation of pre B cells that thereby become small, resting pre II B cells. One original pre B cell with a unique µHC can expand up to 100-fold, but each clone will individually rearrange V_L-to-J_L on the κ-IgLC or λ-IgLC locus, thereby generating greater diversity (Melchers, 2015). Successful light-chain rearrangement, translation and pairing with the µHC is required for the generation of immature, IgM^+ B cells. Self-reactive B cells are negatively selected at this stage through receptor editing, anergy, and deletion. Non-self-reactive immature B cells exit the bone marrow and migrate via the blood into the spleen for further maturation (Chung et al., 2003).

The survival during these early differentiation processes but also the guidance to the respective niches is mediated by signaling via several transmembrane receptors: Activation of c-kit by its ligand stem cell factor (KIT-L) is required for pro B cell survival (Busslinger, 2004). Furthermore, survival and proliferation of pro B cells is promoted by IL-7 that also functions as a differentiation factor (Corfe and Paige, 2012). Binding of IL-7 in pro B cells supports survival by inducing expression of the anti-apoptotic molecules Bcl-2 and myeloid-cell leukemia sequence 1 (MCL1). During development from pro B cell to immature B cells, IL-7R is downregulated and responsiveness to IL-7 decreases (Urbanczyk et al., 2018). A further important function of IL-7 signaling in early B cell development is the regulation of the TF Foxo1. Although to date it remains still elusive to what extent IL-7 regulates Foxo1, it has been shown that Foxo1 deletion causes a developmental block at the pre B cell stage due to lacking expression of IL-7Rα. Foxo1 is a TF involved in the regulation of stress resistance, cell cycle arrest, apoptosis and metabolism (Calnan and Brunet, 2008). Moreover, Foxo1 directly activates expression of RAG1/2 (Amin and Schlissel, 2008) and its regulation is therefore essential during early B cell development. Another important factor during these stages is the chemokine stromal cell-derived factor/CXC chemokine ligand 12 (CXCL12) that is produced and secreted by CXCL12-abundant reticular (CAR) cells (Nagasawa, 2007) and signals via its physiological receptor CXCR4 that is expressed on early B cells and also mature plasma cells. The CXCL12/CXCR4 axis is essential by attracting and/or tethering these cells to their appropriate niches (Nagasawa, 2006). An additional growth factor supporting early B cell

development is Fms-like tyrosine kinase (Flt) 3 ligand that synergizes with IL-7 in the proliferation and differentiation of committed B220-positive pro B cells (Ray et al., 1996).

4.3.1.2 Metabolic control of early B cell development in the bone marrow

Early B cell development is a dynamic process, that is accompanied by changes of intrinsic factors, from proliferative to quiescent states and vice versa, and extrinsic factors, such as changing levels of nutrients, chemo- & cytokines, and O_2 tensions in the environment. Consequently, the metabolism of developing B cells needs to adapt to these changes and support the requirements at different stages, such as rapid biomass accumulation preceding proliferation. While most of the stage-specific, metabolic properties and requirements remain elusive, there are some interesting reports indicating the existence of metabolic checkpoints during these developmental steps: First, previous work showed that the transition from pro to pre B cells is accompanied by a decline in both glycolysis and OxPhos, with the decline in glycolysis being more pronounced, thus resulting in a higher OCR/ECAR ratio. That indicates that developing B cells from pro to pre B cells downregulate their metabolic activity which is accompanied by a shift towards more oxidative metabolism (Stein et al., 2017). The decrease in glycolysis during B cell development could be explained, at least partially, by the function of the TF HIF1α, that becomes stabilized under hypoxic conditions and induces glycolysis by activating gene expression of glucose transporters and enzymes of the glycolytic pathway (Kierans and Taylor, 2021). Interestingly, it has been shown that HIF1α activity is high in human and murine bone marrow pro and pre B cells and decreases at the immature B cell stage. Importantly, this stage specific downregulation of HIF1α activity is required for normal B cell development as genetic prevention of this downregulation resulted in developmental arrest of immature B cells and consequently reduced peripheral B cell numbers (Burrows et al., 2020). A further study that highlights the importance of metabolic regulation, specifically mTOR complex 1 (mTORC1) regulation, during these early B cell transitions revealed that mice with a mb1Cre-mediated, B cell-specific deletion of Raptor, an essential subunit of the mTORC1, exhibited a developmental block at the early pre B cell stage with a complete lack of immature and mature peripheral B cells. These Raptor-deficient pre B cells showed reduced proliferative capacity and survival, and reduced OxPhos and glycolytic metabolic capacity (Iwata et al., 2016). These findings show that mTORC1 activity in pro and pre B cells is essential for further differentiation. But not only mTORC1 activity is important, also its precise regulation. This was shown in Folliculin interacting protein 1 (Fnip1) -/- mice that exhibit a developmental block at the large pre B cell stage. Although the cellular and molecular functions of Fnip1 are unknown, it has been shown to interact with all three subunits of AMPK (α, β, γ), a kinase that becomes activated by changes in AMP/ATP and ADP/ATP ratios and inhibits

mTORC1 activity. Experiments using an AMPK activator revealed that the phosphorylation of S6 was not inhibited, while AMPK is equally phosphorylated in the absence of Fnip1. These results suggest that Fnip1 is not required for activation of AMPK, but for AMPK-mediated inhibition of mTOR (Park et al., 2012). Apparently, the absence of Fnip1 in developing B cells leads to parallel increases in catabolic metabolism and mTOR-mediated anabolism, two energy regulating processes that normally are regulated antagonistically. This underlines that mTORC1 activity alone is not sufficient and its proper regulation at certain stages is required for normal B cell development.

Furthermore, external factors, such as chemokines and cytokines in the bone marrow environment, affect the metabolism of developing B cells: For instance, signaling via CXCR4/CXCL12 in hematopoietic stem cells counteracts metabolic exhaustion and the deletion of CXCR4 results in increased transcription of OxPhos genes (Zhang et al., 2016). Furthermore, binding of IL-7 to the IL-7R in pro B cells activates mTORC1 that supports cell proliferation and metabolism in a myc-dependent manner but is dispensable for survival or Rag1/2 expression (Zeng et al., 2018). Taken together, external stimuli, such as chemo- and cytokines, nutrients, and O_2 tension that regulate cellular metabolism, but also the internal capacity to integrate these signals, play a crucial role in driving early B cell development.

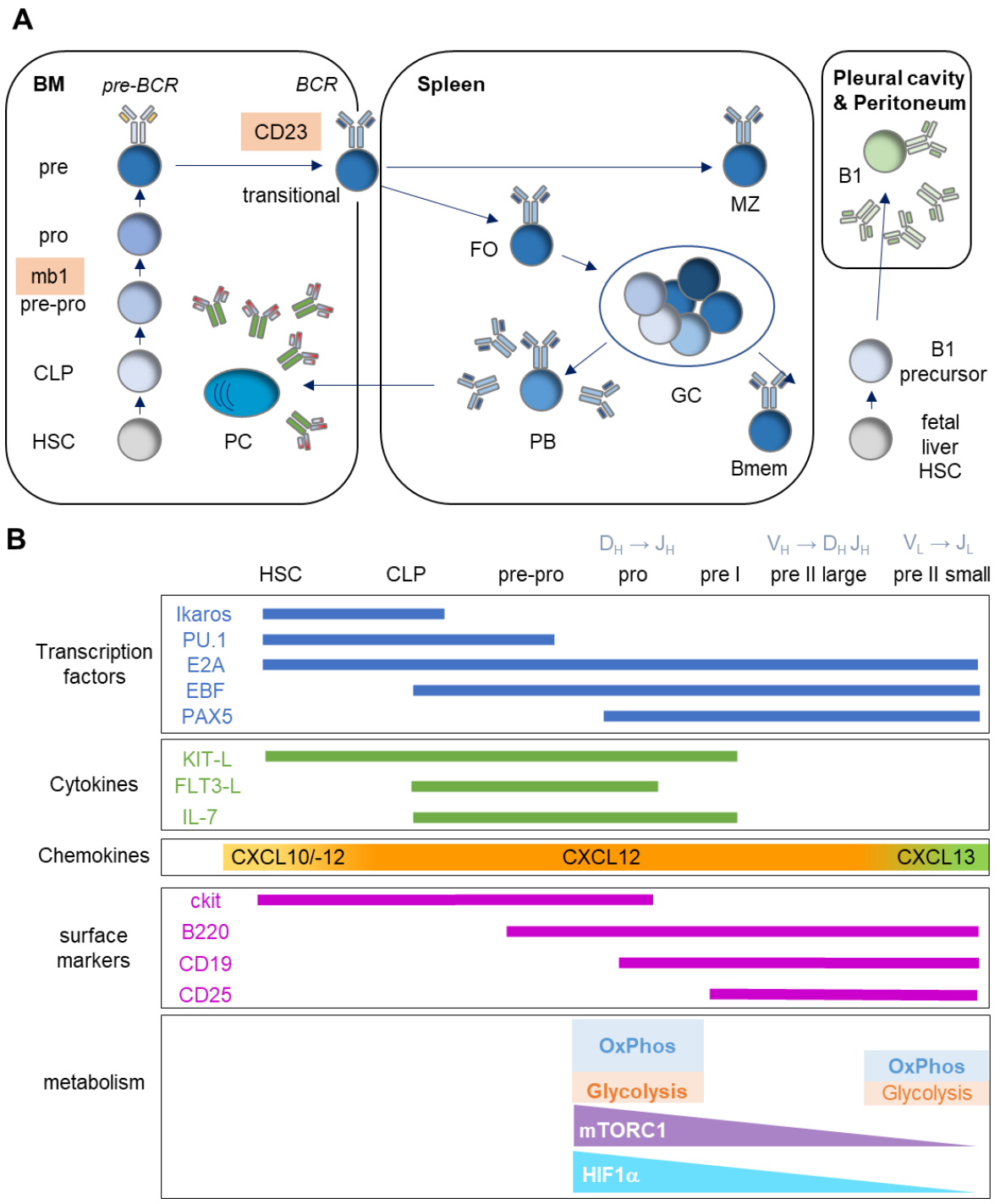

Figure 7 | Murine B cell development, maturation and differentiation in bone marrow and spleen.
A) B cells differentiate from hematopoetic stem cells (HSC) in the bone marrow (BM). After successful µHC arrangement and expression of the pre- B cell receptor (pre-BCR), the B cells leave the bone marrow as immature, transitional B cells. After migration into the spleen, they further differentiate to either follicular B cells (FO) or marginal zone B cells (MZ). After T-dependent activation of FO B cells, they migrate into B cell follicles and induce the formation of germinal centers (GC), where they undergo somatic hypermutation and class switch recombination. After heavy selection, memory B cells (Bmem) and plasma blasts (PB) are generated. The latter further differentiate into long-lived antibody-secreting plasma cells (PCs) that either reside in the spleen or migrate into the bone marrow survival niche. Orange boxes indicate the B cell stages where the respective Cre activity occurs: mb1Cre is active before the pre-BCR checkpoint in pre-pro B cells and CD23Cre is active after the pre-BCR checkpoint but before the GC checkpoint in transitional B cells. **B)** Stage specific activity of certain transcription factors, cytokines, chemokines, surface markers, and metabolic features during early B cell development in the bone marrow. (Urbanczyk et al., 2018)

4.3.1.3 B cell maturation in the spleen

Immature B cells migrate from the bone marrow via the blood into the spleen for further maturation and are termed transitional B cells. Loder et al. first proposed two separate subsets of transitional B cells: T1 B cells that are $IgM^{high}IgD^{-}CD21^{-}CD23^{-}$ and T2 cells that are $IgM^{high}IgD^{+}CD21^{+}CD23^{+}$ (Loder et al., 1999). Newly formed B cells that leave the bone marrow and are still unable to recirculate are T1 B cells. These cells mature to T2 B cells with the expression of surface IgD and CD23. If self-reactive transitional B cells are repeatedly stimulated by self-antigen in the periphery they undergo anergy and are termed T3 B cells (Allman et al., 2001; Hoffman et al., 2016; Pillai, 2009). After positive and negative selection during these stages, these B cells develop into either mature, naïve follicular B cells (FO) or marginal zone B cells (MZ), that express $IgD^{hi}IgM^{+}CD21^{+}CD23^{+}$ and $IgD^{low}IgM^{+}CD21^{+}CD23^{-}$, respectively (Chung et al., 2003; Pillai, 2009).

The two subsets of FO and MZ B cells together make up the B2 B cell compartment, which together with B1 B cells represent the three principal classes of B lymphocytes in the spleen (Hoffman et al., 2016). In contrast to B2 cells, a self-renewing pool of B1 B cells develop from B1 progenitors in the fetal liver with little input from the bone marrow in adulthood. These three subsets can be distinguished by their localization, function, and expression patterns: The follicular B cell compartment contains the majority of mature B cells, which are recirculating cells that mainly home to B cell follicles in secondary lymphoid organs. These follicles are adjacent to T cell zones, which therefore make FO B cells particularly well suited to participate in T cell-dependent (TD) immune responses. MZ B cells on the other hand are sessile and located in the outer white pulp of the spleen between the marginal sinus and the red pulp, which therefore enables them to respond to blood borne pathogens. B1 cells predominantly reside in pleural and peritoneal cavities where they respond to invading pathogens. (Hoek et al., 2010; Pillai, 2009).

The final maturation of transitional B cells into either FO or MZ is reportedly determined by the BCR signaling strength and by activity of the transmembrane receptor Notch2 (Fig 8). While weak BCR signaling induces the development of MZ B cells, relative strong BCR signaling favours the development of FO B cells (Pillai, 2009). MZ B cells express polyreactive BCRs, but also complement receptors CD21 and CD35 (Hoffman et al., 2016). The transmembrane receptor Notch2 belongs to the Notch family genes that play a key role during lymphocyte differentiation. The binding of Notch2 to its ligand delta-like 1 (Dll1) that is expressed on stromal cells or antigen presenting cells results in cleavage of the receptors transmembrane unit and subsequently the release of Notch intracellular fragment (NIC) (Iwahashi et al., 2012). Together with other factors, NIC regulates the expression of Notch2 target genes (Saito et al.,

2003). One reported target gene that was found to be important in Notch2 mediated MZ development is Fos (Iwahashi et al., 2012). Although the majority of target genes remain elusive, it is clear that Notch2 signaling is essential for the generation of MZ, since Notch2 deletion resulted virtually in the absence of MZ B cells, while other B cell populations were normal (Saito et al., 2003). A highly important factor during these transitional stages of B cell maturation, specifically the T1 to T2 transition, is the B cell activation factor from the TNF family (BAFF), which is a trimeric member of the tumour necrosis factor family and is highly abundant in lymphoid follicles. BAFF binding to the BAFF receptor (BAFFR) on newly generated T2 B cells and mature FO B cells induces essential survival signals. Furthermore, beyond its role in B cell survival, BAFF is required for MZ B cell development (Batten et al., 2000). The importance of BAFF signaling in B cells is highlighted in BAFF-deficient mice that exhibit B cell death and immunodeficiency and in mice that have excessive BAFF signaling where it induces lupus-like autoimmunity (Mackay et al., 1999; Schiemann et al., 2001). Interestingly, Patke et al. could show that BAFF activates Akt in a PI3K-dependent manner, thereby promoting metabolic fitness. Additionally, BAFF induces phosphorylation, and consequently inactivation of GSK-3, and phosphorylation with subsequent degradation of Foxo1, with both processes known to play a key role in the regulation of genes required for survival, cell cycle progression, and metabolism (Patke et al., 2006). Taken together, these finding indicate that metabolic capacity of a maturing B cell, availability of nutrients and other external factors in the environment are tightly connected to B cell differentiation processes and interdependent. This notion is supported by findings of Caro-Maldonado et al. that show that anergic B cells are metabolically suppressed: chronic exposure of immature or transitional B cells with self-antigen was genetically induced using anti-hen egg lysozyme transgenic mice and the metabolic capacity of B cells was analysed after anti-IgM stimulation using the Agilent seahorse analyzer. Whereas control B cells increased basal as well as maximal OCR and ECAR upon activation, indicative of OxPhos and glycolysis, respectively, anergic B cells maintained a metabolic phenotype comparable to unstimulated B cells. Conversely, B cells chronically exposed to high BAFF levels exhibited elevated respiratory capacity after LPS-mediated activation. The metabolism of resting B cells was comparable, with the exception that chronically BAFF-exposed B cells had a higher respiratory capacity. B cell activation increased both OCR and ECAR in chronically BAFF exposed and control B cells, and their maximal respiration was comparable, while the basal oxygen consumption of chronically BAFF exposed B cells was significantly higher compared to control B cells. Also, both basal and maximal glycolytic rates were increased in activated B cells after chronic BAFF exposure (Caro-Maldonado et al., 2014). These data show that BAFF regulates the metabolism, which ultimately impacts B cell survival, differentiation, function and activity.

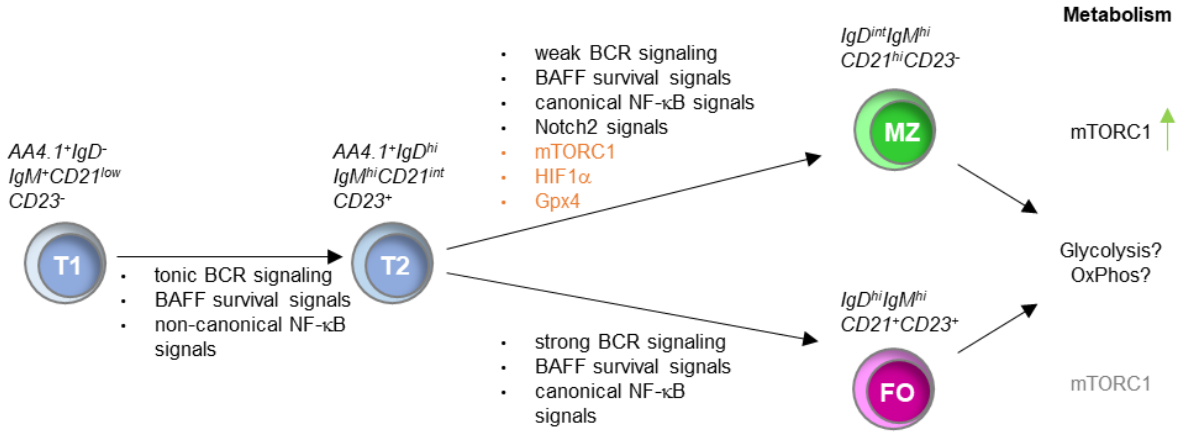

Figure 8 | Murine B cell maturation in the spleen
Newly generated B cells, termed T1 B cells, have yet to acquire the ability to recirculate and are found in the bone marrow and spleen. They mature into T2 B cells that can further mature into either follicular B cells (FO) or marginal zone B cells (MZ). Important known factors during these fate decisions are BCR signaling strength and Notch2 signaling. Metabolic factors (orange) that are especially important for MZ development are mTORC1, HIF1α and Gpx4. Surface markers are indicated in cursive. Adapted and modified from (Pillai, 2009). Further additions and interpretations are based on results from (Muri et al., 2019; Sintes et al., 2017; Zhou et al., 2020).

4.3.2 B cell activation and plasma cell differentiation

4.3.2.1 B cell activation

The mode of B cell activation depends on the B cell subtype, its localization, and also on the nature of the invading pathogen. Generally, B cell activation can be divided into T cell-dependent (TD) and T cell-independent (TI) activation. While FO B cells are mainly activated in a TD manner within GCs that develop in B cell follicles of secondary lymphoid organs upon antigen challenge, MZ and B1 B cells are mainly activated in a TI manner and thereby produce a crucial first antibody response against invading pathogens (Gatto and Brink, 2010; Martin et al., 2001). After antigen activation of MZ B cells and B1 B cells that do not necessarily require BCR-mediated signaling, but rather *toll*-like receptor signaling, these cells differentiate rapidly into plasmablasts that secrete mainly IgM. Although MZ and B1 B cells share these similarities, they differ in their development, topography, phenotype and function (Martin et al., 2001). This combination of TD and TI B cell activation allows rapid IgM production (1-3 days) that bridges the temporal gap until high-affine, GC-derived IgG antibodies are produced (~7 days) (Hoffman et al., 2016). The TD activation of FO B cells, mainly by proteinogenic stimuli, is much more complex and strictly regulated: Resting FO B cells are retained in primary lymphoid follicles in lymph nodes in a CXCR5/CXCL13-dependend manner. After antigen recognition, B cells migrate to the T-B border by expressing CCR7 in search of T cell help. Here, the activated B cells can differentiate into extrafollicular PBs or Bmems independent of GCs for rapid protection via the production of antigen-specific antibodies. Alternatively, B cells remain in the

B cell follicles for the formation of GCs, which requires these aforementioned interactions at the T-B border that induce initial B cell proliferation (Gatto and Brink, 2010).

For engagement in the GC formation, B cells require expression of the proteins Bcl6 and S1PR2. The GC reaction includes B cell-T follicular helper (T_{FH}) cell interactions via MHC2-TCR, B7-CD28, CD40-CD40L, ICOSL-ICOS, PDL1-PD1, and IL21R-IL21 that induce the processes of somatic hypermutation (SHM) and class switch recombination (CSR). The GC can be divided into two functionally distinct zones, termed dark zone and light zone. GC B cells proliferate within the dark zone, while selection for BCR affinity is mediated by follicular dendritic cells (FDCs) that have bound antigen and are located within the light zone (Meyer-Hermann et al., 2012).

After selection and circulation through the light and dark zone, activated B cells differentiate into either Bmems or PCs. Bmems recirculate and are able to rapidly differentiate into PBs or to re-enter the GC reaction after repeated antigen encounter. PCs, on the other hand, home to the BM where they reside as long-lived PCs in survival niches and continuously produce high amounts of high-affine, class-switched antibodies, thereby maintaining a serologic memory independent of repeated antigen exposure (Hoffman et al., 2016).

4.3.2.2 Plasma cell differentiation

The compartment of antibody secreting cells (ASCs) can be divided into PBs and PCs. The former are short-lived, cycling, and found in extrafollicular foci in peripheral lymphoid organs, while the latter are long-lived, non-dividing, found predominantly in the bone marrow and are mostly GC derived (Kallies et al., 2007). These PB/PC subsets can be distinguished by flow cytometry using the surface markers CD19, B220, TACI, and CD138: Proliferating PBs, termed P1, are $CD138^{hi}TACI^{hi}B220^{int}CD19^{int}$, while non-proliferating early P2 PCs are $CD138^{hi}TACI^{hi}B220^{low}CD19^{int}$ and non-proliferating mature P3 PCs are $CD138^{hi}TACI^{hi}B220^{low}CD19^{low}$ (Pracht et al., 2017). Long-lived mature PCs (LLPCs) in the bone marrow are part of the P3 compartment. The transition of a resting B cell into an ASC occurs after B cell activation and represents a lineage switch that requires the coordinated regulation of several hundred gene changes along with major chromatin remodelling (Fig 9A). Whereas key TFs for B cell identity become repressed, ASC-specific TFs become expressed. A long-term stability of these two states, the B cell identity and ASC identity, is mediated by mutually antagonistic regulation amongst the respective TFs. One important TF responsible for B cell lineage commitment of lymphoid progenitors is Pax5 that is expressed throughout B cell development. The role of Pax5 for the conservation of B cell identity becomes highlighted in mature B cells with a conditional deletion of Pax5 that lose their B cell identity and reverse into a progenitor stage (Cobaleda et al., 2007). Another important transcriptional repressor that is expressed throughout B cell differentiation but absent in ASCs is BACH2 with BLIMP1 being

one of its major targets. A further transcriptional repressor of BLIMP1 is BCL6 that is highly expressed and essential in GC B cells by enabling rapid proliferation and tolerance of SHM. The expression of BCL6 is sustained by IL-21 and IRF8, whereas IRF4 and BLIMP1 lead to its repression. Further TFs expressed in B cells are PU.1, IRF8, and SPIB that are downregulated in ASCs in a BLIMP1-dependent manner. The PU.1-IRF8 complexes maintain expression of Pax5, BCL6, and Mef2c and repress BLIMP1 expression. The induction of the ASC transcriptome is initiated by the key TFs IRF4, BLIMP1, and Xbp1 with the former playing already an important role within the GC. Here, IRF4 functions in a dose-dependent manner with low levels promoting CSR by activating Aicda, Pou2af1, and BCL6, whereas high amounts repress BCL6 and induce BLIMP1 expression, thereby inducing the ASC fate. One of the most prominent TFs for the terminal differentiation of B cells is BLIMP1 that is a transcriptional repressor for key regulators of the B cell program such as SPIB, BCL6, MYC, AID, Stat6 and PAX5 (Nutt et al., 2015; Shaffer et al., 2002). BLIMP1 is not detectable in Bmems, but present in PCs generated in primary and secondary responses to TD and TI antigens, but also in a subset of GCBCs that exhibit a partial PC phenotype (Shaffer et al., 2002). BLIMP1 and BCL6 are regulated in GCBCs and ASCs in a developmental feedback loop that functions by the expression of BCL6 in GCBCs which represses BLIMP1, and BLIMP1 expression in ASCs that in turn represses expression of BCL6 (Shaffer et al., 2002). Although BLIMP1 is not required for the initiation of the PC program, it is indispensable for subsequent high Ab production which is in accordance with its higher expression in LLPCs compared to cycling PBs (Kallies et al., 2007; Nutt et al., 2015). Furthermore, ectopic expression of BLIMP1 is sufficient to induce PC differentiation, whereas its deletion results in impaired formation of the ASC compartment highlighting its role in this particular subset (Savitsky and Calame, 2006; Shapiro-Shelef et al., 2003; Turner et al., 1994). BLIMP1 is developmentally upstream of Xbp1 and induces ASC differentiation partially by repressing Pax5 and potentially also BCL6 (Lin et al., 2002; Shaffer et al., 2002). The third key TF for ASC differentiation is XBP1 that is induced by ER stress in several cell types and functions as a mediator of the unfolded protein response (UPR) and is therefore especially important in ASCs, since they have a high rate of Ab synthesis and associated ER stress. Xbp1 is proposed to be repressed in B cells by Pax5 and it promotes immunoglobulin heavy chain (Igh) mRNA processing, Ig secretion and ER remodelling (Nutt et al., 2015).

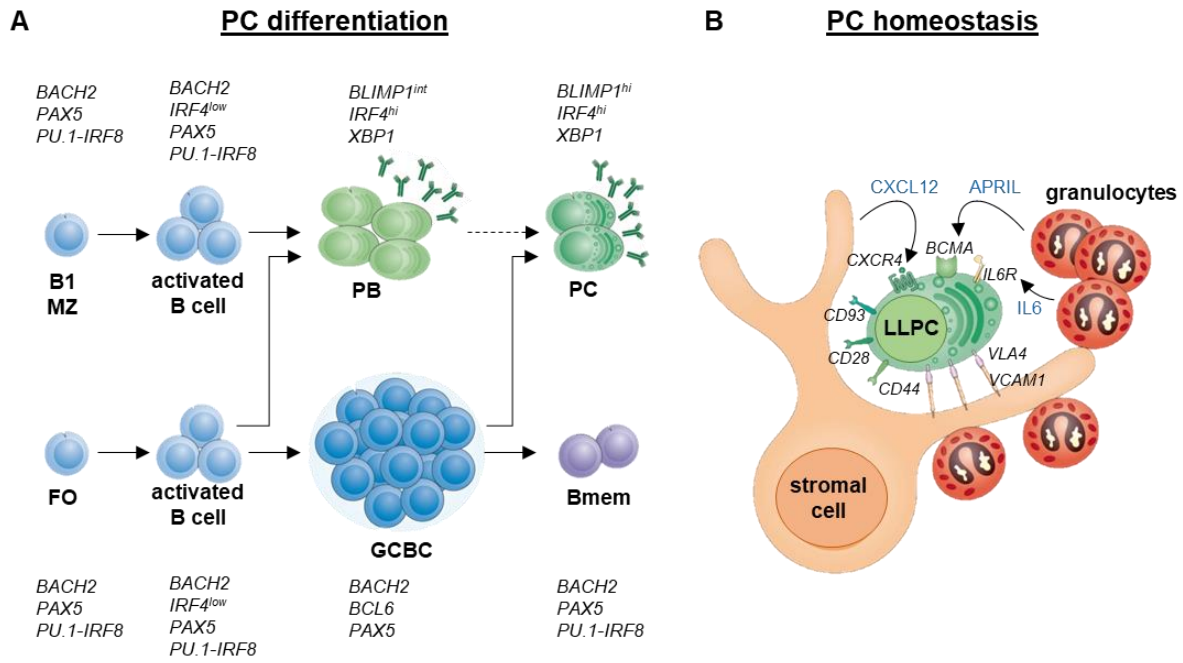

Figure 9 | Model of terminal plasma cell differentiation and long-term survival in the bone marrow niche. **A) Cellular stages of terminal B cell differentiation**. Important transcription factors are indicated in cursive. MZ, marginal zone B cell; FO, follicular B cell; PB, plasma blast; PC plasma cell; Bmem, memory B cell; GCBC, germinal center B cell. **B) Schematic depiction** of a long-lived plasma cell (LLPC) in the bone marrow niche. Surface receptors are indicated in cursive and crucial survival factors that are secreted by cells from the environment, such as stromal cells or granulocytes, are highlighted in blue.

4.3.2.3 Plasma cell homing and survival

Following the generation of PCs, the majority of these cells home into their long-term survival niches located within the bone marrow or the gut. This homing process requires the activation of the protein Sphingosine-1-phosphate receptor 1 (S1PR1) that is needed for efficient egress from secondary lymphoid organs into the blood (Nutt et al., 2015). The recruitment of PCs to sites of inflammation is mediated by the chemokines CXCL9, CXCL10, and CXCL11 that signal via CXCR3, whereas the recruitment and retention in the bone marrow in turn requires signaling via CXCL12/CXCR4. The retention and final maturation of PCs in the bone marrow furthermore require VLA4, CD44, CD28, CD93 and the TFs KLF2, ZBTB20, and Aiolos (Fig 9B). The subsequent survival of PCs requires signaling via the APRIL/BCMA axis that induces expression of the anti-apoptotic protein MCL1, which is essential for the survival of ASCs. These survival factors and cytokines are produced and secreted by CXCL12+VCAM1+ stromal cells and hematopoietic stem cells. The survival of PCs in the bone marrow seems furthermore to be influenced by serum antibodies, as these cells express the inhibitory Fc receptor FcγIIB which, after cross-linking, induces apoptosis as a negative regulatory loop (Nutt et al., 2015; Schuh et al., 2020).

4.3.2.4 Metabolic control of B cell activation and plasma cells

Over the past years it became evident that the activation of B cells is accompanied by metabolic changes that are required to support processes such as proliferation and subsequent survival or antibody secretion of plasma cells. The first important study by Caro-Maldonado et al. showed that LPS or BCR activated B cells increase both glycolysis and OxPhos to the same extent. This is in contrast to activated T cells that disproportionally increase glycolysis, indicating distinct metabolic requirements for different immune cell subsets after activation (Caro-Maldonado et al., 2014). Furthermore, they concluded that efficient mitochondrial electron transport is not essential for Ab production, since the amount of secreted IgM of *in vitro* stimulated B cells that have been treated with Rotenone, an inhibitor of complex I, was comparable to control cells. Interestingly, this was also observed by Price et al., who analysed the effect of further inhibitors of the mtRC on B cells and described that only Rotenone alone did not affect Ab secretion: Treatment with oligomycin, an inhibitor of complex V, or FCCP which is a ionophore functioning as an uncoupling agent, or antimycin A which is an inhibitor of complex III of the mtRC, as well as the combined treatment with antimycin A and rotenone all resulted in decreased Ab production without affecting the viability of the cells (Price et al., 2018). Furthermore, this study showed that *in vitro* LPS activated B cells progressively increased expression of nucleus-encoded OxPhos genes in a BLIMP1-dependent manner. These data show that increased OxPhos is required during B cell activation and PC differentiation with subsequent Ab secretion, although the specific requirements at different stages and mechanisms require further investigation. The requirement of OxPhos in activated B cells caused Waters et al. to analyse mitochondrial remodelling in these cells: First, by activating B cells *in vitro* for 24h with CD40L and IL-4 they showed that these cells mainly import glucose for the synthesis of nucleotides, lipids, and fatty acids. Under these conditions, they concluded that glucose was dispensable for PB differentiation as glucose restriction only impaired the CSR to IgG1 (Waters et al., 2018). Importantly, Waters et al. also analysed mitochondrial remodelling in these cells by live-cell super-resolution imaging and quantitative PCR. They concluded that few, elongated mitochondria remodel to many punctuate mitochondria within the first 24h after CD40L/IL-4 activation of B cells, whereas mtDNA copy numbers and nucleoid numbers remain similar (Waters et al., 2018). GC B cells represent a special subset of activated B cells with distinct transcriptional and metabolic properties. A study by Weisel et al. showed that *ex vivo* GCBCs and *in vitro*-generated GCBCs had minimal glycolytic activity but required the oxidation of fatty acids (FA) (Weisel et al., 2020). These data are in contrast to reports by Jellusova et al. who showed that induction of a HIF1α-mediated glycolytic program in GCBCs is required in these cells (Jellusova et al., 2017). Interpreting these studies with partially contradicting results shows that the metabolic changes and requirements during B cell activation need further

investigation, although the discrepancies can be partially explained by different methods and approaches being used (Boothby et al., 2021).

The metabolic properties of PCs were analysed by Lam et al. and showed differences in the metabolism of short-lived (SLPC) versus long-lived PCs (LLPC): While LLPCs import more glucose compared to SLPCs, they mainly use it for the glycosylation of Abs. However, under metabolic stress LLPCs, in contrast to SLPCs, are able to divert glucose into pyruvate, thereby preventing metabolic exhaustion (Lam et al., 2016). Interestingly, this flexibility in metabolism is a crucial requirement for the longevity of LLPCs, highlighting the importance of regulated metabolism not only in the generation of PCs but also in the survival and longevity.

5. Objective of this work

Understanding molecular mechanisms of immunological processes is a prerequisite for the prevention and treatment of diseases and for the development and improvement of vaccines. B lymphocytes, which represent a major part of the adaptive immune system, have a colourful, semi-nomadic life throughout their development, maturation, activation, and effector function in respect to extrinsic and intrinsic factors: changing environments with various abundance of nutrients, growth factors and cytokines that is accompanied by transient switching between quiescent and proliferative stages or stages of increased Ig secretion. This implies a requirement for rapid metabolic adaptations that support and regulate these processes. Although there have been some interesting findings in the context of B cell metabolism over the past few years, the specific processes at certain B cell stages have not yet been fully elucidated:

It is known that the differentiation of pro B cells to pre B cells in the bone marrow is accompanied by a downregulation of OxPhos and to a greater extent also glycolysis, resulting in a switch towards more oxidative metabolism. Later, the activation of mature B cells is accompanied by a BLIMP1 induced progressive upregulation of OxPhos genes, again indicating the importance of oxidative metabolism. Based on these findings, I hypothesise that mitochondrial function is essential during B cell development, activation, and effector function and that consequently the selection for functional mitochondria must be ensured at certain checkpoints.

How mitochondrial respiration affects early B cell development in the bone marrow and the adaptive immune response *in vivo* has not yet been analysed in detail due to the lack of suitable mouse models. To overcome this limitation and to analyse the function of mitochondrial respiration in B cells, the first aim of this thesis was to establish a mouse model that reduces mitochondrial respiration and OxPhos specifically in B cells.

To address the second aim, I analysed the effects of reduced OxPhos and mitochondrial metabolism during early B cell development in the bone marrow.

Thirdly, I aimed to elucidate the effects of reduced OxPhos and mitochondrial metabolism in B cells on the humoral immune response upon T-dependent and T-independent vaccination.

6. Results

6.1. Analysis of relative mtDNA abundance in murine B cell subsets

Mitochondria carry their own genome coding for 13 mRNAs and the genes for 22 tRNAs and 2 rRNAs necessary for their synthesis in the mitochondrial matrix. All proteins encoded are essential subunits of the mtRC complexes I, III, IV and V, thereby making mtDNA indispensable for function of the respiratory chain and OxPhos. There are no reports regarding the abundance or importance of mtDNA in B cells, a cell type which is known to be dependent on OxPhos, at certain developmental stages for instance after activation (Price et al., 2018). To address this question, mice were immunized with sheep red blood cells (SRBCs), which reliably induces the formation of GCs, and B cell subsets from spleen and bone marrow were sorted by flow cytometry after 10 days (Fig 10A). The relative abundance of mtDNA was analysed using qPCR, quantifying the expression of the mtDNA encoded genes *16s rRNA* and *ND1* normalized to nuclear encoded *hk2* (Fig 10B) (Quiros et al., 2017). Indeed, there were alterations of mtDNA abundance between different B cell subsets detected, indicating differing requirements for OxPhos: While pro and pre B cells have decreased mtDNA levels compared to follicular B cells (FO), marginal zone B cells (MZ) and plasma cells (PC), showed higher levels (Fig 10B). The relative abundance of mtDNA in GCBCs were only slightly increased compared to FO B cells. Interestingly, mtDNA abundance does not correlate with mitochondrial mass or membrane potential, at least within the B cell lineage (Fig 10D, E). Both, mitochondrial mass and membrane potential, were reduced in MZ and the PB/PC compartments compared to FO B cells. Furthermore, while mass and membrane potential were comparable in GCBC, mass was increased, whereas the membrane potential was slightly decreased in pro and pre B cells compared to FO.

To analyse mtDNA abundance during B cell activation, splenic B cells from WT mice were isolated, activated with LPS to induce PB differentiation and analysed as described above. There was a successive and significant increase of the relative mtDNA abundance from resting B cells to d3 activated B cells (Fig 10C), indicating that B cell activation is accompanied by replication of mtDNA.

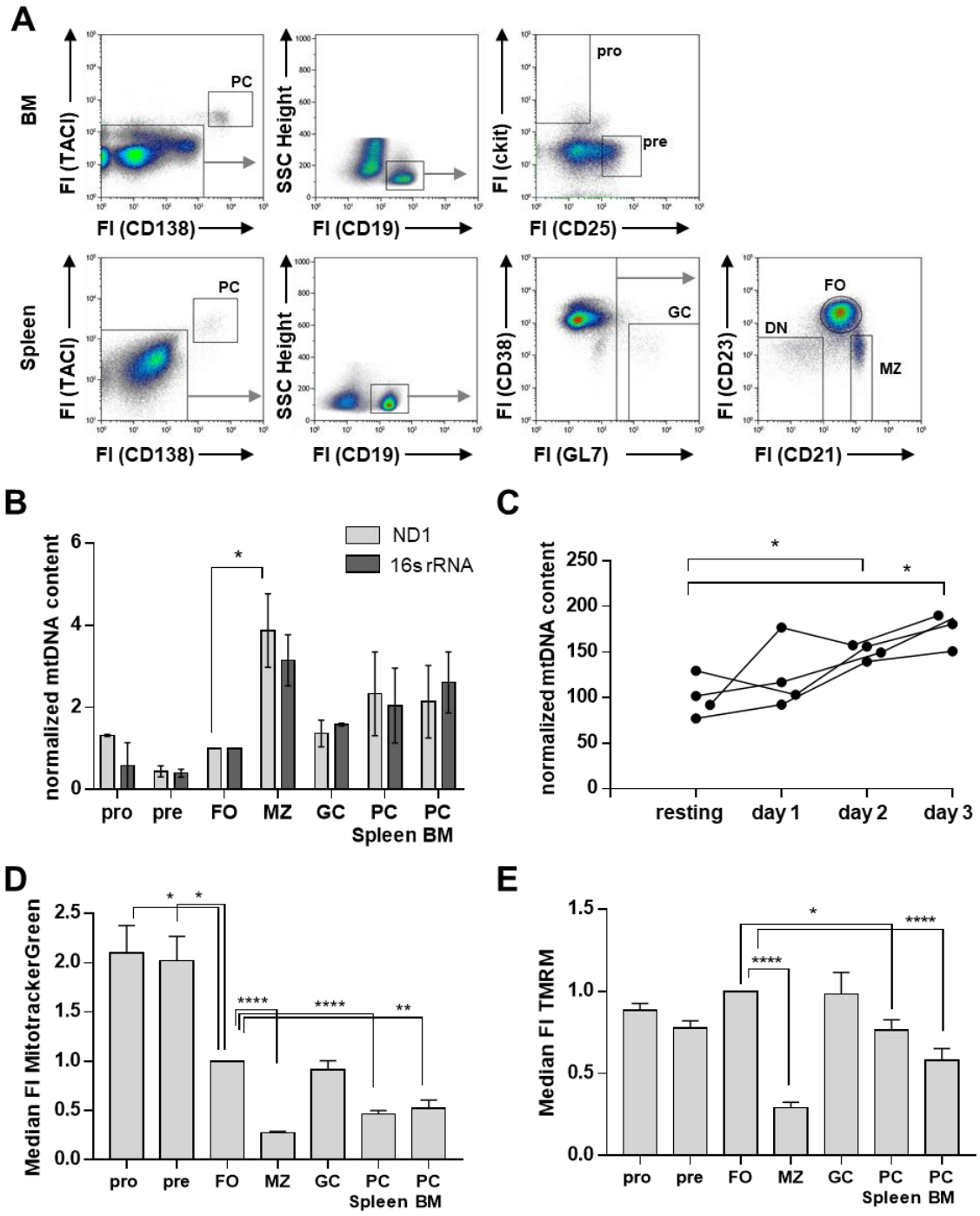

Figure 10 | Analysis of mtDNA, mass and membrane potential in selected murine B cell subsets

Murine B cell subsets were isolated by FACS and relative mtDNA content was determined by abundance of the mitochondrial encoded genes (*16s rRNA, ND1*) normalized to nuclear DNA (*hk2*). **A) Flow cytometric cell sort** of murine B cell subsets from bone marrow (top) and spleen (bottom). **B) Relative mtDNA content** in sorted B cell subsets of SRBC immunized mice. n=4, mean -/+SEM. **C) Naïve splenic B cells were stimulated with LPS** and mtDNA was determined at indicated time points as described in B). n=4 mean -/+ SEM; significance calculated using 2-way ANOVA. **D) Mitochondrial mass** from unimmunized, WT murine B cell subsets was determined by flow cytometry using MitotrackerGreen. Values normalized to FO. N=2, n=4; Bars at mean -/+SEM. Significance was calculated using 2-way ANOVA. **E) Mitochondrial membrane potential** from unimmunized, WT murine B cell subsets was determined by flow cytometry using TMRM. Values normalized to FO. N=2, n=4; Bars at mean -/+SEM. Significance was calculated using 2-way ANOVA.

[Figure partially adapted and modified after (Urbanczyk et al., 2021).]

6.2. Establishing a mouse model with a B cell specific impairment of OxPhos via mtDNA depletion

To determine the importance and downstream effects of the respiratory chain in B cells, mice were generated that carry a dominant negative mutant of the mtDNA helicase Twinkle. The construct (Fig 11A) is located in the ROSA26 locus and contains a CAG promotor (C, cytomegalovirus, A, chicken beta actin, G, rabbit beta globin), a loxP flanked *neo*|Stop sequence (neoR | WWS), the K320E twinkle mutant ("DNT"), and IRES-GFP, allowing the identification of recombined cells (Baris et al., 2015). The expression of Cre results in excision of the Stop sequence, thereby allowing expression of the mutant. The DNT twinkle mutant binds mtDNA, but does not unwind it, thereby preventing essential replication factors from binding. Expression of DNT in B cells results in decreased mtDNA levels, shown exemplarily for resting and LPS activated B cells from DNT/CD23Cre and CD23Cre mice in Fig 11B, and subsequently impaired OxPhos. To analyse the importance of the mtRC specifically in B cells, I activated DNT expression in early pro B cells by crossing DNT mice with mb1Cre mice (Hobeika et al., 2006). The generated DNT/mb1Cre mice had no apparent defects, however they had noticeably less splenocytes (Fig 11C). To further analyse the importance of the respiratory chain during B cell activation and plasma cell differentiation with normal B cell development, I crossed DNT mice with CD23Cre mice (Kwon et al., 2008), which is active in transitional T2 B cells. Splenocyte numbers of DNT/CD23Cre mice were comparable to the respective controls (Fig 11C).

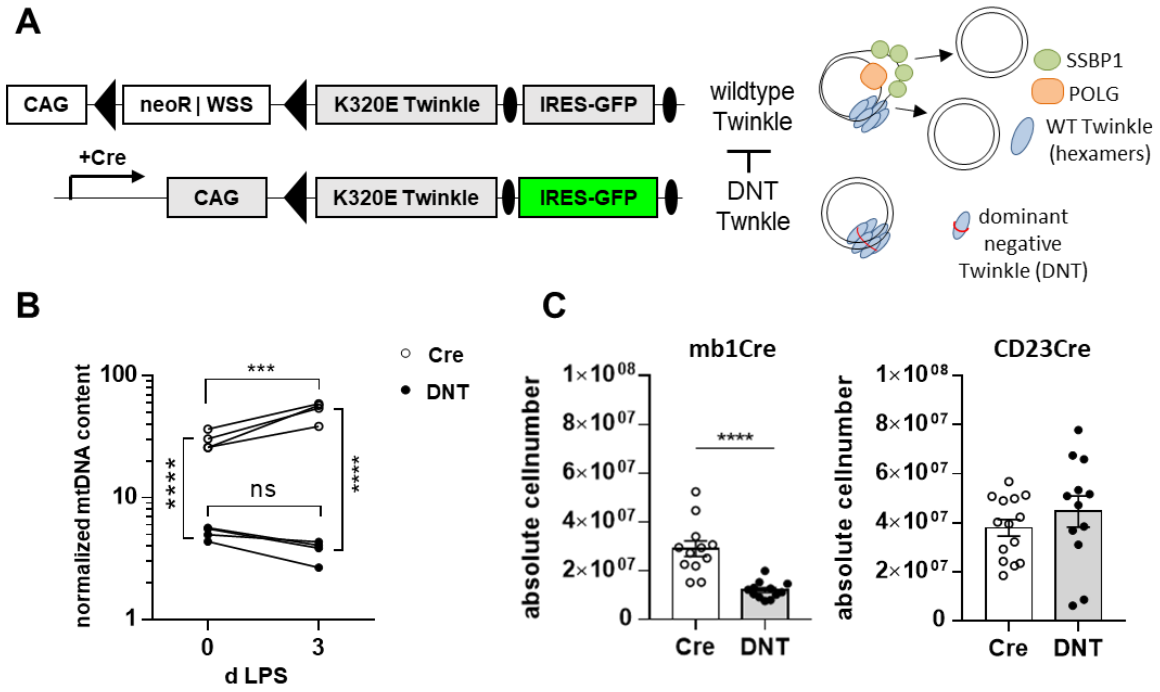

Figure 11 | Mouse model for genetic inhibition of mtDNA replication in B cells
A) Schematic depiction of the construct encoding a dominant negative form of the essential mtDNA helicase TWINKLE (K320E; "DNT" in the following) knocked in into the ROSA26 locus in an inactive conformation (top). After Cre recombination (bottom) a neo|Stop cassette (neoR | WWS) is excised resulting in expression of the dominant-negative twinkle (DNT) mutant and IRES-GFP under a CAG promotor (C, cytomegalovirus, A, chicken beta actin, G, rabbit beta globin). Right: Depicted is the minimal mammalian mtDNA replisome consisting of the polymerase POLγ (POLG), the protein single-stranded DNA binding protein 1 (SSBP1) and the helicase TWINKLE. The DNT mutant is unable to unwind mtDNA and thereby impairing mtDNA replication. **B) Relative expression** of 16s rRNA of naïve and day 3 LPS activated B cells of DNT/CD23Cre and CD23Cre mice. Symbols represent individual mice. N=1; n=4; significance was calculated using 2-way ANOVA. **C) Absolute cell numbers of splenocytes** from DNT/mb1Cre and DNT/CD23Cre mice compared to the respective Cre controls. Bars at mean ± SEM; Symbols represent individual mice. N=2-4; n=4-6; significance was calculated using t-test.
[Figure partially adapted and modified after Urbanczyk et al., 2021.]

6.3. Analysis of B cell development and maturation in unimmunized DNT/mb1Cre mice

To analyse the influence of a dysfunctional respiratory chain in early B cell development, B cell populations from different organs from DNT/mb1Cre and mb1Cre mice as a control were analysed by flow cytometry.

6.3.1. Analysis of early B cell development in the bone marrow

Impairment of mtDNA replication resulted in an accumulation of pro B cells, evident by increased (factor ~1.6) pro B cell numbers and frequencies in DNT/mb1Cre mice compared to mb1Cre mice (Fig 12A, B). In contrast, the numbers and frequencies of pre B cells were drastically reduced in DNT/mb1Cre mice by factor 6.5. While there were about 4% of viable cells, or 1.3 x10^6, pre B cells in the BM of mb1Cre mice, I could detect only 0.6% of viable

cells, or $2x10^5$cells, pre B cells in DNT/mb1Cre animals. The B cell population defined as $ckit^-$ $CD25^-$, which contains immature and mature B cells, was also significantly reduced by factor 3.5, in DNT/mb1Cre mice compared to mb1Cre controls.

Since the successful expression of the µHC is an important checkpoint during B cell development and the observed developmental block occurs at the pre B cell stage in DNT/mb1Cre mice, I analysed intracellular µHC expression by flow cytometry. There were significantly less pro B cells expressing the µHC in DNT/mb1Cre animals (19.8%) compared to mb1Cre controls (34.6%) (Fig 12C, D). The abundance of µHC protein, as indicated by the median of the fluorescent intensity for µHC, was also significantly decreased from ~7 in mb1Cre to ~4 in DNT/mb1Cre mice. Analysing µHC expression in pre B cells showed two distinct populations (Fig 12E, F): IgM^{low} and IgM^{hi} pre B cells. While the medians were comparable within the respective populations, there were significantly less µHC expressing pre B cells in DNT/mb1Cre mice. Especially the frequency of IgM^{hi} cells were reduced in the pre B cell compartment (28% in DNT/mb1Cre compared to 42% in mb1Cre mice). Further analysing the IgM^{low} and IgM^{hi} pre B cells for CD19 and B220 expression showed that IgM^{hi} cells are also $CD19^{hi}$ and $B220^{hi}$ and therefore are probably more mature B cells.

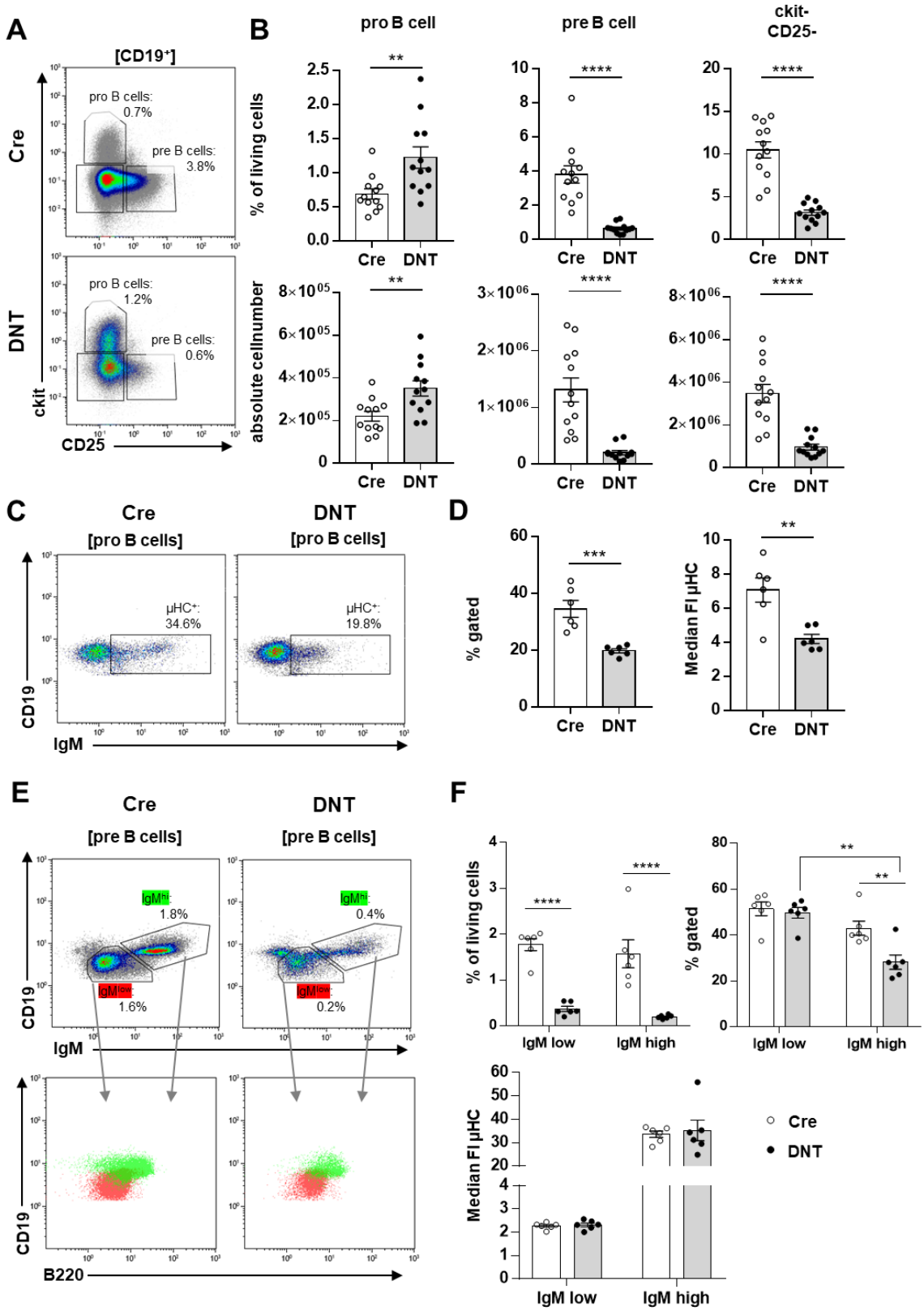

Figure 12 | Analysis of B cell development in the bone marrow of DNT/mb1Cre mice

Bone marrow cells from DNT/mb1Cre and mb1Cre mice were isolated and analysed by flow cytometry. **A) Representative flow cytometric analysis** (merged from 6 mice per genotype) of pro B cells ($CD19^+ckit^+$) and pre B cells ($CD19^+CD25^+$). Numbers indicate the frequency of viable cells **B) Frequencies (top) and absolute cell numbers (bottom)** of pro, pre and $ckit^-CD25^-$ B cells shown in A. Bars at mean ± SEM; Symbols indicate individual mice; N=2, N=6; significance calculated using t-test. **C) Representative flow cytometric analysis** (merged from 6 mice per genotype) of µHC expressing pro B cells. Numbers indicate the frequency of the parent population. **D) Frequency** (left) of μHC^+ pro B cells and median of µHC expression in pro B cells (right). Bars at mean ± SEM; Symbols indicate individual mice; N=1, N=6; significance calculated using t-test**. E) Representative flow cytometric analysis** (merged from 6 mice per genotype) of µHC expressing pre B cells (top) and IgM^{hi} and IgM^{low} pre B cells analysed for CD19 and B220 expression (bottom). Numbers indicate the frequency of viable cells. **F) Frequencies** (top) of μHC^+ pre B cells (frequency of viable cells on the left; frequency of parent population on the right) and median of µHC expression in pre B cells (bottom). Bars at mean ± SEM; Symbols indicate individual mice; N=1, n=6; significance calculated using 2-way ANOVA.

6.3.2. Analysis of early B cell development *in vitro*

To enable thorough analysis of early B cell development with sufficient pro and pre B cell numbers, I used an established protocol for the cultivation of FACS isolated pro B cell *in vitro* using IL-7 supplementation. While high IL-7 concentration (5 ng/ml) induces heavy proliferation of pro B cells, low IL-7 concentration (0.5 ng/ml) induces differentiation, resulting in higher frequencies of pre and immature B cells. Bone marrow cells, pooled of 3 mice per genotype, were used to isolate pro B cells ($CD19^+ckit^+$) by FACS. The analysis was performed on day 7 using flow cytometry. The frequency of viable cells, determined using forward scatter (FS int) and side scatter (SS int), was drastically decreased in pro B cells from DNT/mb1Cre compared to mb1Cre pro B cells (Fig 13A). While mb1Cre cells had a frequency of 82.8% viable cells with low IL-7 and 71.5% with high IL-7, DNT/mb1Cre cells had a viability of only 17.8% with low and 11.6% with high IL-7 (Fig 13B). Differentiation of pro B cells was determined using anti-IgM antibodies, staining intracellular and surface µHC separately (Fig 13C). Under conditions with low IL-7 there were significantly less IgM^+ (both intracellular and surface) cells in DNT/mb1Cre cultures compared to mb1Cre (Fig 13D). Under conditions with high IL-7 the frequency of IgM^+ (intracellular) cells was also decreased in DNT/mb1Cre cultures, whereas the frequency of all IgM^+ cells (intracellular + surface) was comparable, although it should be considered that there are hardly any viable cells detectable in DNT/mb1Cre cultures at all. Since this approach is relatively expensive and time consuming, but DNT/mb1Cre pro B cells hardly survive, with not sufficient cell numbers for further analysis, this strategy was abandoned.

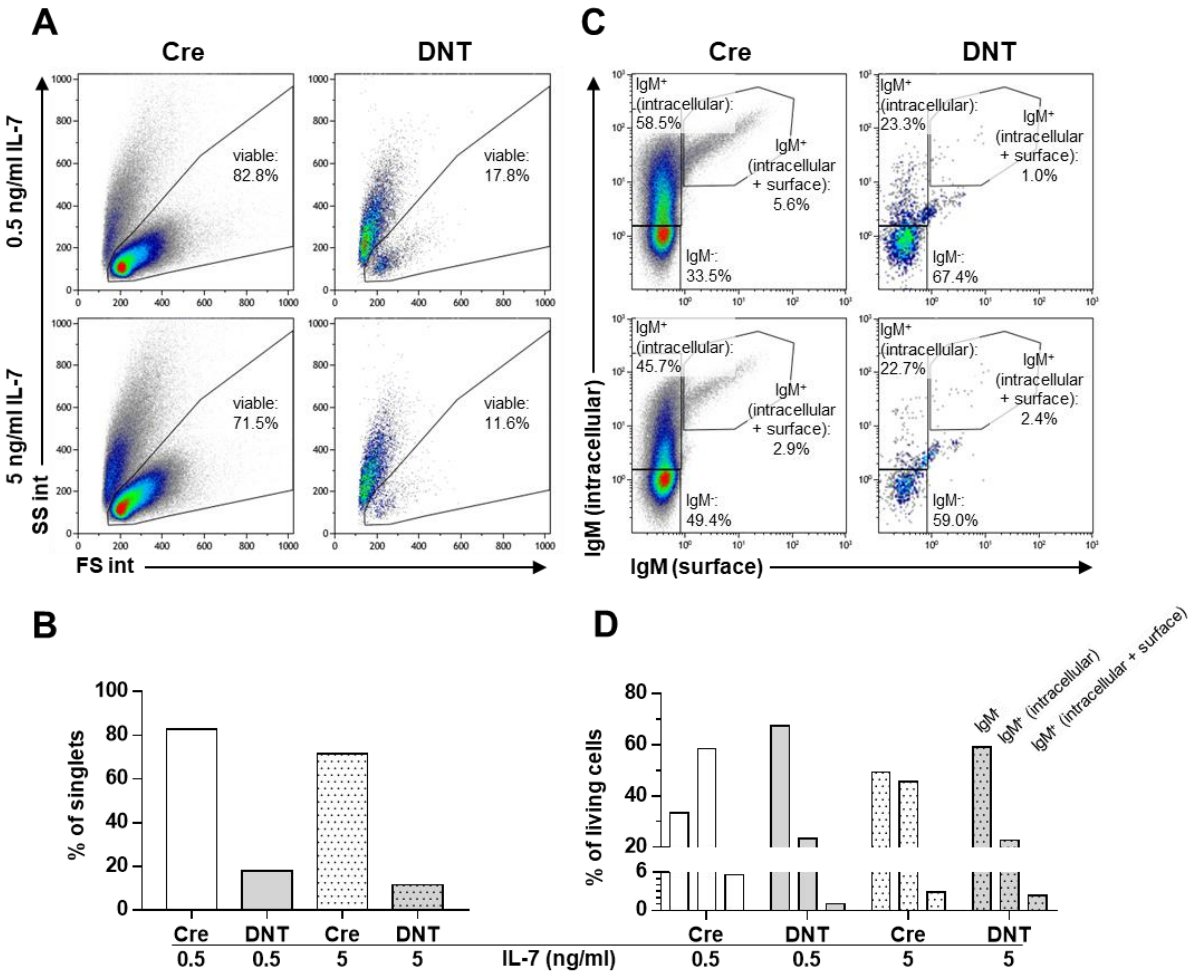

Figure 13 | Analysis of B cell development of DNT/mb1Cre mice *in vitro*
Pro B cells from the BM from DNT/mb1Cre and mb1Cre mice were isolated by FACS and cultivated with IL-7 (low=0.5 ng/ml and high=5ng/ml). Survival and differentiation were determined by flow cytometry at day 7. **A) Flow cytometric analysis** of viable cells using forward scatter (FS int) and side scatter (SS int) for 0.5 ng/ml IL-7 (top) and 5 ng/ml IL-7 (bottom). **B) Quantification of viable cells**; N=1, n=1. **C) Flow cytometric analysis** of intracellular and surface µHC+ B cells using anti-IgM antibodies for 0.5 ng/ml IL-7 (top) and 5 ng/ml IL-7 (bottom). **D) Quantification** of IgM-, gM+ (intracellular) and IgM+ (intracellular + surface) B cells from DNT/mb1Cre and mb1Cre mice; N=1, n=1.

6.3.3. Analysis of mTOR activity in early B cell subsets

The nutrient sensing kinase mTOR is an important mediator of metabolism, gene transcription and anabolic processes, such as cell growth and proliferation. Iwata et al. have shown that mTOR activity is essential during B cell development (Iwata et al., 2016) and that its dysfunction, induced by mb1Cre mediated depletion of it's essential co-factor RAPTOR, also results in a B cell developmental block at the pre B cell stage, similar as observed in mice with mb1Cre induced expression of DNT (Fig 12B). For that reason, I hypothesized that mTOR activity is decreased in DNT/mb1cre mice, as a consequence of impaired OxPhos, resulting in the described developmental block at the pre B cell stage in the BM. To this end I intracellularly analysed phosphorylated RPS6, which is a down-stream target of active mTOR, by flow

cytometry (Fig 14). Interestingly the frequency of pRPS6$^+$ cells was not decreased in pro B cells from DNT/mb1Cre mice (Fig 14A, B). Furthermore, while there was a continuous and significant reduction of pRPS6$^+$ cells in mb1Cre mice during B cell development (45% in pro B cells, 34% in pre B cells and 18% in mature B cells), this mTOR down-regulation was not observed in DNT/mb1Cre mice. On the contrary, the frequency of pRPS6$^+$ cells significantly increased from 43% in pro B cells to 48% in pre B cells, and only then decreased to 28% in mature B cells, which is still significantly more compared to mb1Cre controls. Analysing the median of the fluorescent intensity of pRPS6, which is indicative of the expression intensity, confirmed this observation and showed a similar picture as the described frequencies (Fig 14C). The median for pRPS6 gated on pro B cells was comparable, but the median of pRPS6 gated on pRPS6$^+$ pro B cells was significantly decreased in DNT/mb1Cre mice. The medians of pRPS6 gated on pre and mature B cells was significantly higher in DNT/mb1Cre mice. This data indicates aberrant mTOR activity with impaired down-regulation during B cell development in DNT/mb1Cre mice.

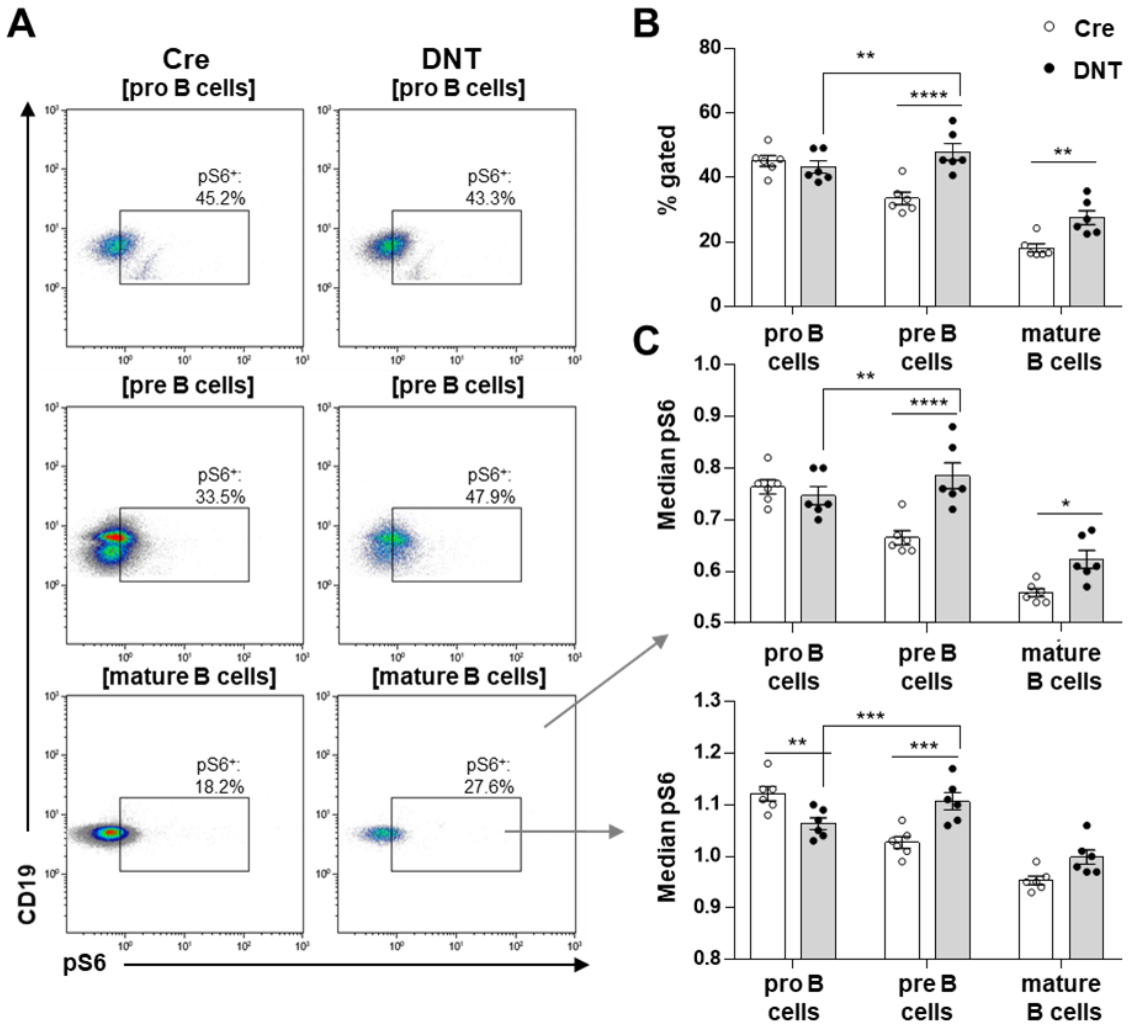

Figure 14 | Analysis of mTOR activity in B cell subsets from the bone marrow of DNT/mb1Cre mice
Bone marrow cells from DNT/mb1Cre and mb1Cre mice were isolated and RPS6 phosphorylation was analysed by flow cytometry. **A) Representative flow cytometric analysis** (merged from 6 mice per genotype) of ps6^{+} pro B cells (top), pre B cells (middle) and mature B cells (bottom). Mature B cells are defined as CD19^{hi}B220^{hi} with the exclusion of pro and pre B cells. Numbers indicate the frequency of the parent population. Gates for pS6^{+} cells were defined using cells stained only with anti-CD19 antibodies. **B) Frequencies of pS6^{+} cells** from the populations shown in A. Bars at mean ± SEM; Symbols indicate individual mice; N=1, N=6; significance calculated using 2-way ANOVA. **C) Median of pS6** from pro, pre and mature B cells (top) and from pS6+ cells within the respective populations (bottom). Bars at mean ± SEM; Symbols indicate individual mice; N=1, N=6; significance calculated using 2-way ANOVA.

6.3.4. B cell maturation in the bone marrow

DNT/mb1Cre mice showed drastically reduced mature B cell numbers and frequencies in the bone marrow (Fig15). While the cell numbers and frequencies of CD19^{+}B220^{+} cells were reduced ~2-fold in DNT/mb1Cre mice, mature CD19^{hi}B220^{hi} B cell numbers were even diminished ~10-fold, indicating impaired B cell maturation (Fig 15A, B). Further analysing CD19/B220 co-expressing cells for abundance of IgM and IgD allowed the identification of 4 BM B cell-subpopulations, with IgM^{-}IgD^{-} B cells being the least reduced in DNT/mb1Cre mice

(3.8% compared to 5.7% in mb1Cre mice). The strongest reduction was observed in the mature IgM^+IgD^+ B cell compartment (~15-fold) from 5% of viable cells ($2x10^6$ cells) in mb1Cre, to 0.4% of viable cells ($1.2x10^5$ cells) in DNT/mb1Cre mice. Both, cell numbers and frequencies of IgM^+IgD^- and IgM^+IgD^{int} B cells were also significantly reduced (~3-fold) in DNT/mb1Cre mice (Fig 15C). Analysing the GFP/DNT expression within the respective B cell populations in DNT/mb1Cre mice showed no particular selection for either of the subsets (Fig 15D, E) and generally an expression frequency of over 90%.

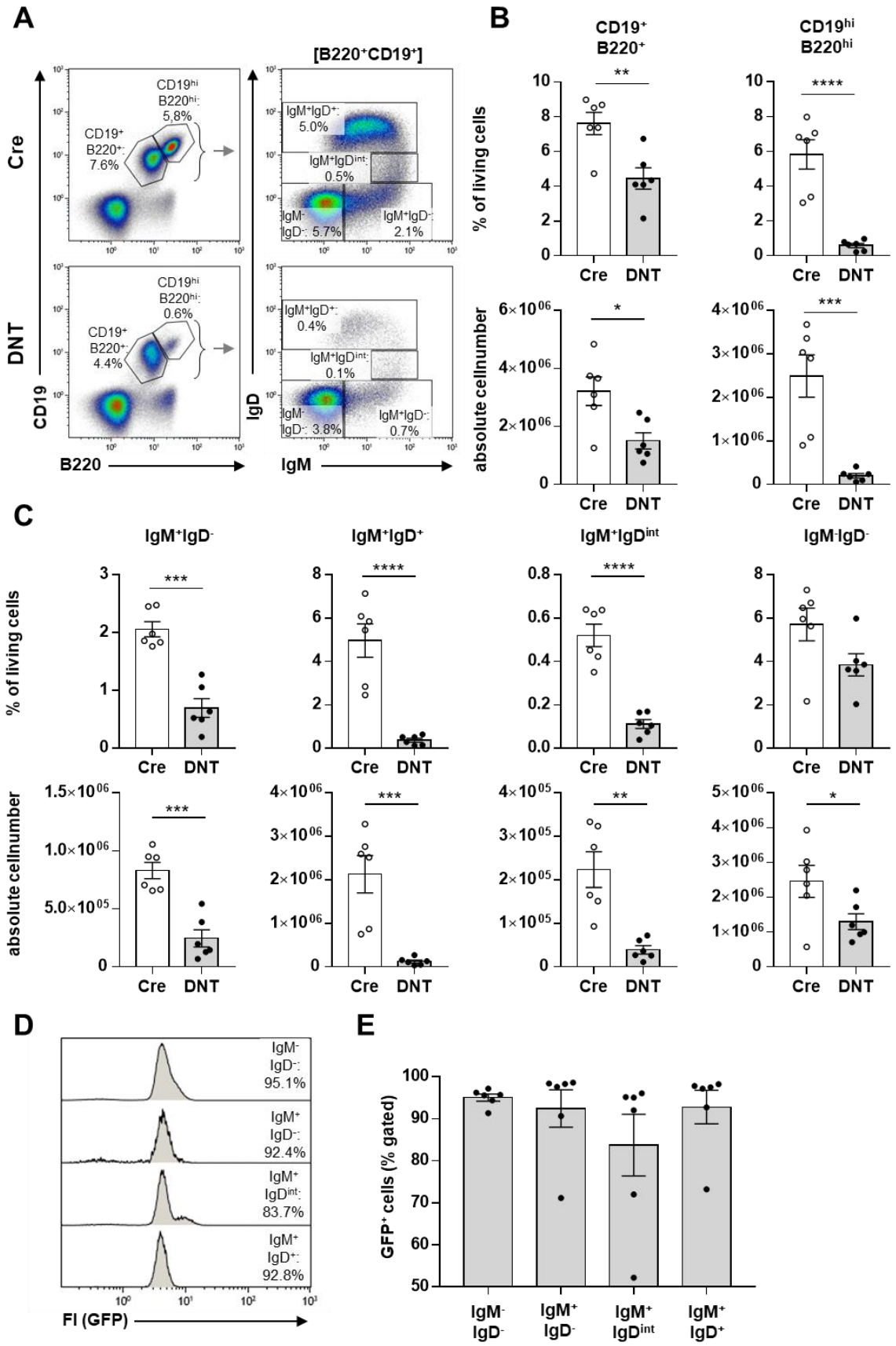

Figure 15 | Analysis of B cell maturation in the bone marrow of unimmunized DNT/mb1Cre mice

Bone marrow cells from DNT/mb1Cre and mb1Cre mice were isolated and analysed by flow cytometry. A) Representative flow cytometric analysis (merged from 6 mice per genotype) using anti CD19 and anti B220 antibodies. CD19 and B220 co-expressing cells were analysed for IgM and IgD expression. Numbers indicate the frequency of the parent population. B) Frequencies (top) and absolute cell numbers (bottom) from $CD19^{+}B220^{+}$ and $CD19^{hi}B220^{hi}$ B cells shown in A. Bars at mean ± SEM; Symbols indicate individual mice; N=1, n=6; significance was calculated using t-test. C) Frequencies (top) and absolute cell numbers (bottom) of $IgM^{-}IgD^{-}$, $IgM^{+}IgD^{-}$, $IgM^{+}IgD^{int}$ and $IgM^{+}IgD^{+}$ B cells shown in A. Bars at mean ± SEM; Symbols indicate individual mice; N=1, n=6; significance was calculated using t-test. D) Representative, merged (from 6 mice) flow cytometric analysis of GFP expressing cells in B cell populations shown in A from DNT/mb1Cre mice. Numbers indicate the frequency of the parent population. E) Frequencies of GFP expressing B cell subsets shown in D. Bars at mean ± SEM; Symbols indicate individual mice; N=1, n=6.

6.3.5. B cell maturation in the spleen

After successful development in the bone marrow, transitional B cells migrate via the blood into the spleen where they further differentiate into either follicular B cells (FO) or marginal zone B cells (MZ) (Melchers, 2015). B cell maturation in the spleen of DNT/mb1Cre mice was analysed by flow cytometry using anti-CD21, anti-CD23, anti-IgM and anti-IgD antibodies (pre-gated on viable $CD19^{+}$ cells to define B cells) (Fig 16A, B). Besides FO B cells and MZ B cells, staining with anti-CD21/anti-CD23 allowed the identification of 2 further B cell subsets: $CD21^{-}CD23^{-}$ and $CD21^{-}CD23^{low}$. The cell numbers of all analysed subsets were significantly decreased in DNT/mb1Cre mice, although to different degrees: While FO B cells were the strongest reduced by a factor ~16, MZ B cells were diminished by factor ~10, $CD21^{-}CD23^{-}$ B cells by factor 4 and $CD21^{-}CD23^{low}$ B cells by factor 3 (Fig 16A, C). The frequencies of FO B cells in DNT/mb1Cre were the strongest reduced B cell population with 4.9% of viable cells compared to 34.6% in mb1Cre mice, MZ B cells were significantly reduced to 1.2% from 5.1%, $CD21^{-}CD23^{-}$ B cells were significantly reduced to 2.0% compared to 3.1% and the frequency of $CD21^{-}CD23^{low}$ B cells was comparable. Using anti-IgM and anti-IgD staining allowed the identification of 4 B cell subsets (Fig 16B). The cell numbers of all 4 subsets were significantly decreased in DNT/mb1Cre mice, again to different degrees: while $IgM^{-}IgD^{-}$ B cells and $IgM^{int}IgD^{int}$ B cells were reduced only two-fold, $IgM^{+}IgD^{-}$ B cells were reduced by factor 8 in DNT/mb1Cre mice and $IgM^{+}IgD^{+}$ B cells by factor 13. The frequencies of $IgM^{-}IgD^{-}$ B cells and $IgM^{int}IgD^{int}$ B cells was comparable between DNT/mb1Cre mice and mb1Cre mice, but the frequency of $IgM^{+}IgD^{-}$ was only 2.6% in DNT/mb1Cre mice compared to 8.7% in mb1Cre mice (Fig 16D). The frequency of $IgM^{+}IgD^{+}$ B cells was with 5.6% also strongly decreased in DNT/mb1Cre mice compared to mb1Cre mice. Analysing the frequencies of DNT/GFP expressing B cells from DNT/mb1Cre mice showed that $CD21^{-}CD23^{low}$ B cells have the highest DNT/GFP expression with 98.2% (Fig 16E, F). The frequency of DNT/GFP expressing FOs was slightly reduced to 96.7%, whereas the frequency of DNT/GFP expressing MZ B cells was only 54.3%, indicating selection against DNT/GFP expressing cells during MZ B cell differentiation. $CD21^{-}CD23^{-}$ B cells showed rather wide scattering between individual mice with a mean DNT/GFP expression of 57.3%. The frequency of DNT/GFP expressing $IgM^{int}IgD^{int}$ and $IgM^{+}IgD^{+}$ B cells was 95.4%, while only 70.3% of $IgM^{+}IgD^{-}$ B cells and 45.1% of IgM-IgD-

B cells showed DNT/GFP expression (Fig 16G, H). In summary, DNT/mb1Cre mice have drastically reduced mature B cell numbers in the spleen. Furthermore, DNT/GFP expression is significantly reduced in MZ compared to FO B cells, indicating that transitional B cells that escaped Cre recombination are selected into the pool of MZ B cells.

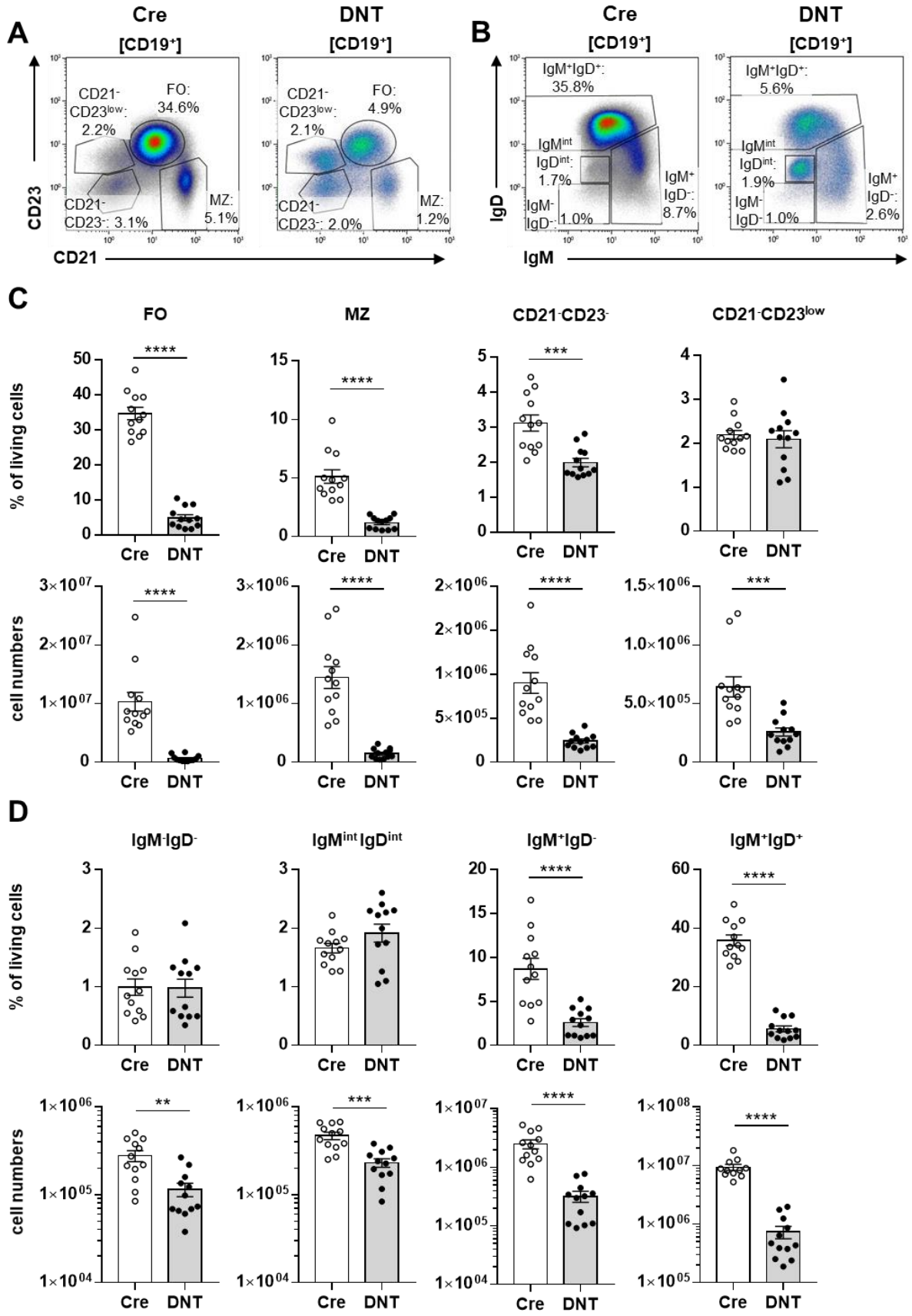
A
Cre
[CD19+]
DNT
[CD19+]
CD21-CD23low: 2.2%
FO: 34.6%
CD21-CD23-: 3.1%
MZ: 5.1%
CD21-CD23low: 2.1%
FO: 4.9%
CD21-CD23-: 2.0%
MZ: 1.2%
CD23
CD21
B
Cre
[CD19+]
DNT
[CD19+]
IgM+IgD+: 35.8%
IgMint IgDint: 1.7%
IgM- IgD-: 1.0%
IgM+ IgD-: 8.7%
IgM+IgD+: 5.6%
IgMint IgDint: 1.9%
IgM- IgD-: 1.0%
IgM+ IgD-: 2.6%
IgD
IgM
C
FO
MZ
CD21-CD23-
CD21-CD23low
% of living cells
cell numbers
Cre
DNT
D
IgM-IgD-
IgMint IgDint
IgM+IgD-
IgM+IgD+
% of living cells
cell numbers
Cre
DNT

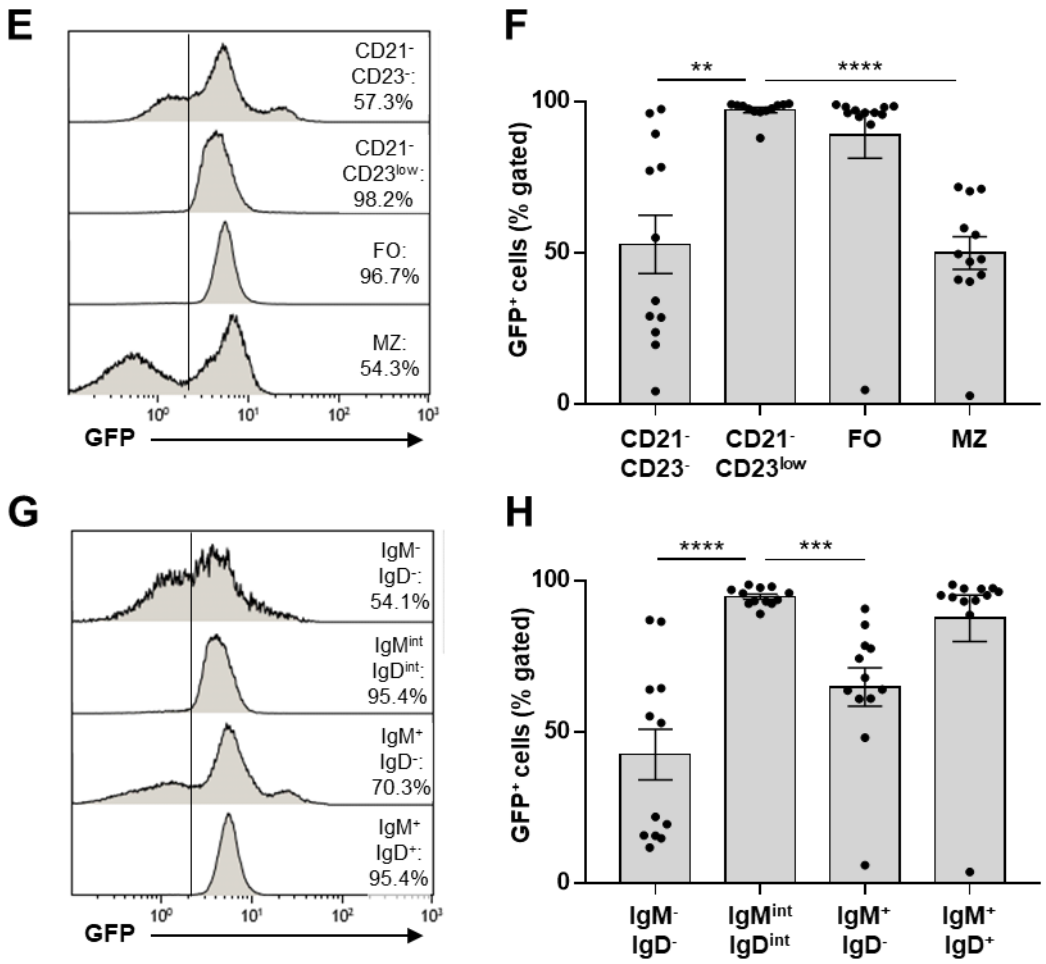

Figure 16 | Analysis of B cell maturation in the spleen of unimmunized DNT/mb1Cre mice

Splenic B cells from unimmunized DNT/mb1Cre and mb1Cre mice were isolated and analysed by flow cytometry. **A) Representative dot blots** (merged from 6 mice per genotype) using anti CD21 and anti CD23 antibodies (pregated on CD19+ cells). Follicular B cells (FO) are $CD21^{+}CD23^{+}$ and marginal zone B cells (MZ) are $CD21^{+}CD23^{low}$. Numbers indicate the frequency of viable cells. **B) Representative dot blots** (merged from 6 mice per genotype) using anti IgM and anti IgD antibodies. Numbers indicate the frequency of viable cells. **C) Frequencies** (top) and absolute cell numbers per spleen (bottom) of FO, MZ, $CD21^{-}CD23^{low}$ and $CD21^{-}CD23^{-}$ B cell subsets shown in A. Bars at mean ± SEM; Symbols indicate individual mice; N=2, n=6; significance was calculated using t-test. **D) Frequencies (top) and absolute cell numbers (bottom)** of B cell subsets defined by expression of IgM and IgD as shown in B. Bars at mean ± SEM; Symbols indicate individual mice; N=2, n=6; significance was calculated using t-test. **E) Representative flow cytometric analysis** (merged from 6 mice) of GFP expressing cells in B cell populations shown in A) from DNT/mb1Cre mice. Numbers indicate the frequency of the parent population. **F) Frequencies** of GFP expressing B cell subsets shown in E. Bars at mean ± SEM; Symbols indicate individual mice; N=2, n=6; significance was calculated using 2-way ANOVA, each subset compared to $CD21^{-}CD23^{low}$ cells. **G) Representative flow cytometric analysis** (merged from 6 mice) of GFP expressing cells in B cell populations shown in B) from DNT/mb1Cre mice. Numbers indicate the frequency of the parent population. **H) Frequencies** of GFP expressing B cell subsets shown in G. Bars at mean ± SEM; Symbols indicate individual mice; N=2, n=6; significance was calculated using 2-way ANOVA, each subset compared to $IgM^{int}IgD^{int}$ B cells.

6.3.6. Germinal center B cells in the Peyer's patches

To determine the formation of germinal centre B cells (GCs) in unimmunized mice, we analysed Peyer's patches, where spontaneous germinal centre reactions occur by flow cytometry using anti-CD19, anti-CD38, anti-CD95 and anti-GL7 antibodies. GC B cells are defined as $CD19^{+}CD38^{low}CD95^{+}GL7^{hi}$. While the frequency of $CD19^{+}$ cells was drastically reduced in DNT/mb1Cre mice (13%) compared mb1Cre mice (65%), the frequency of GCs

was comparable (Fig 17A, B). Interestingly only 51.8% of CD19^{+} B cells from DNT/mb1Cre mice showed DNT/GFP expression with a further significant decrease to 31.8% in GC B cells (Fig 17C, D). These results indicate that B cells that escaped the Cre recombination, and therefore just express the WT TWINKLE protein, are selected for the migration to the Peyer's patches and again favoured during the generation of GC B cells. Taken together, the unchanged frequency of GC B cells in DNT/mb1Cre mice with decreased expression of DNT/GFP in these cells highlights the importance this particular B cell subset and furthermore its dependence on a functional respiratory chain.

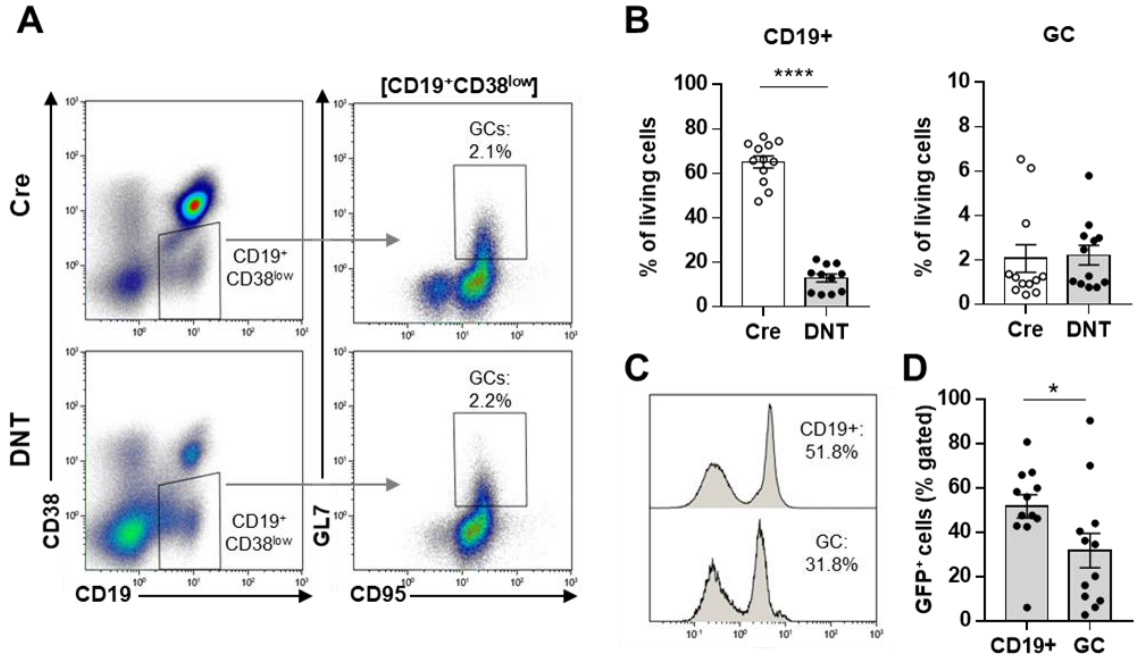

Figure 17 | Analysis of germinal center B cells in the Peyer's patches of unimmunized DNT/mb1Cre mice
Cells from the Peyer's patches of DNT/mb1Cre and mb1Cre mice were isolated and analysed by flow cytometry. **A) Representative dot blots** (merged from 6 mice per genotype) of germinal center B cells (GCs) in the Peyer's patches, defined as CD19^{+}CD38^{low}CD95^{+}GL7^{hi}. Numbers indicate the frequency of viable cells. **B) Frequencies** of CD19^{+} and germinal center B cells (GC), shown in A. **C) Representative flow cytometric analysis** (merged from 6 mice) of GFP expressing cells in CD19+ and germinal center B cells, shown in A), from DNT/mb1Cre mice. **D) Frequencies** of GFP expressing B cells (CD19+) and GC B cells from DNT/mb1Cre mice shown in A and C. Bars at mean ± SEM; Symbols indicate individual mice; N=2, n=6. Statistical significance was calculated using t-test.

6.3.7. Plasma blast and plasma cell populations in the spleen

The activation of B cells, either T-dependently during the germinal centre response or T-independently, results in the generation of antibody-secreting plasma blasts (PB) and plasma cells (PC). The generation of PB/PCs in the spleen was analysed by flow cytometry using anti-TACI, anti-CD138, anti-CD19 and anti-B220 antibodies (Pracht et al., 2017). The frequencies of PB/PCs, defined as TACI^{+}CD138^{+}, in the spleen of DNT/mb1Cre mice was significantly increased, resulting in comparable PB/PC cell numbers (Fig 18A, B). The PB/PC compartment

can be further divided into 4 subpopulations: P0 activated B cells are defined as $CD19^{+}B220^{+}$, P1 PBs are $CD19^{int}$, $B220^{int}$, P2 early PCs are $CD19^{int}B220^{low}$ and P3 mature PCs are $CD19^{low}B220^{low}$ (Fig 18C). The proportions of the subpopulations are altered in DNT/mb1Cre mice with less cells in the P0/P1 compartment and more cells in the P3 compartment (Fig 18D, E). This results in comparable P2 and P3 cell numbers and slightly reduced P0 and P1 cell numbers, although this did not reach statistical significance. The frequency of DNT/GFP expressing cells in DNT/mb1Cre mice decreased during PC differentiation from 83.5% in the P0 compartment, 60.4% in the P1 compartment, 30.6% in the P2 compartment and 27.6% in the P3 compartment (Fig 18F, G). In summary, DNT/mb1Cre mice have comparable PB/PC numbers in the spleen. However, a progressive loss of DNT/GFP expression from P0-P3 indicates a strong requirement on mitochondrial respiration during PC differentiation and maturation.

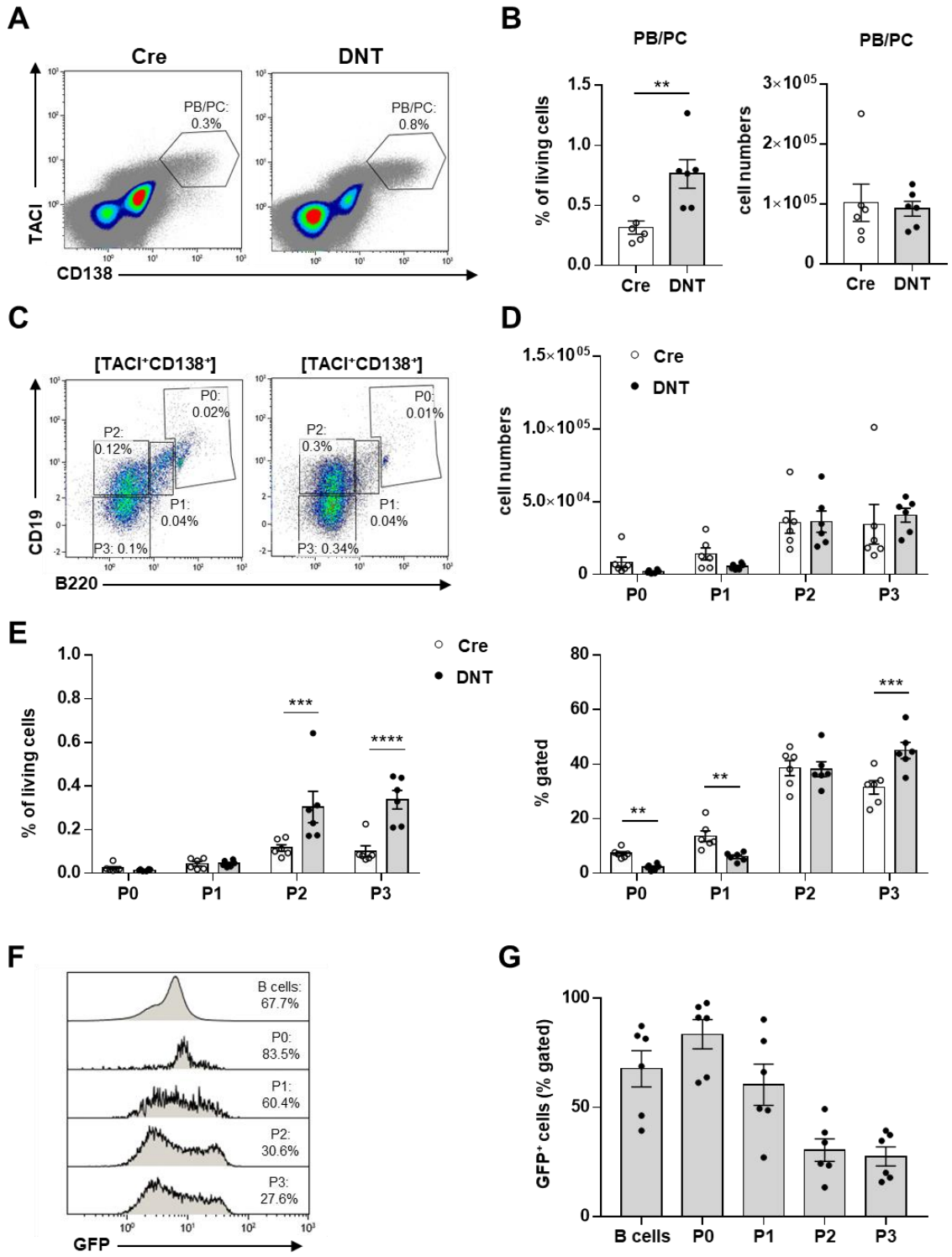

Figure 18 | Analysis of plasma blast and plasma cell populations in the spleen of unimmunized DNT/mb1Cre mice

Splenic cells from DNT/mb1Cre and mb1Cre mice were isolated and analysed by flow cytometry. A**) Representative dot blots** (merged from 6 mice per genotype) using anti TACI and anti CD138 antibodies. Plasmablasts (PB) and plasma cells (PC) are defined as $TACI^+CD138^+$. Numbers indicate the frequency of viable cells. **B) Frequency (left) and absolute cell number (right)** of plasma blasts and plasma cells shown in A. Bars at mean ± SEM; Symbols indicate individual mice; N=1, n=6; significance was calculated using t-test. **C) Representative dot blots** (merged from 6 mice per genotype) using anti CD19 and anti B220 antibodies, pregated on $TACI^+CD138^+$ cells as shown in A. P0 cells are defined as $CD19^+B220^+$, P1 cells are $CD19^{int}$, $B220^{int}$, P2 cells are $CD19^{int}B220^{low}$ and P3 cells are $CD19^{low}B220^{low}$. Numbers indicate the frequency of viable cells. **D) Absolute cell numbers** of PB/PC subpopulations shown in C. **E) Frequencies** of PB/PC subpopulations of living cells (left) and frequencies of $TACI^+CD138^+$ cells (right). **F) Representative flow cytometric analysis** (merged from 6 mice) of GFP expressing cells in B cell populations shown in C) from DNT/mb1Cre mice. Numbers indicate the frequency of the parent population. B cells are defined as $CD19^+TACI^-CD138^-$. **G) Frequencies** of GFP expressing B cell subsets shown in F. Bars at mean ± SEM; Symbols indicate individual mice; N=1, n=6.

6.3.8. Plasma blast and plasma cell populations in the bone marrow

The bone marrow provides a survival niche for PB/PCs, especially for long-lived plasma cells within the P3 compartment. The analysis of PB/PCs in the bone marrow was performed analogous to the spleen with the exception that only the subpopulations P1-P3 are present in the bone marrow. Both, frequency and cell numbers of PB/PCs was reduced by half in DNT/mb1Cre mice (Fig 19A, B). The relative amount of P1 cells was slightly decreased and the relative amount of P2 cells was significantly decreased in DNT/mb1Cre mice, while the relative amount of P3 cells in contrast was significantly increased (Fig 19C-E). This resulted in comparable cell numbers of the P3 compartment. Analysing the DNT/GFP expression within the respective subpopulations showed wide scattering in the P1 compartment between individual mice, with a mean frequency of 57% (Fig 19F, G). Analogous to the spleen, the frequency decreased to 29% in the P2 compartment, but similarly there was no further drop in DNT/GFP expression between the P2 and P3 (33%) compartment detected. These results indicate that B cells with a functional respiratory chain are selected during PC differentiation and replenish the P3 pool within the PB/PC compartment in the bone marrow. This highlights the importance of this particular B cell subset and its requirement for a functional respiratory chain.

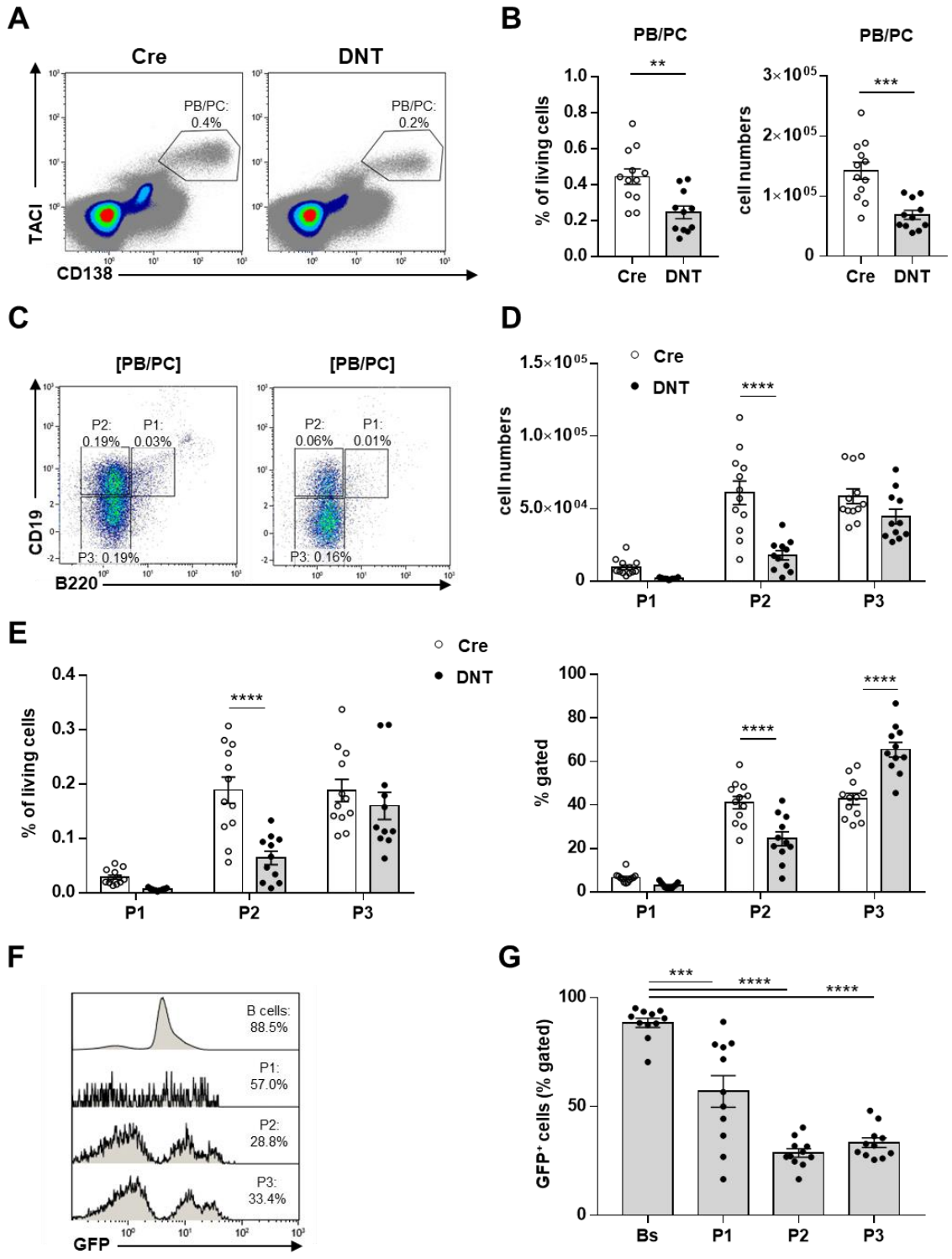

Figure 19 | Analysis of plasmablast and plasma cell populations in the bone marrow of unimmunized DNT/mb1Cre mice

Bone marrow cells from DNT/mb1Cre and mb1Cre mice were isolated and analysed by flow cytometry. **A) Representative dot blots** (merged from 6 mice per genotype) using anti-TACI and anti-CD138 antibodies. Plasmablasts (PB) and plasma cells (PC) are defined as $TACI^+CD138^+$. Numbers indicate the frequency of viable cells**. B) Frequency (left) and absolute cell number (right)** of PBs and PCs shown in A. Bars at mean ± SEM; Symbols indicate individual mice; N=2, n=6; significance was calculated using t-test. **C) Representative dot blots** (merged from 6 mice per genotype) using anti CD19 and anti B220 antibodies, pregated on $TACI^+CD138^+$ cells as shown in A. P1 cells are defined as $CD19^{int}$, $B220^{int}$, P2 cells are $CD19^{int}B220^{low}$ and P3 cells are $CD19^{low}B220^{low}$. Numbers indicate the frequency of viable cells. **D) Absolute cell numbers** of PB/PC subpopulations shown in C. **E) Frequencies** of PB/PC subpopulations of living cells (left) and frequencies of $TACI^+CD138^+$ cells (right). **F) Representative flow cytometric analysis** (merged from 6 mice) of GFP expressing cells in B cell populations shown in C) from DNT/mb1Cre mice. B cells are defined as $CD19^+TACI^-CD138^-$. Numbers indicate the frequency of the parent population. **G) Frequencies** of GFP expressing B cell subsets shown in F. Bars at mean ± SEM; Symbols indicate individual mice; N=2, n=6.

6.3.9. Analysis of serum antibody abundance

To assess, if the aberrant PB/PC populations in spleen and bone marrow of DNT/mb1Cre mice influence antibody levels in the blood serum, the abundance of Ig-isotypes in the serum of unimmunized mice was quantified by ELISA (Fig 20). While the amount of IgM was significantly increased in DNT/mb1Cre mice (0,24 mg/ml compared to 0.18 mg/ml in mb1Cre mice), IgA was significantly decreased (0.36 mg/ml compared to 0.57 mg/ml in mb1Cre). The amount of total IgG was comparable with 3.3 mg/ml in mb1Cre mice and 3.6 mg/ml in DNT/mb1Cre mice. Interestingly there were severe differences in the amounts of the different IgG subclasses in the serum: DNT/mb1Cre mice showed significantly higher levels of IgG2b antibodies (1.9 mg/ml compared to 1.1 mg/ml in mb1Cre mice), whereas the IgG subclasses IgG1, IgG2c and IgG3 were all significantly reduced. While the amount of IgG3 was reduced only by half, the amount of IgG1 and IgG2c was diminished by factor 7 and 8, respectively. This data show that a dysfunctional respiratory chain in B cells affects secreted serum antibody levels, even if only ~30% of the P3 compartment, which contains the long-lived Ab-secreting PCs, do in fact express DNT/GFP and therefore ~70% of mature P3 PCs should be fully functional.

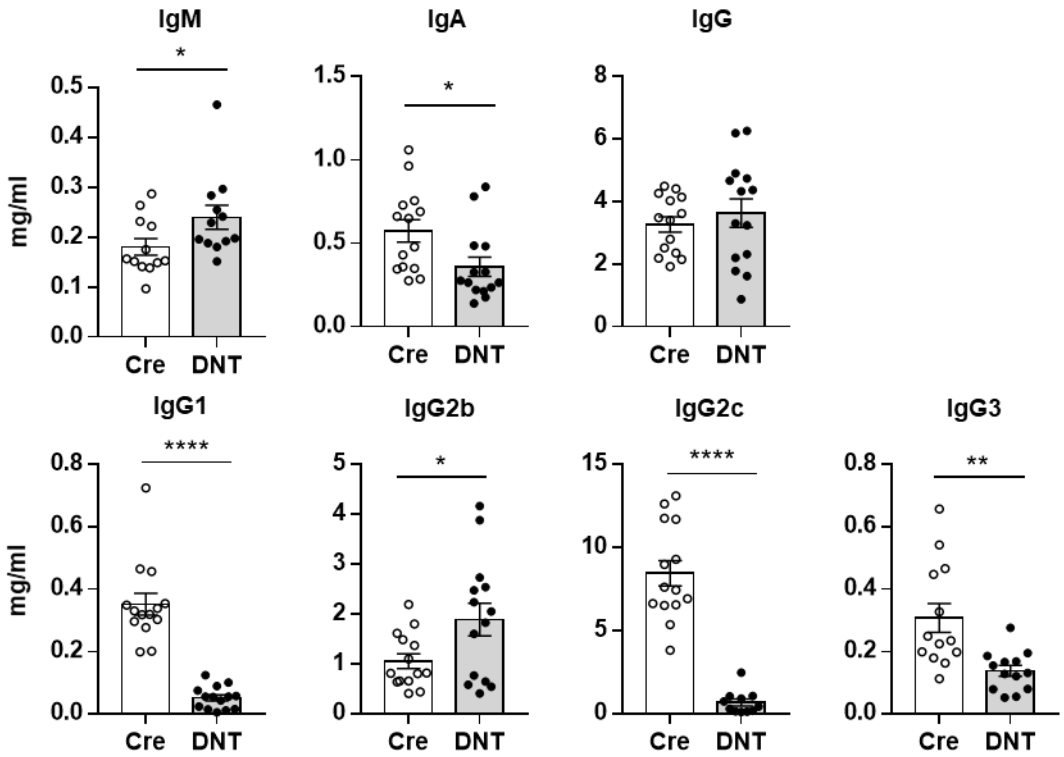

Figure 20 | Analysis of serum antibody levels in unimmunized DNT/mb1Cre mice
Serum from unimmunized DNT/mb1Cre and mb1Cre mice was analysed by ELISA and levels of IgM, IgA and IgG sub-classes were quantified. Bars at mean ± SEM; Symbols indicate individual mice; N=2, n=6; Statistical significance was calculated using t-test.

6.4. Analysis of B cell development and maturation in unimmunized DNT/CD23Cre mice

To analyse the function of the respiratory chain in B cell activation and PC differentiation, DNT/CD23Cre mice were analysed by flow cytometry. Using anti-IgM and anti-IgD antibodies in flow cytometry to define B cell populations in the BM confirmed onset of CD23Cre mediated DNT/GFP expression in transitional B cells (Fig 21A, B). Further analysis, using anti-CD4 and anti-CD8 antibodies to define T cell population in the BM proofed that DNT/GFP is expressed exclusively in B cells (Fig 21C).

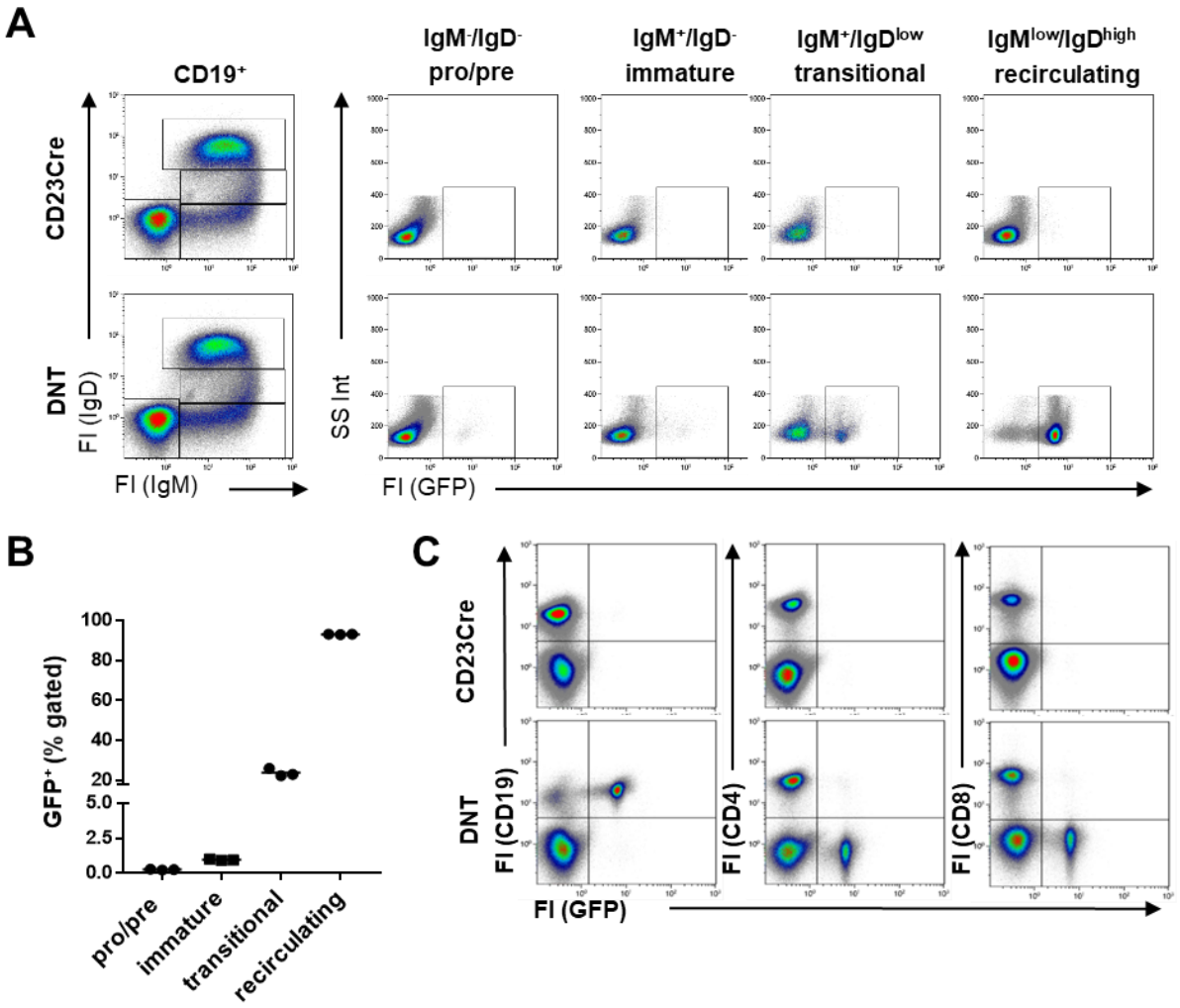

Figure 21 | Analysis of CD23Cre mediated insertion of DNT in B cells

A) Representative, merged flow cytometric analysis of the bone marrow. Viable, CD19+ cells were analysed according to surface expression of IgM and IgD. DNT/GFP expression was further analysed within the defined subpopulations. **B) Frequencies of GFP+ cells** in the subpopulations defined in A). Line at mean; Each line represents one mouse, N=1, n=3. **C) Representative, merged flow cytometric analysis of the spleen**. Viable cells were stained with anti-CD19, -CD4 and -CD8 antibodies and analysed for co-expression of GFP/DNT.
[Figure partially adapted and modified after Urbanczyk et al., 2021.]

6.4.1. B cell maturation in the spleen

B cell maturation in the spleen of DNT/CD23Cre mice was analysed by flow cytometry using anti-CD21, anti-CD23, anti-IgM and anti-IgD antibodies (gated on viable $CD19^+$ cells) (Fig 22A-D). While the frequencies of FOs, MZs, $CD21^-CD23^-$ and $CD21^-CD23^{low}$ B cells were comparable between DNT/CD23Cre and CD23Cre mice, the cell numbers of FOs and $CD21^-CD23^-$ were significantly increased in DNT/CD23Cre mice (Fig 22C). The frequencies and cell numbers of B cell populations defined by anti-IgM and anti-IgD staining, namely $IgM^{int}IgD^{int}$, IgM^+IgD^- and IgM^+IgD^+, were all comparable between DNT/CD23Cre and CD23Cre mice (Fig 22D). Analysing the DNT/GFP expression of the respective subsets in DNT/CD23Cre mice showed differential frequencies: While ~92% of FOs express DNT/GFP, only 87% of MZs, 45%

of $CD21^{-}CD23^{low}$ and 9% of $CD21^{-}CD23^{-}$ B cells expressed DNT/GFP (Fig 22E, F). The subsets defined by anti-IgM and anti-IgD staining also showed different frequencies of DNT/GFP expressing cells: 95% of IgM+IgD+ cells, 53% of $IgM^{int}gD^{int}$ cells and 33% of IgM^{-} IgD^{-} cells expressed DNT/GFP (Fig 22G, H). Taken together, DNT/CD23Cre mice have comparable numbers of mature B cell subsets in the spleen. However, DNT/GFP expression differs between the subsets and is higher in FO compared to MZ B cells, indicating that transitional B cells that escaped Cre recombination are selected into the pool of MZ B cells.

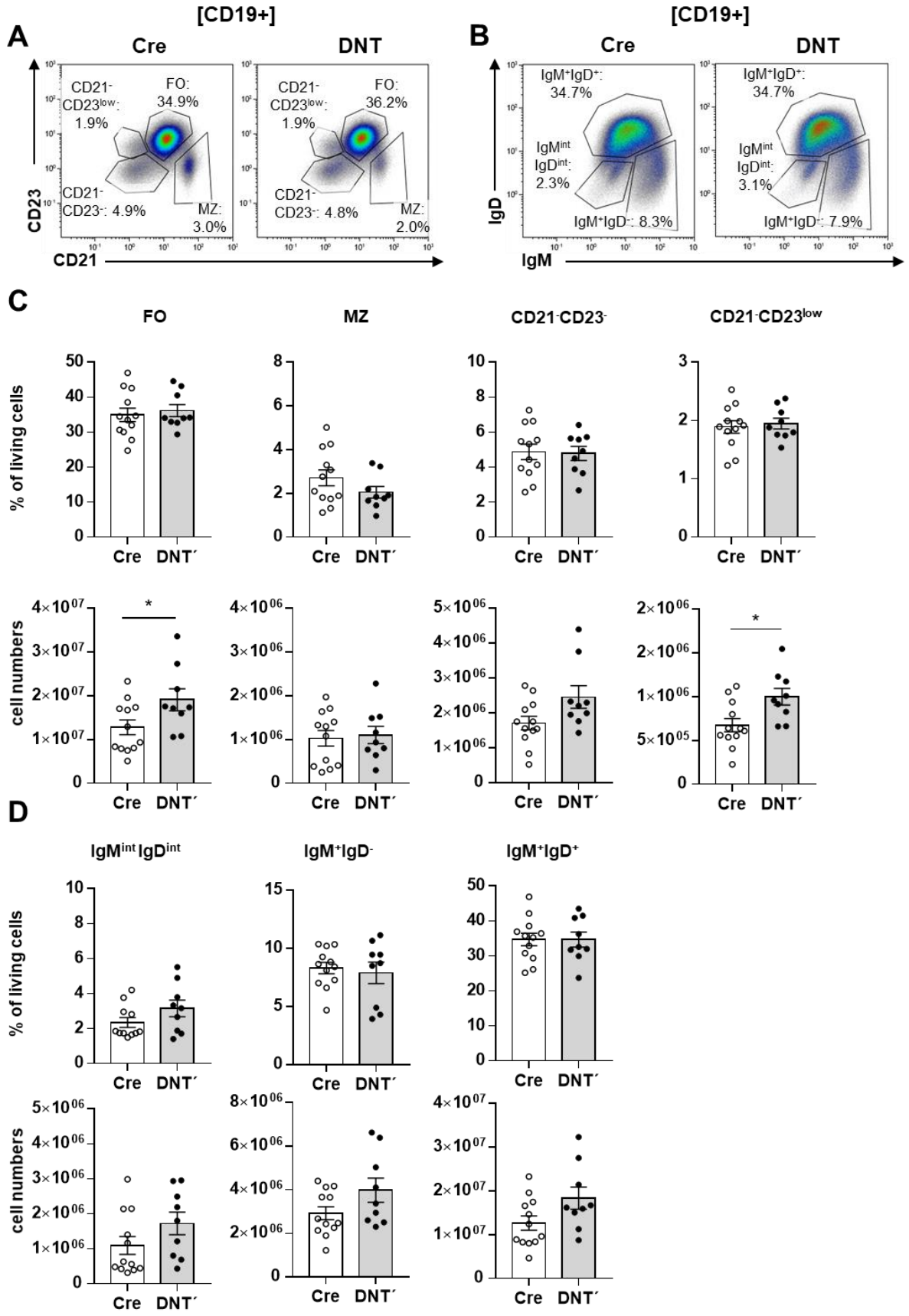
A
[CD19+]
Cre
DNT
CD21-
CD23low:
1.9%
FO:
34.9%
CD21-
CD23-: 4.9%
MZ:
3.0%
FO:
36.2%
CD21-
CD23-: 4.8%
MZ:
2.0%
CD23
CD21
B
[CD19+]
Cre
DNT
IgM+IgD+:
34.7%
IgMint
IgDint:
2.3%
IgM+IgD-: 8.3%
IgMint
IgDint:
3.1%
IgM+IgD-: 7.9%
IgD
IgM
C
FO
MZ
CD21-CD23-
CD21-CD23low
% of living cells
cell numbers
Cre
DNT´
*
D
IgMintIgDint
IgM+IgD-
IgM+IgD+
% of living cells
cell numbers
Cre
DNT´

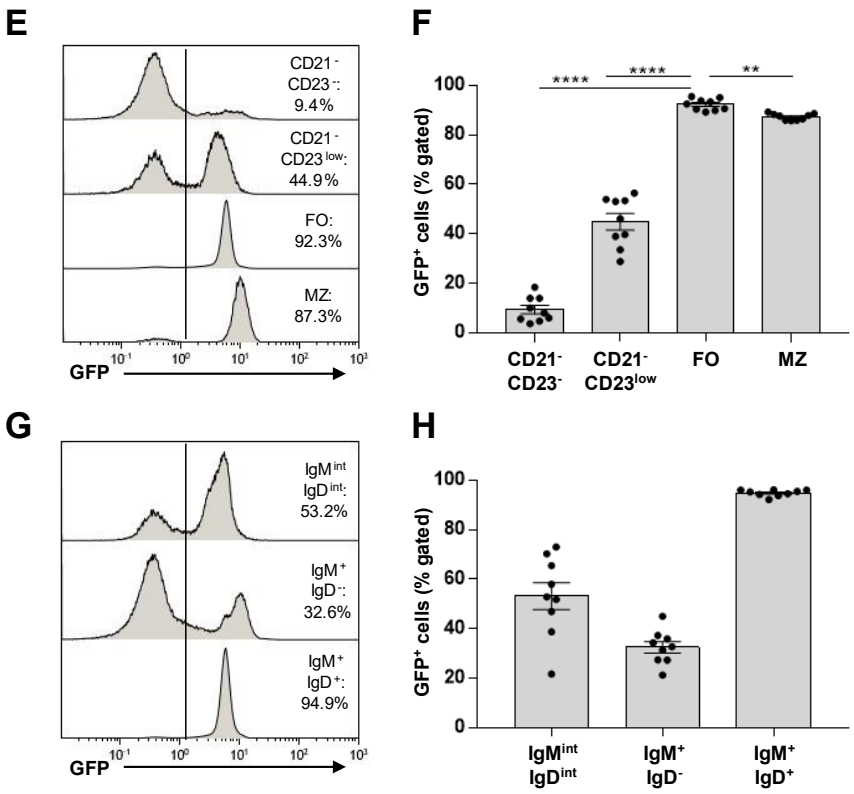

Figure 22 | Analysis of B cell maturation in the spleen from unimmunized DNT/CD23Cre mice
Splenic B cells from unimmunized DNT/CD23Cre and CD23Cre mice were isolated and analysed by flow cytometry. **A) Representative dot blots** (merged from 3 mice per genotype) using anti CD21 and anti CD23 antibodies (pre-gated on CD19+ cells). Follicular B cells (FO) are $CD21^{+}CD23^{+}$ and marginal zone B cells (MZ) are $CD21^{+}CD23^{low}$. Numbers indicate the frequency of viable cells. **B) Representative dot blots** (merged from 3 mice per genotype) using anti IgM and anti IgD antibodies. Numbers indicate the frequency of viable cells. **C) Frequencies (top) and absolute cell numbers (bottom)** of FO, MZ, $CD21^{-}CD23^{low}$ and $CD21^{-}CD23^{-}$ B cell subsets shown in A. Bars at mean ± SEM; Symbols indicate individual mice; N=4, n=2-4; significance was calculated using t-test. **D) Frequencies (top) and absolute cell numbers (bottom)** of B cell subsets defined by expression of IgM and IgD as shown in B. Bars at mean ± SEM; Symbols indicate individual mice; N=4, n=2-3; significance was calculated using t-test. **E) Representative flow cytometric analysis** (merged from 3 mice) of GFP expressing cells in B cell populations shown in A) from DNT/CD23Cre mice. Numbers indicate the frequency of the parent population. **F) Frequencies** of GFP expressing B cell subsets shown in E. Bars at mean ± SEM; Symbols indicate individual mice; N=4, N=2-3; significance was calculated using 2-way ANOVA, each subset compared to follicular B cells (FO). **G) Representative flow cytometric analysis** (merged from 3 mice) of GFP expressing cells in B cell populations shown in B) from DNT/CD23Cre mice. Numbers indicate the frequency of the parent population. H) Frequencies of GFP expressing B cell subsets shown in G. Bars at mean ± SEM; Symbols indicate individual mice; N=4, n=2-3.
[Figure partially adapted and modified after Urbanczyk et al., 2021.]

6.4.2. Germinal center B cells in the Peyer's patches

To analyse the generation of germinal center B cells (GCs) in unimmunized mice, cells from the Peyer's patches were isolated and analysed by flow cytometry using anti-CD19, anti-CD38, anti-CD95 and anti-GL7 antibodies (Fig 23A). GC B cells are defined as $CD19^{+}CD38^{low}CD95^{+}GL7^{hi}$. The frequencies of both CD19+ cells and GC B cells was comparable between DNT/CD23Cre mice and CD23Cre mice (Fig 23B). Interestingly, there was a significant drop of DNT/GFP expressing cells between CD19+ B cells and GC B cells (Fig 23C, D): while 82% of $CD19^{+}$ B cells expressed DNT/GFP, only 16% of GC B cells still expressed the mutant, indicating that GC B cells require a functional respiratory chain.

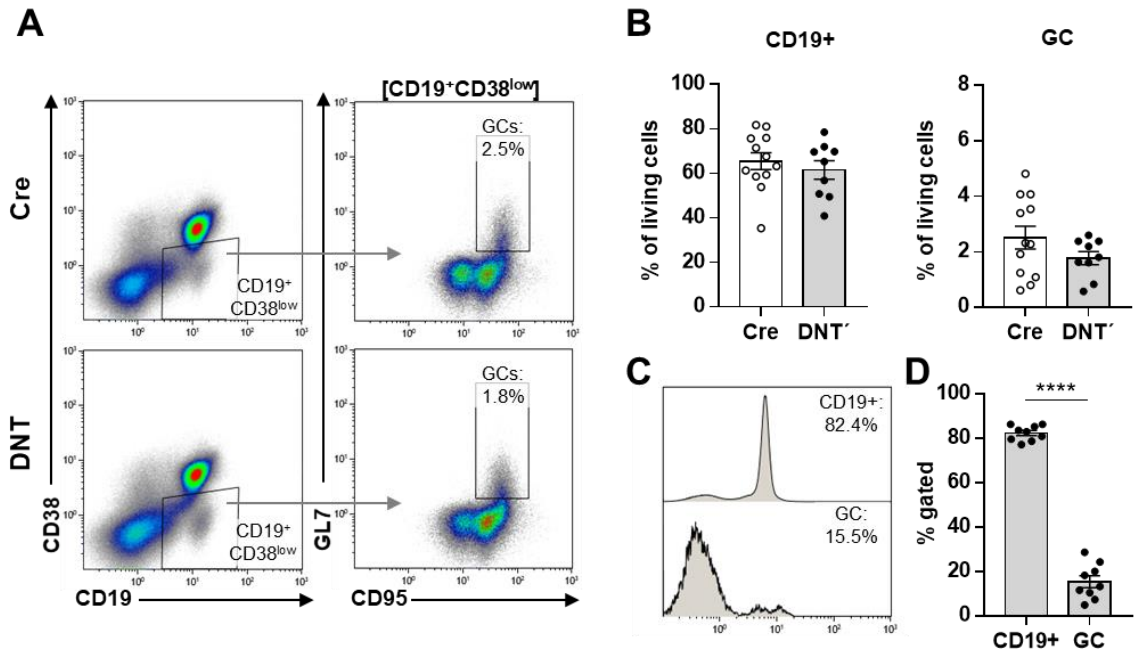

Figure 23 | Analysis of germinal center B cells in the Peyer's patches of unimmunized DNT/CD23Cre mice
Cells from the Peyer's patches of DNT/CD23Cre and CD23Cre mice were isolated and analysed by flow cytometry. **A) Representative dot blots** (merged from 3 mice per genotype) of germinal center B cells (GCs) in the Peyer's patches, defined as $CD19^{+}CD38^{low}CD95^{+}GL7^{hi}$. Numbers indicate the frequency of viable cells. **B) Frequencies** of $CD19^{+}$ and germinal center B cells (GCs), shown in A. **C) Representative flow cytometric analysis** (merged from 3 mice) of GFP expressing cells in CD19+ and germinal center B cells, shown in A), from DNT/CD23Cre mice**. D) Frequencies** of GFP expressing B cells shown in A and C. Bars at mean ± SEM; Symbols indicate individual mice; N=4, n=2-3. Statistical significance was calculated using t-test.
[Figure partially adapted and modified after Urbanczyk et al., 2021.]

6.4.3. Plasma blast and plasma cell populations in the spleen

The generation of PB/PCs in the spleen was analysed by flow cytometry using anti-TACI, anti-CD138, anti-CD19 and anti-B220 antibodies (Fig 24A, C). The frequencies and cell numbers of PB/PCs, defined as $TACI^{+}CD138^{+}$, were comparable between DNT/CD23Cre mice and CD23Cre mice (Fig 24B). Also, the frequencies and cell numbers of P1 PBs, early P2 PCs and mature P3 PCs cells within the PB/PC compartment were comparable (Fig 24D, E), but GFP analysis revealed that there is a significant decrease of DNT/GFP expressing cells during PC development: while 66% of P1 cells showed DNT/GFP expression, it decreased to 28% of P2 cells and 10% of P3 cells (Fig 24F, G).

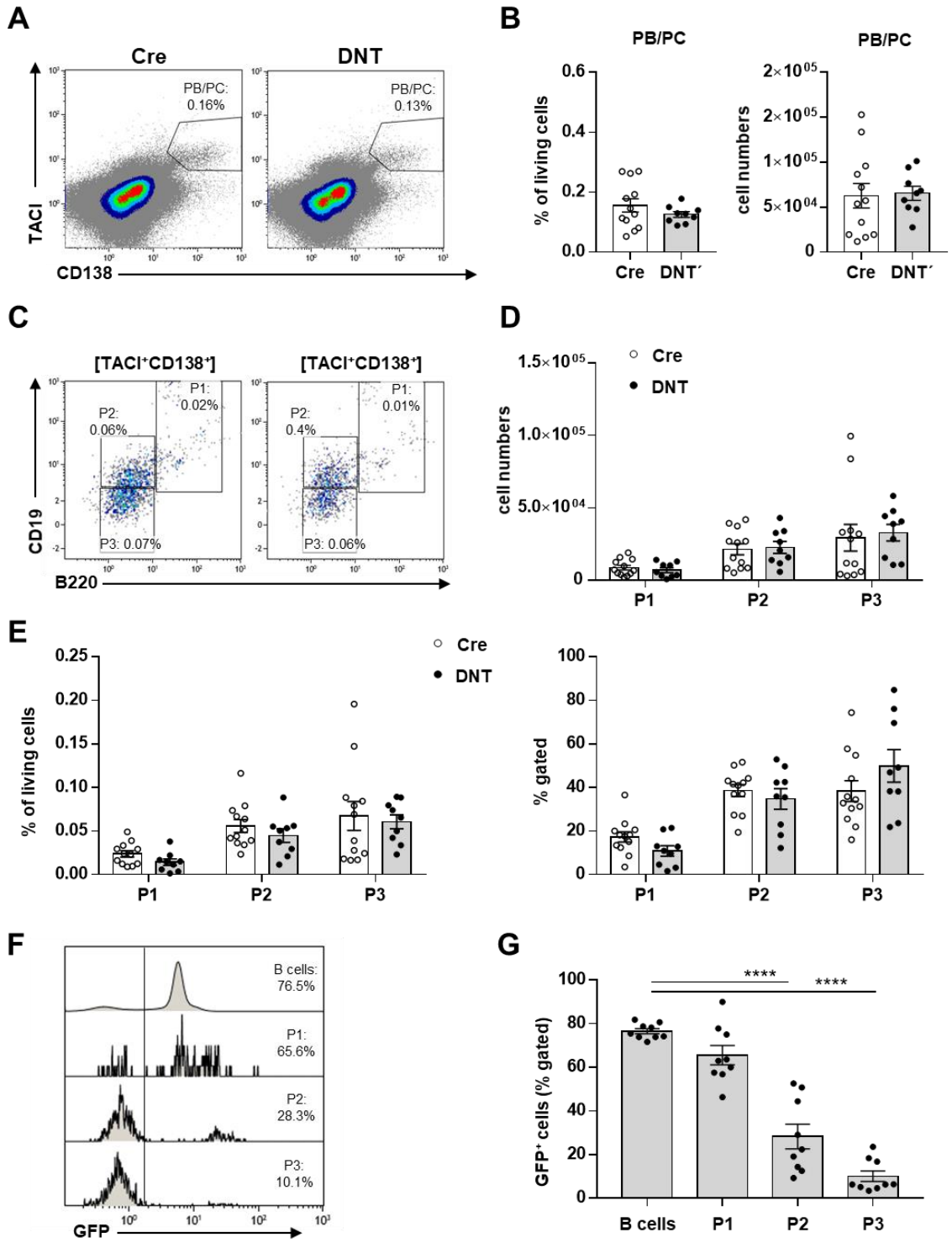

Figure 24 | Analysis of plasmablast and plasma cell populations in the spleen of unimmunized DNT/CD23Cre mice

Splenic cells from DNT/CD23Cre and CD23Cre mice were isolated and analysed by flow cytometry. **A) Representative dot blots** (merged from 3 mice per genotype) using anti-TACI and anti-CD138 antibodies. Plasmablasts (PB) and plasma cells (PC) are defined as $TACI^{+}CD138^{+}$. Numbers indicate the frequency of viable cells. **B) Frequency (left) and absolute cell number (right)** of PBs and PCs shown in A. Bars at mean ± SEM; Symbols indicate individual mice; N=4, n=2-3; significance was calculated using t-test. **C) Representative dot blots** (merged from 6 mice per genotype) using anti CD19 and anti B220 antibodies, pregated on $TACI^{+}CD138^{+}$ cells as shown in A. P1 cells are defined as $CD19^{int}$, $B220^{int}$, P2 cells are $CD19^{int}B220^{low}$ and P3 cells are $CD19^{low}B220^{low}$. Numbers indicate the frequency of viable cells. **D) Absolute cell numbers** of PB/PC subpopulations shown in C. **E) Frequencies** of PB/PC subpopulations of living cells (left) and frequencies of $TACI^{+}CD138^{+}$ cells (right). **F) Representative flow cytometric analysis** (merged from 3 mice) of GFP expressing cells in B cell populations shown in C) from DNT/CD23Cre mice. Numbers indicate the frequency of the parent population. B cells are defined as $CD19^{+}TACI^{-}CD138^{-}$. **G) Frequencies** of GFP expressing B cell subsets shown in F. Bars at mean ± SEM; Symbols indicate individual mice; N=4, n=2-3.
[Figure partially adapted and modified after Urbanczyk et al., 2021.]

6.4.4. Plasma blast and plasma cell populations in the bone marrow

The PB/PC compartment in the bone marrow was comparable to the spleen, with no detectable differences concerning frequencies and cell numbers between DNT/CD23Cre mice and CD23Cre mice (Fig 25A-E). But interestingly there was again a significant drop of DNT/GFP expressing cells from 40% of P1 cells to 9% of P2 and only 3% of P3 cells (Fig 35F, G). These results show that the plasma cell niche in the bone marrow, especially the P3 compartment, is replenished by cells that escaped Cre recombination, showing again the importance of this subset and its dependency on OxPhos and functional mitochondria.

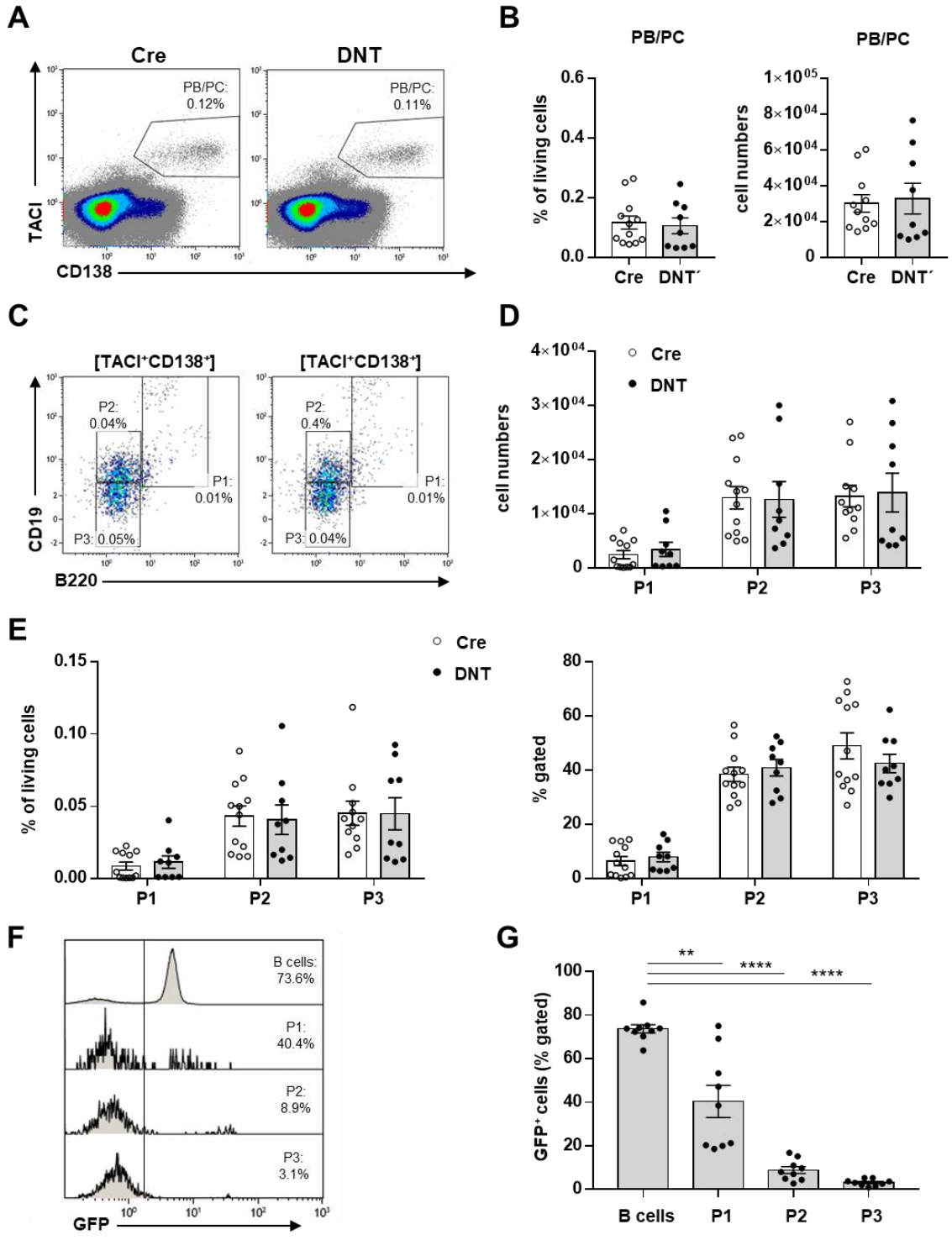
A
Cre
DNT
PB/PC: 0.12%
PB/PC: 0.11%
TACI
CD138
B
PB/PC
PB/PC
% of living cells
cell numbers
Cre
DNT´
C
[TACI⁺CD138⁺]
[TACI⁺CD138⁺]
P2: 0.04%
P1: 0.01%
P3: 0.05%
P2: 0.4%
P1: 0.01%
P3: 0.04%
CD19
B220
D
Cre
DNT
cell numbers
P1
P2
P3
E
Cre
DNT
% of living cells
% gated
F
B cells: 73.6%
P1: 40.4%
P2: 8.9%
P3: 3.1%
GFP
G
GFP⁺ cells (% gated)
B cells
P1
P2
P3

Figure 25 | Analysis of plasmablast and plasma cell populations in the bone marrow of unimmunized DNT/CD23Cre mice

Bone marrow cells from DNT/CD23Cre and CD23Cre mice were isolated and analysed by flow cytometry. **A) Representative dot blots** (merged from 3 mice per genotype) using anti-TACI and anti-CD138 antibodies. Plasma blasts (PB) and plasma cells (PC) are defined as $TACI^{+}CD138^{+}$. Numbers indicate the frequency of viable cells**. B) Frequency (left) and absolute cell number (right)** of PB/PCs shown in A. Bars at mean ± SEM; Symbols indicate individual mice; N=4, n=2-3 significance was calculated using t-test. **C) Representative dot blots** (merged from 3 mice per genotype) using anti CD19 and anti B220 antibodies, pre-gated on $TACI^{+}CD138^{+}$ cells as shown in A. P1 cells are defined as $CD19^{int}$, $B220^{int}$, P2 cells are $CD19^{int}B220^{low}$ and P3 cells are $CD19^{low}B220^{low}$. Numbers indicate the frequency of viable cells. **D) Absolute cell numbers** of PB/PC subpopulations shown in C. **E) Frequencies** of PB/PC subpopulations of living cells (left) and frequencies of $TACI^{+}CD138^{+}$ cells (right). **F) Representative flow cytometric analysis** (merged from 3 mice) of GFP expressing cells in B cell populations shown in C) from DNT/CD23Cre mice. B cells are defined as $CD19^{+}TACI^{-}CD138^{-}$. Numbers indicate the frequency of the parent population. **G) Frequencies** of GFP expressing B cell subsets shown in F. Bars at mean ± SEM; Symbols indicate individual mice; N=4, n=2-3.

[Figure partially adapted and modified after Urbanczyk et al., 2021.]

6.4.5. Analysis of serum antibody abundance

The abundance of Ig isotypes in the serum was quantified by ELISA and showed that levels of IgM were slightly, but not significantly, reduced in DNT/CD23Cre mice (Fig 26). They furthermore had with 0.16 mg/ml compared to 0.29 mg/ml in CD23Cre mice significantly reduced levels of IgA. Total IgG was also significantly reduced (0.9 mg/ml compared to 2.3 mg/ml in CD23Cre mice), with differing levels for the IgG subclasses: IgG1 and IgG2b were comparable, but IgG3 was significantly decreased in DNT/CD23Cre mice with 0.05 mg/ml compared to 0.24 mg/ml in CD23Cre mice. The strongest reduction by factor 54 was observed for IgG2c, which was barely detectable with 0.16 mg/ml in DNT/CD23Cre mice compared to 8.9 mg/ml in CD23Cre mice. These results show that a dysfunctional respiratory chain in B cells decreases the amounts and proportions of secreted Ig isotypes in the serum.

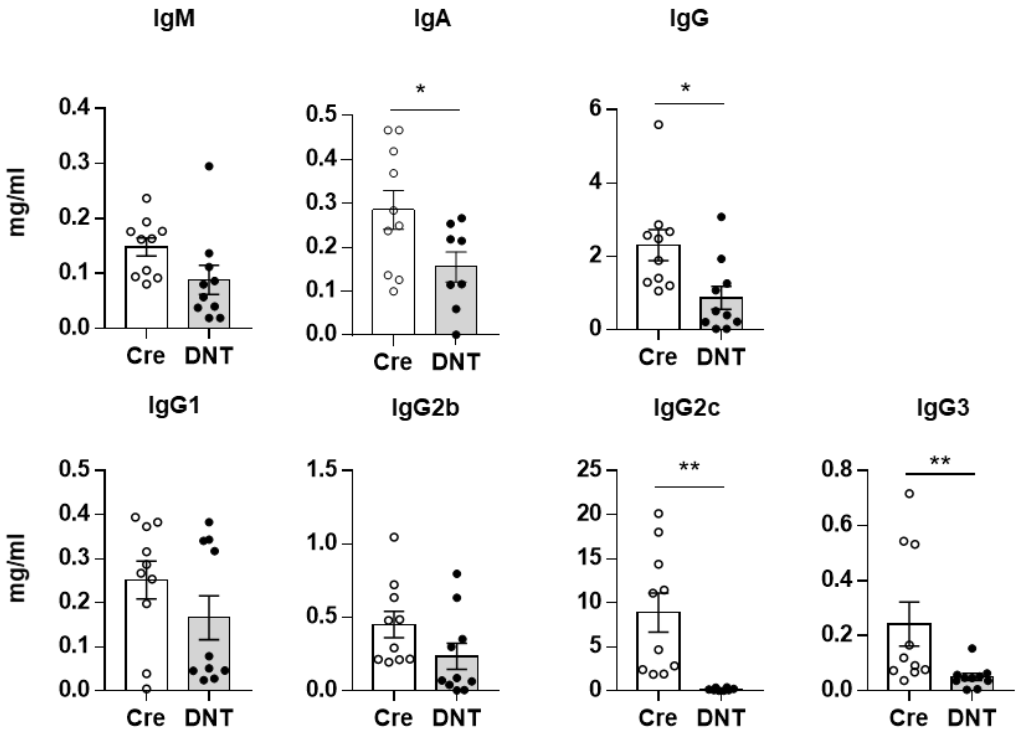

Figure 26 | Analysis of serum antibody levels in unimmunized DNT/CD23Cre mice
Serum from unimmunized DNT/CD23Cre and CD23Cre mice was analysed by ELISA and levels of IgM, IgA and IgG sub-classes were quantified. Bars at mean ± SEM; Symbols indicate individual mice; N=4, n=2-4; Statistical significance was calculated using t-test.
[Figure partially adapted and modified after Urbanczyk et al., 2021.]

6.5. Analysis of immunized DNT/CD23Cre mice

6.5.1. Analysis of the germinal centre reaction in the spleen

Based on the finding that the frequency of DNT/GFP expressing cells of GC B cells was significantly decreased compared to $CD19^+$ B cells in DNT/mb1Cre and DNT/CD23Cre mice, I hypothesised that the GC reaction is impaired. To test this hypothesis mice were immunized *i.p.* with SRBCs and spleen sections were analysed after 10 days using immunohistology and confocal microscopy. The size of the follicular mantle, determined by IgD staining, appeared comparable between the genotypes. However, the GC formation was significantly decreased in DNT/CD23Cre mice, judged by size of the GC, stained with the GC specific markers PNA and GL7 (Fig 27).

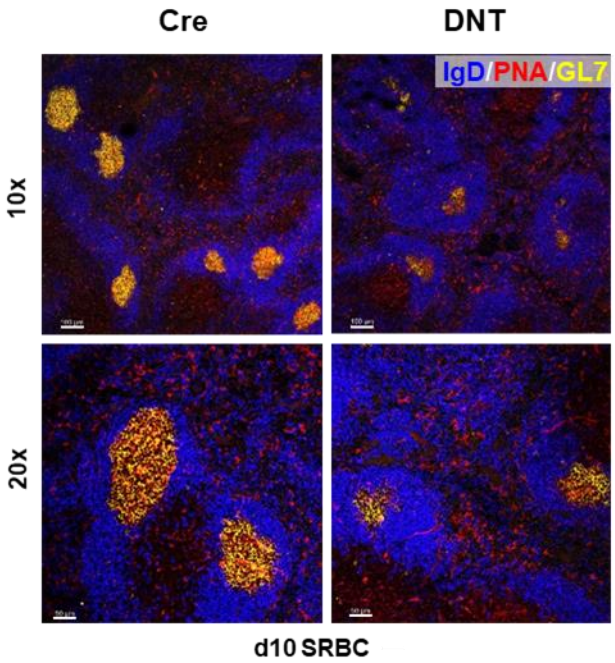

Figure 27 | Influence of DNT/CD23Cre expression on the germinal center formation
Immunohistology of spleen sections from DNT/CD23Cre and CD23Cre SRBC immunized mice (day 10) were stained with IgD (blue), PNA (red) and GL7 (yellow) and analysed using confocal microscopy. Orange areas (PNA^+GL7^+) areas represent the GC, and blue (IgD^+) areas represent the follicular mantle. 10x magnification and 100 µm scale bars in the upper panel; 20x magnification and 50 µm scale bars in the lower panel.
[Figure partially adapted and modified after Urbanczyk et al., 2021.]

6.5.2. Characterization of T-dependently immunized DNT/CD23Cre mice

Both, the decreased frequency in DNT/GFP expression in the GC and PC subsets in unimmunized mice (Fig 23C/D, Fig 24F/G, Fig 25F/G), and the decreased GC formation upon T cell-dependent immunization shown by histology (Fig 27), point to a role of the mtRC during the humoral immune response.

To get detailed insight into the T-dependent immune and memory response, mice were injected *i.p.* with NP-KLH in alum (d0) and boosted after 42 days with NP-KLH in PBS. Serum was taken weekly, and the mice were sacrificed 70 days after primary immunization. The course of the primary and secondary humoral immune response was followed by ELISA and showed that DNT/CD23Cre mice produced comparable amounts of antigen specific IgM in the serum, of both low (NP20) and high (NP4) affinity (Fig 28A). In contrast, low affine, antigen specific IgG was significantly decreased during both, the primary and secondary immune response in DNT/CD23Cre mice. High affine IgG was also significantly decreased during the secondary immune response in DNT/CD23Cre mice. To analyse the frequency and distribution of ASC subsets, flow cytometric analysis of the BM was performed 70 days after immunization (Fig 28B). The total PB and PC compartment, defined by $TACI^+CD138^+$, was comparable between DNT/CD23Cre and Cre mice (Fig 28D). Also, the ratios of P1 PBs, early P2 PCs and

mature P3 PCs were comparable, with slightly decreased P1 cell numbers and increased P3 cell numbers in DNT/CD23Cre mice, although this did not reach mathematical significance. The frequency of antigen-specific PCs, as defined by $TACI^+CD138^+$ and NP^+ on the surface, were significantly decreased in DNT/CD23Cre mice. Although it should be noted that using this method only detects IgM^+ and IgA^+ PB/PCs, as IgG^+ PCs no longer express a surface BCR. Further investigation of DNT/GFP expression revealed that while 3,5% of PCs in DNT/CD23Cre mice were expressing DNT/GFP, they were not NP+, at least on the surface (Fig 28C). The expression of DNT/GFP and surface-staining of NP were exclusive, indicating that B cells with dysfunctional mitochondria are not able to successfully complete PC generation. The subpopulations P1, P2 and P3 showed between 2% and 5% DNT/GFP expression with the highest DNT/GFP expression in the P2 compartment and the lowest in the P3 compartment (Fig 28E/F). Taken together, these data show that DNT/CD23Cre expression dampens the TD immune response, as shown in significantly decreased serum levels of antigen-specific IgG, decreased antigen-specific PCs in the BM, and importantly the finding that antigen-specific PCs in the BM did not express DNT/GFP.

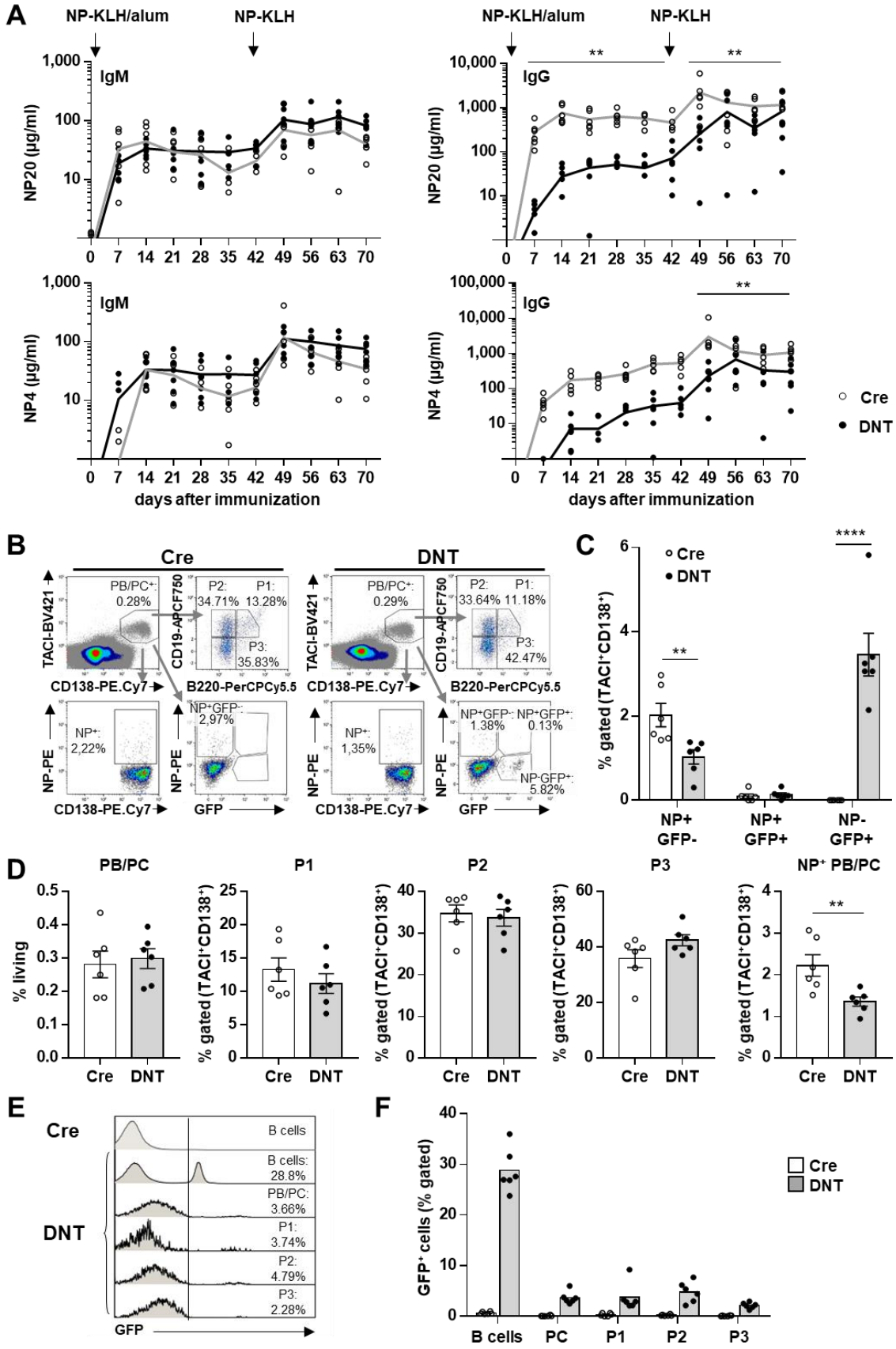

Figure 28 | Analysis of DNT/CD23Cre expression in the T dependent humoral immune response

DNT/CD23Cre and CD23Cre control mice were immunized i.p. with the TD antigen NP-KLH in alum on day 0. To induce a memory immune response, mice were boostered with NP-KLH in PBS i.p. on day 42**. A) Serum** was taken weekly and analysed with ELISA for the presence of NP-specific antibodies with low affinity (upper panel) and high affinity (lower panel) of the isotypes IgM (left) and IgG (right). Line at mean; Symbols indicate individual mice; N=2, n=3; Significance was calculated using 2-way ANOVA of AUC. Mice were sacrificed after 70 days and plasma blasts and cells of the bone marrow were analysed with flow cytometry (B)-F)). **B) Representative, merged flow cytometric analysis** of plasma cells, defined as TACI+CD138+. Further subpopulations were defined according to CD19 and B220 expression: P1 are CD19int B220int, P2 are CD19int B220low, and P3 are CD19low B220low. Antigen specificity was determined by surface staining with NP-PE. Numbers indicate the frequency of viable cells or the parent population. **C) Frequencies** of NP-GFP+, NP+GFP+ and NP+GFP- cells in the TACI+CD138+ compartment shown in B). **D) Frequencies** of total plasma cells in the bone marrow and the proportions of the subpopulations P1, P2, P3 and NP-specific plasma cells shown in B); Data shown as mean values; Symbols indicate individual mice; N=2, n=3; significance was calculated using t-test**. E) Representative, merged flow cytometric analysis** of GFP/DNT expression in the indicated plasma cell populations shown in B). Numbers indicate the frequency of the parent population**. F) Frequencies** of GFP/DNT expressing cells in the indicated plasma cell populations shown in B). B cells are defined as CD19+ with TACI+CD138+ cells excluded. Data shown as mean values; Symbols indicate individual mice; N=2, n=3
[Figure partially adapted and modified after Urbanczyk et al., 2021.]

6.5.3. Characterization of T-independently immunized DNT/CD23Cre mice

In contrast to the TD immune response, where protein antigens are processed and presented on MHC class II molecules for the recognition by helper T cells, the TI immune response does not require T cell help. TI antigens are classified into type I and type II, with the former including mitogenic stimuli such as LPS, poly-IC, or CpG that induce polyclonal B cell activation that is mediated by Toll-like receptors. Type II antigens on the other hand, are polysaccharides that engage the BCR, and thereby induce an antigen-specific B cell response (Obukhanych and Nussenzweig, 2006). Furthermore, while mainly FO B cells engage in TD immune responses, the MZ B cells subset is predominantly activated by TI antigens. Observing an impaired immune response after TD immunization in DNT/CD23Cre mice (Fig28) led to the question whether functional mitochondrial respiration in B cells is also required during a TI antigen challenge. Therefore, DNT/CD23Cre mice and CD23Cre control mice were injected *i.p.* with the type II antigen NP-Ficoll. Serum was taken at day 0, 7 and 14 after immunisation and cells from spleen and bone marrow were analysed by flow cytometry at d7 and d14. The flow cytometric analysis of antigen specific PB/PC subsets was performed as described earlier. Interestingly, there were significantly reduced cell numbers of PB/PCs at both, d7 and d14, in the spleen from DNT/CD23Cre mice (Fig 29A, C). The reduction was about 2-fold on d7 and 2.5-fold on d14. The frequencies of P0-P3 subsets were comparable at both time points in the spleen. In contrast, the PB/PC compartment in the bone marrow was comparable at both time points although a slight reduction, that did not reach statistical significance, was observable on d14 (Fig 29B, D). Again, the frequencies of P1, P2 and P3 cells were comparable at both time points. Interestingly, analysing the frequency of antigen-specific B cells, defined as $CD19^+$ but not $TACI^+CD138^+$, and antigen-specific PB/PCs showed no significant differences between DNT/CD23Cre and CD23Cre mice at all time points and organs (Fig 29E). Intriguingly, analysing the DNT/GFP expression in splenic B cell and PB/PC subsets from DNT/CD23Cre

mice showed a drastic drop of DNT/GFP expressing cells in the P1 compartment (Fig 29F): While 87% of P0 cells expressed DNT/GFP, only 9.3% of P1 cells showed DNT/GFP expression. The frequency of DNT/GFP expressing cells in the P2 compartment was slightly increased to 14.2%, while the P3 compartment showed the lowest DNT/GFP expression of only 5.9%. A similar pattern was observed in the bone marrow, where 14.9% of P1 cells express DNT/GFP that declines to 5.8% in the P2 compartment and 2.7% in the P3 compartment. Analysing the frequency of DNT/GFP expressing antigen-specific PB/PCs in spleen and bone marrow of DNT/CD23Cre mice showed two interesting aspects: There is a strong reduction of DNT/GFP expressing cells in the bone marrow compared to the spleen at all time points, and furthermore there is a strong reduction of DNT/GFP expressing cells in the spleen on d14 compared to d7 (Fig 29F). While 86.3% of antigen-specific PB/PCs in the spleen express DNT/GFP on d7, it decreases to 53.3% on d14. The frequency of DNT/GFP expressing, antigen-specific PB/PCs in the bone marrow was 27% and 29.6% on d7 and d14, respectively.

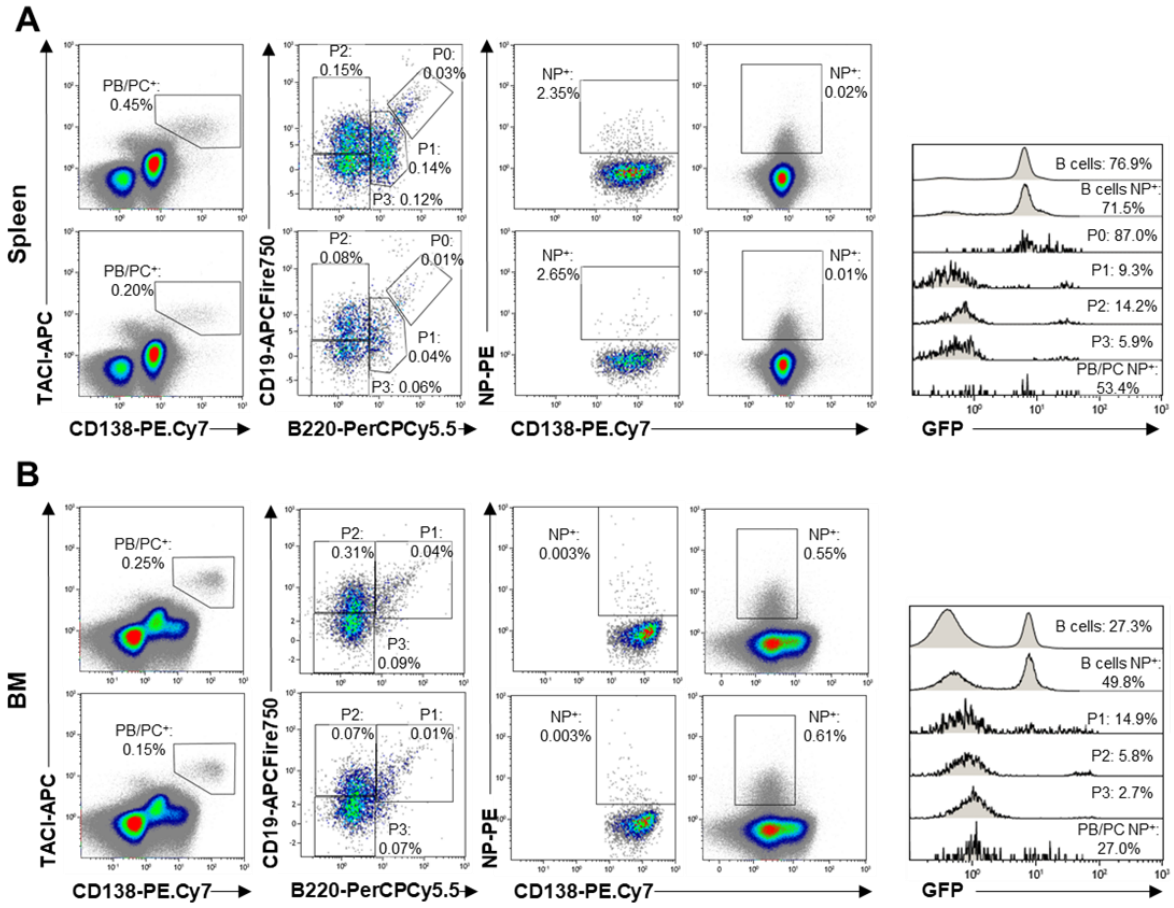
A
Spleen
TACI-APC
CD138-PE.Cy7
PB/PC+: 0.45%
PB/PC+: 0.20%
CD19-APCFire750
B220-PerCPCy5.5
P2: 0.15%
P0: 0.03%
P1: 0.14%
P3: 0.12%
P2: 0.08%
P0: 0.01%
P1: 0.04%
P3: 0.06%
NP-PE
NP+: 2.35%
NP+: 0.02%
NP+: 2.65%
NP+: 0.01%
B cells: 76.9%
B cells NP+: 71.5%
P0: 87.0%
P1: 9.3%
P2: 14.2%
P3: 5.9%
PB/PC NP+: 53.4%
GFP
B
BM
PB/PC+: 0.25%
PB/PC+: 0.15%
P2: 0.31%
P1: 0.04%
P3: 0.09%
P2: 0.07%
P1: 0.01%
P3: 0.07%
NP+: 0.003%
NP+: 0.55%
NP+: 0.003%
NP+: 0.61%
B cells: 27.3%
B cells NP+: 49.8%
P1: 14.9%
P2: 5.8%
P3: 2.7%
PB/PC NP+: 27.0%

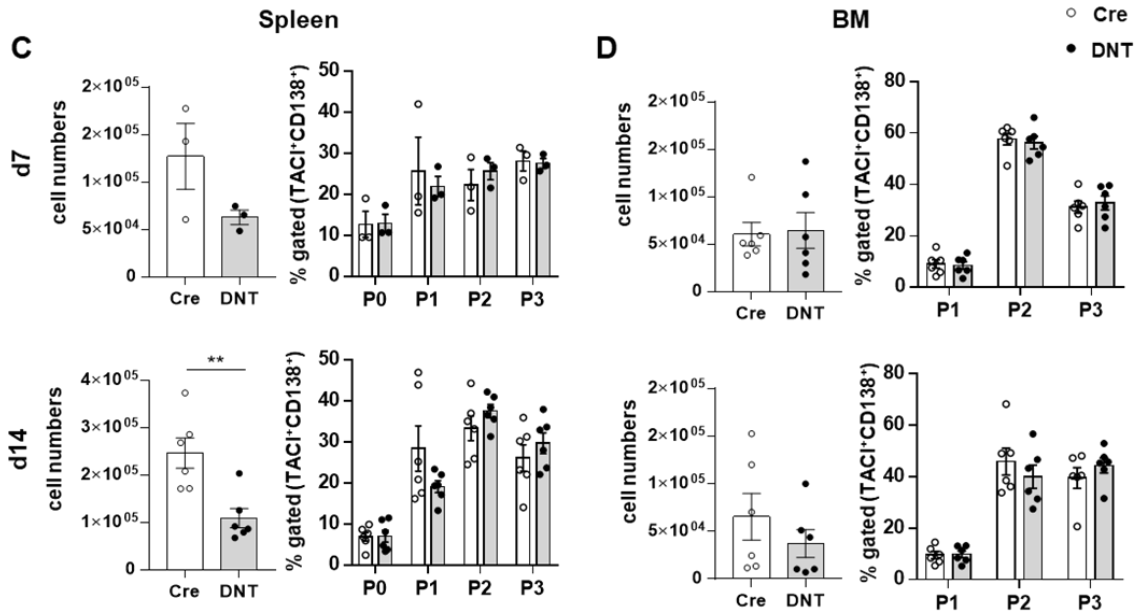
C
Spleen
d7
d14
cell numbers
Cre
DNT
% gated (TACI+CD138+)
P0
P1
P2
P3
**
D
BM
Cre
DNT

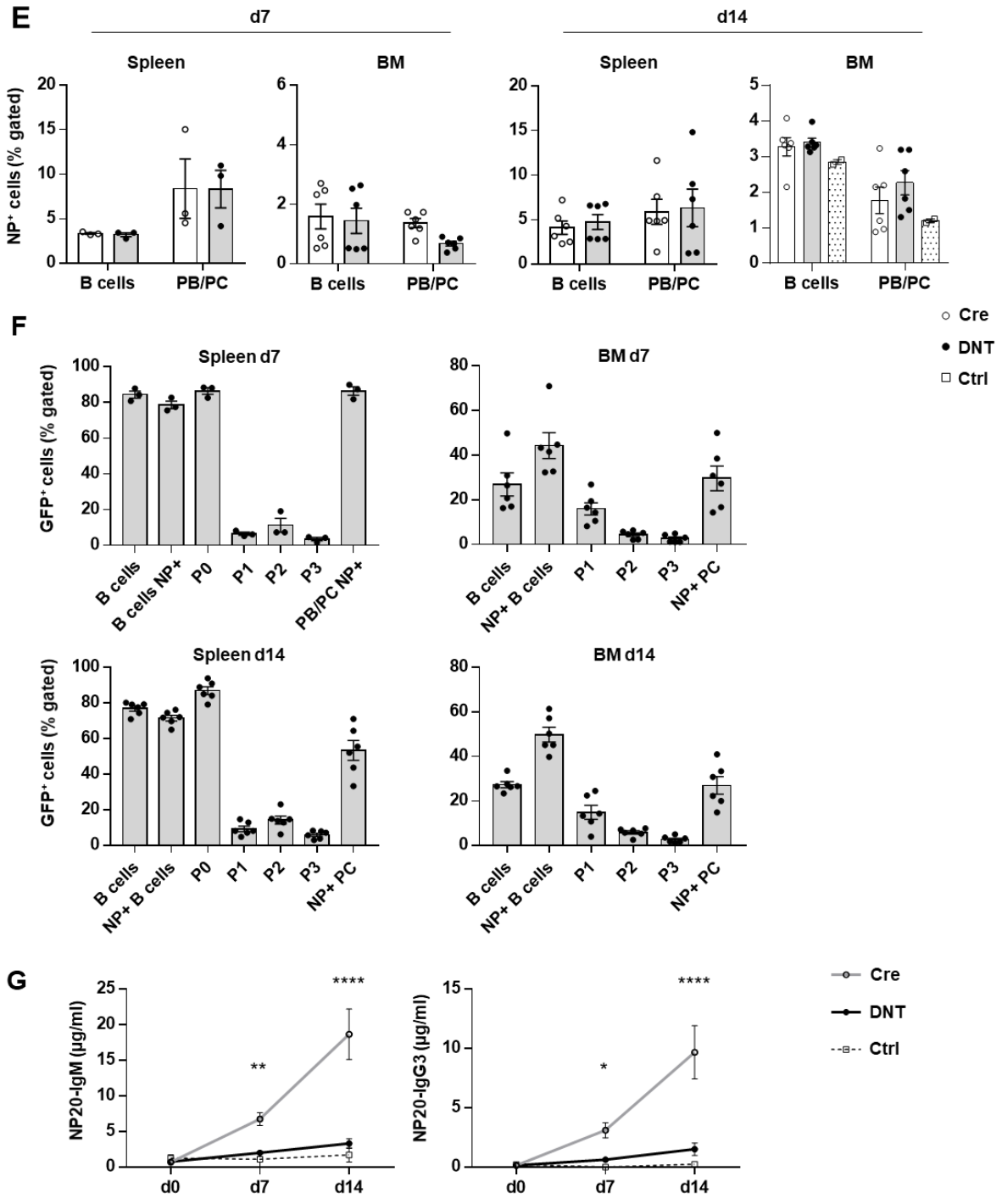

Figure 29 | Analysis of DNT/CD23Cre expression in the T independent humoral immune response

DNT/CD23Cre and CD23Cre control mice were immunized i.p. with the TI antigen NP-Ficoll in PBS on day 0. Serum was taken weekly, animals were sacrificed on d7 and d14 and plasma blasts (PB) and cells (PC) of the spleen and bone marrow were analysed with flow cytometry. One WT mouse per experiment was injected with PBS only and served as a control (Ctrl). **A) Representative, merged flow cytometric analysis** (of 3 mice per genotype) of splenic plasma cells, defined as TACI+CD138+. Further subpopulations were defined according to CD19 and B220 expression: P0 are $CD19^+B220^+$, P1 are CD19int B220int, P2 are CD19int B220low, and P3 are CD19low B220low. Antigen specificity was determined by surface staining with NP-PE. Numbers indicate the frequency of viable cells or the parent population. **B) Representative, merged flow cytometric analysis** (of 3 mice per genotype) of bone marrow plasma cells, defined as TACI+CD138+. Further subpopulations P1, P2, and P3 were defined according to CD19 and B220 as described in A). **C) Cell numbers** of PB/PCs and frequencies of subpopulations (gated on PB/PCs) in the spleen. **D) Cell numbers** of PB/PCs and frequencies of subpopulations (gated on PB/PCs) in the bone marrow. **E) Frequencies** of antigen-specific B cells, defined as $CD19^+$ with $TACI^+CD138^+$ excluded, and antigen-specific PB/PCs, defined as $TACI^+CD138^+$, shown in A) and B) on d7 (left) and d14 (right) after immunization**. F) Frequencies** of GFP/DNT expressing cells in the B and plasma cell populations in the spleen (left) and bone marrow (right) shown in A) and B) on d7 (top) and d14 (bottom) after immunization. B cells are defined as $CD19^+$ with $TACI^+CD138^+$ cells excluded. Line at mean ±SEM; Symbols indicate individual mice; N=2, n=3. **G) Serum** was taken weekly and analysed with ELISA for the presence of NP-specific antibodies with low affinity (NP20) of the isotypes IgM (left) and IgG3 (right). Data shown as mean values ± SEM; N=2, n=3-6; Significance was calculated using 2-way ANOVA.
[Figure partially adapted and modified after Urbanczyk et al., 2021.]

The course of the immune response regarding the generation of antigen-specific Abs was analysed by ELISA (Fig 29G). Remarkably, there were only minimal amounts of antigen-specific IgM and IgG3 detectable at all time points in the serum from DNT/CD23Cre mice, which is in accordance with decreased PB/PC numbers in the spleen. However, the reduction in antigen-specific Abs is much more pronounced than the reduction of PB/PCs, indicating that the majority or PB/PCs do not sufficiently produce and/or secrete Abs. Since more than half of splenic, antigen-specific PB/PCs show DNT/GFP expression, I conclude that the DNT/GFP expressing PB/PCs do not efficiently produce and/or secrete Abs, which would explain the severely reduced levels of antigen-specific Abs in the serum.

Taken together, this experiment showed that mitochondrial respiration in mature and activated B cells is required to successfully mount a TI immune response. This was evident in decreased PB/PC numbers in the spleen on d7 and d14, and most importantly by strongly reduced antigen-specific IgM and IgG3 Abs in the serum.

6.6. *In vitro* analyses of splenic DNT/CD23Cre expressing B cells

To get detailed insights into underlying mechanisms comprising the plasma cell differentiation in DNT/CD23Cre mice, I switched to *in vitro* systems where splenic B cells of DNT/CD23Cre and CD23Cre mice were isolated and activated *in vitro* with LPS or with LPS, α-CD40, α-BCR,

IL4, IL5, RA and TGFβ. While the former robustly induces proliferation and PB differentiation that mainly secrete IgM, the latter induces PB differentiation and CSR to IgA and IgG.

6.6.1. Analysis of mitochondrial morphology in DNT/CD23Cre expressing B cells

Prior to analysing *in vitro* B cell activation and PC differentiation in DNT/CD23Cre mice, I aimed to clarify if decreasing mtDNA levels in B cells affects the structure of mitochondria. To this end, naïve and activated B cells (LPS, day3) were analysed by electron microscopy (Fig 30, pictures kindly provided by Ursula Schlötzer-Schrehardt). The size and number of mitochondria appears to be comparable between DNT/CD23Cre and CD23Cre mice in resting B cells. However, mitochondrial cristae structures in LPS blasts generated from DNT/CD23Cre mice were already visibly loosened at this stage, which is in accordance with decreased mtDNA levels in these cells (Fig 30A, Fig. 11B). These effects of mtDNA depletion on mitochondrial morphology were drastically enhanced on d3 after LPS activation: The mitochondrial cristae structures were completely disrupted at this stage and in addition, the mitochondria were greatly enlarged. The electron density was analysed using ImageJ and was significantly decreased in both, resting and activated B cells, from DNT/CD23Cre mice compared to CD23Cre controls (Fig 30B).

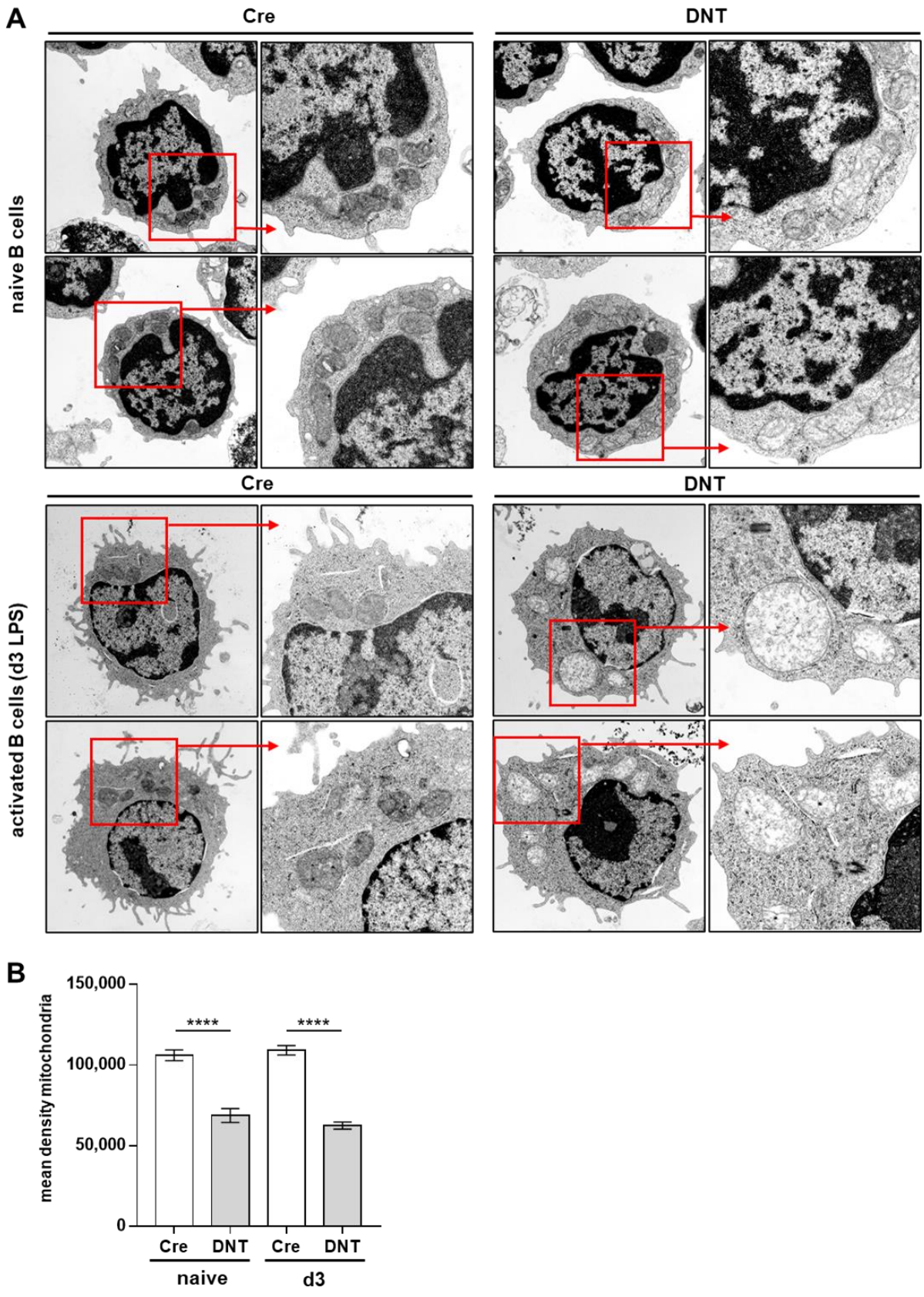

Figure 30 | Electron microscopy of naïve and activated B cells from DNT/CD23Cre mice

A) Splenic B cells (resting or stimulated with LPS for 3d) from DNT/CD23Cre and CD23Cre mice were fixed, embedded and analysed by transmission electron microscopy. Upper panel: naïve B cells (x 10.000, enlargements indicated by arrows: x 21.560), lower panel: d3 LPS blasts (x 6000, enlargements x 16.700). Electron microscopy was kindly performed by Ursula Schlötzer-Schrehardt (Department of Ophthalmology, Erlangen). **B) Electron density** of mitochondria was determined using ImageJ. Data shown as mean values -/+ SEM; significance was calculated using 2-way ANOVA.
[Figure partially adapted and modified after Urbanczyk et al., 2021.]

6.6.2. Analysis of proliferation and survival of LPS activated DNT/CD23Cre expressing B cells

The first question I addressed using *in vitro* analysis was how a dysfunctional mtRC affects the survival and proliferation capacity of activated DNT/CD23Cre expressing B cells. Detection of viable cells was performed by flow cytometry using Annexin-V and PI staining (Fig 31A), on day 3 (top) and day 6 (bottom) after LPS activation (Vermes et al., 1995). Viable cells are defined as Annexin-V^-PI^-, apoptotic cells as Annexin-V^+PI^- and necrotic cells are Annexin$^{+/-}PI^+$. The frequency of viable cells at day 3 was 78% in DNT/CD23Cre expressing cell cultures compared to 70% in Cre control cultures, although this was statistically not significant (Fig 31A, B). While the frequency of necrotic cells was comparable, there were only 4% apoptotic cells in DNT/CD23Cre cultures compare to 7% in Cre control cultures. At day 6 after LPS activation the frequency of viable cells was slightly decreased in DNT/CD23Cre culture, although this was not statistically significant. Since there were less than 20% viable cells in both cultures at this time point, further experiments were performed on day 3 after activation. To analyse the impact of DNT/CD23Cre expression on cell proliferation, splenic B cells were isolated and stained with the cell proliferation dye eFluor450 prior to LPS activation. This fluorescent dye binds to any cellular proteins containing primary amines, and as cells divide, the dye is distributed equally between daughter cells that can be measured as successive halving of the fluorescence intensity of the dye. Cells were analysed by flow cytometry after 3 days (Fig 31C). This experiment revealed that DNT/CD23Cre expressing cells proliferate initially well up to 4 times, but there were significantly less DNT/CD23Cre expressing cells that divided 5 or 6 times (Fig 31D). The cell intrinsic effect of DNT/CD23Cre expression on cell proliferation becomes even more apparent when distinguished between GFP/DNT expressing and non-expressing cells of DNT/CD23Cre mice (Fig 31E, F).

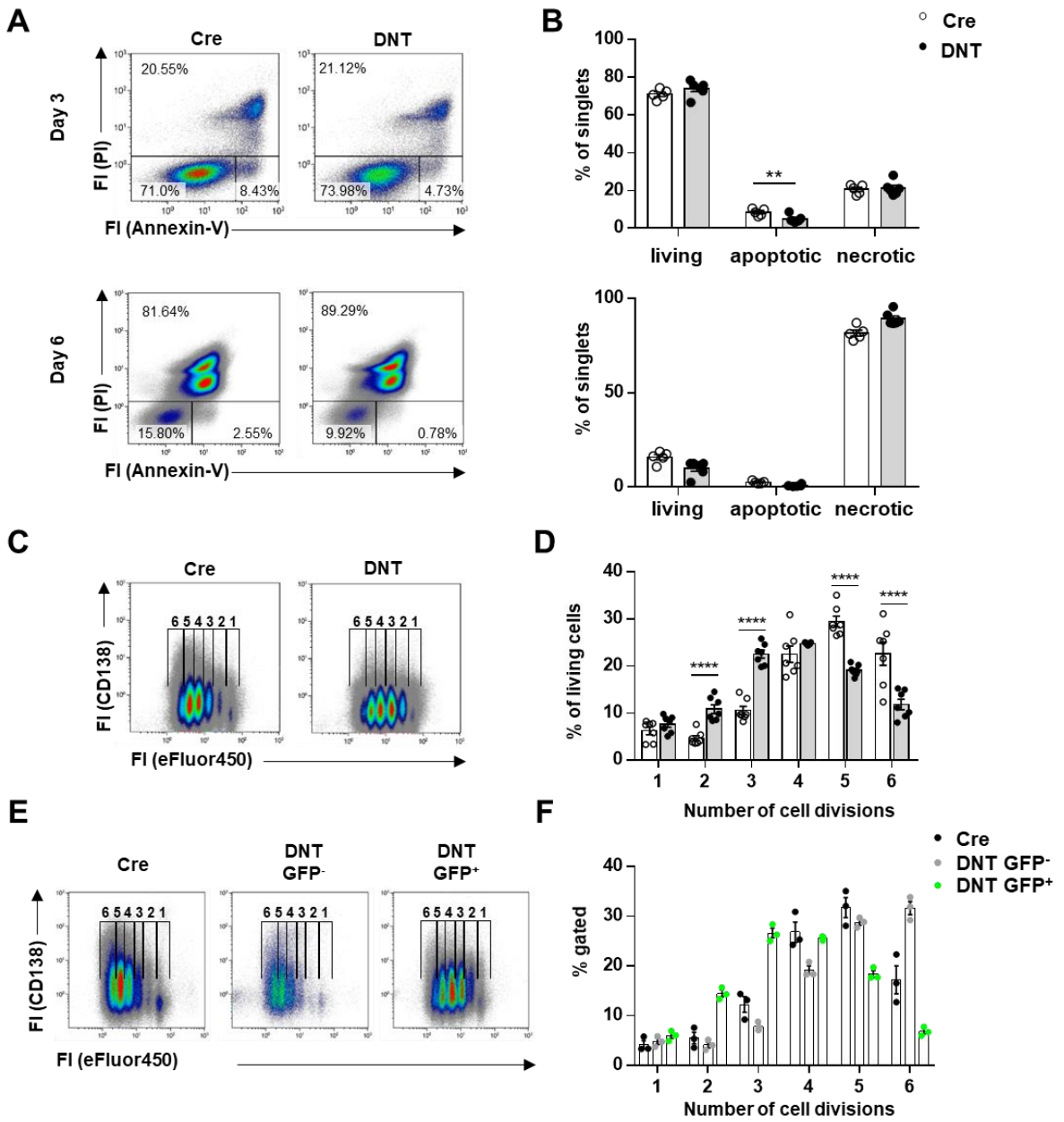

Figure 31 | Analysis of survival and proliferation in DNT/CD23Cre and CD23Cre LPS activated B cells

Splenic B cells from DNT/CD23Cre and CD23Cre mice were isolated, stimulated *in vitro* with LPS and analysed after 3 days. **A) Representative, merged flow cytometric analysis** of cells stained with propidium iodide (PI) and Annexin-V. Living cells are defined as double negative, apoptotic cells are Annexin-V+PI- and necrotic cells are PI+. **B) Frequencies** of living, apoptotic and necrotic cells 3 days after LPS activation shown in A). Data shown as mean values -/+ SEM; N=2, n=2-4; significance was calculated using 2-way ANOVA. **C) Isolated B cells** were labelled with eFluor450 prior to stimulation and analysed after 3 days using flow cytometry. A representative, merged dot blot is shown. **D) Frequencies** of cell populations defined according to the number of cell divisions 3 days after LPS activation. Data shown as mean values -/+ SEM; N=2, n=3; significance was calculated using 2-way ANOVA. **E) Isolated B cells** were labelled with eFluor450 prior to stimulation and analysed after 3 days using flow cytometry. GFP+ and GFP- cells were analysed separately in DNT cultures. A representative, merged dot blot is shown. **F) Frequencies** of cell populations defined according to the number of cell divisions 3 days after LPS activation shown in E. Data shown as mean values -/+ SEM; N=2, n=3; significance was calculated using 2-way ANOVA.

[Figure partially adapted and modified after Urbanczyk et al., 2021.]

6.6.3. Analysis of the influence of DNT/CD23Cre expression on plasma blast differentiation

The decreased frequency of GFP/DNT expressing cells in the plasma cell compartment of DNT/CD23Cre mice (Fig 24F, 25F) indicates an intrinsic impact of a dysfunctional mtRC on PC differentiation. To ensure that further *in vitro* experiments were representative for the *in vivo* phenotype, we first wanted to confirm that DNT/CD23Cre expression impacts PB differentiation *in vitro*. To this end splenic B cells were isolated, activated with LPS and analysed after 3 days using flow cytometry. Activated B cells and PBs were identified by staining with anti-TACI and anti-CD138 (Fig 32A). While the frequency of activated, $TACI^+$ B cells was significantly increased in cultures of DNT/CD23Cre mice, there were significantly less $TACI^+CD138^{high}$ PBs detected (Fig 32B). Comparing the frequencies of GFP/DNT expressing cells in naïve B cells, $TACI^+$ cells and $TACI^+CD138^{high}$ PBs of DNT/CD23Cre mice revealed that the proportion of GFP/DNT expressing cells increases in activated, TACI-expressing cells, but significantly decreases during plasma blast differentiation (Fig 32C, D). There is an initial increase from 74% to 91% of GFP/DNT expressing cells from naïve B cells to activated $TACI^+$ B cells, while only 53% of $TACI^+CD138^{high}$ plasma blasts expressed GFP/DNT. Flow cytometric analysis of intracellular BLIMP1 expression confirmed decreased plasma blast development in DNT/CD23Cre mice (Fig 32E). While the frequency of $CD138^+BLIMP1^-$ cells was comparable between DNT/CD23Cre and CD23Cre mice, there were significantly less $CD138^-BLIMP1^+$ and $CD138^+BLIMP1^+$ cells detected in DNT/CD23Cre cultures (Fig 32F). To determine if the decreased plasma blast development in DNT/CD23Cre mice is a consequence of the observed impaired proliferation, the frequency of $CD138^+$ cells, gated on cells that divided 4 to 6 times, was determined by flow cytometry. Distinghuishing between DNT/GFP-expressing and -non-expressing cells in DNT/CD23Cre mice showed significantly less $CD138^+$ cells in DNT/GFP-expressing cells (Fig 32G, H). These results indicate that a dysfunctional mtRC impaired plasma blast differentiation, at least partially independent of its effect on cell proliferation.

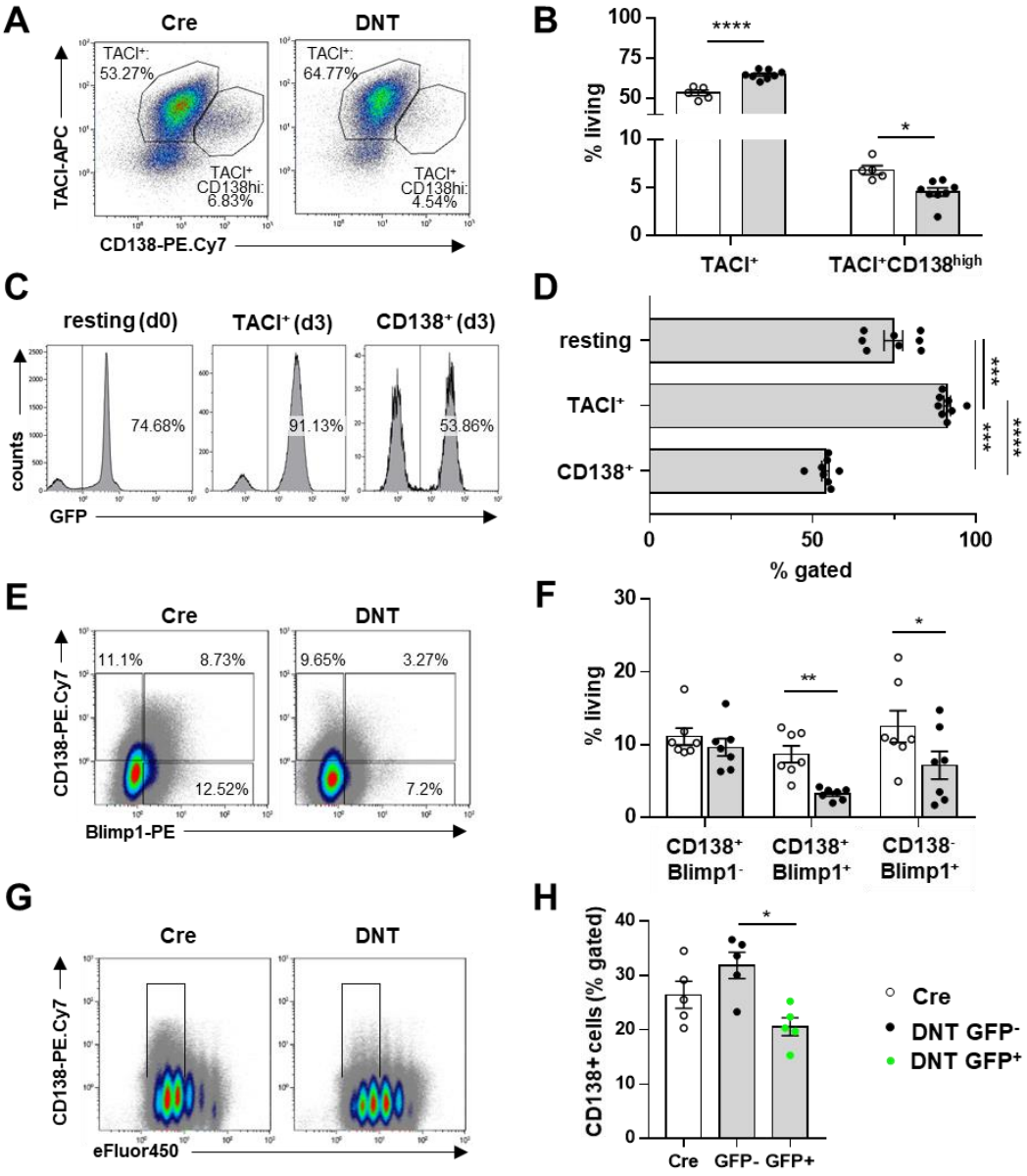

Figure 32 | Flow cytometric analysis of the influence of DNT/CD23Cre expression during in vitro plasma blast differentiation

Splenic B cells from DNT/CD23Cre and CD23Cre mice were isolated, stimulated in vitro with LPS and analysed after 3 days using flow cytometry. **A) Representative, merged flow cytometric analysis** of activated B cells, defined as TACI+, and plasma blasts, defined as CD138+. **B) Frequencies** of TACI+ and CD138+ cells 3 days after LPS activation from DNT/CD23Cre and CD23Cre mice. Data shown as mean values -/+ SEM; N=2, n=2-4; significance was calculated using 2-way ANOVA. **C) Representative, merged flow cytometric analysis** of CD138 and BLIMP1 expressing cells 3 days after LPS activation from DNT/CD23Cre and CD23Cre mice. **D) Frequencies** of CD138+BLIMP1-, CD138+BLIMP1+ and CD138-BLIMP1+ cells shown in C). Data shown as mean values -/+ SEM; N=2, n=3-4; significance was calculated using 2-way ANOVA. **E) Representative, merged flow cytometric analysis** of GFP/DNT expressing naive, TACI+ and CD138+ B cells from DNT/CD23Cre mice. **F) Frequencies** of GFP/DNT expressing cells of the indicated populations shown in A) and E). **G) Representative, merged flow cytometric analysis** of eFluor450 and CD138. Gates were set on cells that divided 4 to 6 times and further analysed for the frequencies of CD138+ cells. **H) Frequencies** of CD138+ cells after 4-6 cell divisions. Bars at mean; Symbols indicate individual mice; N=2, n=2-3; statistical significance was calculated using t-test.
[Figure partially adapted and modified after Urbanczyk et al., 2021.]

Decreased plasma blast differentiation and BLIMP1 expression in DNT/CD23Cre expressing *in vitro* activated B cells was confirmed by Western Blot and qPCR analysis (Fig 33). DNT/CD23Cre and CD23Cre cells were harvested on day 3 and protein abundance was quantified relative to the expression of actin. While the abundance of IRF4 was comparable, there was significantly less BLIMP1, XBP1 and IgM expression in DNT/CD23Cre expressing B cells detectable (Fig 33A, B). Importantly, decreased BLIMP1 expression was also confirmed on transcriptional level using qPCR (Fig 33C).

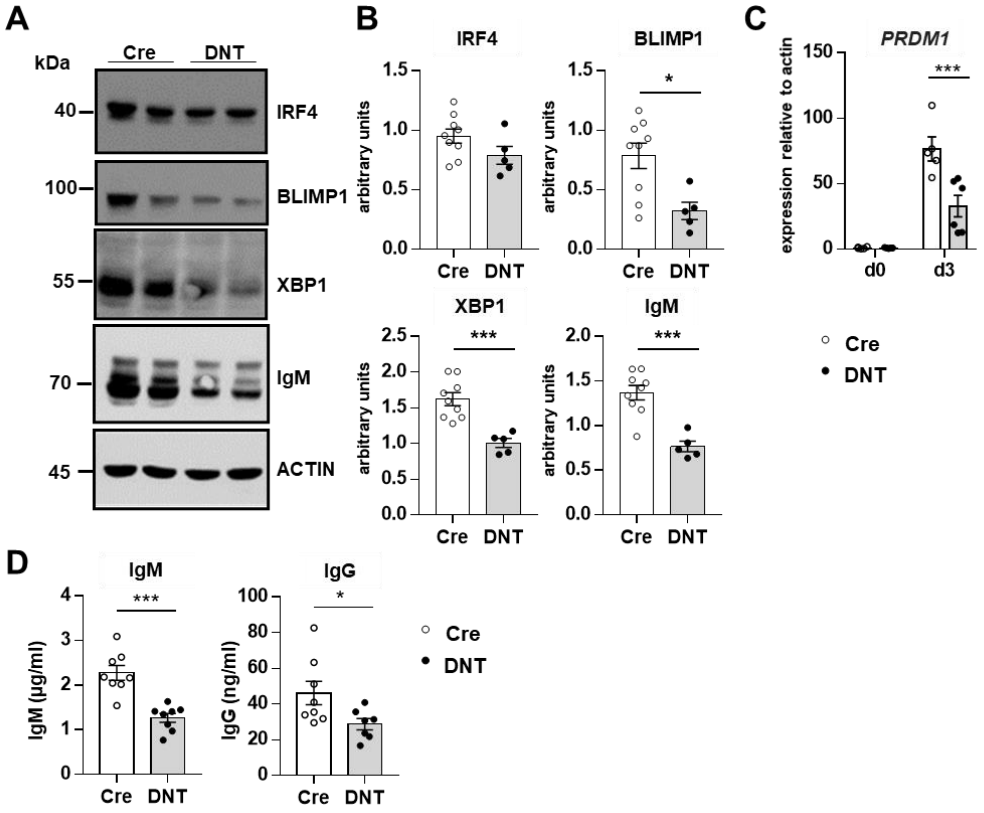

Figure 33 | Analysis of plasma cell markers and Ab secretion in DNT/CD23Cre expressing LPS blasts
Splenic B cells were isolated from DNT/CD23Cre and CD23Cre mice, stimulated in vitro with LPS and analysed after 3 days. **A) Cell lysates** were separated by 10% SDS-PAGE. Proteins were transferred onto a nitrocellulose membrane and stained with antibodies indicated on the right. Standards for molecular mass are depicted on the left. A representative blot with two mice per genotype is shown**. B) Quantification** of IRF4, BLIMP1, XBP1, IgM expression normalized to actin expression from A. Data shown as mean -/+ SEM; Symbols indicate individual mice; N=2, n = 2-4. Significance was calculated using t-test. **C) RNA was isolated** using RNeasy kit (Quiagen) and converted into cDNA. Expression of *PRDM1* which encodes BLIMP1 was evaluated by SYBR Green qPCR, analysed by ΔΔ CT and normalized to actin. Data shown as mean -/+ SEM; Symbols indicate individual mice; N=2, n=3. Significance was calculated using 2-way ANOVA. (qPCR analysis was kindly performed by Leonie Weckwerth and Jana Thomas). **D) The supernatant was harvested** after 3 days, and secreted IgM and IgG was quantified by ELISA. Data shown as mean ± SEM. Symbols indicate individual mice. N=2, n=4. Significance was calculated using t-test.
[Figure partially adapted and modified after Urbanczyk et al., 2021.]

Antibody production was determined by analysing the amounts of secreted antibodies in the supernatant of in vitro activated B cells on day 3 after activation with LPS by ELISA. In accordance with decreased IgM expression in activated DNT/CD23Cre expressing B cells

shown by Western Blot analysis, a significantly reduced amount of secreted IgM and IgG could be shown by ELISA (Fig 33D).

6.6.4. Analysis of the influence of DNT/CD23Cre expression on *in vitro* class switch recombination in B cells

Decreased antigen specific serum IgG in DNT/CD23Cre mice (Fig 28A, 29G) could be a consequence of the observed impaired GC reaction (Fig 27). To get detailed insights into B-cell intrinsic effects of DNT/CD23Cre expression on class switch recombination, splenic B cells were stimulated *in vitro* with LPS, α-CD40, α-BCR, IL4, IL5, RA and TGFβ to induce class switch recombination to IgG and IgA (Chiu et al., 2019, modified by W. Schuh). First, the frequency of viable cells was determined by flow cytometry at day 4, 7 and 9 after activation using viability dye as well as forward and side scatter (Fig 35A). While the frequency of viable cells was comparable on day 4, DNT/CD23Cre expression significantly decreased the frequency of viable cells 7 and 9 days after activation. Furthermore, at these time points drastic morphologic changes were observed in DNT/CD23 expressing activated B cells using forward and side scatter properties in flow cytometry (Fig 35C). Therefore, further class switch recombination analysis was performed on day 4 after activation, when viability and cell morphology were comparable between DNT/CD23Cre and CD23Cre. To analyse the frequency of IgA and IgG class switched B cells, intracellular staining with the respective antibodies and analyses by flow cytometry was performed (Fig 35B). DNT/CD23Cre expressing cells showed decreased class switch recombination since a significant higher percentage of cells still expressed IgM (Fig 35E). The frequency of IgA^+ cells was comparable, but DNT/CD23Cre expression significantly reduced the frequency of IgG^+ cells by ~30%. Further flow cytometric analysis of the frequency of GFP/DNT expressing cells showed significantly less GFP/DNT^+ cells only in the IgA^+ fraction compared to unswitched, IgM^+ cells (Fig 35F, G). These data show that DNT/GFP expression interferes with class switch recombination *in vitro*.

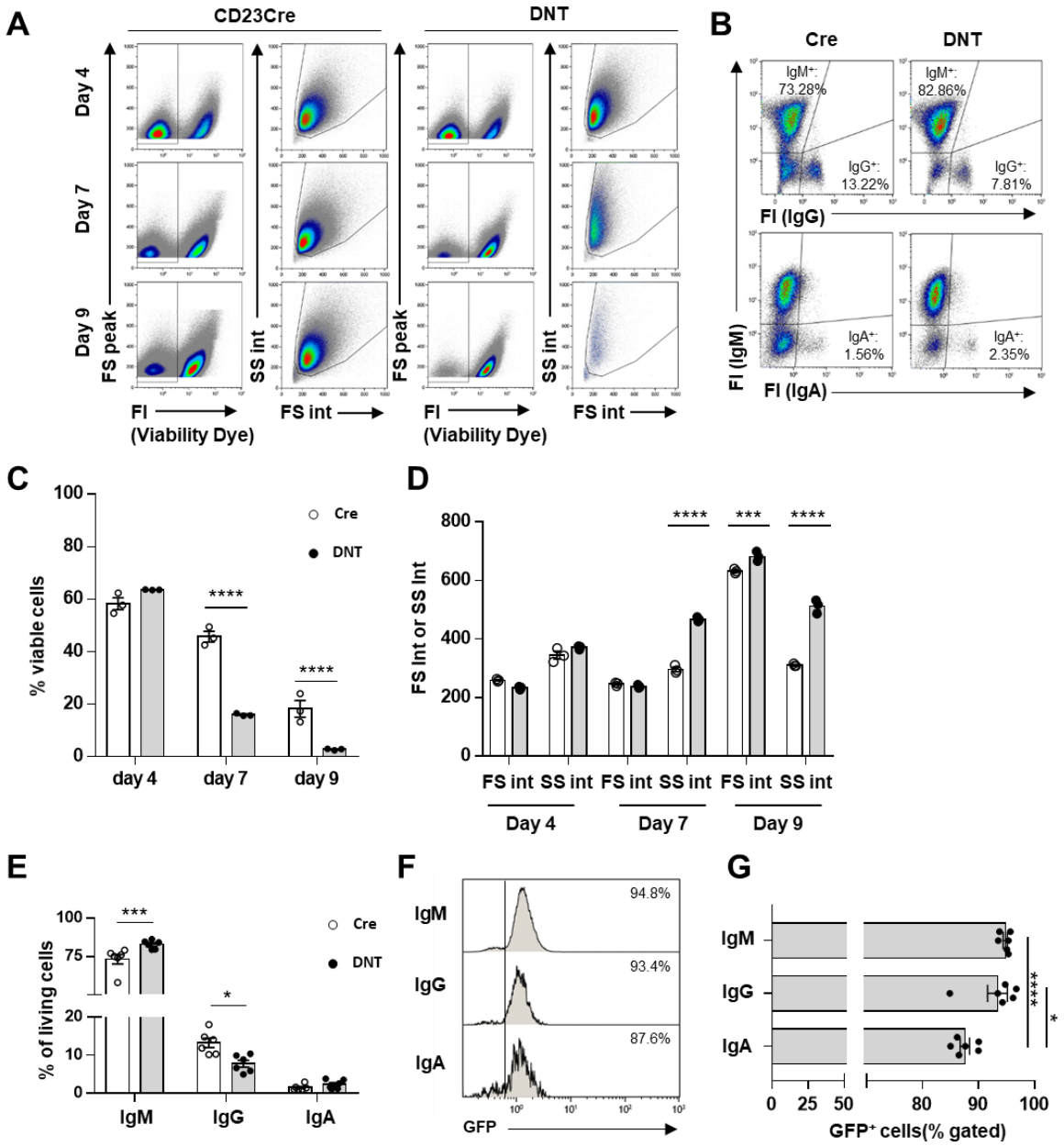

Figure 34 | Analysis of the influence of DNT/CD23Cre expression on in vitro class switch recombination
Splenic B cells from DNT/CD23Cre and CD23Cre mice were isolated and stimulated in vitro with LPS, anti CD40 antibody, IL-4, IL-5, TGFβ and retinoic acid. **A) Representative, merged flow cytometric analysis** of living cells, detected using viability dye and forward/side scatter at indicated time points. **B) Representative, merged flow cytometric analysis** on day 4 after activation. Cells were stained intracellularly with anti-IgM, anti-IgG (top panel) and anti-IgA (bottom panel) **C) Frequencies** of living cells shown in A). Data shown as mean values ± SEM; Symbols indicate individual mice. N=1, n=3. Significance was calculated using 2-way ANOVA. **D) Quantification** of forward and side scatter at indicated time points shown in A). Data shown as mean values ± SEM; Symbols indicate individual mice. N=1, n=3. Significance was calculated using 2-way ANOVA. **E) Frequencies** of unswitched IgM+ and class switched IgG+ and IgA+ cells on day 4 after activation shown in B. Data shown as mean values ± SEM; Symbols indicate individual mice. N=2, n=3. Significance was calculated using 2-way ANOVA**. F) Representative, merged flow cytometric analysis** of GFP/DNT expression in indicated populations shown in B) of DNT/CD23Cre mice. **G) Frequencies** of GFP/DNT expressing cells in indicated populations shown in B) and E) of DNT/CD23Cre mice. Data shown as mean values ± SEM; Symbols indicate individual mice. N=2, n=3. Significance was calculated using 2-way ANOVA.
[Figure partially adapted and modified after Urbanczyk et al., 2021.]

6.6.5. Analysis of metabolic changes induced by DNT/CD23Cre expression

Next, I wanted to clarify how a dysfunctional mtRC affects the metabolism and TCA cycle activity in B cells. The mtRC is fuelled by flux of the TCA cycle, and intermediates of both glycolysis and TCA cycle are important for lipid synthesis. Therefore, it is conceivable that a dysfunctional mtRC has effects on the aforementioned pathways, namely flux of the TCA cycle, glycolysis, and lipid synthesis.

6.6.5.1. Extracellular flux analysis of DNT/CD23Cre expressing B cells

First, to confirm that depleted mtDNA results in decreased OxPhos, splenic B cells were isolated and the oxygen consumption rate (OCR), an indicator of OxPhos activity, was measured using a Seahorse analyzer XFe96. B cells were either left untreated or stimulated with LPS or α-BCR for 6h before measurement. The MitoStress Test (Fig 36A, B) showed that LPS induced the strongest increase in mitochondrial metabolism, measured by basal and maximal respiration, spare respiratory capacity, proton leak, and ATP production, compared to naïve B cells. Stimulation with α-BCR also increased the measured parameters, although to a lesser extent than LPS. Interestingly, basal and maximal respiration, proton leak and ATP production were increased in naïve B cells from DNT/CD23Cre B mice compared to CD23Cre mice. After activation, the mitochondrial activity was comparable, although basal respiration and ATP production was slightly decreased in DNT/CD23Cre expressing B cells. The Glycolysis Stress Test showed that glycolysis was comparable in naïve B cells but increased in activated B cells from DNT/CD23Cre mice (Fig 36C, D). All measured parameters were either comparable between the genotypes or increased in DNT/CD23Cre expressing B cells. To analyse OxPhos activity not only in activated B cells, but also plasma blasts, I analysed the cells on day 3 after LPS activation (Fig 36E, F). At that time point the oxygen consumption was reduced by half in DNT/CD23Cre expressing cells and basal and maximal respiration, spare respiratory capacity, proton leak, and ATP production were decreased, confirming impaired OxPhos induced by mtDNA depletion. The basal extracellular acidification rate (ECAR), indicative of glycolysis, was significantly increased in DNT/CD23Cre expressing LPS blasts, whereas the maximal mean ECAR value was comparable between the two genotypes (Fig 36G). These data imply that DNT/CD23Cre expressing LPS blasts indeed have strongly impaired OxPhos activity and, probably as a consequence, increased glycolysis. Interestingly, naïve and 6h activated B cells show mostly either comparable or increased parameters of both OxPhos and glycolysis in DNT/CD23Cre expressing cells, although it should be reminded that these cells are metabolically rather quiescent and only up-regulate their metabolism upon stimulation.

To analyse mitochondrial and glycolytic ATP production in DNT/CD23Cre expressing B cells upon TD activation, splenic B cells were isolated and activated with either α-IgM, or α-CD40/IL4, or α-IgM/α-CD40/IL4 to mimic T cell help. ATP Rate Assay was performed on day 3 after activation and showed that stimulation with LPS induces the highest ATP production rate for both genotypes (Fig. 37A). However, total ATP production rate was significantly decreased in DNT/CD23Cre expressing B cells upon LPS stimulation, but comparable after α-IgM, α-CD40/IL4, and α-IgM/α-CD40/IL4 stimulation. Analysing mitoATP versus glycoATP production confirmed that DNT/CD23Cre expressing B cells have a highly glycolytic phenotype upon LPS and α-IgM stimulation with a significant and strong increase in glycoATP production in DNT/CD23Cre expressing B cells upon α-IgM stimulation, indicating metabolic flexibility (Fig. 37B, C). Interestingly, this assay showed no differences between DNT/CD23Cre and CD23Cre B cells upon α-CD40/IL4 or α-IgM/α-CD40/IL4 stimulation.

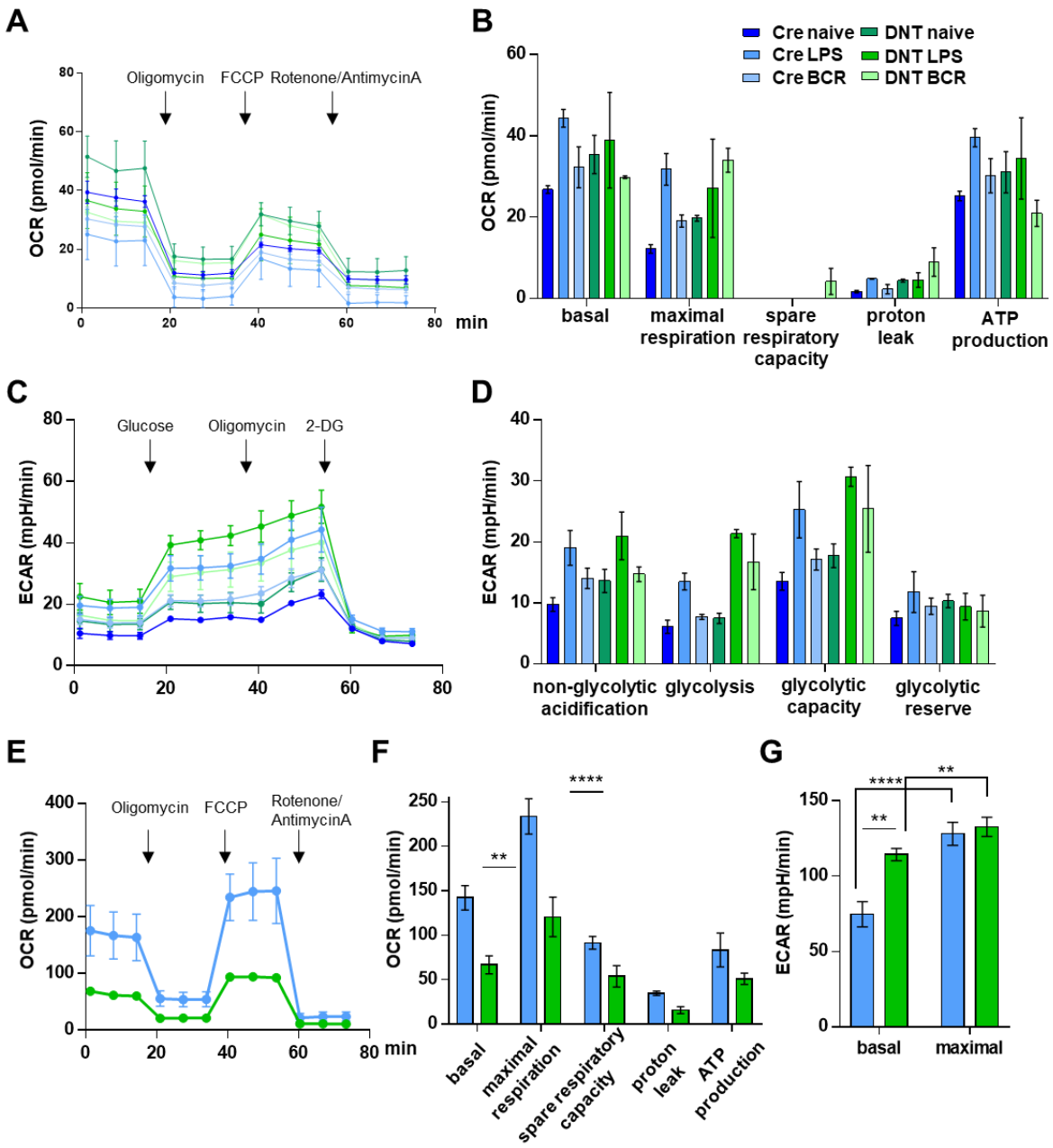

Figure 35 | Extracellular flux analysis of naive and activated B cells from DNT/CD23Cre mice

Splenic B cells from DNT/CD23Cre and CD23Cre mice were isolated and extracellular flux analysis was performed using the Seahorse XFe Analyzer**. A) Naïve B cells were left untreated** or stimulated with either LPS or a-BCR for 6h and oxygen consumption rate (OCR) was determined using extracellular flux analysis measuring basal OCR and after sequential injection of oligomycin, FCCP and Rotenone/Antimycin A. Data shown as mean ± SEM; n = 2-4 mice. **B) Calculated OCR values of basal and maximal respiration**, spare respiratory capacity, proton leak and ATP production. Data shown as mean ± SEM; n = 2-4. **C) Naïve B cells were left untreated** or stimulated with either LPS or a-BCR for 6h and extracellular acidification rate (ECAR) was determined using extracellular flux analysis measuring basal ECAR and after sequential injection of glucose, oligomycin and 2-DG. Data shown as mean ± SEM; n = 2-4 mice. **D) Calculated ECAR values** of non-glycolytic acidification, glycolysis, glycolytic capacity, and glycolytic reserve. Data shown as mean ± SEM; n = 2-4. **E) Splenic B cells were isolated**, activated with LPS and extracellular flux analysis was performed on day 3 as in A). **F) Calculated OCR values of basal** and maximal respiration, spare respiratory capacity, proton leak and ATP production. Data shown as mean ± SEM from N=2, n=2; values from different experiments were normalized using the mean of each genotype; Significance was calculated using 2-way ANOVA. **G) Basal and maximal ECAR values** (after injection of FCCP) from the experiments shown in E) and F). Data shown as mean ± SEM from N=2, n=2; Significance was calculated using 2-way ANOVA.

[Figure partially adapted and modified after Urbanczyk et al., 2021.]

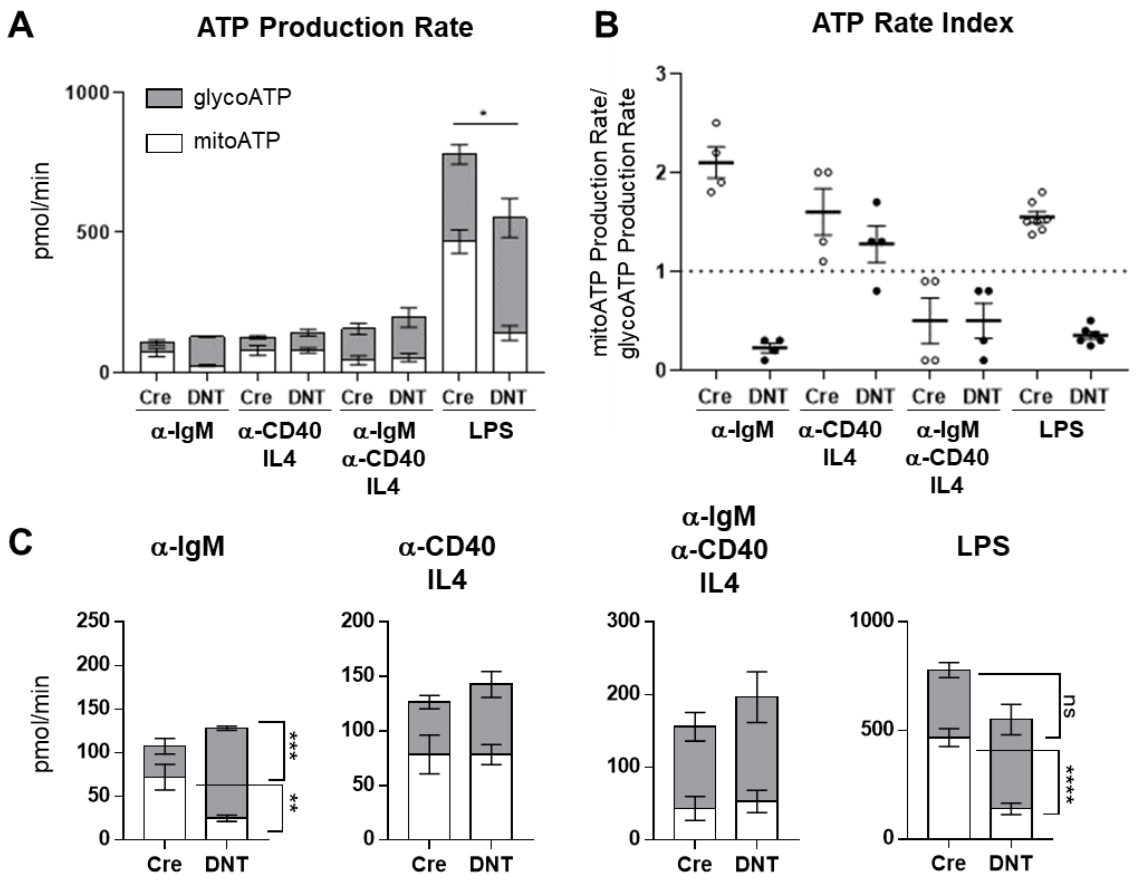

Figure 36 | ATP Rate Assay of activated B cells from DNT/CD23Cre mice

Splenic B cells from DNT/CD23Cre and CD23Cre mice were isolated, stimulated with either LPS, or α-IgM, or α-CD40/IL4, or α-IgM/α-CD40/IL4 and ATP Rate Assay was performed on day 3 after activation using the Seahorse XFe Analyzer. **A) Overview of mitochondrial and glycolytic ATP production rate** was determined measuring basal OCR and after sequential injection of Oligomycin and Rotenone/Antimycin A. Data shown as mean ± SEM; N=1-2, n=4-8; Significance was calculated using one-way ANOVA. **B) ATP Rate Index** is the ratio of the mitoATP Production Rate to the glycoATP Production Rate shown in A). This ratio represents a quantitative metric of the cellular metabolic phenotype. Metabolic indexes greater than 1.0 represent cellular metabolism where greater than 50 % of cellular ATP is derived from mitochondrial through ETC/OXPHOS, while indexes less than 1 indicate greater than 50 % of total ATP is produced by the glycolytic pathway. Since the metabolic index is a ratio-metric measurement, it is highly sensitive to changes or shifts in metabolic phenotype. Data shown as mean ± SEM; N=1-2, n=4-8 **C) Mitochondrial and glycolytic ATP production rate** from A) displayed separately. Data shown as mean ± SEM; N=1-2, n=4-8; Significance was calculated using 2-way ANOVA.
[Figure partially adapted and modified after Urbanczyk et al., 2021.]

6.6.5.2. Analysis of metabolites in DNT/CD23Cre LPS blasts

The next step was to determine how decreased OxPhos and increased glycolysis, as observed by extracellular flux analysis in *in vitro* generated plasma blasts, affects the abundance of metabolites. Measuring glucose, which is imported into the cytosol for glycolysis, and lactate, which is secreted as a by-product of glycolysis, in the supernatant on day 3 after activation showed increased levels of lactate and decreased levels of glucose in DNT/CD23Cre expressing cells (Fig 38A). This result confirms that decreased OxPhos results in increased glycolysis in these cells, as already indicated by the results from extracellular flux analysis. Furthermore, again confirming the seahorse data, luminometric analysis revealed significantly

decreased levels of intracellular ATP on day 3, but not in naïve B cells of DNT/CD23Cre mice (Fig 38B). Both, DNT/CD23Cre and CD23Cre B cells have significantly higher ATP levels on day 3 after LPS activation compared to naïve B cells.

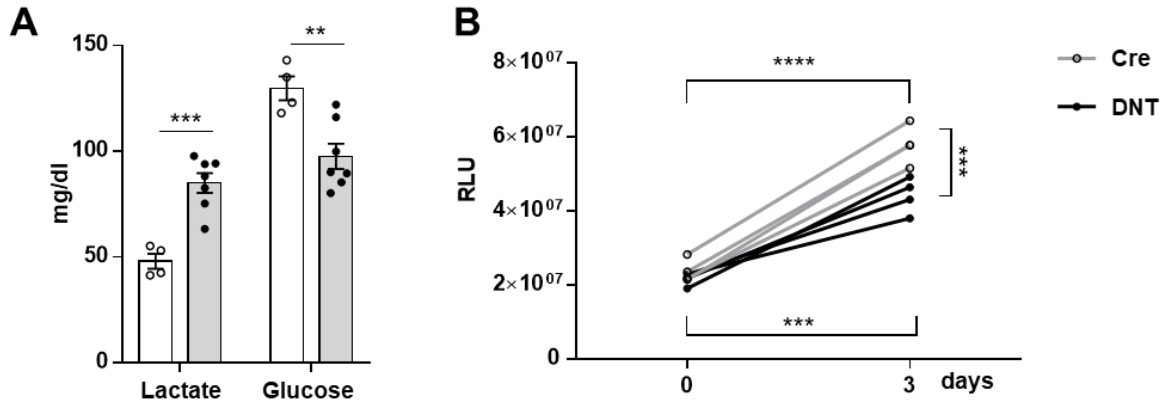

Figure 37 | Analysis of intra- and extra-cellular metabolites in DNT/CD23Cre LPS blasts
Splenic B cells from DNT/CD23Cre and CD23Cre mice were isolated and activated with LPS in vitro. **A) Lactate and glucose** concentrations in the supernatant on day 3 after LPS activation. Data shown as mean ± SEM; symbols indicate individual mice; N=2, n=2-3. Significance was calculated using 2-way ANOVA. **B) Luminometric analysis of intracellular ATP concentration** of naïve and d3 activated B cells. RLU, relative light units. n=4; symbols indicate individual mice; statistical significance was calculated using 2-way ANOVA.
[Figure partially adapted and modified after Urbanczyk et al., 2021.]

Decreased ATP levels of day 3 plasma blasts was also observed using HPLC/MS (Fig 39A). This approach also showed increased levels (both, absolute abundance in pmol/1Mio cells shown in Fig 39A, and relative abundance of DNT/CD23Cre compared to CD23Cre shown in Fig 39B) of fumarate and malate in DNT/CD23Cre expressing cells. Citrate and Isocitrate, on the other hand, were decreased whereas αKG and succinate levels were comparable. Intracellular glucose and Erythrose-4-phosphate (E4P) levels were slightly increased in DNT/CD23Cre expressing cells, whereas 3-Phosphoglyceric acid (3PG), UDPNAG, and PEP were decreased, indicating that these cells utilize glucose not only for glycolysis but also for the pentose phosphate pathway.

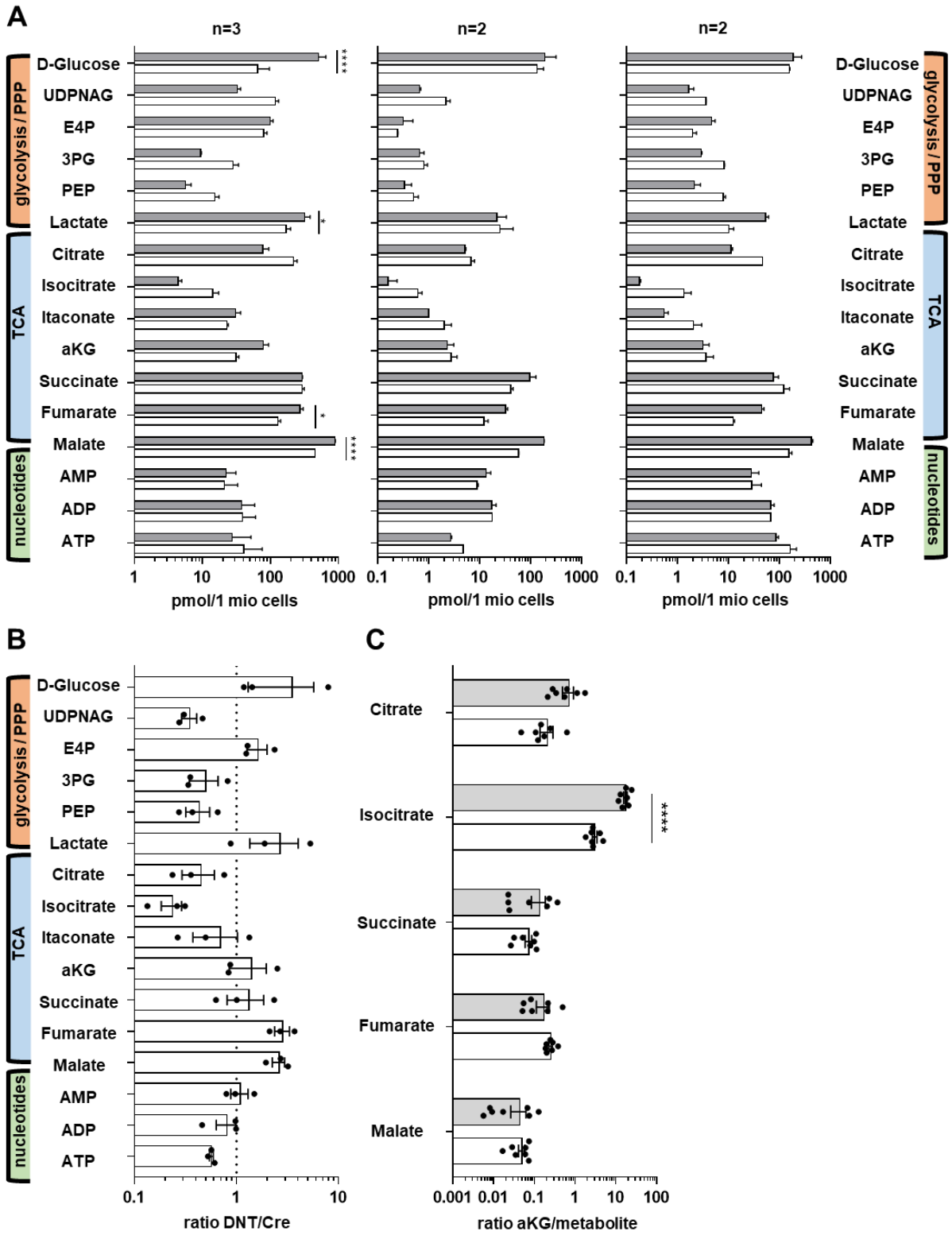

Figure 38 | Mass spectrometric analysis of intracellular metabolites in DNT/CD23Cre LPS blasts

Splenic B cells from DNT/CD23Cre and CD23Cre mice were isolated and analysed on day 3 after *in vitro* LPS activation. **A) HPLC/MS analysis of intracellular metabolites** of FACS sorted B cells (DNT/CD23Cre: viable GFP^+, CD23Cre: viable). Data show the absolute abundance in pmol/10^6 cells of three separate experiments. Bars at mean; N=3, n=2-3; Significance was calculated using 2-way ANOVA. **B) Relative abundance** (DNT/CD23Cre relative to CD23Cre) of intracellular metabolites shown in A. Bars at mean; Dotted line at 1; Symbols show the mean for each experiment; N=3, n=2-3**. C) Relative abundance** (a-ketoglutarate (aKG) relative to respective metabolite) of intracellular metabolites shown in A). Bars at mean; Symbols represent individual mice; N=3, n=2-3. Significance was calculated using 2-way ANOVA. (HPLC/MS analysis was kindly performed by Jörg Hofmann, Department Biology, Division of Biochemistry, Erlangen)
[Figure partially adapted and modified after Urbanczyk et al., 2021.]

6.6.5.3. Analysis of glycerophospholipids in DNT/CD23Cre LPS blasts

Fatty acid synthesis is connected to glycolysis and the TCA cycle. Pyruvate, which is produced by glycolysis, enters the mitochondria, and gets converted to acetyl-CoA with subsequent citrate production. Citrate leaves the mitochondria into the cytosol, where it is cleaved by ATP citrate lyase into acetyl-CoA and oxaloacetate. While oxalacetate returns to the mitochondria as malate, the cytosolic acetyl-CoA can be used for fatty acid synthesis. Since a dysfunctional mtRC resulted in reduced citrate levels, among other changes of metabolites, it is conceivable that fatty acid synthesis is affected in these cells. To answer that question, splenic B cells were isolated, activated with LPS and FACS sorted on day 3 for subsequent direct infusion MS/MS analysis. While the absolute abundance (nMol/mg protein) of phosphatidylglycerol (PG), phosphatidylinositol (PI), phosphatidylcholine (PCh), phosphatidylethanolamine (PE) and phosphatidylserine (PS) was comparable, DNT/CD23Cre expressing B cells had significantly decreased levels specifically of phosphatidic acid (PA) (Fig 40). The distribution of subspecies showed a tendency towards long-chain fatty acids in DNT/CD23Cre expressing B cells for all lipids except PG (Fig 41).

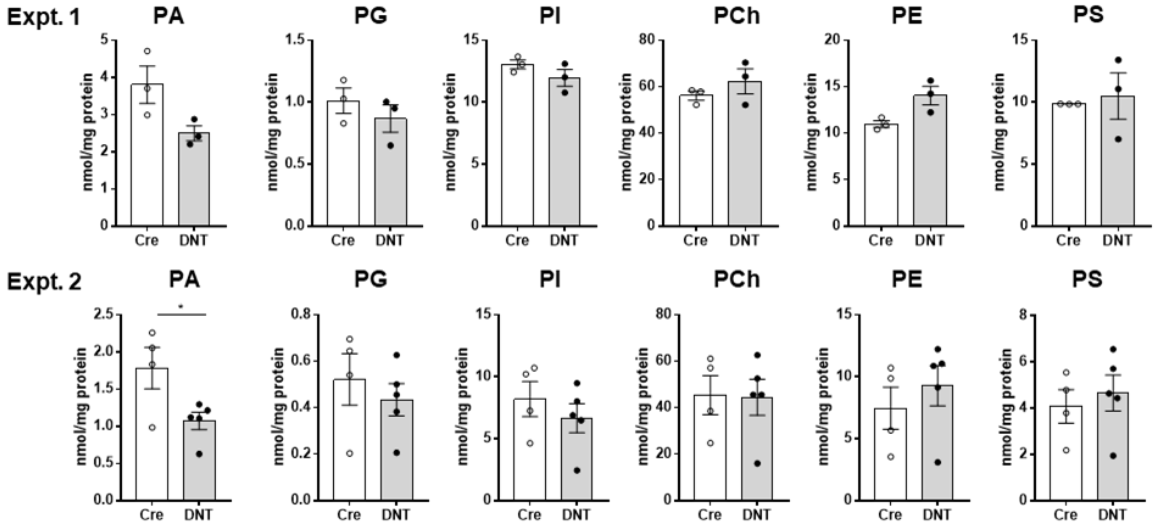

Figure 39 | Analysis of glycerophospholipid composition in DNT/CD23Cre LPS blasts

Splenic B cells from DNT/CD23Cre and CD23Cre mice were isolated and activated with LPS for 3 days. Glycerophospholipids of FACS sorted B cells (DNT/CD23Cre: viable GFP$^+$, CD23Cre: viable) were analysed via direct infusion MS/MS (Shotgun Lipidomics). For technical reasons, the two experiments could not be combined, and the results are shown separately. The absolute abundance (nMol/mg protein) of phosphatidic acid (PA), phosphatidylglycerol (PG), phosphatidylinositol (PI), phosphatidylcholine (PCh), phosphatidylethanolamine (PE) and phosphatidylserine (PS) is shown as mean ± SEM. N=2, n=3-4; significance was calculated for the 2nd experiment using 2-way ANOVA. (Analysis was kindly performed by Susanne Brodesser, Cologne Excellence Cluster on Cellular Stress Responses in Aging-associated Diseases (CECAD), Köln)
[Figure partially adapted and modified after Urbanczyk et al., 2021.]

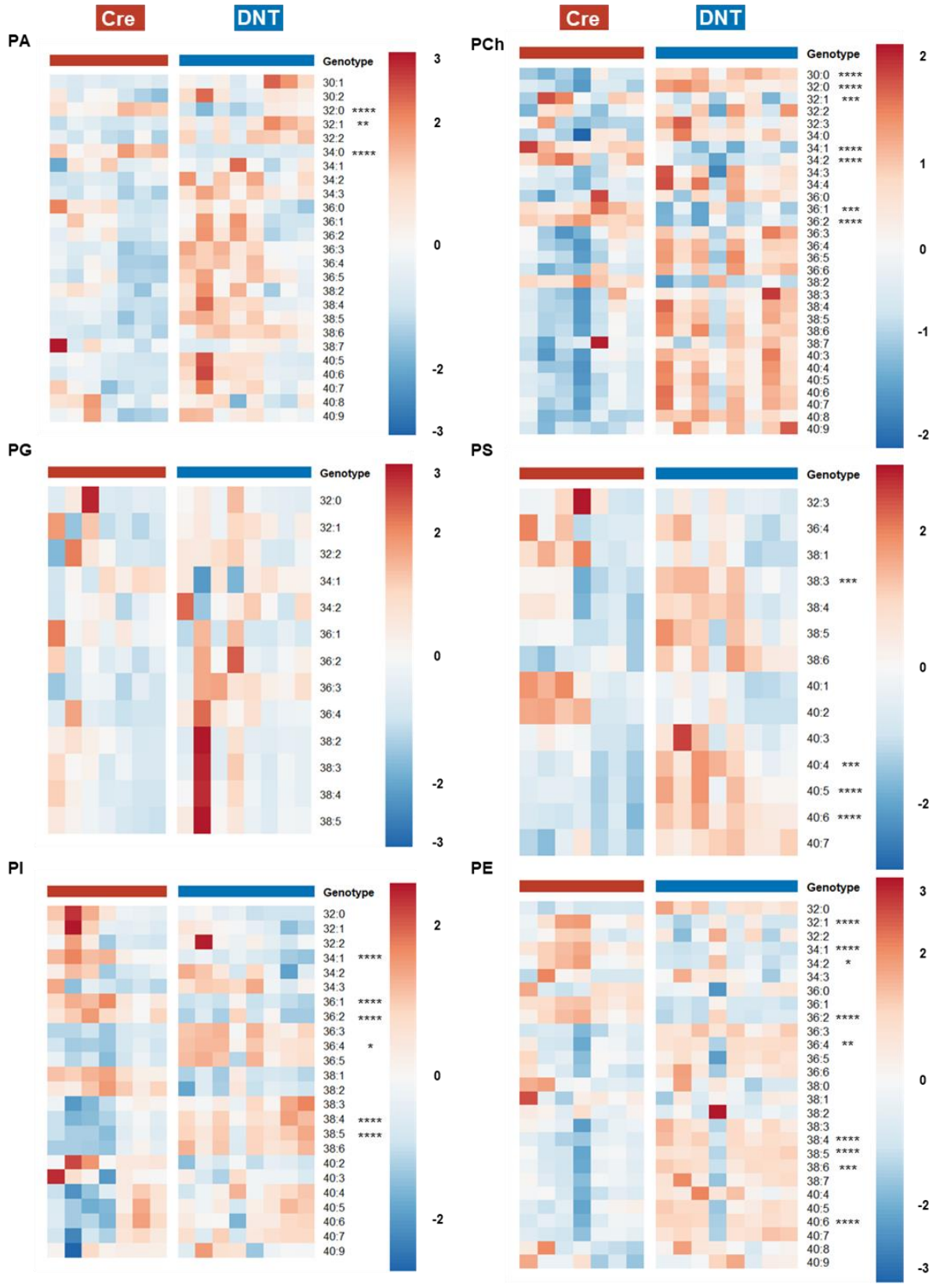

Figure 40 | Analysis of glycerophospholipid subspecies composition in DNT/CD23Cre LPS blasts

The relative abundance (Mol%) of subspecies of phosphatidic acid (PA), phosphatidylglycerol (PG), phosphatidylinositol (PI), phosphatidylcholine (PCh), phosphatidylethanolamine (PE) and phosphatidylserine (PS) is shown heatmaps. Each column represents one mouse. The first number depicts the total number of carbon atoms, the second number the total number of double bonds within the two fatty acyl chains. Combined results from 2 experiments, N=2, n=3-5; statistics calculated using 2-way ANOVA. Related to Figure 40. (Heatmap was kindly generated by Sebastian Schulz using R/pheatmaps). [Adapted from Urbanczyk et al., 2021.]

6.6.5.4. Analysis of mTOR, pAMPK and HIF1α activity in DNT/CD23Cre LPS blasts

The nutrient sensing kinase mTOR plays a crucial role in B cell activation and subsequent plasma cell differentiation (Benhamron et al., 2015; Gaudette et al., 2020), and is directly activated by PA (Yoon et al., 2015), among other activating signals. Since the absolute abundance of PA was reduced in DNT/CD23Cre expressing B cells on day 3 after LPS activation in addition to impaired expression of PC markers and decreased PC differentiation, I hypothesized that mTOR activation may be impaired in these cells. This could be a consequence of decreased levels of PA or/and via activation of pAMPK. pAMPK is a kinase that becomes activated at low energy levels by changes in the AMP/ATP ratio and in its active state leads to mTOR inactivation. Luminometric, mass spectrometric and extracellular flux analysis showed decreased ATP production in DNT/CD23Cre expressing LPS blasts. The transcription factor Hif1α, which becomes activated by hypoxia but also by changes in ratios of αKG to malate and fumarate, is another important player of metabolic homeostasis, inducing a shift to glycolysis when activated. To analyse mTOR, pAMPK and HIF1α activity in DNT/CD23Cre expressing B cells, cell lysates of LPS activated B cells were analysed by Western Blot (Fig 42A). mTOR activity was determined by analysing phosphorylation of RPS6, a down-stream target of active mTOR. pRPS6 was undetectable in naïve B cells, but highly expressed in 24h LPS activated B cells, and still detectable on day 3 after activation. While pRPS6 expression was comparable at 24h after activation, even slightly increased in DNT/CD23Cre expressing B cells, it was decreased on day 3 compared to CD23Cre B cells. pAMPK was only detectable in activated B cells and increased in DNT/CD23Cre B cells at both times points, although the effect was stronger on day 3. Quantifying these data showed a comparable pAMPK/pRPS6 ratio at 24h after activation, but a significant higher pAMPK/pRPS6 ratio at 72h in DNT/CD23Cre expressing B cells (Fig 42B, D). Expression of HIF1α was only detectable at 72h after activation and was significantly increased in DNT/CD23Cre expressing B cells (Fig 42C). In summary, while mTOR activity was decreased, pAMPK and HIF1α were increased in DNT/CD23Cre expressing B cells, probably as a consequence of decreased PA and ATP production, and altered ratios of TCA cycle metabolites, namely αKG to malate/fumarate.

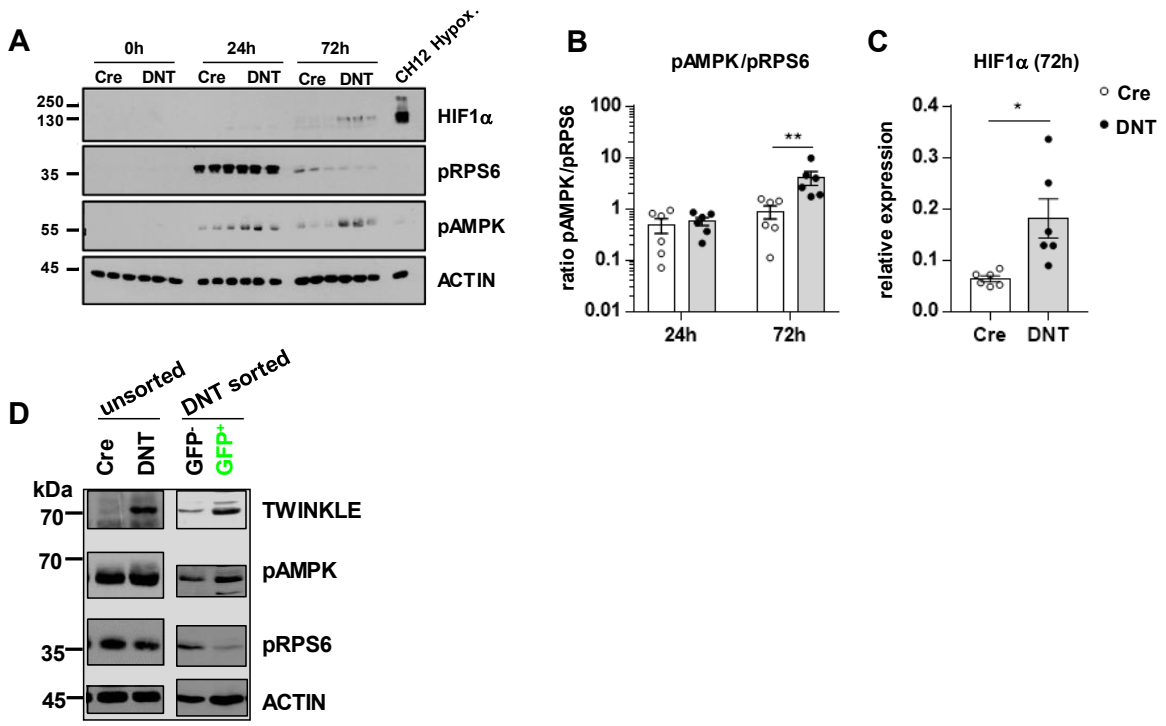

Figure 41 | Analysis of the influence of DNT/CD23Cre expression on mTOR, AMPK and HIF1α activity in LPS activated B cells

Splenic B cells from DNT/CD23Cre and CD23Cre mice were isolated, stimulated *in vitro* with LPS and harvested at indicated time points. Cell lysates were separated by 10% SDS-PAGE. **A) Proteins were transferred** onto a nitrocellulose membrane and stained with antibodies indicated on the right. Standards for molecular mass are depicted on the left. A representative blot with three mice per genotype is shown. **B) Ratio of relative pAMPK/pS6** expression at indicated time points. Data shown as mean values ± SEM. Symbols indicate individual mice. N=2, n=3; significance was calculated using 2-way ANOVA **C) Quantification of HIF1α** expression normalized to actin expression. Data shown as mean ± SEM. Symbols indicate individual mice. N=2, n=3. **D) Left: Unsorted splenic B** cells from CD23CRE and DNT mice were stimulated with LPS for 3d. Right: Splenic B cells from DNT mice were stimulated with LPS for 3d. GFP^+ and GFP^- cells were sorted out. Cell lysates were treated as described in A) and stained with antibodies as indicated on the right. Molecular mass standards are shown on the left (kDa).
[Figure partially adapted and modified after Urbanczyk et al., 2021.]

6.6.6. Analysis of phosphatidic acid liposomes on mTOR activity and PB differentiation in DNT/CD23Cre LPS blasts

It is reported that PA activates mTOR, which can also be achieved by extracellular addition of PA-containing liposomes to *in vitro* cell cultures (Yoon et al., 2015). To investigate, whether the impaired mTOR activity observed in DNT/CD23Cre expressing B cells is resulting from decreased PA production, PA liposomes were added at different time point during *in vitro* B cell activation and plasma blast differentiation. This approach should reveal if artificially increasing PA levels increases mTOR activity, but also if it can restore mTOR activity in DNT/CD23Cre expressing B cells. Activity of mTOR was analysed daily by flow cytometry by staining the cells intracellularly with anti-pRPS6 antibodies (Fig 43A). The PA liposomes were added 5h before measurement. The addition of PA liposomes had overall little effects on the frequencies of viable cells and the frequency of viable cells was comparable between the

genotypes at all time points and every condition (data not shown). Analysing B cells 24h after LPS activation revealed that PA increases pRPS6, both frequency of pRPS6$^+$ cells and the median of pRPS6 fluorescent intensity (FI), with the effect being stronger when added on d0 (Fig 43A, B left panel). While DNT/CD23Cre expressing B cells showed comparable mTOR activity in control cultures, confirming the Western Blot data, the addition of PA did not significantly increase mTOR activity, resulting in significantly decreased medians of pRPS6 FI compared to CD23Cre B cells. At 48h after LPS activation CD23Cre control cultures showed the highest mTOR activity (highest median and frequency of pRPS6$^+$ cells), which was not further enhanced by the addition of PA, indicating that the effects of PA on mTOR activity are time point dependent or/and that mTOR activity is at its maximal capacity, at least in activated B cells (Fig 43A, B middle panel). Addition of PA at this time point (5h before measurement) even decreased the median pRPS6 FI in CD23Cre B cells. While the frequencies of pRPS6$^+$ cells were comparable, the median pRPS6 FI was significantly reduced in DNT/CD23Cre expressing B cells, indicating impaired mTOR activity in these cells. At 72h after LPS activation mTOR activity was strongly down-regulated with no distinct pRPS6$^+$ cells detectable in CD23Cre control cultures and the addition of PA had no enhancing effects (Fig 43A, B right panel). Again, confirming the Western Blot data, DNT/CD23Cre expressing B cells from control cultures had significantly decreased mTOR activity, determined by the median of pRPS6 FI, compared to CD23Cre B cells.

The next question to address was if the artificial alterations of mTOR activity in LPS activated B cells by addition of PA liposomes had effects on plasma blast differentiation, and if this approach would rescue plasma blast differentiation in DNT/CD23Cre expressing cells. Therefore, cells were analysed daily by flow cytometry using anti-TACI and anti-CD138 antibodies. The addition of PA did at no time point increase the frequency of CD138$^+$ plasma blasts in neither DNT/CD23Cre or CD23Cre B cells (Fig 43C). On the contrary, it significantly decreased the frequency at 72h after activation when added on d2 in both genotypes. These results show that while the addition of PA liposomes to LPS activated B cells increases mTOR activity, which is important for subsequent plasma blast differentiation, it did not increase the frequency of CD138$^+$ plasma blasts. Analysing the frequency of DNT/GFP expressing cells confirmed significantly decreased DNT/GFP expression in CD138$^+$ cells compared to TACI$^+$ cells (Fig 43D). The addition of PA on d1-d3 significantly decreased the frequency of DNT/CD23Cre expressing cells, indicating differential effects of PA on DNT/GFP-expressing vs non-expressing cells.

In summary, the addition of PA liposomes at different time points during LPS activation showed that PA increases mTOR activity only within the first 24h after activation. Importantly, this PA-

mediated effect on mTOR is dependent on functional OxPhos, as the addition of PA to DNT/CD23Cre expressing B cells had no effects on mTOR activity.

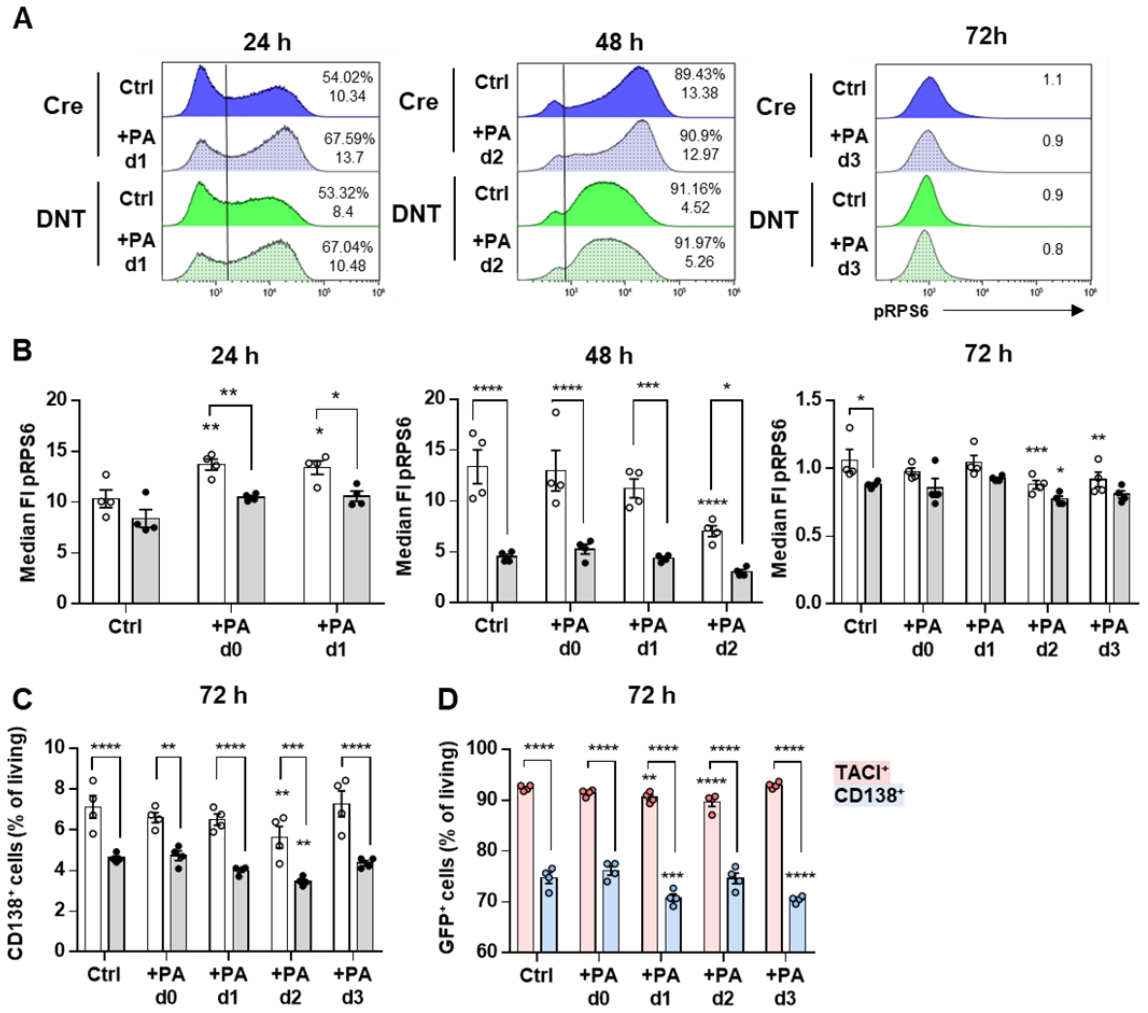

Figure 42 | Analysis of phosphatidic acid addition on mTOR activity and PB/PC differentiation in *in vitro* activated B cells

Splenic B cells from DNT/CD23Cre and CD23Cre mice were isolated, activated with LPS and phosphatidic acid (PA) liposomes were added at the indicated time points. Cells were analysed 24h after activation (left panel), 48h after activation (middle panel) and 72h after activation (right panel). **A) Representative flow cytometric analysis** (merged of 4 mice per genotype) of pRPS6. PA was added on the day of analysis in the shown histograms. Numbers indicate frequency of pRPS6+ cells (top) and median of pRPS6 (bottom). **B) Median of pRPS6** (gated on pRPS6+ cells) shown in A). Data shown as mean ± SEM. Symbols indicate individual mice; n=4; statistical significance was calculated using 2-way ANOVA; **C) Frequency of CD138+ PBs** 72h after LPS activation. Data shown as mean ± SEM. Symbols indicate individual mice; n=4; statistical significance was calculated using 2-way ANOVA. **D) Frequency of DNT/GFP expressing cells**, gated on TACI+ or CD138+ cells, from DNT/CD23Cre mice. Data shown as mean ± SEM. Symbols indicate individual mice; n=4; statistical significance was calculated using 2-way ANOVA.

The significance symbols (*) placed on top of the columns show the difference compared to the untreated controls of the respective genotype while the brackets indicate differences between the genotypes.
[Figure partially adapted and modified after Urbanczyk et al., 2021.]

7. Discussion

The evolution of eukaryotes was enabled by the union of two prokaryotes: an archaeon acquired α–proteobacteria, which come to be known as mitochondria (Archibald, 2015). Although there is still some controversy on the exact evolutionary steps and details, the importance of this event, that is the internalization of energy production via chemiosmosis over membranes, in the generation and maintenance of complex life is undisputed. The fact that mitochondria retained a small part of their genome within the mitochondrial matrix, whereas the majority of genes have over time either become deleted or transferred to the nucleus, highlights its importance for cellular function. The mtDNA genes encode for essential subunits of the respiratory chain and they are highly conserved across species, again highlighting its importance in evolution and life. The probable explanation for retaining genes within the mitochondrial matrix, where mutagenic ROS that can damage DNA is produced, is a requirement for rapid adaptations to changes in energetic demands. B cells continuously experience these drastic changes during their development and differentiation in the bone marrow, spleen, and periphery, with differing availabilities of nutrients and oxygen, but also changes between quiescent and metabolically highly active anabolic states, such as heavy proliferation within the germinal center after TD activation. It is reported that *in vitro* LPS activated B cells upregulated both glycolysis and OxPhos to the same extent (Caro-Maldonado et al., 2014), and that the progressive upregulation of nucleus encoded OxPhos genes is BLIMP1 dependent (Price et al., 2018). Furthermore, Waters et al. showed that OxPhos is fuelled by other nutrients than glucose in α-CD40/IL-4 activated B cells and that they remodel their mitochondria without increasing mtDNA within the first 24h under these conditions (Waters et al., 2018). Yet to date it remains unknown how B cells handle their mtDNA content to support OxPhos at different developmental stages *in vivo* and if selection checkpoints for functional mitochondria exist in this cell type. Therefore, the focus of this project was to investigate how depletion of mtDNA, induced by transgenic expression of a dominant-negative mutant of the mtDNA helicase Twinkle at different B cell stages, affects B cell development, maturation and activation and the humoral immune response.

7.1. Selection for functional mitochondria in early B cell development

It is reported, that B cells down-regulate both, glycolysis and OxPhos, during the differentiation from pro B cells over pre B cells to immature B cells, which are metabolically rather quiescent until activation (Stein et al., 2017; Urbanczyk et al., 2018). Furthermore, the ability to regulate metabolic homeostasis in pro and pre B cells seems to be essential during B cell development, shown by developmental blocks at the pre B cell stage induced by disruption of the mTOR/pAMPK axis (Iwata et al., 2016; Park et al., 2012). While it is mostly known how mTOR

and pAMPK regulate metabolic homeostasis, it remains elusive how dysfunctional mitochondria in turn affect these pathways and their function. Analysing mice that are unable to replicate their mtDNA when entering the pro B cell stage revealed that B cell development is accompanied by selection for functional mitochondria. B cells from DNT/mb1Cre mice show strongly decreased pre B cell differentiation, evident by strongly reduced pre B cell numbers and frequencies and by decreased intracellular expression of the µHC in pro and pre B cells. Interestingly, mTOR activity was increased and the observed downregulation during development in mb1Cre mice was aberrant in DNT/mb1Cre mice, which could be explained by altered OxPhos activity. To address this question, sorted pro B cells were FACS purified and cultivated with IL-7 to enable extracellular flux analysis with sufficient pro and pre B cell numbers. Unfortunately, this approach had to be abandoned because sorted pro B cells from DNT/mb1Cre were not viable in IL-7 *in vitro* cell cultures. Therefore, it remains speculative how genetic prevention of mtDNA replication in pro B cells affects OxPhos and glycolysis. Depending on the degree of mtDNA depletion, current requirements, and nutrient availability, it is conceivable that OxPhos may be decreased in these cells, because essential subunits of the mtRC encoded on mtDNA are lacking. On the other hand, it would also be possible that at this stage compensatory pathways are activated by retrograde signaling that enhance mitochondrial metabolism, similar as observed in Hodgkin and Reed-Sternberg cells (Haumann et al., 2020). In one case or the other, the depletion of mtDNA influences metabolism, which in turn affects further differentiation into pre B cells. I think it is unlikely that the physical absence of mtDNA in pro B cells is responsible for the observed developmental block but instead the metabolic changes, resulting from decreased expression of mtDNA encoded subunits of the mtRC. Nonetheless, the drastically reduced viability of sorted pro B cells in IL-7 cell cultures represents a further indicator that the metabolism is altered in these cells. One possible explanation could be that pro B cells from DNT/mb1Cre are highly dependent on other cytokines deriving from cells of the respective bone marrow niche, that are not present in the cell culture medium. The chemokine stromal cell-derived factor-1 (CXCL12) could be a possible candidate. CXCL12 is produced by reticular CXCL12-abundant (CAR) cells in the bone marrow and its physiological receptor CXCR4 is expressed on pro B cells but also mature plasma cells in the bone marrow, indicating its role in migration, homing and survival of these cells (Nagasawa, 2007, p. 12). Interestingly, it has been shown that the CXCR4/CXCL12 axis counteracts metabolic exhaustion in hematopoietic stem cells (Zhang et al., 2016). Depletion of CXCR4 in these cells increased OxPhos and ROS production, which ultimately resulted in apoptosis. Therefore, it is conceivable that pro B cells from DNT/mb1Cre mice are protected from metabolic exhaustion *in vivo* by CXCL12 that is provided by CAR cells, but are more prone to ROS induced apoptosis *in vitro* due to the absence of CXCL12 in addition to a dysfunctional mtRC. Another possible candidate could be the hypoxia-induced

transcription factor HIF1α, which is highly active in pro B cells and is activated by hypoxia in bone marrow niches (Burrows et al., 2020). Stabilized HIF1α leads to increased glycolysis by enhancing the expression of genes involved in this pathway (Dengler et al., 2014). It is possible that HIF1α is stabilized under hypoxic conditions in the bone marrow and secures the expression of genes involved in glycolysis, whereas under normoxic conditions in cell culture HIF1α is degraded, and glycolytic genes are less expressed. It could be that pro B cells from DNT/mb1Cre are highly dependent on HIF1α mediated glycolysis and that glycolysis may not be sufficiently induced under normoxic conditions in these cells, whereas pro B cells from WT mice under normoxic conditions may have the ability to instead increase their O_2 use and divert their metabolism towards OxPhos (Fig 43). This compensatory adaptation may not be possible in pro B cells from DNT/mb1Cre mice due to a dysfunctional respiratory chain. Taken together, the absence of CXCL12 and the HIF1α degradation, both caused by changing the environment from hypoxic niches in the bone marrow into normoxic cell culture systems, could induce a metabolic shift in pro B cells towards OxPhos that is not possible in pro B cells from DNT/mb1Cre mice due to a dysfunctional mtRC in these cells. Furthermore, these data suggest that pro B cells from DNT/mb1Cre mice use mainly glycolysis for survival and proliferation *in vivo,* but functional mtDNA replication in pro B cells from WT mice increases their metabolic flexibility, thereby enabling their survival also under normoxic conditions outside of their bone marrow niche.

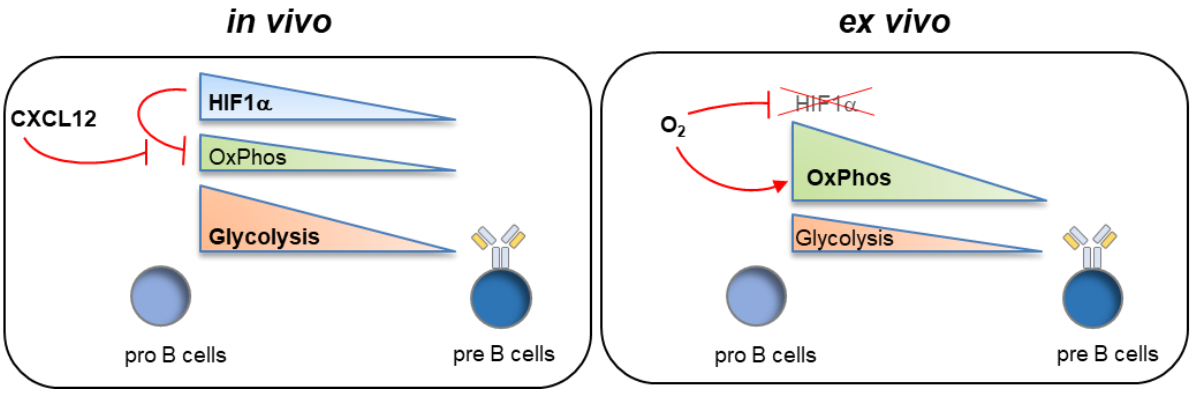

Figure 43 | Proposed model of changes in metabolic activity in *in vivo* versus *ex vivo* pro and pre B cells
Based on findings obtained in this study, I hypothesize that pro B cells in their bone marrow niche preferentially use glycolysis and only minimal OxPhos. This could be mediated by CXCL12, which has been shown to decrease OxPhos in hematopoietic stem cells thereby counteracting metabolic exhaustion, and HIF1α, which may be stabilised under hypoxic conditions in the bone marrow. Isolating pro B cells by flow cytometry and culturing them under normoxic cell culture conditions leads to HIF1α degradation which, in addition to lacking CXCL12 signals, results in a metabolic shift towards OxPhos. This means that WT pro B cells have metabolic flexibility, whereas this metabolic shift towards OxPhos is not possible in DNT/GFP expressing pro B cells

It is furthermore possible that increased glycolytic flux in DNT/mb1Cre pro B cells, which is likely but remains to be shown, occurs at the expense of flux through the PPP. Interestingly, mb1Cre mediated deletion of PP2A, a serine/threonine-protein phosphatase that redirects

glucose from glycolysis into the PPP, results in a developmental block at the pre-BCR stage comparable to DNT/mb1Cre mice (Xiao et al., 2018). However, it remains to be shown to what extend defective OxPhos in pro B cells diverts glucose from the PPP into the glycolysis pathway and if R5P synthesis or NADPH production or both is required at this stage.

The next question to address was how changes in the metabolism of pro B cells, induced by genetic inhibition of mtDNA replication, impair the ability to differentiate into pre B cells. The expression of µHC in pro B cells is an early and essential step in this process, is mediated by the expression of RAG1/2, and is significantly decreased in pro B cells from DNT/mb1Cre mice. This could be caused either by decreased expression of RAG1/2, or by impaired protein translation under normal RAG1/2 expression, or a combination of both. RAG1/2 are directly activated by FOXO1 (Amin and Schlissel, 2008), which is a transcription factor involved in the regulation of stress resistance, cell cycle arrest, apoptosis and metabolism (Calnan and Brunet, 2008). FOXO1 activity is regulated by post-translational modifications, including phosphorylation, acetylation, and ubiquitination resulting in its nuclear export. In addition, metabolic intermediates and by-products, such as ROS, AMP, NAD+ and acetyl-CoA are factors that directly or indirectly regulate FOXO1 activity (Kim and Koh, 2017). Therefore, it seems reasonable that altered the metabolism in pro B cells from DNT/mb1Cre mice leads to aberrant FOXO1 activity, which could result in decreased RAG1/2 expression. This hypothesis is supported by a study analysing mb1Cre mediated deletion of FOXO1. These mice show a comparable phenotype as observed in DNT/mb1Cre mice, with increased pro B cell numbers and developmental block at the pre B cell stage resulting in strongly reduced mature B cells (Dengler et al., 2008). Furthermore, pro B cells from FOXO1$^{-/-}$ pro B cells also failed to expand in IL-7 cultures, what led Dengler et al. to the conclusion that these cells may have defects in proliferation and survival. Therefore, they analysed IL7Rα expression, since IL-7 signaling plays a crucial part in the proliferation and survival of pro B cells. Indeed, expression of IL7Rα was decreased in FOXO1$^{-/-}$ pro B cells in addition to increased Annexin V+ apoptotic cells, which led Dengler et al. to the conclusion that FOXO1$^{-/-}$ pro B cells are prone to apoptosis. In conclusion, it is possible that genetic inhibition of mtDNA replication in pro B cells alters the metabolism and the generation of metabolic intermediates and by-products, which affect FOXO1 activity. This could lead to decreased IL7Rα and RAG1/2 expression, resulting in increased apoptosis of pro B cells and decreased pre B cell differentiation.

A further explanation for impaired pre B cell differentiation could be disrupted activity of mTORC1, which is a nutrient sensing kinase that is involved in the regulation of anabolic processes and metabolism. Mb1Cre mediated disruption of its essential cofactor Raptor also resulted in a similar phenotype observed in DNT/mb1Cre mice with a developmental block at the pre B cell stage and decreased µHC expression (Iwata et al., 2016). However, I observed

comparable mTORC1 activity in pro B cells and increased mTOC1 activity in pre and immature B cells in DNT/mb1Cre mice, indicating impaired down-regulation of mTORC1 in these cells. It should be noted that the downregulation of mTORC1 is also crucial for proper B cell development. This was shown in Fnip1$^{-/-}$mb1Cre mice, that have a developmental block at the pre B cell stage, that is caused by defective AMPK-mediated down-regulation of mTORC1 in these cells (Park et al., 2012). Although the function Fnip1 is unknown, Park et al. could show that the binding of Fnip1 to AMPK is essential for AMPK to inhibit mTORC1. Taken together, these studies highlight the importance of proper mTORC1 regulation during B cell development. Since I could show that the mTORC1 down-regulation during B cell development is impaired in DNT/mb1Cre mice, it is conceivable that the mTORC1/AMPK axis is disrupted in these cells by altered metabolism, that is induced by inhibition of mtDNA replication.

Finally, it is conceivable that mitochondrial ATP production in early B cells might be required for purinergic signaling and migration. While it is appreciated that P2Y receptors are involved in the differentiation of hematopoietic cells, the activity of extracellular nucleotides in the development of lymphoid cells is much less studied (Sak et al., 2003). Yet, the regulated and strong expression of P2X3 receptors in pro and pre B cells that is followed by a drop in expression in immature B cells gives reason to speculate that specifically P2X3 receptor activity is important for the development of early B cells (Fig 44). Since no reports exist in the context of P2X3 receptor function in B cell progenitors, one might speculate that one of the factors that are important during early B cell development, namely IL7 or CXCL12, might induce purinergic signaling via P2X3. It is also possible that P2X3-mediated Ca^{2+} influx is required to support pre-BCR and BCR signaling. If mitochondrial ATP synthesis is required to synergize with chemokine and purinergic signaling, it is possible that pro B cells from DNT/mb1Cre mice fail to deliver the ATP amount that is needed for successful signaling. This would result in impaired differentiation of B cell progenitors, as it was observed in DNT/mb1Cre mice. Therefore, the DNT/mb1Cre model would be well suited to specifically analyse the involvement of mitochondrial ATP production and purinergic signaling in the context of early B cell development.

7.2. Selection for functional mitochondria in B cell maturation

After completion of B cell development in the bone marrow, immature B cells migrate into the spleen as transitional B cells where they further differentiate into either FO or MZ B cells, with the former being predominantly activated in a TD manner in the germinal center while the latter can quickly differentiate into AB-secreting plasma blasts without T-cell help. Interestingly, this step represents a further checkpoint for B cell selection on the basis on functional mitochondria. While the cell numbers and frequencies of both, FO and MZ B cells from

DNT/mb1Cre mice were drastically reduced, as expected from the observed developmental block at the pre B cell stage, tracking DNT/GFP expression revealed a clear disadvantage of DNT/GFP expressing cells in the development of MZ B cells, since only about half of this population showed DNT/GFP expression compared to 97% in FO B cells. This means that B cells that escaped Cre recombination are favoured in the development of MZ B cells. This was also evident when inhibition of mtDNA replication was induced later in transitional T2 B cells using CD23Cre mice, although to a lesser extent where 87% of MZ express DNT/GFP compared to 92% of FO B cells. Since I could demonstrate the existence of a selection checkpoint for functional mitochondria at the pro to pre B cell transition, it is reasonable to assume that immature B cells under normal development, as it should be the case in DNT/CD23Cre mice, have functional mitochondria. Therefore, the onset of DNT/GFP in T2 cells from DNT/CD23Cre mice is not expected to have major effects until B cell activation, since these cells hardly proliferate, compared to pro B cells or GC B cells, and are metabolically rather quiescent (Loder et al., 1999). But still, I observed a statistically significant, albeit slight reduction of DNT/GFP expressing MZ B cell in DNT/CD23Cre mice, indicating that mtDNA replication still occurs after successful B cell development in the bone marrow in transitional T2 B cells, and that mtDNA replication is important in transitional B cells for the subsequent generation of MZ B cells. This could be explained that there are no additional selection checkpoints after TI activation of MZ B cells, in contrast to FO B cells that undergo heavy selection during the germinal center reaction. Therefore, the selection for mitochondrial function must be ensured before the generation of MZ B cells, enabling immediate and sufficient energetic support after activation and later in AB secreting plasma blasts and plasma cells. It is also interesting to note that MZ B cells have a higher mtDNA content compared to FO, which might be an indicator of their increased requirement on OxPhos. Additionally, it is reported that MZ and B1 B cells are poised for PC differentiation in response to TLR agonists: MZ and B1 B cells , in contrast to FO B cells, quickly upregulate the expression of the two key PC differentiation TFs BLIMP1 and Xbp1 upon TLR ligation (Fairfax et al., 2007; Genestier et al., 2007). Taken together, these studies indicate that a selection checkpoint exists in the transitional B cell stage that determines the generation of either FO or MZ B cells. While the studies so far analysed selection parameters concerning BCR signaling strength, Notch2 and NFκB signaling, and anatomical migration and retention, there are no published data analysing the involvement of metabolic capacities at these fate decisions (Iwahashi et al., 2012; Lopes-Carvalho and Kearney, 2004; Pillai, 2009). It is conceivable that to facilitate PC differentiation with enhanced differentiation kinetics in MZ B cells, metabolic support by functional mitochondria must be ensured in advance. The results obtained in this study suggest that therefore functional mitochondria represent a selection criterium in transitional B cells that determine the development of either FO or MZ B cells. At this maturation stage transitional B

cells with higher mtDNA content and functional mitochondria are selected in the pool of MZ B cells. It is conceivable that selection for functional mitochondria in FO B cells occurs at a later time point during activation, probably in the germinal center which is a place known for heavy selection on the basis of different criteria.

Furthermore, also at this developmental stage purinergic signaling, which might be mitochondria-dependent, could be important, since gene expression data shows the regulated expression of several purinergic receptors: Especially P2X4 and P2Y10 expression is increased in immature, mature, FO, and MZ B cells compared to their BM progenitors (Fig 44). It is interesting to note that T cells, also in resting state, engage in purinergic signaling, in order to maintain basal cytosolic Ca2+ homeostasis that enables rapid response after simulation, also by increasing ATP release and further fuelling purinergic signaling via P2X4, one of the receptors that is also expressed in mature B cell subsets. Furthermore, it was shown that the accumulation of extracellular ATP activates P2X7 receptor, resulting in shedding of CD21, CD23, and CD62L from the cell surface. These are the first events in the adhesion cascade leading to integrin interactions and transendothelial migration of leukocytes (Gu et al., 1998; Przybyła et al., 2018; Pupovac et al., 2015). Therefore, it is tempting to speculate that similar mechanisms exist also in B cells, which would require functional mitochondria to support the ATP demand necessary for continuous and/or induced purinergic signaling. If mitochondrial ATP synthesis is required in this context, it is possible that it is impaired in DNT mice, although this needs to be further investigated in the future.

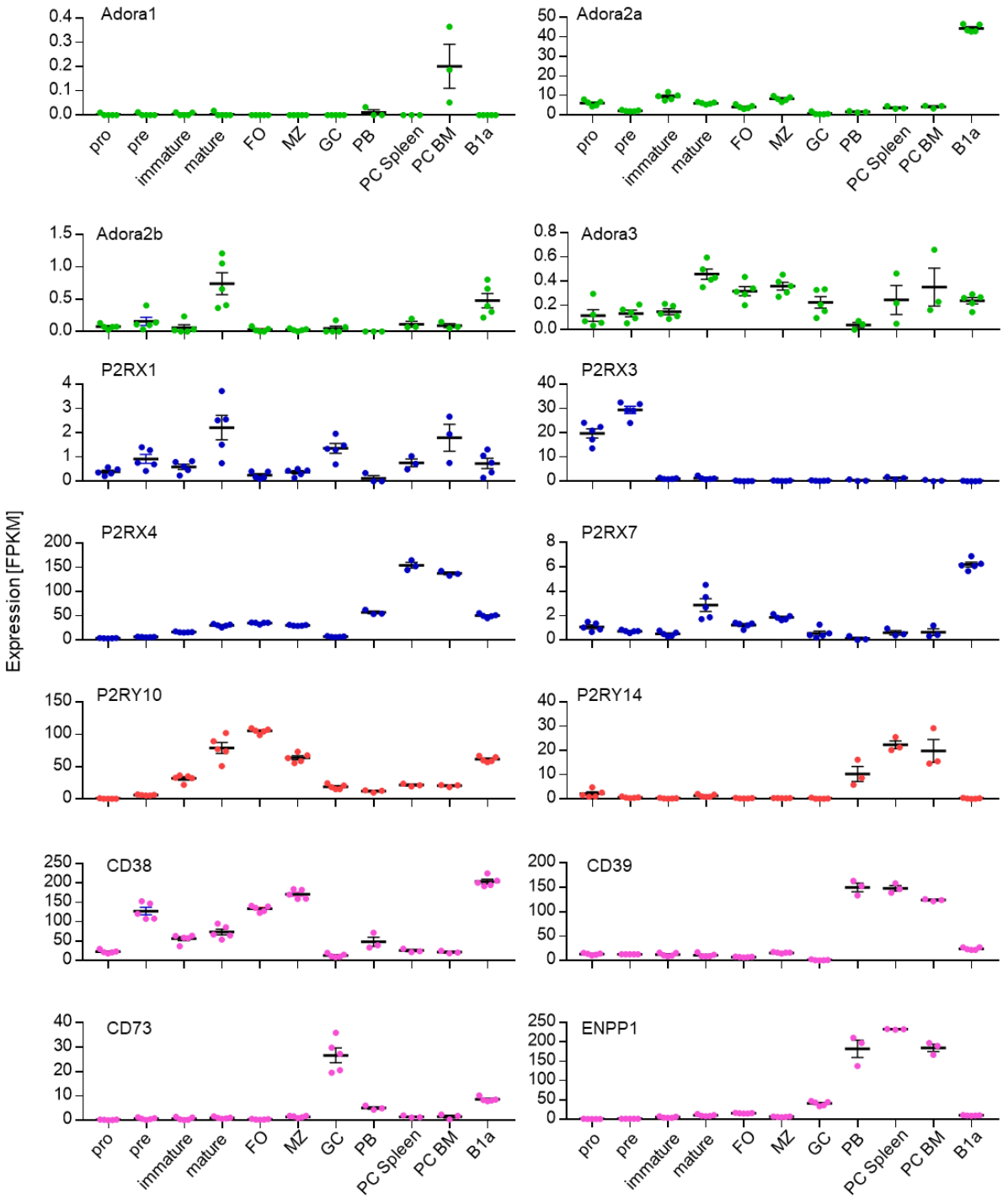

Figure 44 | Expression of purinergic receptors and ectoenzymes in selected B cell subsets

Analysis of RNAseq data from different B cell subsets published in Brazão et al., Blood, 2016 for the expression of selected purinergic receptor and ectoenzyme transcripts in pro B, pre B, immature, mature, follicular (FO), marginal zone (MZ), B1a and germinal center (GC) B cells as well as plasmablasts (PB) and plasma cells (PC). P1 receptors are indicated in green, P2X receptors in blue, P2Y receptors in red, and ectoenzymes in pink. Shown are means of fragments per kilobase per million reads (FPKM) with standard error of the mean (SEM) for n = 3-5 replicates.

7.3. Selection for functional mitochondria in the germinal center

After TD activation, B cells migrate into the germinal center and where they undergo somatic hypermutation and class-switch recombination. After successful selection with the help of FDCs and T_{FH} cells, B cells leave the germinal center as memory B cells or plasma blasts that further mature into plasma cells. Germinal center B cells are highly proliferative, which requires a strong metabolic support. Dividing lymphocytes, but also other proliferative cells, typically rely on anaerobic glycolysis for this purpose. Interestingly, GC B cells are exceptional in that they perform minimal glycolysis but rely on FA oxidation (Weisel et al., 2020), which implies a requirement for a functional respiratory chain. The frequencies of GC B cells from the peyer's patches from unimmunized DNT/mb1Cre and DNT/CD23Cre were comparable to the respective Cre controls. Interestingly, analysing the GFP/DNT expression revealed a strong selection for escaper B cells with a functional respiratory chain. In both mouse model, there is first a significant drop of DNT/GFP expression in $CD19^+$ cells, compared to FO B cells, and a further drop in the GC compartment. The first drop of DNT/GFP expressing cells, that is especially pronounced in DNT/mb1Cre mice, indicate that B cells with a functional respiratory chain are selected for the migration into the Peyer's patches. The second drop of DNT/GFP expressing cells in the GC B cell compartment indicate a further selection checkpoint entering and/or within the germinal center. These results are in accordance with published reports, that show that germinal center B rely on FA oxidation, which requires a functional respiratory chain (Weisel et al., 2020). It is also conceivable that the internalization and processing of antigens but also interactions with T_{FH} and FDC cells are especially energy consuming and may be impaired in B cells with dysfunctional mitochondria. An impairment in these cell-cell contacts or antigen processing could be possible explanations for how this selection might be implemented. Indeed, one particular study by Akkaya et al. supports this idea: They first confirmed that B cells activated with either anti-IgM or CpG or both rapidly increase both OCR and ECAR, indicative of OxPhos and glycolysis respectively, already after a few minutes following activation (Akkaya et al., 2018). Furthermore, they showed that the induction of maximal respiration was mediated by BCR signaling, as inhibition of Syk, Btk, PI3K or JNK decreased maximal OCR. In addition they showed increased mitochondrial metabolism and biogenesis in B cells stimulated with anti-IgM/CpG for 24h: activated B cell had a higher mtDNA content, as shown by a higher ratio of COXI/18S (COXI is mtDNA encoded cytochrome c oxidase subunit I, and 18S is the nuclear encoded 18s ribosomal subunit) and higher expression of TFAM, which is essential for transcriptional activation and organization of mtDNA (Akkaya et al., 2018; Ngo et al., 2014). Yet, anti-IgM stimulation alone did not induce mitochondrial biogenesis. Most interestingly, they showed that the early events following BCR

activation, namely B cell spreading, BCR accumulation at antigen contact-site, and antigen internalization/processing/trafficking were dependent on OxPhos, but not glycolysis. It remains to be confirmed if this is the case in DNT/CDmb1Cre and DNT/CD23Cre mice, but I think it is very likely that a sufficient copy number of mtDNA with continuing mtDNA replication is required during B cell activation, since essential activation processes such as B cell spreading, and antigen processing are dependent on OxPhos-derived ATP. This mechanism would ensure that B cells with higher mtDNA copy number and functional mitochondria have a strong advantage and therefore are predominantly activated and selected.

7.4. Selection for functional mitochondria in plasma cells

Plasma cells can either derive from TI activated MZ or B1 B cells, that are short-lived and secrete IgM, or from TD activated B cells that underwent somatic hypermutation and class-switch recombination in the germinal center, that are long-lived in the bone marrow and secrete IgA, IgM or IgG (Schuh et al., 2020). They can be further divided into 4 subsets in the spleen (P0-P3) and 3 subsets in the bone morrow (P1-P3) according to the expression of CD19 and B220, with P0 and P1 mainly containing proliferating plasma blasts while P2 and P3 are non-proliferating plasma cells (Pracht et al., 2017). Long-lived, mature plasma cells are within in the P3 compartment and have distinct metabolic requirements, as they import glucose mainly for glycosylation of antibodies and import pyruvate into mitochondria to support OxPhos (Lam et al., 2016). Moreover, preceding the plasma cell differentiation, B cells upregulate glycolysis but also OxPhos after activation (Caro-Maldonado et al., 2014). Furthermore, bone marrow plasma cells showed the highest content of mtDNA within the B cell lineage, indicating a higher requirement of mtDNA encoded mtRC subunits in these cells. Therefore, it seems reasonable that at some point during the B cell activation or subsequent plasma cell differentiation the selection for functional mitochondria is ensured. The data obtained in this study strongly confirm this notion: Both mouse model showed that the cell numbers of the P3 compartment from unimmunized were normal, but the majority of these cells do not express DNT/GFP and are therefore B cells, that escaped Cre recombination. These results show first that the homeostasis of the P3 compartment is regulated independently of naïve B cell numbers. This is shown clearly in DNT/mb1Cre mice, that have a developmental block at the pre B cell stage resulting in strongly decreased immature and mature B cell numbers but still have comparable numbers of P3 plasma cells. Moreover, these results show that B cells with functional mitochondria that escaped Cre recombination have a strong advantage and are selected to replenish the pool of mature plasma cells. The fact that in both mouse model the frequency of DNT/GFP expressing plasma cells was highest in P1 plasma blasts and decreased in the P2 and P3 compartment indicate that selection for cells with functional mitochondria still occurs during this stage of plasma cell differentiation and is not restricted to preceding B cell activation or the germinal center reaction. Taken together, while the comparable numbers of P3 plasma

cells in the bone marrow indicate the importance of this subsets and its homeostatic regulation, the strongly decreased frequency of DNT/GFP expressing cells show that B cells with functional mitochondria are selected for plasma cell differentiation, highlighting a strong requirement of OxPhos of this particular subset. This raises the question of how this selection might be implemented. One possibility is via the process of migration itself that is required for plasma cells deriving from the spleen to home into their bone marrow niche and furthermore, is a highly energy-consuming task. In fact, it is reported from human plasma blasts that the CXCL12-mediated migration of plasmablast is dependent on the oxidation of glucose: The CXCL12/CCR4 signaling enhances pyruvate dehydrogenase activity in an AKT-dependent manner to promote OxPhos (Pak et al., 2018). This CXCL12-mediated increase of OxPhos enables the continuous production of sufficient ATP levels that are needed for the phosphorylation of myosin light chains necessary for migration. Since OxPhos is impaired in PB/PCs from DNT mice it is conceivable that CXCL12 signaling is not able to sufficiently increase OxPhos in these cells and that consequently these cells therefore cannot reach their final destination in the bone marrow niche.

But also attachment and/or survival of PCs in the bone marrow niche may be OxPhos dependent and therefore impaired in DNT/CD23Cre and DNT/mb1Cre mice. The connection between metabolism and PC longevity was partially shown by Lam et al.: LLPCs, in contrast to SLPCs, import pyruvate into mitochondria under energetic stress, which was essential for longevity. However, they concluded, based on comparable number and size of mitochondria in LLPCs compared to SLPCs, that “the increased maximal respiratory capacity in LLPCs was not driven by unique cell-intrinsic mitochondrial properties, but by respiratory substrates such as pyruvate which were less available to SLPCs” (Lam et al., 2016). Based on the findings of this thesis I would like to challenge this particular statement, since a sharp drop of GFP expression in the P3 compartment of DNT/mb1Cre mice and DNT/CD23Cre mice compared to the splenic P1 compartment indicates a strong disadvantage of DNT/GFP expressing PCs that is based precisely on cell-intrinsic mitochondrial dysfunction.

A further possibility how of metabolic dysfunction/fitness in PCs is implemented into survival/lifespan might be via purinergic signaling. Unfortunately, only limited, but nonetheless highly interesting, research is available in this context that shows that the ecto-nucleotide pyrophosphatase/phosphodiesterase ENPP1 is upregulated in LLPCs in the BM and is required for their survival or persistence (Wang et al., 2017). Furthermore, RNAseq Data shows a specific upregulation in the PC compartment of a particular set of purinergic receptors, namely P2RX4, P2RY14, and CD39 (Fig 45). Therefore, it is conceivable that continuous mitochondrial ATP production in LLPCs is required for purinergic signaling-mediated survival signals that might be impaired in DNT/GFP expressing PCs.

In summary, decreased DNT/GFP expression in the PC compartment with a drastic drop especially in the P3 compartment of the BM reveal cell-intrinsic, mitochondrial requirements for the generation and longevity of LLPCs.

7.5. Mitochondrial respiration in B cells regulates serum Ig homeostasis

The levels of different Ig isotypes in the serum of unimmunized DNT/mb1Cre and DNT/CD23Cre mice, each with respective Cre controls, were analysed by ELISA. Interestingly, even under these physiological conditions, DNT/GFP expression at these different B cell stages had a profound impact on the Ig homeostasis in the serum: Both DNT/GFP expressing mouse model showed decreased levels of IgA, whereas IgM was slightly decreased in DNT/mb1Cre mice in contrast to DNT/CD23Cre mice that showed increased IgM levels. The IgG isotypes showed great differences between the DNT/mb1Cre and DNT/CD23Cre mice, underlining a tremendous, underestimated B cell intrinsic effect of mitochondrial metabolism on Ig homeostasis. Although it cannot be said from which tissue these Abs originated, it is reasonable to assume that especially P3 cells of the spleen and bone marrow contribute substantial amounts (Pracht et al., 2017). It is important to note that P3 cell numbers were comparable in both DNT/mb1Cre mice and DNT/CD23Cre mice, compared to the respective Cre controls. However, DNT/GFP expression was drastically reduced, especially within the respective P3 compartments in both mouse model. This implicates that mitochondrial metabolism is essential for PB/PC development, and that even the few DNT/GFP expressing B cells surviving competition have a huge impact on Ig homeostasis. One possible explanation could be that few DNT/GFP expressing activated B cells or PB/PCs affect the generation and/or function of Cre escaper PB/PCs in a paracrine fashion. Since DNT/GFP expression primarily results in decreased mtDNA levels, it is conceivable that mtDNA itself might play a role in CSR and/or Ig secretion. Indeed, having an ancestral bacterial origin, mtDNA in the extracellular space activates a plethora of different pattern recognition receptors and innate immune responses, including cGAS-STING, TLR9 and inflammasome formation resulting in, for instance, a robust type I interferon response (Riley and Tait, 2020). Furthermore, and in support of this notion, Ingelsson et al. showed that human lymphocytes, including B cells, rapidly eject mtDNA upon recognition of CpG and non-CpG oligodeoxynucleotides of class C, resulting in priming for antiviral type I IFN production, specifically the secretion of IFN-α. They conclude that mtDNA webs operate as signals in synergy with cytokines and natural Abs (Ingelsson et al., 2018). IFNα in turn, primes B cells for the production and secretion of IFN-γ, which increases the production of IgG2c (Collins, 2016; de Goër de Herve et al., 2011). Therefore, it is conceivable that important CSR signals in the form of extracellular mtDNA

provided by B cells are lacking in DNT/mb1Cre and DNT/CD23Cre mice, which ultimately impacts Ig homeostasis in the serum. However, this remains speculative and would need to be appropriately tested and determined in future experiments.

The most abundantly produced Ab in mouse and human is IgA, which was significantly reduced in the serum of both DNT/mb1Cre and DNT/CD23Cre mice. The majority of IgA-secreting PCs reside in mucosal tissues, primary the gut-associated lymphoid tissues (GALTs), namely the Peyer's patches, but a substantial fraction of IgA^+ PCs, up to 70% in mice, are also found in the bone marrow niche (Pabst and Slack, 2020; Pracht et al., 2017; Schuh et al., 2020). Interestingly, Kunisawa et al. showed that naïve B cells and the generation but not maintenance of IgA+ PCs requires flux of the TCA cycle: Dietary depletion of vitamin B_1, which results in impaired TCA cycle activity, decreases the numbers of naïve B cells in the Peyer's patches. Furthermore, vitamin B_1-mediated maintenance of naïve B cells is required during initiation phase of immunization, but not thereafter for efficient Ab responses against orally or systemically administered antigens, as intestinal IgA^+ PCs, once they are established, mainly utilize glycolysis. Since HPLC/MS analysis of d3 LPS blasts from DNT/CD23Cre mice showed alterations of several TCA metabolites, such as isocitrate, fumarate, and malate, I conclude that defective OxPhos activity results in impaired flux of the TCA cycle in DNT/GFP expressing cells (Fig 46). Therefore, it is possible that DNT/GFP expression in B cells impairs survival of naïve B cells in the Peyer's patches and the generation of IgA^+ PCs. This is supported by the observed decreased frequency of DNT/GFP expressing B cells and GCs in the Peyer's patches, especially from DNT/mb1Cre mice. Consequently, IgA production would be notably decreased, which indeed is the case in both mouse model. Taken together, these results indicate that especially intestinal B cells and their differentiation into IgA^+ PCs require proper flux of the TCA cycle, which apparently presupposes functional mtDNA replication and OxPhos activity.

7.6. Changes in mitochondrial morphology

The mtRC comprises of 5 complexes that reside in the inner mitochondrial membrane, specifically within the cristal membranes. These structures are regulated and formed by a family of mitochondrial-shaping proteins: A group of GTP-dependent dynamin-like proteins, including Optic atrophy 1 (OPA1) and Mitofusin 1,2, and Drp1 as well as a large multiprotein complex termed Mitochondrial contact site and Cristae Organizing System (MICOS) (Cogliati et al., 2016; Stephan et al., 2020). Interestingly, results obtained from this study could show that CD23Cre mediated inhibition of mtDNA replication had a severe impact on mitochondrial

morphology and cristae structures. This was demonstrated by electron microscopy of naïve B cells and on d3 after LPS activation. Although the size of mitochondria was comparable in naïve B cells from DNT/CD23Cre and CD23Cre B mice, a perturbed cristae structure was already visible. This is in accordance with the decreased mtDNA levels that were observed in naïve B cells (Fig 11B). This leads to the conclusion that either mtDNA itself or proteins encoded on mtDNA (or both) are important factors in the formation of cristae structures. Yet, mtDNA itself is packaged in protein complexes termed “nucleoids” that are located in the mitochondrial matrix and the inner mitochondrial membrane whereas the mtDNA encoded proteins reside within the cristae structures (Yan et al., 2019). Furthermore, it has been shown that dimer ribbons of the ATP synthase are located at the apex of cristae membranes and that this arrangement is at least partially responsible for shaping these structures (Strauss et al., 2008). Therefore, I think it is more likely that the lacking mtDNA encoded proteins are responsible for the observed impaired cristae formation or stabilization. Interestingly, d3 LPS activated B cells with strongly reduced mtDNA content and OxPhos activity from DNT/CD23Cre mice displayed mitochondria that completely lack cristae structures, were highly electron-lucent and hugely enlarged in size. It is reported from studies on human cancer cell lines that the electron density of mitochondria is dependent on the metabolic state of the cell: during glycolysis mitochondria maintain an orthodox state, whereas they switch to a condensed configuration when performing OxPhos due to condensation of the mitochondrial matrix and expansion of the cristal spaces (Rossignol et al., 2004). This could explain the observed electron-lucent mitochondria of DNT/CD23Cre B cells that exhibit strongly reduced OxPhos. It is interesting to note that DNT/CD23Cre B cells do not clear these mitochondria although they apparently are unable to sufficiently perform OxPhos. In addition, these mitochondria are greatly enlarged, which together indicated that the clearance of mitochondria, termed mitophagy, and/or mitochondrial fission/fusion processes may be impaired in these cells. Interestingly, there are several reports where mtDNA depletion resulted in enlarged, electron-lucent mitochondria with disrupted cristae structures: Hepatocytes from human patients with Hepatocerebral Mitochondrial DNA Depletion Syndrome also showed enlarged mitochondria with reduced cristae structures, indicating the importance of mtDNA encoded proteins on cristae formation also *in vivo* in humans (Freisinger et al., 2006). These morphological changes are also observed in mtDNA-deficient human osteosarcoma 143B cells and SH-SY5Y neuroblastoma cells , indicating its importance also in the context of cancer (Chen et al., 2016; Holmuhamedov et al., 2003; Sherer et al., 2000). Unfortunately, none of these reports discuss possible explanations. It is possible that dysfuntional mitochondria result in signals that lead to increased fusion and decreased fission in order to compensate for their dysfunction.

7.7. Metabolic changes in DNT/CD23Cre expressing B cells

B cells experience drastic changes during their lifetime concerning nutrient and oxygen availability, environmental signals, and changes between resting and proliferating phases. Going through these changes, the B cells metabolism must be flexible and support the current energetic demands. Over the past few years, it became clear that the metabolic activity of immune cells is not only supportive during activation and differentiation phases, but even decisive. For instance are glycolysis and FA synthesis key features of LPS activated macrophages, whereas IL-4 activated macrophages mainly use OxPhos and FA oxidation (O'Neill et al., 2016). And effector T cells are highly glycolytic in contrast to memory T cells that display mainly oxidative metabolism (van der Windt and Pearce, 2012). Therefore, metabolism represents the bridge connecting environmental signals with cellular differentiation, function, and outcome. In B cells both OxPhos and glycolysis are upregulated after activation to the same extent (Caro-Maldonado et al., 2014). Of course, the *in vivo* conditions are differing from *ex vivo* yet analysing the metabolism of *ex vivo* LPS activated B cells gives insights into how a defective mtRC affects the cells metabolism. Interestingly, naive DNT/CD23Cre B cells had already a strongly reduced mtDNA content, yet extracellular flux analysis showed comparable OxPhos that was even increased in DNT/CD23Cre B cells after 6h activation. This contrasts with d3 after activation where respiration was reduced by half in DNT/CD23Cre B cells. The comparable respiration in naive B cells could be explained by the fact that mitochondrial morphology and cristae structure were loosened, which was shown using electron microscopy, but apparently, they were still functional for respiration. It is possible that in DNT/CD23Cre B cells at this stage the defects of mtRC assembly are compensated by the activation of retrograde signaling pathways that induce mitochondrial biogenesis and function, as observed in classic Hodgkin and Reed–Sternberg lymphoma cells (Haumann et al., 2020). However, the proliferation that accompanies B cell activation results in strongly reduced mtDNA levels in DNT/CD23Cre B cells on d3 after LPS stimulation, whereas WT B cells increased their mtDNA content during this time. At this time point, electron microscopy revealed drastically enlarged mitochondria with completely disrupted mitochondrial cristae structure in DNT/CD23Cre mice. The defects in mtRC assembly can no longer be compensated and result in strongly reduced oxygen consumption, which was expected and thereby confirmed. This raises the question of how other metabolic pathways are affected by decreased OxPhos. Especially with keeping in mind that survival and initial proliferation were comparable, indicating a compensatory upregulation of other pathways for energetic support. Under conditions where oxygen consumption is not possible, cells typically increase glycolysis. In the presence of oxygen it is termed aerobic glycolysis and was discovered as the "Warburg effect" in cancer cells (Vander Heiden et al., 2009). And indeed, glycolysis was increased in cells with a defective mtRC on

d3 after LPS stimulation, as shown by increased ECAR in extracellular flux analysis and increased lactate and decreased glucose levels in the supernatant. Metabolic flexibility and a shift towards glycolysis in DNT/CD23Cre expressing B cells was also clearly visible in the ATP Rate Assay of LPS, or α-IgM, or α-CD40/IL4, or α-IgM/a-CD40/IL4 activated B cells (d3). This approach furthermore revealed different metabolic phenotypes after the respective stimulations: Whereas α-IgM alone results in a mainly mitochondrial phenotype, at least in CD23Cre controls, the addition of α-CD40/IL4 leads towards more glycolytic ATP production. Importantly, DNT/CD23Cre expressing B cells showed great flexibility and were able to compensate ATP production upon α-IgM, or α-CD40/IL4, or α-IgM/a-CD40/IL4 stimulation by increasing glycolysis.

This switch towards glycolysis in DNT/CD23Cre expressing B cells could be mediated by the TF HIF1α that becomes activated under hypoxic but also under pseudo-hypoxic conditions. HIF1α is continuously expressed and degraded in the cytosol via oxygen-dependent hydroxylation by PHDs with subsequent ubiquitinoylation for proteasomal degradation by the von Hippel-Lindau protein (VHL). Under hypoxia, when HIF1α cannot be hydroxylated, it becomes stabilized, transported to the nucleus and results as a dimer with the HIF1b subunit in the transcription of HIF target genes. Essentially all glycolytic enzymes are directly upregulated by HIFs (Dengler et al., 2014), thereby mediating the metabolic switch from oxidative metabolism towards glycolysis. The stabilization of HIF1α under normoxic conditions is for instance mediated by metabolites: The PHD mediated hydroxylation of HIF1α requires beside oxygen also iron, ascorbate, and a-ketoglutarate. But the binding of a-ketoglutarate is in competition with the TCA cycle derived metabolites fumarate and succinate, and the ratios of these metabolites to a-ketoglutarate determine the activity of PHD. Therefore, altered TCA activity resulting in an accumulation of fumarate and/or succinate can induce HIF1α stabilization under normoxic conditions. The abundance of intracellular metabolites was determined on d3 after LPS activation by HPLC/MS analysis and indeed showed an accumulation of fumarate, which could explain HIF1α stabilization in DNT/CD23Cre B cells (Fig 45). In general, there was a reduction of metabolites upstream of the succinate dehydrogenase (SDH), namely citrate, isocitrate and itaconate, and accumulation of metabolites downstream of SDH detectable. It should be noted that the SDH is complex II of the mtRC, it connects and participates in both, TCA cycle and OxPhos, and it is the only mtRC complex that is entirely encoded in the nucleus. Metabolites of the glycolysis pathway were also altered with a slight increase of glucose and erythrose-4-phosphate (E4P) and a reduction of 3PG and PEP, indicating that DNT/DC23Cre expressing B cells divert their glucose into the pentose phosphate pathway, which could explain their initial ability to survive and proliferate. Moreover, this approach confirmed a reduction in intracellular ATP levels on d3, which was

also shown by extracellular flux analysis and luminometric analysis, and an increase of AMP, resulting in an altered AMP/ATP ratio.

Since both, glycolysis and TCA cycle, generate metabolites that are important for lipid synthesis and both pathways are altered in DNT/CD23Cre expressing LPS blasts, it is expected that the intracellular lipid composition is consequently also altered. This was confirmed using direct infusion MS/MS (Shotgun Lipidomics) that showed a significant and specific reduction of the saturated, short-chained phospholipid phosphatidic acid (PA). This turns out to be highly interesting, since PA has a unique role as being both, a key building block for phospholipid synthesis and a major lipid second messenger (Tanguy et al., 2019). It is the simplest phospholipid and constitutes only a minor fraction of the total cell lipids (Ammar et al., 2014), and its reduction was the only significant alteration concerning the absolute phospholipid abundance in DNT/CD23Cre expressing B cells. There are three main pathways producing PA: The LPAAT pathway, that is mainly required for *de novo* synthesis of phospholipids, and the DGK and PLD pathways, that are mainly activated by growth factors (Foster et al., 2014). The LPAAT pathway for PA production is especially interesting in this context, because it requires intermediates that are generated in both, glycolysis and the TCA cycle: Glycolysis derived G3P becomes doubly acetylated with a fatty acid, that is produced in the cytosol from TCA cycle derived citrate, which is exported into the cytosol and converted to acetyl-CoA. Although the abundance of G3P was not analysed in this study it is conceivable that it is reduced because of increase glucose diversion into the PPP. Additionally, the observed reduction of citrate in DNT/CD23Cre expressing B cells supports this idea. Taken together, this study shows that a functional mtRC and OxPhos is required in activated B cells for proper flux of the TCA cycle, and ultimately the regulation of glycolysis and the synthesis of PA.

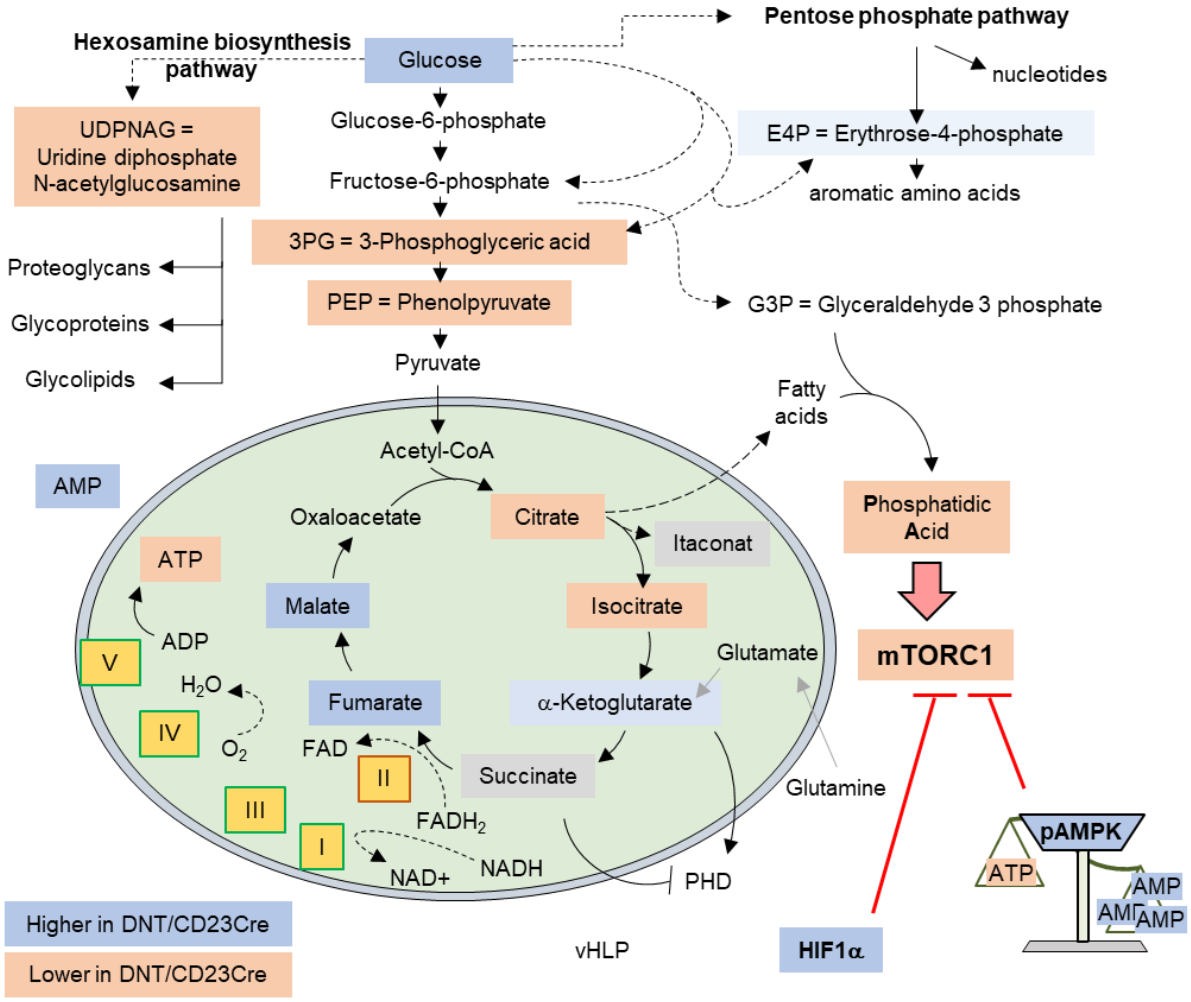

Figure 45 | Model of metabolic changes induced by impaired mitochondrial respiration.
Roman letters indicate OxPhos complexes I-V, complexes outlined in green contain mtDNA-encoded subunits. Metabolites and factors decreased in DNT B cells are shown in orange colour, increased metabolites and factors are indicated in blue colour, and unchanged in grey. G3P, Glyceraldehyde-3-phosphate, 3PG, 3-Phosphoglycerate, E4P, Erythrose-4-Phosphate, NAD, Nicotinamide adenine dinucleotide, NADPH, Nicotinamide Adenine Dinucleotide phosphate, FAD, Flavine Adenine Dinucleotide, FADH2, Flavine Adenine Dinucleotide Dihydrate, PHD, prolyl hydroxylase domain-containing enzymes, vHLP, von-Hippel-Lindau-protein, HIF1α, hypoxia-inducible-factor 1a.

7.8. Metabolic regulation of mTORC1

The findings that proper mtRC assembly and concomitant OxPhos activity are required for the generation of PA are especially important because they connect metabolic dysfunction with cell signaling via mTORC1. This key kinase integrates information about nutrient abundance and environmental cues and balances anabolic and catabolic processes in the cell (Saxton and Sabatini, 2017). Furthermore, it has been shown that mTORC1 plays an important role during B cell activation and subsequent plasma cell differentiation (Benhamron et al., 2015; Gaudette et al., 2020; Jones et al., 2016). Interestingly, PA is a direct activator of mTORC1 (Foster, 2013; Yoon et al., 2011b), while pAMPK, which is activated by a decreased AMP/ATP ratio, is an inhibitor of mTORC1 (Hindupur et al., 2015; Shaw, 2009). One of the downstream

targets of mTORC1 is pRPS6 and its phosphorylation was analysed in this study to investigate mTORC1 activity in B cells with a dysfunctional mtRC (Hindupur et al., 2015). The results obtained from western blot and FACS analysis showed a significant reduction in mTOR activity on d2 and d3 after LPS activation in DNT/CD23Cre expressing B cells. There are several possible explanations for this observation (Fig 46): First, it was shown that DNT/CD23Cre expressing B cells have increased pAMPK, which is probably caused by the observed decreased AMP/ATP ratio. Secondly, impaired OxPhos resulted in decreased PA levels in activated B cells, which is a direct activator of mTORC1. That could mean that continuous PA synthesis via the *de novo* pathway may be required for sustained mTORC1 activation, which ultimately depends on OxPhos for proper flux of the TCA cycle and glycolysis and the resulting generation of required metabolites. And third, impairment of OxPhos and the following metabolic changes resulted in HIF1α stabilization under normoxic conditions in d3 LPS blasts from DNT/CD23Cre mice. The exact regulatory mechanisms between HIF1α and mTORC1 are controversial, depend on the cell type and therefore require further investigation: Several studies showed that mTORC1 is an upstream activator of HIF1 α function (Hudson et al., 2002; Land and Tee, 2007; Xia et al., 2012), yet only limited research exist on how HIF1α activity in turn affects mTORC1: Whereas hypoxia promoted mTORC1 activity in pulmonary arterial vascular smooth muscle cells (Krymskaya et al., 2011) and cancer cells (Doan et al., 2019), interestingly it is reported for B cells that sustained hypoxia or genetic HIF1α induction inhibited mTORC1 activity during B cell activation and consequently impaired plasma cell differentiation (Cho et al., 2016). Activated B cells from DNT/CD23Cre mice have defective respiration that alters flux of the TCA cycle. This results in stabilization of HIF1α induced by accumulation of TCA intermediates (Bailey and Nathan, 2018). In accordance with the study from Cho et al. it is conceivable that the HIF1α stabilization in DNT/CD23Cre B cells, that is induced by metabolic alterations, represents an additional pathway of mTORC1 inhibition in these cells (Cho et al., 2016).

7.9. Mitochondrial respiration in B cells is required for the humoral immune response

To analyse what role mitochondrial respiration in B cells plays *in vivo* during the immune response, I immunized DNT/CD23Cre mice with the TD antigen NP-KLH and the TI antigen NP-Ficoll in two separate sets of experiments. The generation of PB/PCs in the spleen and bone marrow were analysed by flow cytometry, whereas the abundance of antigen-specific Abs in the serum was determined by ELISA. Both immunization models resulted in a diminished humoral immune response in DNT/CD23Cre mice as shown by decreased levels

of antigen-specific antibodies and decreased generation of DNT/GFP expressing, antigen-specific PB/PCs. Therefore, the first conclusion that can be drawn is that B cells require mitochondrial respiration for their effector function during the humoral immune response. This is in accordance with reports showing that activated B cells increase mitochondrial respiration but also glycolysis, as well as reports showing a progressive upregulation of OxPhos genes after LPS activation (Caro-Maldonado et al., 2014; Price et al., 2018). These metabolic changes occur early after B cell activation within 15 minutes and interestingly, especially OxPhos, in contrast to glycolysis, is required for early antigen induced BCR functions, namely B cell spreading and BCR accumulation at the antigen contact site. Also antigen internalization and trafficking to acidic compartments is dependent on OxPhos, but not glycolysis (Akkaya et al., 2018). Intriguingly, Akkaya et al. also showed increased mtDNA content in stimulated B cells for 24h with CpG or CpG/anti-IgM (Akkaya et al., 2018). However, DNT/CD23Cre expressing B cells showed comparable or even slightly higher OCR 6h after LPS or anti-IgM stimulation, which could be due to the activation of compensatory mechanisms as discussed above. Therefore, it remains to be determined in the future, if the early activation events such as B cell spreading, BCR accumulation, and antigen processing and trafficking are impaired in DNT/CD23Cre expressing B cells. Importantly, mitochondrial respiration is also reported to be required during later important B cell activation processes, namely CSR and SHM: The coupled analysis of single cell RNA sequencing and BCR mutations revealed that GC B cells acquiring higher-affinity mutations showed elevated expression of OxPhos genes (Chen et al., 2021). Furthermore, they also observed decreased frequencies of GC B Cells and NP-specific IgG1 ASCs in Cox10 deficient mice after NP-KLH immunization. Cox10 deficiency also leads to impaired OxPhos activity, since it is required for the assembly of complex IV of the ETC. They additionally showed in these mice that GC B cells require OxPhos not only for clonal expansion, but importantly for efficient positive selection. Concluding from these findings it is conceivable that CSR, SHM, and positive selection during the TD immune response are impaired in DNT/CD23Cre mice which might explain decreased levels of high-affine IgG antibodies after NP-KLH immunization. Although Chen et al. could convincingly show the connection between mitochondrial respiration and clonal expansion/positive selection within the germinal center, precise mechanisms remain speculative, and possibly include fine-tuning of cell cycle phases and division (Chen et al., 2021).

The process of CSR on the other hand, may be connected to mitochondrial respiration via purinergic signaling. This notion is supported by studies showing that the coordinate stimulation of BCR and TLR results in rapid release of ATP stored in Ca2+ sensitive secretory vesicles. The subsequent ectoenzymatic activity of CD39 and CD73 is then required for the induction of CSR (Schena et al., 2013). Accordingly, CD73 expression is progressively upregulated in GC B cells upon immunization where it is required for successful generation of

BM PCs in the late phase of the primary immune response (Conter et al., 2014). Schena et al. also showed the direct effect of extracellular adenosine on CSR by treatment of isolated naïve B cells and Bmems with a specific CD73 inhibitor and adenosine: Whereas treatment with CD73 inhibitor significantly affected the generation of isotype switches Ig of both naïve B cells and Bmems, the addition of adenosine significantly increased the generation of class-switched B cells (Schena et al., 2013). These purinergic signaling processes require continuous production of ATP that is mainly provided by mitochondria, which are precisely colocalized with the purinosome for this purpose (Huang et al., 2021). Taken together, these finding allow the suggestion that OxPhos activity in B cells is required for CSR by continuously providing ATP that is needed for extracellular, CD73-mediated adenosine production, which in turn is important for successful CSR. This could explain the decreased, class-switched Ab levels after immunization in DNT/CD23Cre mice, as well as decreased CSR of isolated DNT/GFP expressing B cells *in vitro* (Fig 28A, 29G, 35E, F).

One striking observation is that the TI immune response appears to be more dependent on functional mitochondria compared to the TD immune response: Whereas TD immunization of DNT/CD23Cre mice resulted in the generation of antigen-specific IgM Abs, only minimal antigen-specific IgM levels were detectable after TI immunization. One possible explanation could be that MZ and B1 B cells, compared to FO B cells, are particularly dependent on mitochondrial respiration, as these subsets are predominantly activated after TI immunization, whereas TD immunization mainly induces GC formation by FO B cells (Daly et al., 2020). Several results obtained in this study but also published data support this idea: First, resting MZ B cells, compared to FO B cells, have a higher mtDNA content. Second, I observed a clear selection of Cre escaper B cells into the MZ compartment of DNT/mb1Cre mice, highlighting a low tolerance for defective mitochondria in the development of MZ B cells. Therefore, MZ B cells, which are in a preactivated state and show accelerated differentiation kinetics upon stimulation, may be especially dependent on mitochondrial respiration and may not be able to sufficiently mount the immune response under DNT/GFP expression (Oliver et al., 1999). This is also evident in decreased MZ B cell numbers in DNT/CD23Cre mice on d7 after TI immunization: Whereas unimmunized CD23Cre mice had ~$1x10^6$ MZ B cells, this number was increased to ~$2x10^6$ MZ B cells in immunized mice, which is in accordance with published results showing a peak of antigen-specific MZ B cells on d5 after immunization (Vinuesa et al., 1999). Importantly, MZ B cells numbers from unimmunized DNT/CD23Cre mice were with ~$1x10^6$ cells comparable, however this number was even reduced to ~$0.5x10^6$ MZ B cells on d7 after immunization. Therefore, I speculate that OxPhos activity, which presupposes functional mtDNA replication, is required for antigen-induced MZ B cell proliferation, although this would need to be formally shown since it is possible that proliferation is comparable,

whereas apoptosis may be increased (or a combination of decreased proliferation and increased apoptosis).

A further explanation could be that both TD and TI activated B cells require OxPhos, however the selection for functional mitochondria might more efficient during the TD immune response, which would mean that Cre escaper B cells are more efficiently selected and subsequently differentiate into functional, antigen-specific PB/PCs. The results obtained in this study support this idea, since the compartment of antigen-specific PB/PCs in the bone marrow was devoid of DNT/GFP expression on d70 after TD immunization using NP-KLH (Fig 28F) whereas antigen-specific IgM titers were comparable (Fig 28A), indicating that B cells that escaped Cre recombination are selected for the generation of antigen-specific PCs. However, it appears that selection for B cells with functional respiration, meaning for Cre escaper B cells, occurs also during a TI immune response: Whereas 83% of antigen-specific PB/PCs in the spleen express DNT/GFP on d7, the frequency drops to 53% on d14 (Fig 29F). This means that although selection for functional mitochondria occurs also during the TI immune response, still the majority of generated PB/PCs express DNT/GFP and are apparently not functional. This would also be in accordance with the drastic gap between reduced PB/PC numbers in the spleen, but almost absent antigen-specific Abs in the serum observed upon TI immunization using NP-Ficoll. In summary, these data show that mitochondrial respiration is not only required for the differentiation of PB/PCs, but more importantly for their effector function.

4.1 Concluding remarks

This thesis aimed at elucidating how mitochondrial respiration in B cells affects their development in the bone marrow, their activation, and ultimately the adaptive immune response *in vivo*. For this purpose, mice with a B cell specific inhibition of mtDNA replication, which ultimately results in impaired mitochondrial respiration, were generated and analysed. The combination of *in vivo* and *ex vivo* experiments allowed the identification of selection checkpoints for functional mitochondria and underlying metabolic changes accompanying B cell activation and subsequent plasma cell differentiation. Concluding the findings discussed above, I could show that mtDNA replication is required for B cell development in the bone marrow at the pre B cell transition (Fig 46A). Furthermore, transitional B cells with functional mtDNA replication are favoured in the selection for marginal zone B cell development that also exhibit a higher mtDNA content compared to FO B cells. Importantly, antigen specific antibody titers were decreased upon TD-immunization and basically absent upon TI-immunization, highlighting the importance of mitochondrial respiration in B cells for the humoral immune response. Mechanistically, it was shown that impaired OxPhos activity in *in vitro* activated B cells results in increased glycolysis, altered flux of the TCA cycle, and decreased generation of PA. Furthermore, these metabolic changes increased pAMPK and HIF1α activity, whereas consequently mTORC1 and BLIMP1 were reduced, which ultimately results in impaired plasma blast differentiation (Fig 46B).

In summary, this thesis identified mitochondrial respiration, which presupposes functional mtDNA replication, as crucial factor during B cell development, plasma cell differentiation and ultimately the humoral immune response.

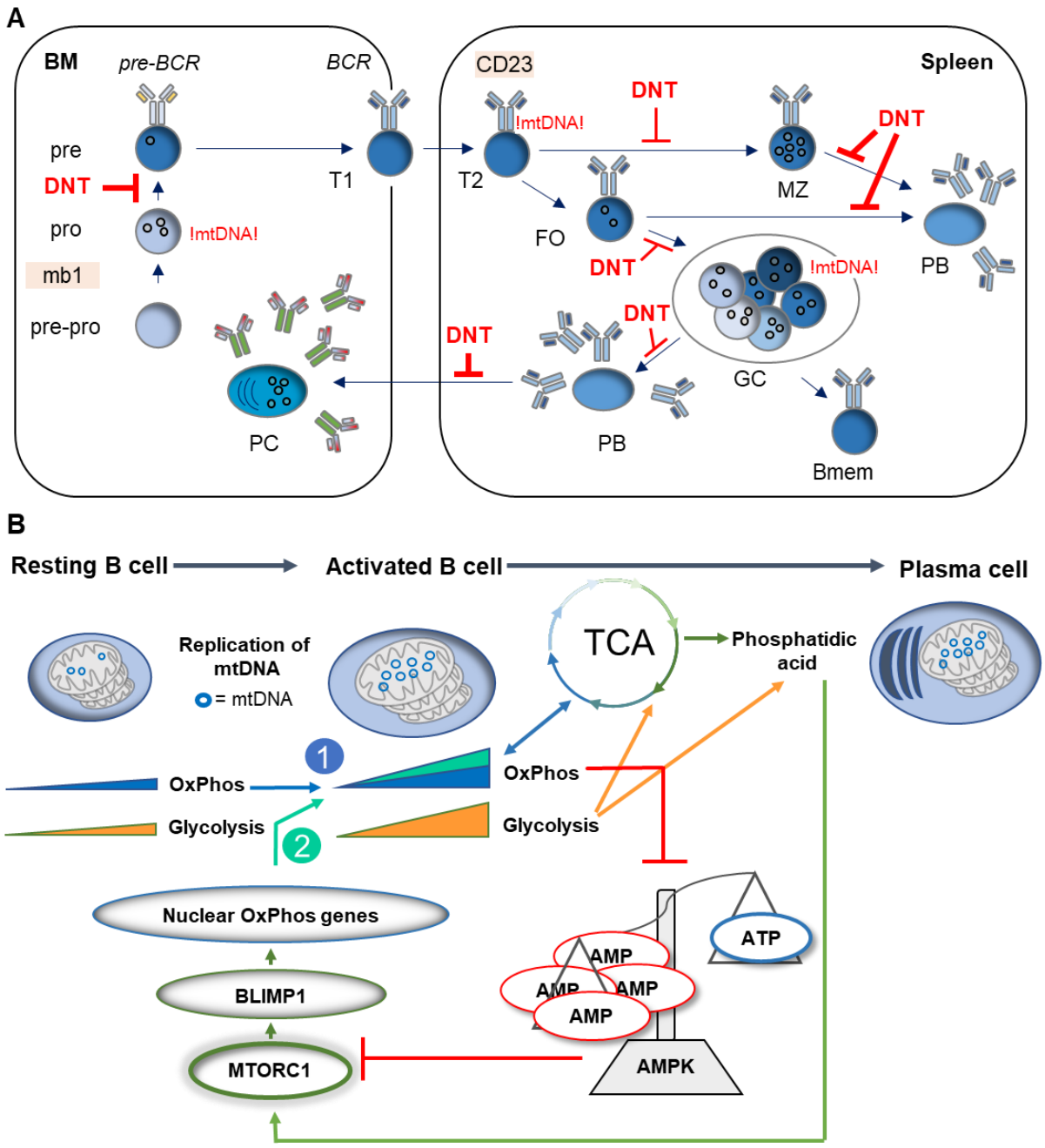

Figure 46 | A) Proposed model of mtDNA replication and content in B cells

Schematic of relative mtDNA content during B cell development and differentiation. Stages with increased mtDNA replication are indicated in „!mtDNA!"; blocks during differentiation that are induced by expression of a dominant negative mtDNA helicase („DNT") (either by mb1Cre or CD23Cre recombination) are indicated in red (thickness of lines indicate degree of blockage); the relative mtDNA abundance of selected B cell subsets was determined by qPCR and is represented by amounts of circles. Interpretations are based on findings obtained in this study.

B) Integrated model of OxPhos controlled plasma cell differentiation

Proposed model of OxPhos controlled plasma cell differentiation showing that LPS activated B cells replicate mtDNA which is essential for increasing OxPhos activity. This initial increase in OxPhos (1) is required for proper TCA flux, which is important for the continuous generation of phosphatidic acid. Phosphatidic acid activates mTORC1 and BLIMP1 is expressed, which leads to a progressive upregulation of nuclear encoded OxPhos genes, thereby further increasing OxPhos (2). Combined upregulation of mtDNA encoded essential mtRC subunits and nuclear mtRC components ensures full OxPhos activity which prevents AMPK activation and preserves mTORC1 activity. This positive feedback loop between OxPhos and BLIMP1 expression ensures the generation of plasma cells harboring functional mitochondria. [Figure adapted and modified from Urbanczyk et al., interpretations include findings from (Price et al., 2018; Yoon et al., 2011b)].

8. Material

8.1. Consumables

Table 1: Consumables

Products	Company
96-well megablocks	Sarstedt
96-well plates (U-/F-bottom)	Greiner bio-one
Cannulas	BD
Cell culture flasks	Greiner bio-one
Cell strainers	Corning Life Sciences
Cover slips	ThermoFisher, Chemometec
FACS tubes	Micronic
Filter systems	Merck Millipore, Sarstedt, Sysmex
Filter tips	Nerbe plus
Microscope slides	ThermoFisher
Microtainer tubes	BD
Multi-well cell culture plates	Greiner bio-one
NC counting slides A8	ChemoMetec
Nitrocellulose membrane	Amersham
PCR reaction tubes	Peqlab
Petri dishes	Sarstedt
Polypropylene round bottom tubes	Falcon
Reaction tubes	Eppendorf, BD
Seahorse Cell Culture Microplate	Agilent
Seahorse Cartridge	Agilent
Round bottom tubes	Falcon, Sarstedt
Serological pipettes	Greiner bio-one, Sarstedt
Serum tube	BD
Syringes	BD
Whatman paper	GE Healthcare
X-ray film CL-Xposure	Thermo Scientific

8.2. Commercial Kits

Table 2: Commercial kits

Product name	Company	Catalogue number

AnnexinV Apoptosis Detection Kit APC	eBioscience	88-8007-74
ATP Luminescence Assay	Roche	11699709001
CellCount and Viability Solution 13	Chemometec	910-3013
DNeasy Blood & Tissue Kit	Quiagen	69504
EasySep™ Mouse B Cell Isolation Kit	StemCell	19854
FIX&PERM Cell Kit	Dianova	GAS-002-1-CE/IVD
RevertAid First Strand cDNA Synthesis Kit	Thermo Scientific	K1622
SYBR™ Green PCR Master Mix	Applied Biosystems™	4309155

8.3. Chemicals and reagents

All chemicals and reagents were obtained at analytical quality from Carl Roth or Sigma Aldrich, if not stated otherwise.

Table 3: Chemicals & reagents

Reagent	Company	Catalogue number
100bp DNA ladder	New England BioLabs	N3231S/L
Agarose	PeqLab	732-2789
Albumin fraction V (BSA)	Carl Roth	8076.4
anti-CD40	purified from FGK cells	
Antimycin A	Sigma-Aldrich	A-8674
APS	Carl Roth	9592.3
BSA, fatty acid free	Sigma-Aldrich	A3803
DAPI	Carl Roth	28717-90-3
DMSO	Molecular Probes	C10634
dNTPs	Genaxxon Bioscience	M3018 - M3021
Ethidium bromide	Carl Roth	2218
EtOH	Merck	1.00983.2500
FCCP	Sigma-Aldrich	C2920
Fetal calf serum (FCS)	Gibco	10270-106
Glucose	Carl Roth	HN06.3
Glutaraldehyde	Carl Roth	4995.1
H_2SO_4	Merck	
Imject alum adjuvants	ThermoFisher	77161
Interleukin-4	Miltenyi Biotec	130-097-761
Interleukin-5	PeproTech	215-15
L-Glutamine	Gibco	25030-24
LPS	Sigma-Aldrich	L3012

Mowiol 4-88	Calbiochem	47-590-4100GM
Milk Powder	Carl Roth	T145.3
NaN_3	Carl Roth	26628-22-8
NP_{20}-BSA	Biosearch Technolgies	N-5050H-10
NP_4-BSA	Biosearch Technolgies	N-5050L-10
NP_{24}-KLH	Biosearch Technologies	N-5060-5
Oligomycin	Sigma-Aldrich	75351
PageRuler Prestained Protein Ladder	Thermo Scientific	26616
p-Cumaric acid	Carl Roth	9908.2
Penicillin-streptomycin	Gibco	15140-122
Phosphate-Buffered Saline (PBS), 1x	Gibco	14190-094
PMSF	Sigma-Aldrich	329-98-6
Poly-L-Lysine	Sigma-Aldrich	P8920
Ponceau S	Carl Roth	5938.1
Propodium iodide	Sigma-Aldrich	
Proteinase K	Peqlab	04-1076
Rapamycin	Sigma-Aldrich	53123-88-9
Rotenone	Sigma-Aldrich	R8875
SDS	Carl Roth	151-21-3
Taq Buffer	Genaxxon Bioscience	
Taq Polymerase	Genaxxon Bioscience	M3001.5000
TEMED	Carl Roth	2367.3
Tris	Carl Roth	4855.3
Tween-20	Carl Roth	P1379

8.4. Buffer, Solutions and Media

Table 4: Buffers, solutions and medium used for this thesis (self-made)

Reagent	Composition	Solvent
Antibody dilution	3g/100ml BSA 0.1ml/100ml Tween-20 0.1ml/100ml NaN_3	PBS
Anode buffer 1	25mM Tris 20/100ml MeOH	dH_2O
Anode buffer 2	300mM Tris	dH_2O

	20/100ml MeOH	
Cathode buffer	40mM 6-Aminocaproic acid 20ml/100ml MeOH	dH_2O
Cell sorting buffer	2% FCS 5mM EDTA	PBS
DNA loading buffer, 5x	10mM EDTA 25% glycerol 0.025% xylencyanol	
ECL	10ml/100ml 1M Tris pH 8.5 1ml/100ml 250mM Luminol 0.45ml/100ml 90mM p-Cumaric acid	dH_2O
ELISA Wash buffer	0.5ml/l Tween-20	PBS
ELISA coating buffer	35mM $NaHCO_3$ 15mM Na_2CO_3	dH_2O
ELISA Stop solution	0.5M H_2SO_4	dH_2O
FACS buffer	2% FCS 0.05% NaN_3	PBS
2.5% Glutaraldehyde	2.5g/100ml Gluteraldehyde	PBS
Mowiol	0.4g/ml Mowiol 4-88 1g/ml glycerol	dH_2O
PBND buffer	50mM KCl 10mM Tris-HCl pH 8.4 2.5mM $MgCl_2$ 1mg/ml gelatine 0.45% NP40 0.45% Tween20	dH_2O
Phosphate-Buffered Saline (PBS), 10x	1.37M NaCl 27mM KCl 81mM Na_2HPO_4 8mM KH_2PO_4	dH_2O
Ponceau S	1g/l Ponceau S	dH_2O
Protein loading buffer	10g/100ml SDS 40ml/100ml 1M Tris pH6.8 10ml/100ml b-ME 50m/100ml Bromophenol blue	Glycerol
R10 medium	10% FCS	RPMI1640

	2mM L-glutamine 1mM sodium pyruvate 100U/ml penicillin 100µg/ml streptomycin 50µM β-mercaptoethanol	
Seahorse coating buffer	1mg/100ml poly-L-lysine	TE
Seahorse medium	1mM Pyruvate 2mM Glutamine 10mM Glucose	
Solution 13	30mg/ml Acridine orange 100µg/ml DAPI	dH_2O
TAE buffer	40mM Tris/HCl pH 8.5 20mM sodium acetate 1mM EDTA	dH_2O
TBS-T	8.77g/l NaCl 2.42g/l Tris 1ml/l Tween-20 adjust pH 7.4 with HCl	dH2O
1M Tris/HCl pH 6.8	1M Tris adjust pH 6.8 with HCl	dH_2O
1M Tris pH 8.5	1M Tris adjust pH 8.5 with HCl	dH_2O

Table 5: Buffers, solutions and medium (bought)

Name	company	comment
30% Acrylamid	Roth	Rotiphorese Gel 30
β-Merpatoethanol	Gibco	50mM
EDTA solution	Invitrogen	0.5M EDTA Ultrapure pH 8.0
Ethidium bromide	Roth	1% ethidium bromide solution in water
FCS	Gibco	
Glutamine	Gibco	200mM
H_2O_2	AppliChem	35% solution
OptiMEM	Gibco	
PBS	Gibco	
PenStrep	Gibco	10,000 U/ml Penicillin 10,000mg/ml Streptomycin

Pyruvate (sodium)	Gibco	100mM
qPCR SYBR green	Applied Biosystems	
RPMI	Gibco	
Seahorse calibrant	Agilent	
Seahorse XF RPMI medium	Agilent	

8.5. Oligonucleotides

All oligonucleotides were obtained from Invitrogen at desalted quality and were dissolved in ultra-pure H_2O as 100µM stock solutions.

Table 6: Oligonucleotides used in this thesis

Name	internal ID	sequence (5'-3')	use
DNT fwd	5699	TGTCGCAAATTAACTGTGAATC	genotyping
DNT rev (I)	5700	GATATGAAGTACTGGGCTCTT	
DNT rev (II)	5701	AAAGTCGCTCTGAGTTGTTATC	
mb1 fwd	2153	CTGCGGGTAGAAGGGGGTC	genotyping
mb1 rev	2154	CCTTGCGAGGTCAGGGAGCC	
Cre fwd	2819	ACCTCTGATGAAGTCAGGAAGAAC	
Cre rev	2820	GGAGATGTCCTTCACTCTGATTCT	
CD23Cre fwd (I)	6326	CAGATGCTGTCCTACACCCA	genotyping
CD23Cre rev (II)	6328	TGAGTCACAGAAAGGAGGGG	
CD23Cre rev (III)	6329	TCCCTGAACATGTCCATCAG	
Prdm1 fwd	4440	ACACACAGGAGAGAAGCCACATGA	qPCR
Prdm1 rev	4441	TCGAAGGTGGGTCTTGAGATTGCT	
Actin fwd	3027	TGGAATCCTGTGGCATCCATGAAAC	qPCR
Actin rev	3028	TAAAACGCAGCTCAGTAACAGTCC	
HK2 fwd	6261	GCCAGCCTCTCCTGATTTTAGTGT	qPCR
HK2 rev	6262	GGGAACACAAAAGACCTCTTCTGG	
ND1 fwd	6259	CTAGCAGAAACAAACCGGGC	qPCR
ND1 rev	6260	CCGGCTGCGTATTCTACGTT	
16s rRNA	6257	CCGCAAGGGAAAGATGAAAGAC	qPCR
16s rRNA	6258	TCGTTTGGTTTCGGGGTTTC	

8.6. Antibodies and fluorescent dyes

Table 7: Antibodies used for FACS

Antigen	Conjugate	Company	Clone	Dilution	Catalogue number
B220	PerCPCy5.5	eBioscience	Ra3-6b2	100	103236
B220	BV421	biolegend	Ra3-6b2	100	103251
Blimp 1	PE	eBioscience	clone 567	50	12-9850-82
CD11b	BV510	biolegend	M1/70	200	101263
CD11c	APC.Cy7	biolegend	N418	200	117323
CD138	PE.Cy7	biolegend	281-2	1500	142514
CD19	BV421	biolegend	6D5	100	115538
CD19	BV510	biolegend	6D5	50	115545
CD19	APCFire750	biolegend	6D5	400	115558
CD21/35	BV421	biolegend	7E9	100	123421
CD23	PE	eBioscience	B3D4	400	12-0232-82
CD23	APC.Cy7	biolegend	B3B4	200	101629
CD25	APC	Biolegend	PC61	800	102012
CD25	APC.Cy7	Biolegend	PC61	800	102025
CD25	BV421	biolegend	PC61	200	102033
CD38	PE	biolegend	90	1500	102707
CD38	APC.Cy7	biolegend	90	1000	102728
CD38	PerCPCy5.5	biolegend	90	100	102722
CD3e	PE	eBioscience	145-2c11	300	12-0031
CD4	PE	BD	RPA-T4	800	555347
CD4	PE	eBioscience	gk1.5	800	12-0041-82
CD8a	PE	eBioscience	53-6.7	800	12-0081
CD8a	APC	eBioscience	53-6.7	800	17-0081
ckit	BV421	BD Pharmingen	2B8	100	562609
ckit	APC	eBioscience	2b8	1000	17-1171
GL7	AF647	BD Pharmingen	GL7	500	561529
GL7	Pacific Blue	biolegend	GL7	100	144614
IgA	AF647	Southern Biotech		10000	1040-31

IgA	BV421	BD Bioscience	C10-1	800	743293
IgA	AF647	Southern Biotech	1040-31	10000	1040-31
IgA	BV421	BD Bioscience	C10-1	800	743293
IgD	AF647	Southern Biotech	1120-31	1500	1120-31
IgG	PerCPCy5.5	biolegend	Poly4053	800	405314
IgM	Cy5	Southern Biotech	1020-15	5000	1020-15
IgM	PE	Southern Biotech	1021-09	1000	1021-09
pS6	PE	eBioscience	cupk43k	50	12-9007-42
TACI	PE	eBioscience	eBio8F10-3	100	12-5942
TACI	APC	eBioscience	eBio8F10-3	1000	17-5942
TACI	BV421	BD Pharmingen	8F10	600	742840

Table 8 | Antibodies used for ELISA and Western Blot

Antigen	Species	Conjugate	Company	Catalogue number	Usage
Actin	rabbit	Unlabeled	Sigma-Aldrich	A2066	Western Blot
anti-rabbit	goat	HRP	Jackson Immuno Research	111-035-046	Western Blot
anti-rat	goat	HRP	Jackson Immuno Research	112-035-071	Western Blot
Blimp1	rat	Unlabeled	Santa Cruz	sc-47732	Western Blot
HIF1a	rabbit	Unlabeled	Cayman	10006421	Western Blot
IgA	goat	HRP	Southern Biotech	1040-05	ELISA

IgA	goat	Unlabeled	Southern Biotech	1040-01	ELISA
IgG	goat	HRP	Southern Biotech	1030-05	ELISA
IgG	goat	Unlabeled	Southern Biotech	1030-01	ELISA
IgG1	goat	HRP	Southern Biotech	1071-05	ELISA
IgG1	goat	Unlabeled	Southern Biotech	1071-01	ELISA
IgG2b	goat	HRP	Southern Biotech	1090-05	ELISA
IgG2b	goat	Unlabeled	Southern Biotech	1091-01	ELISA
IgG2c	goat	Unlabeled	Southern Biotech	1078-01	ELISA
IgG2c	goat	HRP	Southern Biotech	1078-05	ELISA
IgG3	goat	HRP	Southern Biotech	1100-05	ELISA/ Western Blot
IgG3	goat	Unlabeled	Southern Biotech	1100-01	ELISA
IgM	goat	Unlabeled	Southern Biotech	1020-01	ELISA
IgM	goat	HRP	Southern Biotech	1020-05	ELISA/ Western Blot
IgM F(ab)2 fragment, µ chain-specific	goat	Unlabeled	Jackson Immuno Research	115-006-075	B cell activation
IRF4	rabbit	Unlabeled	Cell Signaling	4948	Western Blot
pAMPK	rabbit	Unlabeled	Cell Signaling	2535	Western Blot
pS6	rabbit	Unlabeled	Cell Signaling	4858	Western Blot
TWINKLE	rabbit	Unlabeled	Abcam	187517	Western Blot

XBP1	rabbit	Unlabeled	Cell Signaling	12782	Western Blot

Table 9: Fluorescent dyes used for labeling of viable and fixed cells

Dye	Dilution/ Concentration	Company	Catalogue number
Cell Proliferation Dye eFluor™ 450	5mM	eBioscience	65-0842-85
Fixable Viability Dye eFluor™ 780	15.000	eBioscience	65-0865-14
MitoTracker Green FM	20nM	Cell signaling	9074S
TMRM	20nM	Sigma-Aldrich	T5428

8.7. Software

Table 10: Software used for data acquisition, analysis and graphics

Software	Version	Utilization
GraphPad Prism	7.0	Data presentation, statistical analysis
ImageJ (Fiji)	1.52a	Western Blot analysis
Kaluza	2.1	Flow cytometric analysis
Microsoft Office	2108	Data analysis and presentation
NucleoView	2.1.25.12	Cell counting
Pyrat	4.4.1-494	Mouse management
Wave	2.6.3.5	Seahorse analysis
Zotero	5.0.96.3	Citation management

8.8. Mouse strains

Table 11: Mouse strains used for *in vivo* experiments and *in vitro* analyses of primary B cells

Internal name	Nomenclature	Reference
DNT	R26-K320E-Twinkle loxP+/-	(Baris et al., 2015)
mb1Cre	Cd79atm1(cre)Reth	(Hobeika et al., 2006)
CD23Cre	Tg(Fcer2a-cre)5Mbu	(Kwon et al., 2008)

9. Methods

9.1. Animal housing

All mice used in this study were bred under pathogen free conditions and kept in the Franz-Penzoldt-Center and animal facility of the Nikolaus-Fiebiger-Center (Erlangen). DNT mice were crossed to either mb1Cre or CD23Cre mice and animals with $DNT^{+/-}Cre^{+/-}$ were used in the experiments. The respective $Cre^{+/-}$ littermates served as controls. Littermates with $DNT^{-/-}$ $Cre^{-/-}$ were used in wildtype experiments. All experiments were performed according to the guidelines of the Federation of European laboratory animal science association (FELASA B).

9.2. Genotyping of mice

Biopsies from mice were collected from ear or tail and stored on -70°C until further use. Genomic DNA was extracted by lysis of the biopsies in 100µl (ear) or 150µl (tail) PBND buffer supplemented with 1:200 proteinase K over night at 56°C and 550rpm in a thermomixer. Enzymatic digestion was terminated by heat inactivation at 95°C for 10min, samples were centrifuged at 13.000rpm for 2min at RT and stored at 4°C until further use. The PCR reaction mix and respective PCR programs are shown in tables 12 and 13, respectively. After the PCR run, samples were supplemented with loading buffer and loaded on an agarose gel. For this purpose, agarose was boiled in 1x TAE buffer in the microwave and, after cooling down, supplemented with ethidium bromide (1:10.000 from 1% stock solution). After gel electrophoresis at 120V for 40-60min, ethidium bromide-stained PCR products were visualized under UV light using gel documentation system. The expected sizes of the PCR products are shown in table 14.

Table 12: Genotyping PCR reaction mix

	DNT	mb1/Cre	CD23Cre
Component	**Volume [µl]**	**Volume [µl]**	**Volume [µl]**
10x Taq reaction buffer (including 15mM MgCl2)	2	2	2
dNTPs (10mM stock)	0,3	0,3	0,3
Taq Polymerase (5U/µl)	0,3	0,3	0,3
primer I (10µM stock)	1	1	2,5
primer II (10µM stock)	1	1	1
primer III (10µM stock)	1	-	2,5
H_2O	11,4	12,4	8,4
genomic DNA	3	3	3

Table 13: Genotyping PCR programs

	DNT			mb1/Cre			CD23Cre		
Reaction step	**Temp [°C]**	**Time [min]**	**cycles**	**Temp [°C]**	**Time [min]**	**cycles**	**Temp [°C]**	**Time [min]**	**cycles**
Initial denaturation	94	3		94	2		94	2	
Denaturation	94	0,5		94	0,5		94	5s	
Annealing	56	0,75	40x	61	0,5	33x	61	5s	30x
Elongation	72	1		72	1		72	20s	
Final elongation	72	10		72	3		72	5	
Cooling	4	∞		4	∞		4	∞	

Table 14: Expected fragment sizes of PCR products

DNT	mb1/Cre	CD23Cre
WT: 570bp DNT. 380bp	WT: 417bp Cre: 500bp	WT: 368bp Cre: 283bp

9.3. Immunization of mice

Sheep red blood cells (SRBCs): The stock suspension of SRBCs (approximately $4x10_9$ cells/ml) was washed 3 times with 5ml PBS under sterile conditions and centrifuged at 1000rcf for 5min at 4°C. After carefully discarding the supernatant by pipetting, the cell pellet was resuspended in the desired volume of PBS. Per mouse, $2x10^9$ SRBCs in 200µl PBS were injected intraperitoneally using an insulin syringe.

NP-Ficoll: 25µg NP-Ficoll were injected per mouse. For this purpose, a 1mg/ml stock solution (in PBS and stored at -20°C), was mixed with PBS in a 1:3 ratio and injected intraperitoneally using an insulin syringe.

NP-KLH: 100µg NP_{29}-KLH were injected per mouse. For this purpose, lyophilized NP_{29}-KLH was diluted in PBS to a stock concentration of 1mg/ml and stored at 4°C. Upon immunization, the stock solution was mixed with an equal amount of the adjuvance alum by rotating for 1h at RT. 200µl of the NP-KLH alum mix per mouse were injected intraperitoneally using an insulin syringe.

9.4. Preparation of primary murine cells

Prior to organ preparation, mice were euthanized by CO_2 followed by cranial dislocation. The dead animal was sprayed with 70% ethanol before skinning. Generally, the cell suspensions were handled and stored on ice and centrifuged at 1400rpm for 7min at 4°C.

Blood was obtained by cardiac puncture using an insulin syringe and transferred into a serum tube.

Peritoneal cells were collected by carefully flushing the peritoneal cavity with 5ml PBS using a blue cannula.

Spleen was removed upon carefully opening the abdomen and transferred into 5ml 2% FCS on ice. For the isolation of splenic cells, the spleen was gently meshed through a 70µm cell strainer into a petri dish using a syringe stamp. After transferring the cell suspension into a 15ml reaction tube, petri dish and cell strainer were rinsed with 2ml 2% FCS.

Bone marrow cells were collected from the femur (and depending on required cell number also tibia) of both hind legs. For this purpose, muscles tissue was removed using scissors and tissues before cutting the articular surfaces. The bone marrow cells were flushed with 10ml 2% FCS using a 27G cannula into a 15ml reaction tube.

Peyer's patches preparation was performed in a similar fashion to the spleen.

After centrifugation, erythrocytes were lysed by resuspending the cell pellet in 5ml red blood cell-lysis buffer. After incubating for 5min at room temperature, the reaction was stopped by addition of 5ml 2% FCS cells were pelleted by centrifugation. After resuspending the pellet in the appropriate volume of 2% FCS, the cell suspension was filtered through a 30µm mesh filter and kept on ice until further use.

9.5. Cell counting

Cell numbers were determined automatically using the nucleocounter NC3000, which allows the detection of dead cells (DAPI positive) within total cells (acridine orange (AO) positive). For this purpose, cell suspensions were diluted (usually in a 1:1 ratio) and 95µl of this dilution was mixed with 5µl "solution 13" (DAPI+AO). For subsequent cell counting, 10µl of the final solution was transferred into an 8-well slide and measured in the nucleocounter NC3000.

9.6. B cell isolation

Splenocytes were prepared as described above and naïve B cell were isolated using the EasySep *Mouse B cell isolation negative selection* kit (StemCell Technologies) according to the manufacturer's instructions. Purity was confirmed by flow cytometry using anti CD19 antibodies and usually exceeded >95%.

9.7. Cultivation of primary murine B cells in vitro

Splenic B cells were cultured in R10 medium at 37°C and 5% CO_2. The supplements and cell numbers used for the respective stimuli are shown in table 15. Stimulation for CSR adapted from (Chiu et al., 2019) and modified by W. Schuh.

Table 15: Concentrations of cell culture supplements and cell numbers used for in vitro B cell activation

Stimulation	Additive(s)	End concentration	Seeded cell number
LPS	LPS	10µg/ml	$0.5x10^6$/ml
CSR	LPS	10µg/ml	$0.1x10^6$/ml
	IL4	100U/ml	
	IL5	10ng/ml	
	TGFb	5ng/ml	
	Retinoic acid	5nM	
	α-CD40	10µg/ml	
α-BCR	α-IgM	10µg/ml	$1x10^6$/ml

9.8. Flow cytometric analysis

9.8.1. Staining of surface proteins

For the flow cytometric analysis 0.5-3x10^6 cells were pelleted in FACS tubes by centrifugation at 1500rpm for 5min at 4°C. After aspirating the supernatant, cells were resuspended in 50µl staining mix (FACS buffer + FC-Block 1:100 + Abs) and incubated on ice in the dark for 15min. Cells were washed by addition of 500-750µl FACS buffer, pelleted by centrifugation, resuspended in 150µl FACS buffer and stored on ice until analysis using the Beckman Coulter Gallios flow cytometer.

9.8.2. Staining of intracellular proteins

For the analysis of intracellular proteins, cells were fixed and permeabilised with the Nordic MUbio FIX&PERM Kit. After surface staining, cells were washes and resuspended in 50µl reagent A (fix solution) and incubated for 15min at RT in the dark. After washing, the cells were resuspended in 50µl of solution B (permeabilization solution) also containing the antibody of interest in the respective dilution. After final washing, cells were resuspended in 150µl for flow cytometric analysis.

9.8.3. Determination of viability

The frequency of viable cells was determined using the eBioscience AnnexinV Apoptosis Detection Kit APC according to manufacturer's instructions. AnnexinV-APC and PI were used in a 1:40 dilution. Viable cells are defined as $AnnexinV^-PI^-$, apoptotic cells are $AnnexinV^+PI^-$ and necrotic cells are $Annexin^{+/-}PI^+$.

9.8.4. Analysis of proliferation

The proliferation rate of *in vitro* activated, splenic B cells was determined by staining the cells with the Cell Proliferation Dye eFluor 450 (eBioscience). For this purpose, freshly isolated, splenic B cells were washed once with PBS, centrifuged at 1500rpm and 4°C for 5min and resuspended at a density of 1x10^6cells/ml in 5µM eFluor 450 diluted in PBS. After incubation (10min, 37°C, dark), 4-5 volumes of complete medium were added, and the samples incubated on ice for 5min. The cells were washed twice in medium before seeding them for subsequent cultivation.

9.8.5 Common gating strategy for viable cells and exclusion of autofluorescence

First, autofluorescence was excluded, if possible, using two empty channels that were included beforehand in the compensation matrix. Singlets were defined via FS Int (forward scatter intensity) and FS Peak (forward scatter peak) and further gated for total viable cells using FS int and SS int. The obtained cell number of the viable cell gate was used for calculation of

population frequencies. Within the gate for viable cells, an additional extended lymphocyte gate was set which was used for further definition of cell populations.

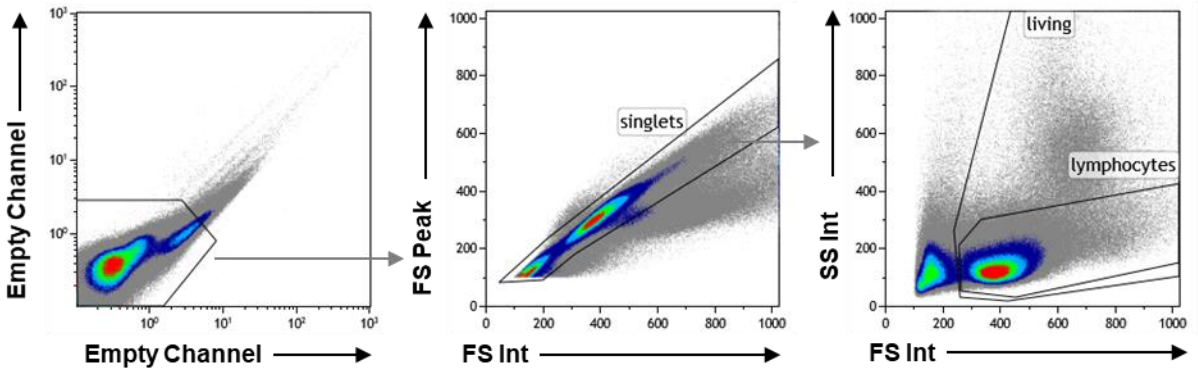

Figure 47 | Common pre-gating strategy (exemplary shown for spleen)

9.9. Determination of mtDNA content

9.9.1. DNA extraction

Cell pellets (1x10^{6}cells per sample) were resuspended in PBS and DNA was isolated using the DNeasy Blood & Tissue Kit (Quiagen) according to manufacturer's instructions.

9.9.2. RT-qPCR

To quantify the mtDNA amount relative to genomic DNA, RT-qPCR for mtDNA encoded and nucleus encoded genes was performed (Quiros et al., 2017). Samples were measured in triplicates and 35ng/well DNA were used. Quantification of mitochondrial and genomic DNA was conducted using an Applied Biosystems 7300 real time PCR system with the ThermoFisher SYBR Green Master Mix. For this purpose, 7µl of diluted DNA was mixed with a master mix made up from 0.25μl gene specific forward primer, 0.25μl gene specific reverse primer and 7.5μl SYBR Green. Reactions were performed in MicroAmp Optical 96-well reaction plates in technical triplicates by default. After an initial 10min denaturation step at 95°C real time quantification of PCR product accumulation was tracked during 40 cycles of a 95°C, 15sec and 60°C, 60sec 2-step PCR reaction followed by determination of a dissociation curve. No template controls (RNA or H_2O instead of DNA), interpretation of dissociation curve and amplification curves were used for quality control of reactions.

9.10. Measurement of Lactate and Glucose in cell culture supernatant

The supernatant of LPS activated B cells was harvested after 3 days by centrifugation and analysed using the SUPER GL compact analyzer according to the manufacturer's instructions (kindly performed by AG Mougiakakos)

9.11. Intracellular ATP measurement

The level of intracellular ATP was determined using the ATP Bioluminescence Assay Kit HS II (Roche) according to manufacturer's instructions. For this purpose, $5x10^4$ cells of d3 LPS cultures were harvested by centrifugation at 1500rpm and 4°C for 5min.

9.12. ELISA

96-well flat-bottom microtiter plates were coated with 50µl/well using ELISA coating buffer supplemented with 1µg/ml of the respective capture antibody or NP_{20}-BSA/NP_4-BSA and incubated overnight at 4°C. For antigen specific ELISA, standard lanes were coated with the respective capture antibody to allow quantification. Plates were washed 3 times with ELISA wash buffer and blocked for 1h at room temperature with 200µl/well ELISA blocking buffer. Samples were pre-diluted in ELISA blocking buffer according to table 16. The standards were diluted in blocking buffer to 200ng/ml. After discarding the blocking buffer, pre-diluted serum samples and immunoglobulin standards were applied in 1:2 serial dilutions and incubated for 1h at room temperature. After discarding the samples and washing the plates 3 times, 50µl/well of the respective detection antibody diluted 1:1000 in ELISA blocking buffer were added to the plates and incubated for 1h at room temperature. After finally washing the plates 3 times, 50µl/well of ELISA TMB substrate reagent was added to the plates. The reaction was stopped by adding 50µl/well ELISA acid stop solution. Optical density (oD) was measured at 450nm on a FLUOstar Omega Microplate Reader (BMG Labtech). Data analysis was performed using 5-parameter fit and linear regression of the MARS software.

Table 16 | Pre-dilution of sera and supernatant for ELISA

Antibody Isotype	Serum Dilution (non-immunized or 0-14d after immunization)	Serum Dilution (21d-35d after immunization)	Serum Dilution (42d-70d after immunization)	d3 LPS blasts Supernatant
IgA	1.000			
IgG total	10.000			1

IgG1	1.000			
IgG2b	1.000			
IgG2c	1.000			
IgG3	1.000			
IgM	1.000			1
IgM NP-spezifisch	250	500	2000	
IgG NP-spezifisch	250	500	2000	

9.13. Extracellular flux analysis

Extracellular flux analysis was performed using the Seahorse XFe96 Extracellular Flux Analyzer.

One day prior to the assay: Cartridge was calibrated with 200µl/well calibrant buffer and the cell plate was coated with 100µl/well poly-L-lysine (10µg/ml in TE buffer). Both were incubated overnight at 37°C without CO_2.

Day of the assay: Cell plate was washed 3 times with H_2O. The cells are resuspended in the respective Seahorse assay medium at the required density (500.000 naïve B cells/well; 250.000 d3 LPS blasts/well; measured at least in triplicates) and 180µl/well were added to the plate. After short centrifugation to enhance attachment, the cells were incubated for 45-60min at 37°C without CO_2. In the meantime, the cartridge was loaded with the respective inhibitors according to table 17 diluted in the respective assay medium. Protocol and data analysis was performed according to manufacturer's instructions using the Wave software.

Table 17: Seahorse inhibitors und concentrations

Assay	Inhibitor	10x solution (in assay medium)	Final well	Port
Glyko Stress Test	Glucose	100mM	10mM	A (20µl)
	Oligomycin	10µM	1µM	B (22µl)
	2-DG	500mM	50mM	C (25µl)
Mito Stress Test	Oligomycin	10µM	1µM	A (20µl)
	FCCP	10µM	1µM	B (22µl)
	Rotenone +	5µM	0.5µM	C (25µl)
	Antimycin A	5µM	0.5µM	
ATP Rate Assay	Oligomycin	10µM	1.5µM	A (20µl)

	Rotenone +	5µM	0.5µM	B (22µl)
	Antimycin A	5µM	0.5µM	

9.14. Western Blot

The cells were washed with cold PBS (centrifugation at 1500rpm for 5min at 4°C) and lysed on ice for 30min in lysis-buffer supplemented with 1mM PMSF. After centrifugation for 10min at 14.000rpm at 4°C, the supernatant was transferred into a fresh tube, mixed with an equal volume of loading buffer and denaturated at 95°C for 10min. The samples were stored at -20°C until loaded onto a sodium dodecyl sulfate (SDS) polyacrylamide gel according to table 18 prepared in a Hoefer 16x18cm chamber.

Table 18: SDS polyacylamid gel preparation

Component	**separation gel 10%**	**stacking gel 4%**
1M Tris/HCl pH 8.8	11.7ml	-
1M Tris/HCl pH 6.8	-	1.49ml
H_2O	2.5ml	8.4ml
10% SDS	310µl	120µl
30% Acrylamid	15.6ml	1.68ml
APS	650µl	600µl
TEMED	15.6µl	12µl

Samples and PageRuler Prestained Protein Ladder as marker for molecular weight were loaded into the gel chambers and proteins were electrophoresed at 60-70mA (max. 400V, 60W) per gel for 2-3h or at 8mA (max. 100V, 20W) per gel overnight in Laemmli loading buffer. The proteins were transferred onto a nitrocellulose membrane at 400mM (max. 50V, 10W) for 45min in the following stacking order (from top to bottom) in a PerfectBlue semi-dry blot chamber:

whatman paper soaked in cathode buffer
polyacrylamid gel
nitrocellulose membrane in anode buffer 1
whatman paper soaked in anode buffer 1

whatman paper soaked in anode buffer 2

Next, the membrane was stained with Ponceau-S solution for 1min and unspecific staining removed with dH_2O to subsequently document the total proteins transferred. After washing 3 times with TBST (each 5-10min), the membrane was blocked for 30-60min with 5% w/v skimmed milk powder in TBST. Proteins of interest were detected by incubating the membrane with the respective primary antibody in antibody dilution solution for 1h at RT or overnight at 4°C. After washing 3 times as described before, the membrane was incubated for 1h with the secondary horseradish peroxidase (HRP) conjugated antibody diluted 1:10.000 in 5% skimmed milk powder in TBST. After final 3 washing steps, the membrane is incubated with enhanced chemiluminescence (ECL) solution (table 19) for 1min before exposing the membrane to X-ray films within Amersham pharmacia biotech Hypercassette (10sec - 5min exposure time, depending on a first trial film with 1min exposure) in a dark room. X-ray films were developed using an Agfa Curix 60, molecular weight standards were transferred with a pen, and X-ray films were scanned for subsequent quantification by densitometry analysis with ImageJ. For this purpose, band intensities were measured, and background of X-ray films was subtracted. The protein expression was normalized to expression of β-Actin.

Table 19: ECL solution mix

ECL component	Volume
1M Tris pH 8.5	2ml
H_2O	17.7ml
90mM p-Cumaric acid	90µl
250mM Luminol	200µl
H_2O_2	6µl

9.15. Lipidomics

Glycerophospholipids (PC, PE, PI, PS, PG, PA) in B cells were analysed by Nano-Electrospray Ionization Tandem Mass Spectrometry (Nano-ESI-MS/MS) with direct infusion of the lipid extract (Shotgun Lipidomics): 14 to 45 x 106 cells were homogenized in 300 µl of Milli-Q water using the Precellys 24 Homogenisator (Peqlab, Erlangen, Germany) at 6.500 rpm for 30 sec. The protein content of the homogenate was routinely determined using bicinchoninic acid. To 100 µl of the homogenate 400 µl of Milli-Q water, 1.875 ml of methanol/chloroform 2:1 (v/v) and internal standards (125 pmol PC 17:0-20:4, 132 pmol PE 17:0-20:4, 118 pmol PI 17:0-20:4, 131 pmol PS 17:0-20:4, 62 pmol PG 17:0/20:4, 75 pmol PA 17:0/20:4 Avanti Polar Lipids) were added. Lipid extraction and Nano-ESI-MS/MS analysis were performed as previously described (V et al., 2015). Endogenous glycerophospolipids were quantified by referring their peak areas to those of the internal standards. The calculated glycerophospolipid amounts were

normalized to the protein content of the tissue homogenate. Sample preparation and analysis was kindly performed by Susanne Brodesser (Cologne Excellence Cluster on Cellular Stress Responses in Aging-associated Diseases (CECAD), Köln)

9.16. Metabolomics

9.16.1. Perchloric acid extraction

Splenic B cells were isolated and activated with LPS as described before and viable cells, only GFP+ for DNT, were sorted after 3 days using flow cytometry, washed with PBS, transferred into a 2ml reaction tube, and stored at -70°C until further use.

For perchloric acid extraction of cell extracts, samples were dipped in liquid N_2 before adding 500µl 1M perchloric acid. After vortexing and dipping the samples again in liquid N_2, 500µl of 0,1M perchloric acid were added. The tube was gently warmed using the hand and vortexed or resuspended using a pipette. As soon as the pellet is dissolved, the samples were centrifuged for 2min at 14.000rpm and 4°C and 900µl of the supernatant were transferred into a fresh, cooled (on ice) 2ml reaction tube. In two consecutive steps, 25µl 5M K_2CO_3 was added, and the safety lid was closed after the second time. Tubes were inverted and incubated for 5min on ice. The reaction tubes were carefully opened (facing away from the body) and pH was checked using indicator paper. If necessary, pH was adjusted using K_2CO_3 until pH 6-7. Samples are centrifuged for 2min at 14.000rpm and 4°C and the supernatant was transferred into a fresh, cooled reaction tube. Cell extracts were stored at -70°C and handled on dry ice until analysis.

9.16.2. Mass Spectrometric analysis

Metabolic profiles were determined as previously published and kindly performed by Jörg Hofmann (Department Biology, Division of Biochemistry, Erlangen) (Hofmann et al., 2011).

9.17. Electron Microscopy

Cells were collected by centrifugation and fixed overnight in 2.5% glutaraldehyde (Carl Roth, 4995.1) in PBS. Further treatment for electron microscopy preparation and analysis was kindly performed by the lab of Ursula Schlötzer-Schrehardt (Department of Ophthalmology, Erlangen), as described previously (Td et al., 2020).

9.18. Immunohistology

Mice were immunized with SRBCs, sacrificed after 10 days and spleens were embedded in OCT medium (Tissue-Tek). Cryotome sections of 8µm were prepared, fixed in acetone,

blocked (with 20 µg/ml α-CD16/23 in 1% PBS, 10% FCS, 2% BSA) and stained with α-IgD-AF647, PNA-Rhodamine and α-GL7-PacificBlue.

9.19. Liposome production

Liposome production was based on a published method (Poschenrieder et al., 2016) originally developed for the production of polymersomes, which are the artificial counterparts of liposomes. Here, 11.4 mL of vesicle buffer (10 mM TRIS HCl, 150 mM NaCl, pH 8.0) were poured into unbaffled miniaturized stirred tank reactors (BioREACTOR48, 2mag, Munich, Germany) and stirred at 4,000 rpm at 25°C using an S type stirrer. Then, 600 µL of the dissolved phospholipid 16:0 PA (1,2-dipalmitoyl-sn-glyero-3-phosphate) (10 mM in chloroform) were injected under stirring, leading to a whitish highly dispersed emulsion. The reactor shell, originally made of polystyrene, has been replaced by borosilicate glass, in order to avoid damaging by the chloroform. The process was continued, until the solution became transparent, indicating the evaporation of the chloroform, which was the case after 6 hours. Subsequently, the solution was centrifuged at 13,000 rpm in a tabletop centrifuge to remove precipitates. The liposomes in the supernatant were then concentrated to 1,5 mg mL-1 by centrifugation for 50 min at 50,000 g and resuspending of the resulting pellet in the appropriate amount of vesicle buffer. The quality of the liposomes during and after the production process was monitored via dynamic light scattering using a Zetasizer NS (Malvern, Worcestershire, UK) as reported (Poschenrieder et al., 2016). The liposome production was kindly performed by Florian Golombek (Lab of Kathrin Castiglione, Department of Chemical and Biological Engineering, Erlangen)

9.20. Statistical analysis

Statistical analysis was performed using the GraphPad Prism software 7.00. First, outliers were detected using ROUT test and excluded from following analysis. The remaining values were tested for Gaussian distribution with the Shapiro-Wil normality test. For comparison of two groups, data sets that passed the normality test were analysed for statistical significance using the two-tailed unpaired t test. Data sets that did not pass the normality test were compared for statistical significance with the two-tailed Mann-Whitney test. For comparison of two groups with multiple subgroups, 2-way ANOVA was used. P-values <0.05 were indicated as statistically significant: * $p \leq 0.05$ ** $p \leq 0.01$ *** $p \leq 0.001$ **** $p \leq 0.0001$.

10. Appendix

10.1. Abbreviations

Abbreviation	Meaning
$^{-}$	Negative (expression)
$^{+}$	Positive (expression)
aa	Amino acid
Ab	Antibody
ACLY	ATP Citrate Lyase
ADP	Adenosine diphosphate
AF	Alexa Fluor
AID	Activation-induced cytidine deaminase
AMP	Adenosine monophosphate
AMPK	5' adenosine monophosphate-activated protein kinase
APC	Antigen-presenting cell
APRIL	A proliferation-inducing ligand
ASC	Antibody-secreting cell
ATP	Adenosine triphosphate
BAFF	B cell activating factor
BCL6	B cell lymphoma 6 protein homolog
BCMA	B cell maturation antigen
BCR	B cell receptor
BLIMP1	B lymphocyte-induced maturation protein 1
BM	Bone marrow
Bmem	memory B cell
bp	Base pairs
BSA	Bovine serum albumin
BV	Brilliant Violet TM
Ca^{2+}	Calcium
CD	Cluster of differentiation
CLP	Common lymphoid progenitor
CSR	Class switch recombination
CXCL	C-X-C motif chemokine ligand
CXCR	C-X-C motif chemokine receptor
DC	Dendritic cell
ddH_2O	Double-distilled water

DHAP	Dihydroxyacetone phosphate
DMSO	Dimethyl sulfoxide
DNA	Deoxyribonucleic acid
DNT	dominant-negative TWINKLE
dNTP	Deoxynucleoside triphosphate
DZ	Dark zone
e.g.	Exempli gratia (for example)
E4P	Erythrose 4-phosphate
EBF	Early B cell factor 1
ECAR	extracellular acidification rate
EDTA	Ethylenediaminetetraacetic acid
ELISA	Enzyme-linked Immunosorbent Assay
ETC	electron transport chain
FA	fatty acid
FACS	Fluorescence-activated cell sorting
FAD	flavin adenine dinucleotide
Fc	Fragment crystallizable
FCCP	Carbonyl cyanide-p-trifluoromethoxyphenylhydrazone
FCS	Fetal calf serum
FO	follicular B cell
FS	Forward Scatter
fwd	Forward
GAP	Glyceraldehyde 3-phosphat
GC	Germinal centre
GCBC	Germinal centre B cell
GFP	Green fluorescent protein
HC	Heavy chain
HIF1α	Hypoxia-inducible factor 1-alpha
HRP	Horseradish peroxidase
HSC	Hematopoietic stem cell
i.e.	*Id est* (that means)
i.p.	Intraperitoneally
IFN	Interferon
Ig	Immunoglobulin
IL(R)	Interleukin (receptor)
int	Intermediate (expression)
IRF	Interferon-regulatory factor

KLH	Keyhole limpet hemocyanin
LC	Light chain
LFA-1	Lymphocyte function-associated antigen 1
LLPC	long-lived plasma cell
low	Low (expression)
LPS	Lipopolysaccharide
MHC	Major histocompatibility complex,
MIM	mitochondrial inner membrane
mRNA	messenger RNA
mtDNA	mitochondrial DNA
mTORC1	mammalian target of rapamycin complex 1
mtRC	mitochondrial respiratory chain
mtSSB	mitochondrial single-stranded DNA-binding protein
MZ	Marginal zone (B cells)
n.s.	Not significant
NAD^+	Nicotinamide adenine dinucleotide
NFκB	Nuclear factor kappa B
NP	(4-Hydroxy-3-nitrophenyl)acetyl
O_2	oxygen
OCR	oxygen consumption rate
OxPhos	oxidative phosphorylation
Pax5	Paired box 5
PB	Plasma blast
PBS	Phosphate-buffered saline
PC	Plasma cell
PCh	Phosphatidylcholine
PCR	Polymerase-Chain-Reaction
PE	Phycoerythrin
PerCP	Peridinin chlorophyll protein
Pi3K	Phosphoinositide 3-kinase
PKC	Protein kinase C
POLG	mitochondrial DNA polymerase subunit gamma
PPP	Pentose phosphate pathway
pre-BCR	pre-B cell receptor
R5P	Ribose 5-phosphate
RAG 1/2	Recombination activating gene 1/2

rev	Reverse
ROS	Reactive oxygen species
RPMI	Roswell memorial park institute medium
RPS6	Ribosomal protein S6
SANDO	sensory ataxic neuropathy with dysarthria and ophthalmoparesis
SHM	Somatic hypermutation
SLC	Surrogate light chain
SLE	systemic lupus erythematosus
SLPC	short-lived plasma cell
SRBC	Sheep red blood cell
SS	Side Scatter
Syk	Spleen tyrosine kinase
TACI	Transmembrane activator and cyclophilin ligand interactor
TCA	tricarboxylic acid (cycle)
TCR	T cell receptor
TD	T cell-dependent
Temp.	Temperature
TF	Transcription factor
TI	T cell-independent
TLR	Toll-like receptor
tRNA	transfer RNA
VCAM-1	Vascular cell adhesion molecule 1
VDJ	Variable, diversity, joining
VLA4	Very late antigen 4
WT	Wildtype
Xbp1	X-box binding protein 1
Δp	Proton Motive Force
Δψμ	(electrochemical) Mitochondrial membrane potential
α-KG	Alpha-ketoglutarate

10.2. Units, prefixes, and Greek letters

Table 20: Definition of Units

Symbol	Meaning
°C	degree Celsius
A	Ampere
d	day

Da	Dalton
FI	fluorescence intensity
g	gram
h	hour
l	litre
m	meter
M	Mol
min	minute
rpm	rounds per minute
sec	second
U	unit
V	Volt
W	Watt

Table 21: Definition of prefixes

Symbol	Meaning
k	kilo (10^{+3})
c	centi (10^{-2})
m	milli (10^{-3})
µ	micro (10^{-6})
n	nano (10^{-9})

Table 22: Definition of greek letters

Symbol	Meaning
α	alpha
β	beta
γ	gamma
δ, Δ	delta
κ	kappa
λ	lambda
µ	mu
ψ	psi

10.3. Figure index

10.4. Table index

10.5. Bibliography

Akkaya, M., Traba, J., Roesler, A.S., Miozzo, P., Akkaya, B., Theall, B.P., Sohn, H., Pena, M., Smelkinson, M., Kabat, J., Dahlstrom, E., Dorward, D.W., Skinner, J., Sack, M.N., Pierce, S.K., 2018. Second signals rescue B cells from activation-induced mitochondrial dysfunction and death. Nat. Immunol. 19, 871–884. https://doi.org/10.1038/s41590-018-0156-5

Allman, D., Lindsley, R.C., DeMuth, W., Rudd, K., Shinton, S.A., Hardy, R.R., 2001. Resolution of Three Nonproliferative Immature Splenic B Cell Subsets Reveals Multiple Selection Points During Peripheral B Cell Maturation. J. Immunol. 167, 6834–6840. https://doi.org/10.4049/jimmunol.167.12.6834

Amin, R.H., Schlissel, M.S., 2008. Foxo1 directly regulates the transcription of recombination-activating genes during B cell development. Nat. Immunol. 9, 613–622. https://doi.org/10.1038/ni.1612

Ammar, M.-R., Kassas, N., Bader, M.-F., Vitale, N., 2014. Phosphatidic acid in neuronal development: A node for membrane and cytoskeleton rearrangements. Biochimie, From Membranes to Pathologies 107, 51–57. https://doi.org/10.1016/j.biochi.2014.07.026

Angelini, C., 2014. SANDO (Sensory Ataxic Neuropathy, Dysarthria, Ophthalmoparesis), in: Angelini, C. (Ed.), Genetic Neuromuscular Disorders: A Case-Based Approach. Springer International Publishing, Cham, pp. 259–260. https://doi.org/10.1007/978-3-319-07500-6_59

Archibald, J.M., 2015. Endosymbiosis and Eukaryotic Cell Evolution. Curr. Biol. 25, R911–R921. https://doi.org/10.1016/j.cub.2015.07.055

Athenstaedt, K., Daum, G., 1999. Phosphatidic acid, a key intermediate in lipid metabolism. Eur. J. Biochem. 266, 1–16. https://doi.org/10.1046/j.1432-1327.1999.00822.x

Auten, R.L., Davis, J.M., 2009. Oxygen Toxicity and Reactive Oxygen Species: The Devil Is in the Details. Pediatr. Res. 66, 121–127. https://doi.org/10.1203/PDR.0b013e3181a9eafb

Bailey, P.S.J., Nathan, J.A., 2018. Metabolic Regulation of Hypoxia-Inducible Transcription Factors: The Role of Small Molecule Metabolites and Iron. Biomedicines 6. https://doi.org/10.3390/biomedicines6020060

Bao, Y., Ledderose, C., Graf, A.F., Brix, B., Birsak, T., Lee, A., Zhang, J., Junger, W.G., 2015. mTOR and differential activation of mitochondria orchestrate neutrophil chemotaxis. J. Cell Biol. 210, 1153–1164. https://doi.org/10.1083/jcb.201503066

Baris, O.R., Ederer, S., Neuhaus, J.F.G., von Kleist-Retzow, J.-C., Wunderlich, C.M., Pal, M., Wunderlich, F.T., Peeva, V., Zsurka, G., Kunz, W.S., Hickethier, T., Bunck, A.C., Stöckigt, F., Schrickel, J.W., Wiesner, R.J., 2015. Mosaic Deficiency in Mitochondrial Oxidative Metabolism Promotes Cardiac Arrhythmia during Aging. Cell Metab. 21, 667–677. https://doi.org/10.1016/j.cmet.2015.04.005

Batten, M., Groom, J., Cachero, T.G., Qian, F., Schneider, P., Tschopp, J., Browning, J.L., Mackay, F., 2000. Baff Mediates Survival of Peripheral Immature B Lymphocytes. J. Exp. Med. 192, 1453–1466.

Benhamron, S., Pattanayak, S.P., Berger, M., Tirosh, B., 2015. mTOR activation promotes plasma cell differentiation and bypasses XBP-1 for immunoglobulin secretion. Mol. Cell. Biol. 35, 153–166. https://doi.org/10.1128/MCB.01187-14

Berg, J.M., Tymoczko, J.L., Stryer, L., 2002a. Phosphatidate Is a Common Intermediate in the Synthesis of Phospholipids and Triacylglycerols. Biochem. 5th Ed.

Berg, J.M., Tymoczko, J.L., Stryer, L., 2002b. The Citric Acid Cycle. Biochem. 5th Ed.

Berg, J.M., Tymoczko, J.L., Stryer, L., Berg, J.M., Tymoczko, J.L., Stryer, L., 2002c. Biochemistry, 5th ed. W H Freeman.

Boothby, M.R., Raybuck, A., Cho, S.H., Stengel, K.R., Haase, V.H., Hiebert, S., Li, J., 2021. Over-Generalizing About GC (Hypoxia): Pitfalls of Limiting Breadth of Experimental Systems and Analyses in Framing Informatics Conclusions. Front. Immunol. 12, 1523. https://doi.org/10.3389/fimmu.2021.664249

Burnstock, G., Knight, G.E., Greig, A.V.H., 2012. Purinergic Signaling in Healthy and Diseased Skin. J. Invest. Dermatol. 132, 526–546. https://doi.org/10.1038/jid.2011.344

Burrows, N., Bashford-Rogers, R.J.M., Bhute, V.J., Peñalver, A., Ferdinand, J.R., Stewart, B.J., Smith, J.E.G., Deobagkar-Lele, M., Giudice, G., Connor, T.M., Inaba, A., Bergamaschi, L., Smith, S., Tran, M.G.B., Petsalaki, E., Lyons, P.A., Espeli, M., Huntly, B.J.P., Smith, K.G.C., Cornall, R.J., Clatworthy, M.R., Maxwell, P.H., 2020. Dynamic regulation of hypoxia-inducible factor-1α activity is essential for normal B cell development. Nat. Immunol. 21, 1408–1420. https://doi.org/10.1038/s41590-020-0772-8

Busslinger, M., 2004. Transcriptional Control of Early B Cell Development. Annu. Rev. Immunol. 22, 55–79. https://doi.org/10.1146/annurev.immunol.22.012703.104807

Calnan, D.R., Brunet, A., 2008. The FoxO code. Oncogene 27, 2276–2288. https://doi.org/10.1038/onc.2008.21

Campello, S., Lacalle, R.A., Bettella, M., Mañes, S., Scorrano, L., Viola, A., 2006. Orchestration of lymphocyte chemotaxis by mitochondrial dynamics. J. Exp. Med. 203, 2879–2886. https://doi.org/10.1084/jem.20061877

Caro-Maldonado, A., Wang, R., Nichols, A.G., Kuraoka, M., Milasta, S., Sun, L.D., Gavin, A.L., Abel, E.D., Kelsoe, G., Green, D.R., Rathmell, J.C., 2014. Metabolic Reprogramming Is Required for Antibody Production That Is Suppressed in Anergic but Exaggerated in Chronically BAFF-Exposed B Cells. J. Immunol. 192, 3626–3636. https://doi.org/10.4049/jimmunol.1302062

Chang, C.-R., Blackstone, C., 2007. Cyclic AMP-dependent protein kinase phosphorylation of Drp1 regulates its GTPase activity and mitochondrial morphology. J. Biol. Chem. 282, 21583–21587. https://doi.org/10.1074/jbc.C700083200

Chaplin, D.D., 2010. Overview of the Immune Response. J. Allergy Clin. Immunol. 125, S3-23. https://doi.org/10.1016/j.jaci.2009.12.980

Chen, D., Wang, Y., Manakkat Vijay, G.K., Fu, S., Nash, C.W., Xu, D., He, D., Salomonis, N., Singh, H., Xu, H., 2021. Coupled analysis of transcriptome and BCR mutations reveals role of OXPHOS in affinity maturation. Nat. Immunol. 1–10. https://doi.org/10.1038/s41590-021-00936-y

Chen, H., Wang, J., Liu, Z., Yang, H., Zhu, Y., Zhao, M., Liu, Y., Yan, M., 2016. Mitochondrial DNA depletion causes decreased ROS production and resistance to apoptosis. Int. J. Mol. Med. 38, 1039–1046. https://doi.org/10.3892/ijmm.2016.2697

Chiu, H., Jackson, L.V., Oh, K.I., Mai, A., Ronai, Z.A., Ruggero, D., Fruman, D.A., 2019. The mTORC1/4E-BP/eIF4E Axis Promotes Antibody Class Switching in B Lymphocytes. J. Immunol. 202, 579–590. https://doi.org/10.4049/jimmunol.1800602

Cho, S.H., Raybuck, A.L., Stengel, K., Wei, M., Beck, T.C., Volanakis, E., Thomas, J.W., Hiebert, S., Haase, V.H., Boothby, M.R., 2016. Germinal centre hypoxia and regulation of antibody qualities by a hypoxia response system. Nature 537, 234–238. https://doi.org/10.1038/nature19334

Chung, J.B., Silverman, M., Monroe, J.G., 2003. Transitional B cells: step by step towards immune competence. Trends Immunol. 24, 342–348. https://doi.org/10.1016/S1471-4906(03)00119-4

Circu, M.L., Aw, T.Y., 2010. REACTIVE OXYGEN SPECIES, CELLULAR REDOX SYSTEMS AND APOPTOSIS. Free Radic. Biol. Med. 48, 749–762. https://doi.org/10.1016/j.freeradbiomed.2009.12.022

Clark, M.R., Mandal, M., Ochiai, K., Singh, H., 2014. Orchestrating B cell lymphopoiesis through interplay of IL-7 receptor and pre-B cell receptor signalling. Nat. Rev. Immunol. 14, 69–80. https://doi.org/10.1038/nri3570

Cobaleda, C., Jochum, W., Busslinger, M., 2007. Conversion of mature B cells into T cells by dedifferentiation to uncommitted progenitors. Nature 449, 473–477. https://doi.org/10.1038/nature06159

Cogliati, S., Enriquez, J.A., Scorrano, L., 2016. Mitochondrial Cristae: Where Beauty Meets Functionality. Trends Biochem. Sci., Special Issue: Mitochondria & Metabolism 41, 261–273. https://doi.org/10.1016/j.tibs.2016.01.001

Collins, A.M., 2016. IgG subclass co-expression brings harmony to the quartet model of murine IgG function. Immunol. Cell Biol. 94, 949–954. https://doi.org/10.1038/icb.2016.65

Conter, L.J., Song, E., Shlomchik, M.J., Tomayko, M.M., 2014. CD73 expression is dynamically regulated in the germinal center and bone marrow plasma cells are diminished in its absence. PloS One 9, e92009. https://doi.org/10.1371/journal.pone.0092009

Corfe, S.A., Paige, C.J., 2012. The many roles of IL-7 in B cell development; mediator of survival, proliferation and differentiation. Semin. Immunol. 24, 198–208. https://doi.org/10.1016/j.smim.2012.02.001

Daly, C.A., Spurrier, M.A., Jennings-Gee, J.E., Haas, K.M., 2020. B Cell Subsets Differentially Contribute to the T Cell–Independent Memory Pool. J. Immunol. 205, 2362–2374. https://doi.org/10.4049/jimmunol.1901453

de Goër de Herve, M.-G., Durali, D., Dembele, B., Giuliani, M., Tran, T.-A., Azzarone, B., Eid, P., Tardieu, M., Delfraissy, J.-F., Taoufik, Y., 2011. Interferon-Alpha Triggers B Cell Effector 1 (Be1) Commitment. PLoS ONE 6. https://doi.org/10.1371/journal.pone.0019366

del Pozo, M.A., Nieto, M., Serrador, J.M., Sancho, D., Vicente-Manzanares, M., Martínez, C., Sánchez-Madrid, F., 1998. The two poles of the lymphocyte: specialized cell compartments for migration and recruitment. Cell Adhes. Commun. 6, 125–133. https://doi.org/10.3109/15419069809004468

Dengler, H.S., Baracho, G.V., Omori, S.A., Bruckner, S., Arden, K., Castrillon, D.H., DePinho, R.A., Rickert, R.C., 2008. Distinct roles for Foxo1 at multiple stages of B cell differentiation. Nat. Immunol. 9, 1388–1398. https://doi.org/10.1038/ni.1667

Dengler, V.L., Galbraith, M., Espinosa, J.M., 2014. Transcriptional Regulation by Hypoxia Inducible Factors. Crit. Rev. Biochem. Mol. Biol. 49, 1–15. https://doi.org/10.3109/10409238.2013.838205

Doan, H., Parsons, A., Devkumar, S., Selvarajah, J., Miralles, F., Carroll, V.A., 2019. HIF-mediated Suppression of DEPTOR Confers Resistance to mTOR Kinase Inhibition in Renal Cancer. iScience 21, 509–520. https://doi.org/10.1016/j.isci.2019.10.047

Doughty, C.A., Bleiman, B.F., Wagner, D.J., Dufort, F.J., Mataraza, J.M., Roberts, M.F., Chiles, T.C., 2006. Antigen receptor–mediated changes in glucose metabolism in B lymphocytes: role of phosphatidylinositol 3-kinase signaling in the glycolytic control of growth. Blood 107, 4458–4465. https://doi.org/10.1182/blood-2005-12-4788

Dufort, F.J., Gumina, M.R., Ta, N.L., Tao, Y., Heyse, S.A., Scott, D.A., Richardson, A.D., Seyfried, T.N., Chiles, T.C., 2014. Glucose-dependent de Novo Lipogenesis in B Lymphocytes. J. Biol. Chem. 289, 7011–7024. https://doi.org/10.1074/jbc.M114.551051

Fairfax, K.A., Corcoran, L.M., Pridans, C., Huntington, N.D., Kallies, A., Nutt, S.L., Tarlinton, D.M., 2007. Different Kinetics of Blimp-1 Induction in B Cell Subsets Revealed by Reporter Gene. J. Immunol. 178, 4104–4111. https://doi.org/10.4049/jimmunol.178.7.4104

Fang, Y., Vilella-Bach, M., Bachmann, R., Flanigan, A., Chen, J., 2001. Phosphatidic Acid-Mediated Mitogenic Activation of mTOR Signaling. Science 294, 1942–1945. https://doi.org/10.1126/science.1066015

Foster, D.A., 2013. Phosphatidic acid and lipid-sensing by mTOR. Trends Endocrinol. Metab. 24, 272–278. https://doi.org/10.1016/j.tem.2013.02.003

Foster, D.A., Salloum, D., Menon, D., Frias, M.A., 2014. Phospholipase D and the maintenance of phosphatidic acid levels for regulation of mammalian target of rapamycin (mTOR). J. Biol. Chem. 289, 22583–22588. https://doi.org/10.1074/jbc.R114.566091

Freisinger, P., Fütterer, N., Lankes, E., Gempel, K., Berger, T.M., Spalinger, J., Hoerbe, A., Schwantes, C., Lindner, M., Santer, R., Burdelski, M., Schaefer, H., Setzer, B., Walker, U.A., Horváth, R., 2006. Hepatocerebral Mitochondrial DNA Depletion Syndrome Caused by Deoxyguanosine Kinase (DGUOK) Mutations. Arch. Neurol. 63, 1129. https://doi.org/10.1001/archneur.63.8.1129

Friedl, P., Weigelin, B., 2008. Interstitial leukocyte migration and immune function. Nat. Immunol. 9, 960–969. https://doi.org/10.1038/ni.f.212

Garrett, n.d. Biochemistry 4th Edition.
Gatto, D., Brink, R., 2010. The germinal center reaction. J. Allergy Clin. Immunol. 126, 898–907. https://doi.org/10.1016/j.jaci.2010.09.007
Gaudette, B.T., Jones, D.D., Bortnick, A., Argon, Y., Allman, D., 2020. mTORC1 coordinates an immediate unfolded protein response-related transcriptome in activated B cells preceding antibody secretion. Nat. Commun. 11, 723. https://doi.org/10.1038/s41467-019-14032-1
Ge, T., Yang, J., Zhou, S., Wang, Y., Li, Y., Tong, X., 2020. The Role of the Pentose Phosphate Pathway in Diabetes and Cancer. Front. Endocrinol. 11. https://doi.org/10.3389/fendo.2020.00365
Genestier, L., Taillardet, M., Mondiere, P., Gheit, H., Bella, C., Defrance, T., 2007. TLR Agonists Selectively Promote Terminal Plasma Cell Differentiation of B Cell Subsets Specialized in Thymus-Independent Responses. J. Immunol. 178, 7779–7786. https://doi.org/10.4049/jimmunol.178.12.7779
Gnoni, G.V., Priore, P., Geelen, M.J.H., Siculella, L., 2009. The mitochondrial citrate carrier: metabolic role and regulation of its activity and expression. IUBMB Life 61, 987–994. https://doi.org/10.1002/iub.249
Gray, M.W., 2012. Mitochondrial Evolution. Cold Spring Harb. Perspect. Biol. 4. https://doi.org/10.1101/cshperspect.a011403
Gu, B., Bendall, L.J., Wiley, J.S., 1998. Adenosine triphosphate-induced shedding of CD23 and L-selectin (CD62L) from lymphocytes is mediated by the same receptor but different metalloproteases. Blood 92, 946–951.
Guak, H., Krawczyk, C.M., 2020. Implications of cellular metabolism for immune cell migration. Immunology 161, 200–208. https://doi.org/10.1111/imm.13260
Gustafsson, C.M., Falkenberg, M., Larsson, N.-G., 2016. Maintenance and Expression of Mammalian Mitochondrial DNA. Annu. Rev. Biochem. 85, 133–160. https://doi.org/10.1146/annurev-biochem-060815-014402
Hagman, J., Lukin, K., 2006. Transcription factors drive B cell development. Curr. Opin. Immunol., Lymphocyte development / Tumour immunology 18, 127–134. https://doi.org/10.1016/j.coi.2006.01.007
Haumann, S., Boix, J., Knuever, J., Bieling, A., Vila Sanjurjo, A., Elson, J.L., Blakely, E.L., Taylor, R.W., Riet, N., Abken, H., Kashkar, H., Hornig-Do, H.-T., Wiesner, R.J., 2020. Mitochondrial DNA mutations induce mitochondrial biogenesis and increase the tumorigenic potential of Hodgkin and Reed-Sternberg cells. Carcinogenesis. https://doi.org/10.1093/carcin/bgaa032
Hindupur, S.K., González, A., Hall, M.N., 2015. The Opposing Actions of Target of Rapamycin and AMP-Activated Protein Kinase in Cell Growth Control. Cold Spring Harb. Perspect. Biol. 7, a019141. https://doi.org/10.1101/cshperspect.a019141
Hobeika, E., Thiemann, S., Storch, B., Jumaa, H., Nielsen, P.J., Pelanda, R., Reth, M., 2006. Testing gene function early in the B cell lineage in mb1-cre mice. Proc. Natl. Acad. Sci. U. S. A. 103, 13789–13794. https://doi.org/10.1073/pnas.0605944103
Hoek, K.L., Gordy, L.E., Collins, P.L., Parekh, V.V., Aune, T.M., Joyce, S., Thomas, J.W., Van Kaer, L., Sebzda, E., 2010. Follicular B cell trafficking within the spleen actively restricts humoral immune responses. Immunity 33, 254–265. https://doi.org/10.1016/j.immuni.2010.07.016
Hoffman, W., Lakkis, F.G., Chalasani, G., 2016. B Cells, Antibodies, and More. Clin. J. Am. Soc. Nephrol. CJASN 11, 137–154. https://doi.org/10.2215/CJN.09430915
Hofmann, J., Börnke, F., Schmiedl, A., Kleine, T., Sonnewald, U., 2011. Detecting Functional Groups of Arabidopsis Mutants by Metabolic Profiling and Evaluation of Pleiotropic Responses. Front. Plant Sci. 2. https://doi.org/10.3389/fpls.2011.00082
Holmuhamedov, E., Jahangir, A., Bienengraeber, M., Lewis, L.D., Terzic, A., 2003. Deletion of mtDNA disrupts mitochondrial function and structure, but not biogenesis. Mitochondrion 3, 13–19. https://doi.org/10.1016/S1567-7249(03)00053-9
Huang, Z., Xie, N., Illes, P., Di Virgilio, F., Ulrich, H., Semyanov, A., Verkhratsky, A., Sperlagh, B., Yu, S.-G., Huang, C., Tang, Y., 2021. From purines to purinergic signalling:

molecular functions and human diseases. Signal Transduct. Target. Ther. 6, 1–20. https://doi.org/10.1038/s41392-021-00553-z

Hudson, C.C., Liu, M., Chiang, G.G., Otterness, D.M., Loomis, D.C., Kaper, F., Giaccia, A.J., Abraham, R.T., 2002. Regulation of hypoxia-inducible factor 1alpha expression and function by the mammalian target of rapamycin. Mol. Cell. Biol. 22, 7004–7014. https://doi.org/10.1128/mcb.22.20.7004-7014.2002

Hudson, G., Deschauer, M., Busse, K., Zierz, S., Chinnery, P.F., 2005. Sensory ataxic neuropathy due to a novel C10Orf2 mutation with probable germline mosaicism. Neurology 64, 371–373. https://doi.org/10.1212/01.WNL.0000149767.51152.83

Ingelsson, B., Söderberg, D., Strid, T., Söderberg, A., Bergh, A.-C., Loitto, V., Lotfi, K., Segelmark, M., Spyrou, G., Rosén, A., 2018. Lymphocytes eject interferogenic mitochondrial DNA webs in response to CpG and non-CpG oligodeoxynucleotides of class C. Proc. Natl. Acad. Sci. 115, E478–E487. https://doi.org/10.1073/pnas.1711950115

Iwahashi, S., Maekawa, Y., Nishida, J., Ishifune, C., Kitamura, A., Arimochi, H., Kataoka, K., Chiba, S., Shimada, M., Yasutomo, K., 2012. Notch2 regulates the development of marginal zone B cells through Fos. Biochem. Biophys. Res. Commun. 418, 701–707. https://doi.org/10.1016/j.bbrc.2012.01.082

Iwata, T.N., Ramírez, J.A., Tsang, M., Park, H., Margineantu, D.H., Hockenbery, D.M., Iritani, B.M., 2016. Conditional Disruption of Raptor Reveals an Essential Role for mTORC1 in B Cell Development, Survival, and Metabolism. J. Immunol. Author Choice 197, 2250–2260. https://doi.org/10.4049/jimmunol.1600492

Jellusova, J., Cato, M.H., Apgar, J.R., Ramezani-Rad, P., Leung, C., Chen, C., Richardson, A.D., Conner, E.M., Benschop, R.J., Woodgett, J.R., Rickert, R.C., 2017. GSK3 is a metabolic checkpoint regulator in B cells. Nat. Immunol. 18, 303–312. https://doi.org/10.1038/ni.3664

Jones, D.D., Gaudette, B.T., Wilmore, J.R., Chernova, I., Bortnick, A., Weiss, B.M., Allman, D., 2016. mTOR has distinct functions in generating versus sustaining humoral immunity. J. Clin. Invest. 126, 4250–4261. https://doi.org/10.1172/JCI86504

Kallies, A., Hasbold, J., Fairfax, K., Pridans, C., Emslie, D., McKenzie, B.S., Lew, A.M., Corcoran, L.M., Hodgkin, P.D., Tarlinton, D.M., Nutt, S.L., 2007. Initiation of plasma-cell differentiation is independent of the transcription factor Blimp-1. Immunity 26, 555–566. https://doi.org/10.1016/j.immuni.2007.04.007

Kierans, S.J., Taylor, C.T., 2021. Regulation of glycolysis by the hypoxia-inducible factor (HIF): implications for cellular physiology. J. Physiol. 599, 23–37. https://doi.org/10.1113/JP280572

Kim, S., Koh, H., 2017. Role of FOXO transcription factors in crosstalk between mitochondria and the nucleus. J. Bioenerg. Biomembr. 49, 335–341. https://doi.org/10.1007/s10863-017-9705-0

Krebs, H.A., 1948. The tricarboxylic acid cycle. Harvey Lect. Series 44, 165–199.

Krymskaya, V.P., Snow, J., Cesarone, G., Khavin, I., Goncharov, D.A., Lim, P.N., Veasey, S.C., Ihida-Stansbury, K., Jones, P.L., Goncharova, E.A., 2011. mTOR is required for pulmonary arterial vascular smooth muscle cell proliferation under chronic hypoxia. FASEB J. 25, 1922–1933. https://doi.org/10.1096/fj.10-175018

Kwon, K., Hutter, C., Sun, Q., Bilic, I., Cobaleda, C., Malin, S., Busslinger, M., 2008. Instructive role of the transcription factor E2A in early B lymphopoiesis and germinal center B cell development. Immunity 28, 751–762. https://doi.org/10.1016/j.immuni.2008.04.014

Kwong, J.Q., Henning, M.S., Starkov, A.A., Manfredi, G., 2007. The mitochondrial respiratory chain is a modulator of apoptosis. J. Cell Biol. 179, 1163–1177. https://doi.org/10.1083/jcb.200704059

Lam, W.Y., Becker, A.M., Kennerly, K.M., Wong, R., Curtis, J.D., Llufrio, E.M., McCommis, K.S., Fahrmann, J., Pizzato, H.A., Nunley, R.M., Lee, J., Wolfgang, M.J., Patti, G.J., Finck, B.N., Pearce, E.L., Bhattacharya, D., 2016. Mitochondrial Pyruvate Import Promotes Long-Term Survival of Antibody-Secreting Plasma Cells. Immunity 45, 60–73. https://doi.org/10.1016/j.immuni.2016.06.011

Land, S.C., Tee, A.R., 2007. Hypoxia-inducible Factor 1α Is Regulated by the Mammalian Target of Rapamycin (mTOR) via an mTOR Signaling Motif *. J. Biol. Chem. 282, 20534–20543. https://doi.org/10.1074/jbc.M611782200

Larsson, N.-G., 2010. Somatic Mitochondrial DNA Mutations in Mammalian Aging. Annu. Rev. Biochem. 79, 683–706. https://doi.org/10.1146/annurev-biochem-060408-093701

Ledderose, C., Junger, W.G., 2020. Mitochondria Synergize With P2 Receptors to Regulate Human T Cell Function. Front. Immunol. 11. https://doi.org/10.3389/fimmu.2020.549889

Ledderose, C., Liu, K., Kondo, Y., Slubowski, C.J., Dertnig, T., Denicoló, S., Arbab, M., Hubner, J., Konrad, K., Fakhari, M., Lederer, J.A., Robson, S.C., Visner, G.A., Junger, W.G., 2018. Purinergic P2X4 receptors and mitochondrial ATP production regulate T cell migration. J. Clin. Invest. 128, 3583–3594. https://doi.org/10.1172/JCI120972

Lin, K.-I., Angelin-Duclos, C., Kuo, T.C., Calame, K., 2002. Blimp-1-Dependent Repression of Pax-5 Is Required for Differentiation of B Cells to Immunoglobulin M-Secreting Plasma Cells. Mol. Cell. Biol. 22, 4771–4780. https://doi.org/10.1128/MCB.22.13.4771-4780.2002

Locasale, J.W., 2018. New concepts in feedback regulation of glucose metabolism. Curr. Opin. Syst. Biol. 8, 32–38. https://doi.org/10.1016/j.coisb.2017.11.005

Loder, B.F., Mutschler, B., Ray, R.J., Paige, C.J., Sideras, P., Torres, R., Lamers, M.C., Carsetti, R., 1999. B Cell Development in the Spleen Takes Place in Discrete Steps and Is Determined by the Quality of B Cell Receptor–Derived Signals. J. Exp. Med. 190, 75–90.

Lopes-Carvalho, T., Kearney, J.F., 2004. Development and selection of marginal zone B cells. Immunol. Rev. 197, 192–205. https://doi.org/10.1111/j.0105-2896.2004.0112.x

Mackay, F., Woodcock, S.A., Lawton, P., Ambrose, C., Baetscher, M., Schneider, P., Tschopp, J., Browning, J.L., 1999. Mice Transgenic for Baff Develop Lymphocytic Disorders along with Autoimmune Manifestations. J. Exp. Med. 190, 1697–1710.

Martin, F., Oliver, A.M., Kearney, J.F., 2001. Marginal Zone and B1 B Cells Unite in the Early Response against T-Independent Blood-Borne Particulate Antigens. Immunity 14, 617–629. https://doi.org/10.1016/S1074-7613(01)00129-7

McCarron, J.G., Wilson, C., Sandison, M.E., Olson, M.L., Girkin, J.M., Saunter, C., Chalmers, S., 2013. From Structure to Function: Mitochondrial Morphology, Motion and Shaping in Vascular Smooth Muscle. J. Vasc. Res. 50, 357–371. https://doi.org/10.1159/000353883

Medzhitov, R., Janeway Jr, C.A., 2000. How does the immune system distinguish self from nonself? Semin. Immunol. 12, 185–188. https://doi.org/10.1006/smim.2000.0230

Melchers, F., 2015. Checkpoints that control B cell development. J. Clin. Invest. 125, 2203–2210. https://doi.org/10.1172/JCI78083

Meyer-Hermann, M., Mohr, E., Pelletier, N., Zhang, Y., Victora, G.D., Toellner, K.-M., 2012. A Theory of Germinal Center B Cell Selection, Division, and Exit. Cell Rep. 2, 162–174. https://doi.org/10.1016/j.celrep.2012.05.010

Milenkovic, D., Matic, S., Kühl, I., Ruzzenente, B., Freyer, C., Jemt, E., Park, C.B., Falkenberg, M., Larsson, N.-G., 2013. TWINKLE is an essential mitochondrial helicase required for synthesis of nascent D-loop strands and complete mtDNA replication. Hum. Mol. Genet. 22, 1983–1993. https://doi.org/10.1093/hmg/ddt051

Mullen, A.R., Wheaton, W.W., Jin, E.S., Chen, P.-H., Sullivan, L.B., Cheng, T., Yang, Y., Linehan, W.M., Chandel, N.S., DeBerardinis, R.J., 2011. Reductive carboxylation supports growth in tumor cells with defective mitochondria. Nature 481, 385–388. https://doi.org/10.1038/nature10642

Muri, J., Thut, H., Bornkamm, G.W., Kopf, M., 2019. B1 and Marginal Zone B Cells but Not Follicular B2 Cells Require Gpx4 to Prevent Lipid Peroxidation and Ferroptosis. Cell Rep. 29, 2731-2744.e4. https://doi.org/10.1016/j.celrep.2019.10.070

Nagasawa, T., 2007. The chemokine CXCL12 and regulation of HSC and B lymphocyte development in the bone marrow niche. Adv. Exp. Med. Biol. 602, 69–75. https://doi.org/10.1007/978-0-387-72009-8_9

Nagasawa, T., 2006. Microenvironmental niches in the bone marrow required for B-cell development. Nat. Rev. Immunol. 6, 107–116. https://doi.org/10.1038/nri1780

Ngo, H.B., Lovely, G.A., Phillips, R., Chan, D.C., 2014. Distinct structural features of TFAM drive mitochondrial DNA packaging versus transcriptional activation. Nat. Commun. 5, 3077. https://doi.org/10.1038/ncomms4077

Nutt, S.L., Hodgkin, P.D., Tarlinton, D.M., Corcoran, L.M., 2015. The generation of antibody-secreting plasma cells. Nat. Rev. Immunol. 15, 160–171. https://doi.org/10.1038/nri3795

Obukhanych, T.V., Nussenzweig, M.C., 2006. T-independent type II immune responses generate memory B cells. J. Exp. Med. 203, 305–310. https://doi.org/10.1084/jem.20052036

Oliver, A.M., Martin, F., Kearney, J.F., 1999. IgMhighCD21high Lymphocytes Enriched in the Splenic Marginal Zone Generate Effector Cells More Rapidly Than the Bulk of Follicular B Cells. J. Immunol. 162, 7198–7207.

O'Neill, L.A.J., Kishton, R.J., Rathmell, J., 2016. A guide to immunometabolism for immunologists. Nat. Rev. Immunol. 16, 553–565. https://doi.org/10.1038/nri.2016.70

Pabst, O., Slack, E., 2020. IgA and the intestinal microbiota: the importance of being specific. Mucosal Immunol. 13, 12–21. https://doi.org/10.1038/s41385-019-0227-4

Pak, H.-K., Nam, B., Lee, Y.K., Kim, Y.-W., Roh, J., Son, J., Chung, Y.-S., Choe, J., Park, C.-S., 2018. Human Plasmablast Migration Toward CXCL12 Requires Glucose Oxidation by Enhanced Pyruvate Dehydrogenase Activity via AKT. Front. Immunol. 9, 1742. https://doi.org/10.3389/fimmu.2018.01742

Park, H., Staehling, K., Tsang, M., Appleby, M.W., Brunkow, M.E., Margineantu, D., Hockenbery, D.M., Habib, T., Liggitt, H.D., Carlson, G., Iritani, B.M., 2012. Disruption of Fnip1 reveals a metabolic checkpoint controlling B lymphocyte development. Immunity 36, 769–781. https://doi.org/10.1016/j.immuni.2012.02.019

Patke, A., Mecklenbräuker, I., Erdjument-Bromage, H., Tempst, P., Tarakhovsky, A., 2006. BAFF controls B cell metabolic fitness through a PKCβ- and Akt-dependent mechanism. J. Exp. Med. 203, 2551–2562. https://doi.org/10.1084/jem.20060990

Pillai, S., 2009. The follicular versus marginal zone B lymphocyte cell fate decision 11.

Poschenrieder, S.T., Wagner, S.G., Castiglione, K., 2016. Efficient production of uniform nanometer-sized polymer vesicles in stirred-tank reactors. J. Appl. Polym. Sci. 133. https://doi.org/10.1002/app.43274

Pracht, K., Meinzinger, J., Daum, P., Schulz, S.R., Reimer, D., Hauke, M., Roth, E., Mielenz, D., Berek, C., Côrte-Real, J., Jäck, H.-M., Schuh, W., 2017. A new staining protocol for detection of murine antibody-secreting plasma cell subsets by flow cytometry. Eur. J. Immunol. 47, 1389–1392. https://doi.org/10.1002/eji.201747019

Price, M.J., Patterson, D.G., Scharer, C.D., Boss, J.M., 2018. Progressive Upregulation of Oxidative Metabolism Facilitates Plasmablast Differentiation to a T-Independent Antigen. Cell Rep. 23, 3152–3159. https://doi.org/10.1016/j.celrep.2018.05.053

Przybyła, T., Sakowicz-Burkiewicz, M., Pawełczyk, T., 2018. Purinergic signalling in B cells. Acta Biochim. Pol. 65, 1–7. https://doi.org/10.18388/abp.2017_1588

Pupovac, A., Geraghty, N.J., Watson, D., Sluyter, R., 2015. Activation of the P2X7 receptor induces the rapid shedding of CD23 from human and murine B cells. Immunol. Cell Biol. 93, 77–85. https://doi.org/10.1038/icb.2014.69

Quiros, P.M., Goyal, A., Jha, P., Auwerx, J., 2017. Analysis of mtDNA/nDNA ratio in mice. Curr. Protoc. Mouse Biol. 7, 47–54. https://doi.org/10.1002/cpmo.21

Ray, R.J., Paige, C.J., Furlonger, C., Lyman, S.D., Rottapel, R., 1996. Flt3 ligand supports the differentiation of early B cell progenitors in the presence of interleukin-11 and interleukin-7. Eur. J. Immunol. 26, 1504–1510. https://doi.org/10.1002/eji.1830260715

Ribeiro, J.A., Sebastião, A.M., 2010. Caffeine and adenosine. J. Alzheimers Dis. JAD 20 Suppl 1, S3-15. https://doi.org/10.3233/JAD-2010-1379

Riley, J.S., Tait, S.W., 2020. Mitochondrial DNA in inflammation and immunity. EMBO Rep. 21. https://doi.org/10.15252/embr.201949799

Rossignol, R., Gilkerson, R., Aggeler, R., Yamagata, K., Remington, S.J., Capaldi, R.A., 2004. Energy Substrate Modulates Mitochondrial Structure and Oxidative Capacity in Cancer Cells. Cancer Res. 64, 985–993. https://doi.org/10.1158/0008-5472.CAN-03-1101

Rottenberg, H., 1975. The measurement of transmembrane electrochemical proton gradients. J. Bioenerg. 7, 61–74. https://doi.org/10.1007/BF01558427

Sadofsky, M.J., 2001. The RAG proteins in V(D)J recombination: more than just a nuclease. Nucleic Acids Res. 29, 1399–1409.

Saito, T., Chiba, S., Ichikawa, M., Kunisato, A., Asai, T., Shimizu, K., Yamaguchi, T., Yamamoto, G., Seo, S., Kumano, K., Nakagami-Yamaguchi, E., Hamada, Y., Aizawa, S., Hirai, H., 2003. Notch2 Is Preferentially Expressed in Mature B Cells and Indispensable for Marginal Zone B Lineage Development. Immunity 18, 675–685. https://doi.org/10.1016/S1074-7613(03)00111-0

Sak, K., Boeynaems, J.-M., Everaus, H., 2003. Involvement of P2Y receptors in the differentiation of haematopoietic cells. J. Leukoc. Biol. 73, 442–447. https://doi.org/10.1189/jlb.1102561

Savitsky, D., Calame, K., 2006. B-1 B lymphocytes require Blimp-1 for immunoglobulin secretion. J. Exp. Med. 203, 2305–2314. https://doi.org/10.1084/jem.20060411

Saxton, R.A., Sabatini, D.M., 2017. mTOR Signaling in Growth, Metabolism, and Disease. Cell 168, 960–976. https://doi.org/10.1016/j.cell.2017.02.004

Schena, F., Volpi, S., Faliti, C.E., Penco, F., Santi, S., Proietti, M., Schenk, U., Damonte, G., Salis, A., Bellotti, M., Fais, F., Tenca, C., Gattorno, M., Eibel, H., Rizzi, M., Warnatz, K., Idzko, M., Ayata, C.K., Rakhmanov, M., Galli, T., Martini, A., Canossa, M., Grassi, F., Traggiai, E., 2013. Dependence of immunoglobulin class switch recombination in B cells on vesicular release of ATP and CD73 ectonucleotidase activity. Cell Rep. 3, 1824–1831. https://doi.org/10.1016/j.celrep.2013.05.022

Schiemann, B., Gommerman, J.L., Vora, K., Cachero, T.G., Shulga-Morskaya, S., Dobles, M., Frew, E., Scott, M.L., 2001. An Essential Role for BAFF in the Normal Development of B Cells Through a BCMA-Independent Pathway. Science 293, 2111–2114. https://doi.org/10.1126/science.1061964

Schuh, W., Mielenz, D., Jäck, H.-M., 2020. Unraveling the mysteries of plasma cells. Adv. Immunol. 146, 57–107. https://doi.org/10.1016/bs.ai.2020.01.002

Shaffer, A.L., Lin, K.-I., Kuo, T.C., Yu, X., Hurt, E.M., Rosenwald, A., Giltnane, J.M., Yang, L., Zhao, H., Calame, K., Staudt, L.M., 2002. Blimp-1 Orchestrates Plasma Cell Differentiation by Extinguishing the Mature B Cell Gene Expression Program. Immunity 17, 51–62. https://doi.org/10.1016/S1074-7613(02)00335-7

Shapiro-Shelef, M., Lin, K.-I., McHeyzer-Williams, L.J., Liao, J., McHeyzer-Williams, M.G., Calame, K., 2003. Blimp-1 Is Required for the Formation of Immunoglobulin Secreting Plasma Cells and Pre-Plasma Memory B Cells. Immunity 19, 607–620. https://doi.org/10.1016/S1074-7613(03)00267-X

Shaw, R.J., 2009. LKB1 and AMPK control of mTOR signalling and growth. Acta Physiol. Oxf. Engl. 196, 65–80. https://doi.org/10.1111/j.1748-1716.2009.01972.x

Sherer, T.B., Trimmer, P.A., Parks, J.K., Tuttle, J.B., 2000. Mitochondrial DNA-depleted neuroblastoma (Rho°) cells exhibit altered calcium signaling. Biochim. Biophys. Acta BBA - Mol. Cell Res. 1496, 341–355. https://doi.org/10.1016/S0167-4889(00)00027-6

Sintes, J., Gentile, M., Zhang, S., Garcia-Carmona, Y., Magri, G., Cassis, L., Segura-Garzón, D., Ciociola, A., Grasset, E.K., Bascones, S., Comerma, L., Pybus, M., Lligé, D., Puga, I., Gutzeit, C., He, B., DuBois, W., Crespo, M., Pascual, J., Mensa, A., Aróstegui, J.I., Juan, M., Yagüe, J., Serrano, S., Lloreta, J., Meffre, E., Hahne, M., Cunningham-Rundles, C., Mock, B.A., Cerutti, A., 2017. mTOR intersects antibody-inducing signals from TACI in marginal zone B cells. Nat. Commun. 8, 1462. https://doi.org/10.1038/s41467-017-01602-4

Stein, M., Dütting, S., Mougiakakos, D., Bösl, M., Fritsch, K., Reimer, D., Urbanczyk, S., Steinmetz, T., Schuh, W., Bozec, A., Winkler, T.H., Jäck, H.-M., Mielenz, D., 2017. A defined metabolic state in pre B cells governs B-cell development and is counterbalanced by Swiprosin-2/EFhd1. Cell Death Differ. 24, 1239–1252. https://doi.org/10.1038/cdd.2017.52

Stephan, T., Brüser, C., Deckers, M., Steyer, A.M., Balzarotti, F., Barbot, M., Behr, T.S., Heim, G., Hübner, W., Ilgen, P., Lange, F., Pacheu-Grau, D., Pape, J.K., Stoldt, S., Huser, T., Hell, S.W., Möbius, W., Rehling, P., Riedel, D., Jakobs, S., 2020. MICOS assembly controls mitochondrial inner membrane remodeling and crista junction redistribution to mediate cristae formation. EMBO J. 39, e104105. https://doi.org/10.15252/embj.2019104105

Stincone, A., Prigione, A., Cramer, T., Wamelink, M.M.C., Campbell, K., Cheung, E., Olin-Sandoval, V., Grüning, N.-M., Krüger, A., Alam, M.T., Keller, M.A., Breitenbach, M., Brindle, K.M., Rabinowitz, J.D., Ralser, M., 2015. The return of metabolism: biochemistry and physiology of the pentose phosphate pathway. Biol. Rev. 90, 927–963. https://doi.org/10.1111/brv.12140

Strauss, M., Hofhaus, G., Schröder, R.R., Kühlbrandt, W., 2008. Dimer ribbons of ATP synthase shape the inner mitochondrial membrane. EMBO J. 27, 1154–1160. https://doi.org/10.1038/emboj.2008.35

Tanguy, E., Wang, Q., Moine, H., Vitale, N., 2019. Phosphatidic Acid: From Pleiotropic Functions to Neuronal Pathology. Front. Cell. Neurosci. 13. https://doi.org/10.3389/fncel.2019.00002

Td, S., U, S.-S., A, H., W, S., J, W., Sr, S., Th, W., Hm, J., D, M., 2020. TFG is required for autophagy flux and to prevent endoplasmic reticulum stress in CH12 B lymphoma cells. Autophagy. https://doi.org/10.1080/15548627.2020.1821546

Turner, C.A., Mack, D.H., Davis, M.M., 1994. Blimp-1, a novel zinc finger-containing protein that can drive the maturation of B lymphocytes into immunoglobulin-secreting cells. Cell 77, 297–306. https://doi.org/10.1016/0092-8674(94)90321-2

Urbanczyk, S., Baris, O.R., Hofmann, J., Golombek, F., Castiglione, K., Meng, X., Bozec, A., Mougiakakos, D., Schulz, S.R., Schuh, W., Schlötzer-Schrehardt, U., Steinmetz, T.D., Brodesser, S., Wiesner, R.J., Mielenz, D., 2021. Mitochondrial function is essential for humoral immunity by controlling flux of the TCA cycle, phosphatidic acid and mTOR activity in B cells. bioRxiv 2021.01.14.426649. https://doi.org/10.1101/2021.01.14.426649 (Cell Reports, in revision)

Urbanczyk, S., Stein, M., Schuh, W., Jäck, H.-M., Mougiakakos, D., Mielenz, D., 2018. Regulation of Energy Metabolism during Early B Lymphocyte Development. Int. J. Mol. Sci. 19. https://doi.org/10.3390/ijms19082192

V, K., Je, B., J, B., Rh, R., Ht, H.-D., Dr, R., N, S., S, B., S, T., Re, L., Rj, W., P, V., Cb, B., S, H., H, B., H, L.-W., P, S., Tm, M., 2015. A keratin scaffold regulates epidermal barrier formation, mitochondrial lipid composition, and activity. J. Cell Biol. 211. https://doi.org/10.1083/jcb.201404147

van der Windt, G.J.W., Pearce, E.L., 2012. Metabolic switching and fuel choice during T-cell differentiation and memory development. Immunol. Rev. 249, 27–42. https://doi.org/10.1111/j.1600-065X.2012.01150.x

Vander Heiden, M.G., Cantley, L.C., Thompson, C.B., 2009. Understanding the Warburg Effect: The Metabolic Requirements of Cell Proliferation. Science 324, 1029–1033. https://doi.org/10.1126/science.1160809

Vermes, I., Haanen, C., Steffens-Nakken, H., Reutelingsperger, C., 1995. A novel assay for apoptosis. Flow cytometric detection of phosphatidylserine expression on early apoptotic cells using fluorescein labelled Annexin V. J. Immunol. Methods 184, 39–51. https://doi.org/10.1016/0022-1759(95)00072-i

Vinuesa, C.G. de, O'Leary, P., Sze, D.M.-Y., Toellner, K.-M., MacLennan, I.C.M., 1999. T-independent type 2 antigens induce B cell proliferation in multiple splenic sites, but exponential growth is confined to extrafollicular foci. Eur. J. Immunol. 29, 1314–1323. https://doi.org/10.1002/(SICI)1521-4141(199904)29:04<1314::AID-IMMU1314>3.0.CO;2-4

Wang, H., Gonzalez-Garcia, I., Traba, J., Jain, S., Conteh, S., Shin, D.-M., Qi, C., Gao, Y., Sun, J., Kang, S., Abbasi, S., Naghashfar, Z., Yoon, J., DuBois, W., Kovalchuk, A.L., Sack, M.N., Duffy, P., Morse, H.C., 2017. ATP-degrading ENPP1 is required for survival (or persistence) of long-lived plasma cells. Sci. Rep. 7, 17867. https://doi.org/10.1038/s41598-017-18028-z

Waters, L.R., Ahsan, F.M., Wolf, D.M., Shirihai, O., Teitell, M.A., 2018. Initial B Cell Activation Induces Metabolic Reprogramming and Mitochondrial Remodeling. iScience 5, 99–109. https://doi.org/10.1016/j.isci.2018.07.005

Weisel, F.J., Mullett, S.J., Elsner, R.A., Menk, A.V., Trivedi, N., Luo, W., Wikenheiser, D., Hawse, W.F., Chikina, M., Smita, S., Conter, L.J., Joachim, S.M., Wendell, S.G., Jurczak, M.J., Winkler, T.H., Delgoffe, G.M., Shlomchik, M.J., 2020. Germinal center B cells selectively oxidize fatty acids for energy while conducting minimal glycolysis. Nat. Immunol. 21, 331–342. https://doi.org/10.1038/s41590-020-0598-4

Xia, Y., Choi, H.-K., Lee, K., 2012. Recent advances in hypoxia-inducible factor (HIF)-1 inhibitors. Eur. J. Med. Chem. 49, 24–40. https://doi.org/10.1016/j.ejmech.2012.01.033

Xiao, G., Chan, L.N., Klemm, L., Braas, D., Chen, Z., Geng, H., Zhang, Q.C., Aghajanirefah, A., Cosgun, K.N., Sadras, T., Lee, J., Mirzapoiazova, T., Salgia, R., Ernst, T., Hochhaus, A., Jumaa, H., Jiang, X., Weinstock, D.M., Graeber, T.G., Müschen, M., 2018. B cell-specific diversion of glucose carbon utilization reveals a unique vulnerability in B cell malignancies. Cell 173, 470-484.e18. https://doi.org/10.1016/j.cell.2018.02.048

Yan, C., Duanmu, X., Zeng, L., Liu, B., Song, Z., 2019. Mitochondrial DNA: Distribution, Mutations, and Elimination. Cells 8. https://doi.org/10.3390/cells8040379

Yoo, H.C., Yu, Y.C., Sung, Y., Han, J.M., 2020. Glutamine reliance in cell metabolism. Exp. Mol. Med. 52, 1496–1516. https://doi.org/10.1038/s12276-020-00504-8

Yoon, M.-S., Rosenberger, C.L., Wu, C., Truong, N., Sweedler, J.V., Chen, J., 2015. Rapid Mitogenic Regulation of the mTORC1 Inhibitor, DEPTOR, by Phosphatidic Acid. Mol. Cell 58, 549–556. https://doi.org/10.1016/j.molcel.2015.03.028

Yoon, M.-S., Sun, Y., Arauz, E., Jiang, Y., Chen, J., 2011a. Phosphatidic acid activates mammalian target of rapamycin complex 1 (mTORC1) kinase by displacing FK506 binding protein 38 (FKBP38) and exerting an allosteric effect. J. Biol. Chem. 286, 29568–29574. https://doi.org/10.1074/jbc.M111.262816

Yoon, M.-S., Sun, Y., Arauz, E., Jiang, Y., Chen, J., 2011b. Phosphatidic Acid Activates Mammalian Target of Rapamycin Complex 1 (mTORC1) Kinase by Displacing FK506 Binding Protein 38 (FKBP38) and Exerting an Allosteric Effect. J. Biol. Chem. 286, 29568–29574. https://doi.org/10.1074/jbc.M111.262816

Youle, R.J., van der Bliek, A.M., 2012. Mitochondrial Fission, Fusion, and Stress. Science 337, 1062–1065. https://doi.org/10.1126/science.1219855

Zeng, H., Yu, M., Tan, H., Li, Y., Su, W., Shi, H., Dhungana, Y., Guy, C., Neale, G., Cloer, C., Peng, J., Wang, D., Chi, H., 2018. Discrete roles and bifurcation of PTEN signaling and mTORC1-mediated anabolic metabolism underlie IL-7–driven B lymphopoiesis. Sci. Adv. 4, eaar5701. https://doi.org/10.1126/sciadv.aar5701

Zhang, Y., Dépond, M., He, L., Foudi, A., Kwarteng, E.O., Lauret, E., Plo, I., Desterke, C., Dessen, P., Fujii, N., Opolon, P., Herault, O., Solary, E., Vainchenker, W., Joulin, V., Louache, F., Wittner, M., 2016. CXCR4/CXCL12 axis counteracts hematopoietic stem cell exhaustion through selective protection against oxidative stress. Sci. Rep. 6, 37827. https://doi.org/10.1038/srep37827

Zhou, W., Cao, L., Jeffries, J., Zhu, X., Staiger, C.J., Deng, Q., 2018. Neutrophil-specific knockout demonstrates a role for mitochondria in regulating neutrophil motility in zebrafish. Dis. Model. Mech. 11. https://doi.org/10.1242/dmm.033027

Zhou, Y., Zhang, Y., Han, J., Yang, M., Zhu, J., Jin, T., 2020. Transitional B cells involved in autoimmunity and their impact on neuroimmunological diseases. J. Transl. Med. 18, 131. https://doi.org/10.1186/s12967-020-02289-w

10.6. Publications

Cossarizza, … , **Urbanczyk, S**., ..., 2019. Guidelines for the use of flow cytometry and cell sorting in immunological studies (second edition). Eur. J. Immunol. 49, 1457–1973. https://doi.org/10.1002/eji.201970107

Finger, Y., Habich, M., Gerlich, S., **Urbanczyk, S**., van de Logt, E., Koch, J., Schu, L., Lapacz, K.J., Ali, M., Petrungaro, C., Salscheider, S.L., Pichlo, C., Baumann, U., Mielenz, D., Dengjel, J., Brachvogel, B., Hofmann, K., Riemer, J., 2020. Proteasomal degradation induced by DPP9-mediated processing competes with mitochondrial protein import. EMBO J. 39, e103889. https://doi.org/10.15252/embj.2019103889

Parma, B., Ramesh, V., Gollavilli, P.N., Siddiqui, A., Pinna, L., Schwab, A., Marschall, S., Zhang, S., Pilarsky, C., Napoli, F., Volante, M**., Urbanczyk, S**., Mielenz, D., Schrøder, H.D., Stemmler, M., Wurdak, H., Ceppi, P., 2021. Metabolic impairment of non-small cell lung cancers by mitochondrial HSPD1 targeting. J. Exp. Clin. Cancer Res. 40, 248. https://doi.org/10.1186/s13046-021-02049-8

Reimer, D., Meyer-Hermann, M., Rakhymzhan, A., Steinmetz, T., Tripal, P., Thomas, J., Boettcher, M., Mougiakakos, D., Schulz, S.R., **Urbanczyk, S**., Hauser, A.E., Niesner, R.A., Mielenz, D., 2020. B Cell Speed and B-FDC Contacts in Germinal Centers Determine Plasma Cell Output via Swiprosin-1/EFhd2. Cell Rep. 32, 108030. https://doi.org/10.1016/j.celrep.2020.108030

Stein, M., Dütting, S., Mougiakakos, D., Bösl, M., Fritsch, K., Reimer, D., **Urbanczyk, S**., Steinmetz, T., Schuh, W., Bozec, A., Winkler, T.H., Jäck, H.-M., Mielenz, D., 2017. A defined metabolic state in pre B cells governs B-cell development and is counterbalanced by Swiprosin-2/EFhd1. Cell Death Differ. 24, 1239–1252. https://doi.org/10.1038/cdd.2017.52

Urbanczyk, S., Stein, M., Schuh, W., Jäck, H.-M., Mougiakakos, D., Mielenz, D., 2018. Regulation of Energy Metabolism during Early B Lymphocyte Development. Int. J. Mol. Sci. 19. https://doi.org/10.3390/ijms19082192

Urbanczyk, S., Baris, O.R., Hofmann, J., Golombek, F., Castiglione, K., Meng, X., Bozec, A., Mougiakakos, D., Schulz, S.R., Schuh, W., Schlötzer-Schrehardt, U., Steinmetz, T.D., Brodesser, S., Wiesner, R.J., Mielenz, D., 2021. Mitochondrial function is essential for humoral immunity by controlling flux of the TCA cycle, phosphatidic acid and mTOR activity in B cells. bioRxiv 2021.01.14.426649. https://doi.org/10.1101/2021.01.14.426649

11. Acknowledgments

Nach einigen Jahren intensiver Arbeit ist das Werk vollbracht, und ich kann hiermit versuchen Worte zu finden, um mich bei denjenigen zu bedanken, die mich auf diesem Weg begleitet und unterstützt haben.

Zuallererst möchte ich ganz herzlich meinem Doktorvater Dirk Mielenz für diese wundervolle und vor allem sehr lehrreiche Zeit danken! Der Dank gilt nicht nur für die Bereitstellung dieses interessanten Themas, sondern auch für die stetige Begleitung, die super Betreuung und die unvergesslichen Gespräche. Ohne das mir entgegengebrachte Vertrauen und die damit verbundenen Freiheiten in der Ausübung meiner wissenschaftlichen Arbeit, wäre diese Dissertation nicht zu diesem Werk geworden... Vielen Dank!

Des Weiteren möchte ich mich bei Lars Nitschke bedanken für die Übernahme des Erstgutachtens und bei Thomas Winkler und Robert Slany für die Übernahme der mündlichen Prüfung.

Außerdem bedanke ich mich ganz herzlich bei Hans-Martin Jäck, sowohl für seine fachlichen Ratschläge und Kommentare, als auch für das Ermöglichen an zahlreichen Konferenzen und Workshops teilzunehmen.

Besonderer Dank gebührt meinen langjährigen Kollegen/-innen, die einfach eine wundervolle Begleitung waren, und sowohl durch ihre fachliche Hilfe als auch durch viel Spaß das (Arbeits-) Leben enorm verschönert haben: (Doro-) Thea Reimer, Tobit Steinmetz, Sebastian Schulz, Jens Wittner, Katharina Pracht und Stefan Hofmann.

Den „Neuankömmlingen“ der AG Mielenz Leonie Weckwerth und Jana Thomas möchte ich für ihre Bereitstellung praktischer Hilfe danken. Ich wünsche euch viel Erfolg und Spaß auf eurem weiteren Weg in Richtung Promotion!

Auch bei den Post-Docs Wolfgang Schuh und Jürgen Wittmann möchte ich mich für die Hilfe und konstruktives Feedback bedanken.

Außerdem möchte ich mich ganz herzlich bei Manuela Hauke und Edith Roth bedanken, bei denen ich jederzeit freundliche Hilfe (auch bei doofen Fragen) erhalten habe.

Für stetige Hilfe beim Thema Tierpflege möchte ich mich bei Heidi von Berg bedanken, die sich stets gewissenhaft um meine Mäuse gekümmert hat.

Des Weiteren danke ich Uwe Appelt und Markus Mrotz für das Sortieren meiner Zellen und zugehöriges Entwerfen von Sort-Strategien auf dem Dach.

Außerdem möchte ich mich ganz herzlich bei Lisa Lang bedanken, die sich über Jahre hinweg zuverlässig um ziemlich alles Organisatorisches gekümmert hat, was mir ermöglicht hat, mich

voll und ganz auf die Wissenschaft zu konzentrieren. Anja Schwarz danke ich diese Arbeit übernommen zu haben.

Auch den zahlreichen Kooperationspartnern möchte ich für ihre Beitrage zu dieser Arbeit danken: Jörg Hofmann, Ursula Schlötzer-Schrehardt, Dimitrios Mougiakakos, Susanne Brodesser, Florian Golombek und Kathrin Castiglione. Besonderer Dank geht an Rudolf Wiesner und Olivier Baris für die Bereitstellung der DNT Maus und Hilfe rund um das Thema Mitochondrien.

Außerdem danke ich allen TRR130 Kollegen/-innen für unvergessliche Momente und wunderschöne Zeiten auf unseren zahlreichen Winterschools und Meetings. Agnes Giniewski danke ich für das Organisieren, welches das erst ermöglicht hat.

Im Zusammenhang mit dem IRTG und jährlichen Winterschools möchte ich mich außerdem ganz herzlich bei meinem Thesis Advisory Committee bestehend aus Julia Jellusova und Anja Hauser für das hilfreiche und konstruktive Feedback bedanken.

Zu guter Letzt gebührt unendlicher Dank meinen Freunden und besonders meiner Familie und meinem Partner Kalli, ohne deren bedingungslose Liebe und unermüdliche Unterstützung auf jedwede erdenkliche Weise ich niemals so weit gekommen wäre.

Iraké Oni!

12. Declaration

Ich erkläre: „Ich habe die vorgelegte Dissertation selbständig und ohne unerlaubte fremde Hilfe und nur mit Hilfen angefertigt, die ich in der Dissertation angegeben habe. Alle Textstellen, die wörtlich oder sinngemäß aus veröffentlichten oder nicht veröffentlichten Schriften entnommen sind, und alle Angaben, die auf mündlichen Auskünften beruhen, sind als solche kenntlich gemacht. Bei den von mir durchgeführten und in der Dissertation erwähnten Untersuchungen habe ich die Grundsätze guter wissenschaftlicher Praxis eingehalten, wie sie in den „Richtlinien der Friedrich-Alexander-Universität Erlangen- Nürnberg zur Sicherung guter wissenschaftlicher Praxis“ niedergelegt sind.”

Erlangen, 07.01.2021

Sophia Urbanczyk

“And if my thought-dreams could be seen
They’d probably put my head in a guillotine
But it’s alright Ma,
It’s life, and life only”

(Bob Dylan)